



UNIVERSIDADE FEDERAL DE MINAS GERAIS
INSTITUTO DE CIÊNCIAS BIOLÓGICAS – ICB
DEPARTAMENTO DE FISILOGIA E BIOFÍSICA
PROGRAMA DE PÓS-GRADUAÇÃO EM CIÊNCIAS BIOLÓGICAS:
FISILOGIA E FARMACOLOGIA

EXPRESSÃO DE RECEPTORES DE INOSITOL 1,4,5-TRIFOSFATO
DO TIPO 3 É UM EVENTO FINAL COMUM AO
DESENVOLVIMENTO DO CARCINOMA HEPATOCELULAR

Rodrigo Machado Florentino

Orientadora: Maria de Fátima Leite

Coorientadora: Fernanda de Oliveira Lemos

Belo Horizonte

2020

RODRIGO MACHADO FLORENTINO

**EXPRESSÃO DE RECEPTORES DE INOSITOL 1,4,5-TRIFOSFATO
DO TIPO 3 É UM EVENTO FINAL COMUM AO
DESENVOLVIMENTO DO CARCINOMA HEPATOCELULAR**

Tese apresentada ao Programa de Pós-Graduação em Ciências Biológicas: Fisiologia e Farmacologia, do Instituto de Ciências Biológicas da Universidade Federal de Minas Gerais, como requisito obrigatório para obtenção do título de Doutor em Ciências Biológicas.

Área de concentração: Fisiologia

Orientadora: Maria de Fátima Leite

Coorientadora: Fernanda de Oliveira Lemos

Belo Horizonte

2020

043 Florentino, Rodrigo Machado.
Expressão de receptores de inositol 1,4,5-trifosfato do tipo 3 é um evento final comum ao desenvolvimento do carcinoma hepatocelular [manuscrito] / Rodrigo Machado Florentino. - 2020.
158 f. : il. ; 29,5 cm.

Orientadora: Maria de Fátima Leite. Coorientadora: Fernanda de Oliveira Lemos.

Tese (doutorado) - Universidade Federal de Minas Gerais, Instituto de Ciências Biológicas. Programa de Pós-Graduação em Fisiologia e Farmacologia.

1. Fisiologia. 2. Carcinoma Hepatocelular. 3. Receptores de Inositol 1,4,5-Trifosfato. 4. Sinalização do Cálcio. 5. Proliferação de Células. 6. Apoptose. I. Leite, Maria de Fátima. II. Lemos, Fernanda de Oliveira. III. Universidade Federal de Minas Gerais. Instituto de Ciências Biológicas. IV. Título.

CDU: 612

"EXPRESSÃO DE RECEPTORES DE INOSITOL 1,4,5-TRIFOSFATO DO TIPO 3 É UM EVENTO FINAL COMUM AO DESENVOLVIMENTO DO CARCINOMA HEPATOCELULAR"

RODRIGO MACHADO FLORENTINO

Tese de Doutorado defendida e aprovada, no dia **19 de junho de 2020**, pela Banca Examinadora constituída pelos seguintes professores:



PROFA. DRA. JULIANA DE ASSIS SILVA GOMES ESTANISLAU
ICB/UNIVERSIDADE FEDERAL DE MINAS GERAIS



PROF. DR. JADER DOS SANTOS CRUZ
ICB/UNIVERSIDADE FEDERAL DE MINAS GERAIS




PROFA. DRA. REGINA COELI DOS SANTOS GOLDENBERG
IBCCF/UFRJ



PROF. DR. LUCIANO DE FIGUEIREDO BORGES
EPM/UNIFESP



DRA. FERNANDA DE OLIVEIRA LEMOS
ICB/UNIVERSIDADE FEDERAL DE MINAS GERAIS
COORIENTADORA



PROFA. DRA. MARIA DE FÁTIMA LEITE
ICB/UNIVERSIDADE FEDERAL DE MINAS GERAIS
ORIENTADORA

Programa de Pós-Graduação em Ciências Biológicas - Fisiologia e Farmacologia
Instituto de Ciências Biológicas - Universidade Federal de Minas Gerais - UFMG

Belo Horizonte, 19 de junho de 2020

Esse trabalho foi realizado no Laboratório de Sinalização de Cálcio, Departamento de Fisiologia e Biofísica do Instituto de Ciências Biológicas da Universidade Federal de Minas Gerais. Esta tese contou com auxílio financeiro da Coordenação de Aperfeiçoamento de Pessoal de Nível Superior (CAPES), Conselho Nacional de Desenvolvimento Científico e Tecnológico (CNPq) e Fundação de Amparo à Pesquisa de Minas Gerais (FAPEMIG).

“Pode-se encontrar a felicidade mesmo nas horas mais sombrias
se a pessoa se lembrar de acender a luz!”

Alvo Dumbledore

AGRADECIMENTOS

Agradeço primeiramente à minha família por serem simplesmente o que são! Aos meus pais, Aureliana e Oscar, meu muito obrigado por terem me acompanhado durante todo o percurso e por ter me dado todo o apoio necessário para chegar até aqui! Ao meu irmão, Daniel, agradeço o apoio, mesmo distante, mas sabendo que sempre presente!

Agradeço a todos do *Calcium Lab* pela oportunidade de aprender todos os dias! Toda experiência vivida com os que passaram por esse laboratório e aos que atualmente lutam comigo todos os dias, meu muito obrigado! A oportunidade de conviver com pessoas diversas, com objetivos e bagagens diferentes, me fez crescer como ser humano e me fez aprender como devo e como quero me portar frente a diversas situações! Obrigado, Professora Maria de Fátima Leite, pela orientação ao longo dos últimos 7 anos! Obrigado Fernanda de Oliveira Lemos, por ter aceitado a missão de ser minha coorientadora! Obrigado aos meus companheiros (não só) de bancada: Andressa França, Antônio Carlos Melo Lima Filho, Dabny Missiagia, Marcone Loiola, Sandhra Maria, Kemper Nunes, Gilson Nogueira e Taquinho!

Agradeço também aos meus amigos, do COLUNI, da Farmácia, do ICB e os outros que se agregaram durante a caminhada! Muito obrigado!

Agradeço à Universidade Federal de Minas Gerais!

Agradeço aos professores pela partilha do conhecimento!

Agradeço aos animais utilizados nesse projeto!

Agradeço aos pacientes que cederam as amostras para o estudo!

Agradeço a todos que contribuíram de alguma forma para que esse trabalho fosse realizado!

MUITO OBRIGADO!

SUMÁRIO

LISTA DE FIGURAS	8
LISTA DE ABREVIÇÕES	10
RESUMO	12
ABSTRACT	14
INTRODUÇÃO	15
Sinalização intracelular de cálcio	16
Receptores de Inositol 1,4,5-trifosfato	18
Carcinoma hepatocelular e epigenética	20
OBJETIVOS	23
Objetivo geral	24
Objetivos específicos	24
MATERIAIS E MÉTODOS	25
Avaliação do perfil de metilação do DNA na região promotora do ITPR humano	26
Análise dos dados de sobrevivência em pacientes com carcinoma hepatocelular	26
Animais e tratamento hipometilante do DNA	27
Modelo murino de carcinoma hepatocelular	28
Cultura primária de hepatócitos	28
Estudo do perfil de metilação da região promotora do gene ITPR3 em camundongos.....	28
<i>Real time</i> PCR	29
<i>Western blot</i>	30
Imunofluorescência	30
Imunohistoquímica	31
Sinalização de cálcio <i>in vitro</i>	31
Sinalização de cálcio <i>in vivo</i>	32
Hepatectomia parcial	33
Células HepG2 <i>knockout</i> para ITPR3	34
Apoptose	34

Co-localização de ITPR3 e mitocôndria	35
Análise estatísticas dos dados	35
RESULTADOS E DISCUSSÃO	36
CONCLUSÃO	73
REFERÊNCIAS BIBLIOGRÁFICAS	75
ANEXOS	88

LISTA DE FIGURAS

FIGURA 1. Sinalização de Cálcio	17
FIGURA 2. Esquema do tratamento hipometilante do DNA	27
FIGURA 3. Esquema de análise dos sinais nucleares de cálcio <i>in vivo</i>	33
FIGURA 4. Expressão de Inositol 1,4,5-trifosfato em células hepáticas	38
FIGURA 5. ITPR3 é expresso em carcinoma hepatocelular humano e está relacionado a um pior prognóstico	40
FIGURA 6. Expressão de ITPR3 no desenvolvimento do carcinoma hepatocelular em modelo murino	43
FIGURA 7. Metilação do DNA regula a expressão de ITPR3 em humanos	45
FIGURA 8. Análise da metilação do DNA em amostras de carcinoma hepatocelular humano	47
FIGURA 9. Tratamento com 5'-aza diminui a metilação do DNA na região promotora do gene para ITPR3 em camundongos sem causar dano hepático	50
FIGURA 10. Desmetilação do DNA da região promotora do <i>ITPR3</i> libera sua expressão em hepatócitos	53
FIGURA 11. Sinalização de cálcio <i>in vitro</i>	56
FIGURA 12. Sinalização de cálcio <i>in vivo</i>	58
FIGURA 13. Expressão de ITPR3 aumenta a capacidade proliferativa dos hepatócitos	61
FIGURA 14. Expressão de ITPR1 e ITPR2 após hepatectomia parcial	62
FIGURA 15. ITPR3 torna células de carcinoma hepatocelular resistentes a apoptose ..	66

FIGURA COMPLEMENTAR 1. Análise da metilação do DNA na região promotora do gene <i>ITPR1</i> e <i>ITPR2</i>	89
---	-----------

LISTA DE ABREVIACOES

5'-aza: 5'-azacitidina

5mC: 5-metil citosina

ALP: fosfatase alcalina

ALT: aminotransferase de alanina

AST: aminotransferases de aspartato

ATP: trifosfato de adenosina ou adenosina trifosfato

AVP: vasopressina

Ca²⁺: íon cálcio

CHC: carcinoma hepatocelular

CO₂: dióxido de Carbono

CpG: Citosina-fosfato-Guanina

CRISPR: *Clustered Regularly Interspaced Short Palindromic Repeats*

CXCL-10: *C-X-C motif chemokine 10*

DAB: 3, 3 -diaminobenzidina

DEN: dietilnitrosamina

DMEM: *Dulbecco's Modified Eagle's Medium*

DMSO: Dimetilsulfóxido

DNA: ácido desoxirribonucleico

DNMT: DNA methyltransferase

GFP: *Green Fluorescent Protein*

GGT: gamaglutiltransferase

GSD: *Glycogen Storage Disease*

HBV: vírus da Hepatite B

HCV: vírus da Hepatite C

HE: hematoxilina e eosina

InsP₃: Inositol 1,4,5-trisfosfato

ITPR: receptor de Inositol 1,4,5-trisfosfato

KO: *knockout*

mRNA: RNA mensageiro

Na⁺: íon sódio

NASH: *non-alcoholic steatohepatitis*

NF- κ B: *Nuclear Fator kappa B*

Nrf2: *nuclear factor erythroid 2-related factor 2*

NSB: *non-specific binding*

O₂: *oxigênio*

PBS: *Phosphate Buffered Saline*

PCNA: *Proliferating Cell Nuclear Antigen*

PCR: *Polymerase Chain Reaction*

RNA: *ácido ribonucleico*

SAM: *S-adenosil-L-metionina*

STA: *estaurosporina*

TOMM20: *mitochondrial import receptor subunit TOM20 homolog*

WT: *Wild Type*

RESUMO

Introdução: O carcinoma hepatocelular (CHC) é a terceira cause de morte entre os cânceres em todo o mundo. Várias doenças hepáticas crônicas são fatores predisponentes ao CHC. Diferentes vias de sinalização já foram identificadas na patogênese do CHC, porém nenhuma via comum foi reportada. A sinalização intracelular de cálcio (Ca^{2+}) regula a proliferação de hepatócitos saudáveis e de células tumorais, podendo vir a ser um alvo no desenvolvimento do CHC. **Objetivo:** Investigar se a metilação do DNA regula a expressão dos receptores de Inositol 1,4,5-trifosfato do tipo 3 (ITPR3) em hepatócitos saudáveis e se a desregulação desse processo está envolvida na tumorigênese hepática. **Métodos:** A expressão do ITPR3 em amostras de fígado humano, células hepáticas tumorais e fígado de camundongo foi realizada combinando a análise dos níveis de metilação do DNA na região promotora do gene *ITPR3* e a caracterização dos efeitos da expressão de ITPR3 na proliferação celular e no processo apoptótico. A expressão *de novo* de ITPR3 foi avaliada em hepatócitos murino, assim como a sinalização de Ca^{2+} e a capacidade regenerativa do fígado. **Resultados:** ITPR3 não é expresso ou é expresso em baixa quantidade em hepatócitos normais, mas sua expressão é aumentada em amostras de CHC de diferentes etiologias e está relacionada a uma menor sobrevida do paciente. O DNA da região promotora do gene *ITPR3* é altamente metilado em hepatócitos saudáveis, encontrando-se significativamente desmetilado em pacientes com CHC. Administração de um agente desmetilante em camundongos resultou na expressão de ITPR3 em algumas áreas do fígado, culminando com um aumento na sinalização de Ca^{2+} . Essa expressão *de novo* de ITPR3 resultou em uma maior proliferação dos hepatócitos, aumentando a capacidade regenerativa do fígado. A deleção de ITPR3 em células de CHC humano resultou em um aumento do apoptose. **Conclusão:** Juntos, os

resultados sugerem que a expressão *de novo* de ITPR3 é um evento comum ao CHC e pode estar envolvida na patogênese da doença.

Palavras-chaves: Carcinoma hepatocelular, ITPR3, sinalização de cálcio, proliferação celular, apoptose.

ABSTRACT

Background: Hepatocellular carcinoma (HCC) is the second leading cause of cancer death worldwide. Several types of chronic liver disease predispose to HCC, and several different signaling pathways have been implicated in its pathogenesis, but no common molecular event has been identified. Calcium (Ca^{2+}) signaling regulates the proliferation of both normal hepatocytes and liver cancer cells and can be a target in the HCC development. **Objective:** We investigated the role of the protein involved on the intracellular Ca^{2+} signaling in HCC. **Design:** Expression analyses of the type 3 isoform of the inositol 1, 4, 5-trisphosphate receptor (ITPR3) in human liver samples, liver cancer cells and mouse liver were combined with the evaluation of DNA methylation profiles of ITPR3 promoter in HCC and characterization of the effects of ITPR3 expression on cellular proliferation and apoptosis. The effects of *de novo* ITPR3 expression on calcium signaling and liver growth were evaluated in mice. **Results:** ITPR3 was absent or expressed in low amounts in hepatocytes from normal liver, but was expressed in HCC specimens from three independent patient cohorts, regardless of the underlying cause of chronic liver disease, its increased expression level was associated with poorer survival. The ITPR3 gene was heavily methylated in control liver specimens but was demethylated at multiple sites in specimens of patient with HCC. Administration of a demethylating agent in a mouse model resulted in ITPR3 expression in discrete areas of the liver, and Ca^{2+} signalling was enhanced in these regions. In addition, cell proliferation and liver regeneration were enhanced in the mouse model, and deletion of ITPR3 from human HCC cells enhanced apoptosis. **Conclusions:** These results provide evidence that *de novo* expression of ITPR3 typically occurs in HCC and may play a role in its pathogenesis.

Keywords: Hepatocellular carcinoma, ITPR3, calcium signaling, cell proliferation, apoptosis.

INTRODUÇÃO

INTRODUÇÃO

Sinalização intracelular de cálcio

Devido a sua capacidade de regular diversas funções celulares, o íon cálcio (Ca^{2+}) é considerado um importante mensageiro intracelular. Para que cada função seja desempenhada de forma correta, alterações nas concentrações de Ca^{2+} devem ocorrer de forma efetiva e em regiões específicas da célula, como por exemplo: variações no Ca^{2+} nuclear levam à transcrição genética e à proliferação celular, enquanto o Ca^{2+} mitocondrial regula os processos de metabolização lipídica e apoptose (HARDINGHAM *et al.*, 1996; RODRIGUES *et al.*, 2007; FERIOD *et al.*, 2014; GOMES *et al.*, 2005; GUERRA *et al.*, 2011). Nos hepatócitos, para que seja iniciado o processo de liberação de Ca^{2+} é necessário que um agonista se ligue ao seu receptor, seja ele acoplado a proteína G ou receptores do tipo tirosina-quinase, como mostrado na FIGURA 1. Dada essa ligação, haverá ativação de fosfolipase C (PLC), presente na membrana plasmática e também no envelope nuclear, que fará a quebra de fosfolípides de membrana (fosfatidil Inositol 4,5-bifosfato - PIP₂), gerando diacilglicerol (DAG) e Inositol 1,4,5-trifosfato (InsP₃). O InsP₃, se difunde pelo citoplasma até encontrar os receptores para InsP₃ (ITPR), localizados na membrana do retículo endoplasmático e/ou nucleoplasmático. Havendo a ligação, ocorre uma mudança conformacional no ITPR, fazendo com que os estoques internos de Ca^{2+} no retículo endoplasmático e/ou nucleoplasmático sejam liberados (BERRIDGE *et al.*, 2003).

Em altas concentrações, o Ca^{2+} pode ser tóxico para a célula, levando à morte. Para evitar esse processo, mecanismos foram desenvolvidos para remover esse íon após sua liberação. Um desses mecanismos é a ativação de transportadores de membrana que removem o Ca^{2+} para fora da célula, como Ca^{2+} -ATPase ou trocador de $\text{Na}^+/\text{Ca}^{2+}$. Outro mecanismo é a captura de Ca^{2+} pela mitocôndria através da ação do *mitochondrial* Ca^{2+}

uptake 1 (MCU1) ou pela ação da *sarco/endoplasmic Ca²⁺ ATPase* (SERCA), que transfere os íons do citoplasma para o retículo endoplasmático (OLIVEIRA *et al.*, 2014).

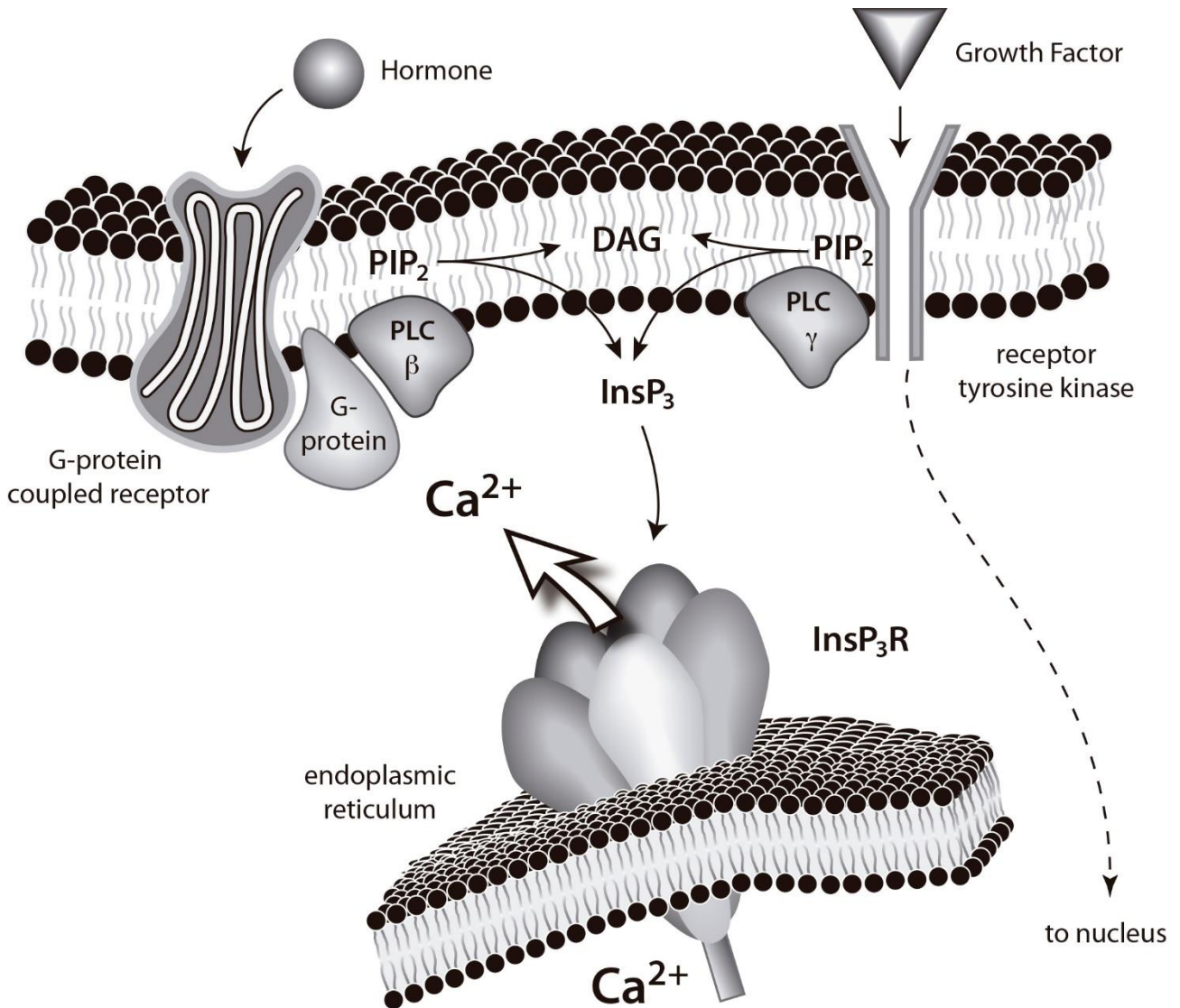


FIGURA 1. Sinalização de Cálcio. Após a ligação de um agonista a um receptor acoplado à proteína G ou ao receptor tirosina-quinase, como no caso dos fatores de crescimento, ocorre a hidrólise do PIP₂ pela PLC, gerando DAG e InsP₃. O InsP₃ liga-se ao seu receptor ITPR no retículo endoplasmático que age como canal que permite a liberação de Ca²⁺ para o citosol ou núcleo. Ref: Leite, MF *et.al*, 2010 – *The Liver: Biology and Pathobiology*; John Wiley and Sons). NOTA: Atualizações foram feitas recentemente e a sigla para os receptores de Inositol 1,4,5-trifosfato mudou de InsP₃R para ITPR.

Receptores de Inositol 1,4,5-trifosfato

Formado por uma sequência de aproximadamente 2700 aminoácidos, as subunidades dos ITPRs são formados por três importantes partes: uma região N-terminal, onde se encontra a sequência de ligação do InsP_3 , uma região C-terminal, responsável pela formação do poro por onde os íons Ca^{2+} são liberados e entre as duas extremidades existe uma região regulatória que sofre ação de outras moléculas, regulando por exemplo a localização da expressão desses receptores (JIANG *et al.*, 2002; SHAH *et al.*, 2015). O ITPR em si é formado por quatro subunidades idênticas, logo, faz-se necessário quatro moléculas de InsP_3 para ativar a liberação de Ca^{2+} . É descrita a existência de três isoformas do ITPR: tipo 1 (ITPR1), tipo 2 (ITPR2) e tipo 3 (ITPR3), apresentando homologia de aproximadamente 70% nas sequências de aminoácidos que as formam (MIKOSHIBA, 2007). Todas as isoformas são ativadas pelo mesmo ligante, o InsP_3 , sendo que cada isoforma apresenta diferentes graus de afinidade. O ITPR2 é a isoforma com maior afinidade ao InsP_3 , enquanto o ITPR3 é a isoforma com menor afinidade (NEWTON *et al.*, 1994).

No fígado, o ITPR1 representa 20% dos ITPRs em hepatócitos. Essa isoforma é distribuída por todo o citoplasma e sugere-se que ela estabeleça um acoplamento entre a mitocôndria e o retículo endoplasmático, sendo a responsável pela sinalização de Ca^{2+} mitocondrial (GUERRA *et al.*, 2011; FERIOD *et al.*, 2016). O ITPR2, em condições fisiológicas, representa 80% do ITPRs em hepatócitos. Essa isoforma está concentrada em uma região especializada do retículo endoplasmático, sob a membrana canalicular, e regula a inserção e ativação de transportadores importantes para a secreção biliar (HERNANDEZ *et al.*, 2007; FERIOD *et al.*, 2016). O ITPR3 está presente em quantidades insignificantes em hepatócitos em condições fisiológicas, porém estudos preliminares demonstram aumento da expressão dessa isoforma em carcinoma

hepatocelular (LEITE *et al.*, 2003) e em situações agudas e crônicas de injúria hepática (LEMOS *et al.*, 2020 e dados não publicados). Os mecanismos e as funções da expressão de ITPR3 nos hepatócitos em casos de doença hepática ainda são poucos conhecidos, mas estudos recentes, como reportado por Lemos e colaboradores, vem construindo esse conhecimento.

Os colangiócitos, outro tipo celular encontrado no fígado e responsável por formar os ductos biliares, diferentemente dos hepatócitos, expressam as três isoformas do ITPR. ITPR1 e ITPR2 juntos somam 20% dos ITPRs nesse tipo celular e são distribuídos pelo citoplasma. Já o ITPR3, isoforma majoritária nos colangiócitos, é encontrado predominantemente na região apical da célula, ou seja, voltada para o lúmen dos ductos biliares. Estudos mostraram que a sinalização mediada por ITPR3 nos colangiócitos regulam a liberação de água e eletrólitos, diluindo a bile e permitindo seu escoamento até a vesícula biliar (SHIBAO *et al.*, 2003). Em algumas condições clínicas, como septicemia e hepatite alcoólica, a expressão da isoforma 3 do ITPR se encontra diminuída, o que leva a um quadro clínico de colestase (FRANÇA e LIMA FILHO *et al.*, 2019). Alguns fatores de transcrição já foram descritos como os responsáveis por causar a diminuição da expressão de ITPR3 em colangiócitos, entre eles o *nuclear factor erythroid 2-related factor 2* (Nrf2), *factor nuclear kappa B* (NF-κB) e micro RNA 506 (WEERACHAYAPHORN *et al.*, 2015; FRANÇA e LIMA FILHO *et al.*, 2019 e ANANTHANARAYANAN *et al.*, 2015).

Carcinoma hepatocelular e epigenética:

Segundo o Observatório Global do Câncer da Organização Mundial da Saúde (OMS), em 2040, o carcinoma hepatocelular (CHC) será responsável por mais de 1.200.000 mortes e terá uma incidência de mais de 1.300.000 novos casos por ano. Atualmente, o CHC é a sexta causa de mortes entre os cânceres e anualmente, mais de 800 mil casos são diagnosticados (GLOBOCAN, 2018). O CHC se origina da cronificação de doenças hepáticas e é uma doença que requer tempo para se desenvolver. Entre as principais doenças hepáticas que se cronificam dando origem ao CHC, podemos destacar as infecções pelos vírus da Hepatite B e Hepatite C, o consumo crônico de álcool e atualmente, com mais destaque a esteatohepatite não alcoólica (*non-alcoholic steatohepatitis* - NASH) (EL-SERAG *et al.*, 2007). De maneira geral, as etiologias acima mencionadas utilizam de mecanismos próprios para gerar o dano hepático e, em resposta a esse estresse, o fígado ativa sua maquinaria de reparo no qual o tecido lesado é encapsulado ou substituído por uma matriz constituída principalmente de colágeno do tipo I, dando origem à fibrose (SCHUPPAN & AFDHAL, 2008). A extensão da fibrose não se relaciona somente com a doença hepática em si, mas também com fatores ambientais e com o próprio indivíduo. A cirrose, gerada pelo avanço da fibrose hepática, gera um quadro clínico no qual os septos fibróticos alteram o fluxo sanguíneo, levando à uma hipertensão portal e alterando a funcionalidade dos hepatócitos (SCHUPPAN & AFDHAL, 2008). É sabido que com a progressão da fibrose/cirrose, fatores de transcrição responsáveis por conferir a identidade dos hepatócitos, os chamados *Liver-enriched transcription factor* (LETf), apresentam sua expressão diminuída, levando a uma perda da diferenciação dos hepatócitos e contribuindo para a progressão do dano hepático (LIU *et al.*, 2012; GUZMAN-LEPE *et al.*, 2018). A presença da cirrose é um fator

predeterminante para o surgimento do CHC, atualmente 90% dos CHC registrados na parte ocidental do globo está relacionada à cirrose (FORNER *et al.*, 2018).

No complexo processo de carcinogênese, uma das primeiras alterações a surgir é a do perfil genético. Genes que participam da proteção celular, chamados de genes *housekeeping*, são suprimidos, ou seja, apresentam sua expressão diminuída e juntamente com tal fato, oncogenes e genes pró-metastáticos passam a ser expressos (JONES *et al.*, 1999; FEITELSON *et al.*, 2002; EHERLICH, 2002). Genes como *alpha fetoprotein* (AFP), *Rat Sarcoma virus* (RAS), c-FOS, c-JUN, *rhodopsin* (RHO), *transforming growth factor alpha* (TGF- α) e *hepatocyte growth factor* (HGF), são alguns dos genes alterados no fígado, resultando em uma maior proliferação celular e contribuindo para o processo de carcinogênese (ZHANG *et al.*, 2010).

A expressão gênica está sob o comando de várias formas de regulação, entre elas a epigenética, que são alterações que regulam a expressão de genes sem alterar a estrutura fundamental do material genético. Esses padrões epigenéticos são reversíveis e estão suscetíveis a modificações ambientais, podendo causar mudanças fenotípicas herdáveis pela mitose e transmitidas ao longo de gerações aos descendentes (TANG E HO, 2007). As principais modulações epigenéticas descritas na literaturas são: modificações nas histonas, a metilação do DNA e os RNAs não codificantes, micro RNA e *long non coding RNA* (HANDY *et al.*, 2011). As modificações de histonas e a metilação do DNA, são capazes de modular a transcrição por intermédio da modificação da acessibilidade à cromatina, causada pelas alterações nos nucleossomos ou diretamente no DNA (LUND *et al.*, 2004; D’ALESSIO *et al.*, 2006). Enquanto os RNA não codificantes podem atuar como reguladores pós-translacionais ou até mesmo exercendo papel de fatores de transcrição, se ligando à região promotora do gene (XIAO *et al.*, 2017).

A metilação do DNA é a alteração epigenética mais bem descrita na literatura e a que mais afeta o DNA. Esse processo é capaz de regular a expressão genética por meio de adições covalentes, realizadas pelas enzimas DNA metiltransferases (DNMTs), de um grupamento metil (CH₃) na posição 5' do anel de citosina localizado nas ilhas CpG, pares de Citosina-fosfato-Guanina (FEINBERG, 2001; BIRD, 1992). A hipermetilação das ilhas CpG, localizadas nas regiões promotoras de genes *housekeeping* e a hipometilação de oncogenes têm papel significativo na progressão de tumores (ROTHHAMMER *et al.*, 2007). Com o recente avanço da bioengenharia e manipulação genética, terapias baseadas na epigenética vem sendo discutidas e estudadas (DAWSON *et al.*, 2012).

Considerando o envolvimento dos processos epigenéticos na progressão tumoral e a expressão de ITPR3 em condições de doenças hepáticas, incluindo o carcinoma hepatocelular, buscamos verificar a ocorrência e a relação desses dois eventos no desenvolvimento do CHC causado por diferentes doenças de base. O estudo da expressão do ITPR3 em hepatócitos e sua possível participação no processo de formação dos tumores hepáticos possibilitará a ampliação dos conhecimentos sobre a gênese dessa patologia, o estudo de novos biomarcadores para a detecção e avaliação da progressão da doença, bem como a identificação de alvos terapêuticos para o tratamento específico.

OBJETIVOS

OBJETIVOS

Objetivo geral

Investigar se a metilação do DNA regula a expressão dos receptores de Inositol 1,4,5-trifosfato do tipo 3 (ITPR3) em hepatócitos e se a desregulação desse processo está envolvida na tumorigênese hepática.

Objetivos específicos

- Avaliar se a expressão de ITPR3 está sob o controle da metilação do DNA.
- Avaliar se a expressão de ITPR3 altera a proliferação celular dos hepatócitos e capacidade regenerativa do fígado;
- Avaliar se a expressão de ITPR3 participa do processo de formação do tumor hepático e qual sua contribuição para o desenvolvimento e progressão do mesmo.

MATERIAIS E MÉTODOS

MATERIAIS E MÉTODOS

Avaliação do perfil de metilação do DNA na região promotora do ITPR humano

Os níveis de metilação do DNA humano foram coletados em bancos de dados disponíveis gratuitamente para acesso. Os controles foram retirados do banco de dado *Gene Expression Omnibus - GEO*. Para controle, foram selecionados 23 indivíduos, de idade entre 33-57 anos, sendo 47% do sexo masculino e 53% do sexo feminino. Os dados dos pacientes com tumor hepático do tipo CHC foram retirados *The Cancer Genome Atlas – TCGA*. Quarenta pacientes compõem esse grupo e apresentam idade média de 59 anos, sendo 65% homens e 35% mulheres. Os níveis de metilação do DNA (*beta value*) foram obtidos utilizando DNA genômico do fígado e o método *Illumina Human Methylation 450* em ambos os bancos de dados. As ilhas CpG dentro da região promotora dos ITPRs foram selecionadas utilizando os seguintes ID_REF: ITPR1 (cg24699271; cg03918306; cg04251662; cg06716686; cg09407429; cg14643330; cg21024916; cg21858376), ITPR2: (cg02569086; cg03966406; cg16175911; cg18238734; cg24082826; cg25960567) e ITPR3 (cg02066343; cg02084729; cg02478409; cg03489495; cg05234888; cg08355863; cg09209803; cg12650926; cg12913957; cg14639225; cg16400825; cg19889152; cg20706766; cg22065976; cg24603235; cg27193704). A porcentagem de ilhas CpG na região promotora do ITPR3 humano foi obtida no site *Ensembl*.

Análise dos dados de sobrevivência em pacientes com carcinoma hepatocelular

Os dados gerados a partir do *The Cancer Genome Atlas – TCGA* foram usados para dividir os pacientes em dois grupos de acordo com os níveis de mRNA para ITPR3. O primeiro grupo, 39 de 370 pacientes (10,5%), apresentou expressão elevada de ITPR3

Modelo murino de carcinoma hepatocelular

Camundongos C57/BL6 machos com 2 semanas de idade foram injetados com uma dose intraperitoneal única de 50 mg/kg de dietilnitrosamina (DEN). Salina foi utilizada para o tratamento de animais do grupo controles. Os fígados dos animais foram coletados após 6, 9 e 12 meses do tratamento. Fixados em formol e embebidos por parafina, cortes de 5 µm foram utilizados para imunomarcção de ITPR3. Esse procedimento foi realizado em parceria com a *Yale University* e protocolado sob o registro #2012-07602.

Cultura primária de hepatócitos

Hepatócitos foram isolados do fígado dos animais adultos controles e tratados com 5'-aza através da perfusão com colagenase como já previamente descrito por Boyer em 1990. A cultura primária dessas células foi realizada a 37 °C sob 5% CO₂/95% O₂ em meio William contendo 10% de soro fetal bovino, 50 unidades/mL de penicilina e 50 g/mL de estreptomicina. Os hepatócitos primários foram utilizados até 4 - 6 horas do isolamento. A medida de viabilidade destas células foi realizada através do teste de exclusão com azul de Tripan e somente culturas com viabilidade acima de 85% foram utilizadas.

Estudo do perfil de metilação da região promotora do gene *ITPR3* em camundongos

Para avaliar o perfil de metilação da região promotora do gene que codifica o ITPR3, DNA genômico foi extraído de hepatócitos controles e tratados com 5'-aza

utilizando o kit de extração DNAeasy Blood and Tissue (Qiagen) de acordo com instruções do fabricante. Logo em seguida, o DNA extraído foi tratado com bissulfito, utilizando o kit EZ DNA Methylation-Gold (Zymo Research). Após conversão do DNA com bissulfito, parte da região promotora do gene que codifica o *ITPR3* foi amplificada por meio de PCR convencional e utilizando os seguintes primers específicos: 5'-AAGCCGTCTAGAGAACGCCC-3' (*forward*) e 5'-CCACACACATGCAAATCCCG-3' (*reverse*). A amplificação do produto da PCR foi verificada utilizando gel de 1% de agarose. Em seguida, o produto foi sequenciado e foi possível identificar as regiões metiladas e não metiladas na região promotora do gene *ITPR3*. As citosinas não metiladas das ilhas CpG, durante o tratamento das amostras com bissulfito, foram convertidas à uracila e identificadas no sequenciamento.

Real time PCR

RNA mensageiro total dos hepatócitos isolados foi extraído com Trizol (Sigma) de acordo com as instruções do fabricante. DNA complementar foi gerado a partir de 1µg de RNA usando o Kit de Transcrição Reversa de Alta Capacidade cDNA (Life Technologies). Análises de qPCR foram realizadas com SYBR Green PCR Supermix (Bio-Rad) usando o sistema CFX96 Real Time PCR (Bio-Rad). Primes para *ITPR3* de camundongo foram utilizados e a expressão relativa de RNA mensageiro determinado pelo método comparativo *Ct* usando GAPDH como o gene de referência. As sequencias dos primers utilizados foram: 5'-TATGCAGTTTCGGGACCACC-3' (*ITPR3 forward*), 5'-TGCCCTTGTACTCGTCACAC-3' (*ITPR3 reverse*), 5'-GACAGTCAGCCGCATCTTCT-3' (*GAPDH forward*) e 5'-GCGCCCAATACGACCAAATC-3' (*GAPDH reverse*).

Western blot

Proteínas totais ou frações nucleares e citoplasmáticas dos hepatócitos foram extraídas como descrito por GUIMARÃES *et al.*, 2017 e DIMAURO *et al.* 2012, respectivamente. 40 ou 80 µg do lisado proteico foram separadas utilizando gel de 10 % de bis-acrilamida (Bio-Rad) seguido de transferência das proteínas para membrana de PVDF. Ligações não específicas foram bloqueadas utilizando uma solução 5% albumina bovina em TBST 1x, incubado por 1 hora à temperatura ambiente. As marcações de interesse foram feitas incubando as membranas overnight a 4 °C com os seguintes anticorpos: anti-ITPR1 (1:1000; Santa Cruz), anti-ITPR2 (1:1000; Santa Cruz), anti-ITPR3 (1:1000; Millipore), caspase clivada 3 (1:1000; Cell Signaling), anti-GAPDH (1:5000; Santa Cruz), anti-β actina (1:5000; Santa Cruz) e anti-Histone H3 (1:1000; Santa Cruz). As membranas foram incubadas com anticorpos secundários acoplados à peroxidase (Sigma) durante 2 horas a temperatura ambiente. As revelações das imunomarcações foram feitas utilizando reagente ECL (Bio-Rad), e as quantificações das marcações foram realizadas utilizando o software *Image J*, como descrito por GUIMARÃES *et al.*, 2017.

Imunofluorescência

Hepatócitos isolados foram plaqueados em lamínulas 22x22 cm revestidas com colágeno do tipo I (Sigma). Após 2-4 horas para aderência, as células foram fixadas utilizando paraformaldeído a 4% (Electron Microscopy Science) e permeabilizadas com 0,05% de Triton X-100 (Sigma). Após lavagem com *Phosphate Buffered Saline - PBS* (Sigma) as ligações inespecíficas foram inativadas com uma solução de bloqueio (10%

albumina bovina, 0,05% Triton X-100, 5% soro de cavalo em PBS) por 1 hora à temperatura ambiente. Anti-ITPR3 (1:100; Millipore) foi utilizado para a imunomarcação com incubação por 2 horas a temperatura ambiente. O anticorpo secundário conjugado a Alexa 488 (1:200; Life Technologies) e TO-PRO 3 (1:1000; Thermo Fisher Scientific), para marcação do núcleo, foram incubados à temperatura ambiente por 1 hora. As imagens foram coletadas utilizando microscópio confocal Zeiss LSM 510. A especificidade da marcação do anticorpo primário foi feita omitindo sua utilização no chamado *non-specific binding* – NSB.

Imunohistoquímica

Cortes de 5 µm de tecido hepático humano e animal fixados em formol e emblocados em parafina foram desparafinizados e a recuperação de antígeno foi feita utilizando tampão citrato (10 mM, pH = 6.0) contendo 0,6% de peróxido de hidrogênio. O sistema de Detecção Novolink (Leica Biosystems) foi usado nas etapas subsequentes como descrito anteriormente por FONSECA *et al*, 2018. Anticorpos primários anti-ITPR3 (1:100; Sigma), anti-PCNA (1:100; Abcam) e anti-5mC (1:400; Zymo Research) foram incubados overnight à temperatura ambiente seguido de incubação com polímero, para amplificação do sinal, por 40 minutos também à temperatura ambiente. DAB foi usado para detecção do sinal. As imagens foram obtidas utilizando microscópio óptico (Zeiss). A quantificação das células positivas para ITPR3, PCNA e 5mC, foi avaliada por um observador externo e um *score* de marcação positiva foi utilizado: *score* 0 para 0 – 25% de células marcadas; *score* 1 para 25 – 50% das células marcadas; *score* 2 para 50 – 75% células marcadas e *score* 3 para 75 – 100% células marcadas. A utilização das biopsias humanas foi aprovada pelo Comitê de Ética da UFMG pelo número de protocolo 71206617.8.0000.5149.

Sinalização de cálcio *in vitro*

Hepatócitos isolados foram plaqueados em lamínulas 22x22 cm revestidas com colágeno do tipo I (Sigma). Após 2-4 horas para aderência, os hepatócitos foram marcados utilizando a sonda para cálcio, Fluo-4/AM (Thermo Fisher Scientific) por 15 minutos a 37 °C sob atmosfera de 5% CO₂/95% O₂ em meio William contendo 10% de soro fetal bovino, 50 unidades/mL de penicilina e 50 g/mL de estreptomicina. Em seguida as células foram transportadas para o microscópio confocal onde foram mantidas sob perfusão de HEPES 1x (130 mM NaCl, 5 mM KCl, 1 mM MgSO₄, 1,2 mM KH₂PO₄, 1,25 mM CaCl₂, 5 mM glicose, 19,7 mM HEPES), pH 7,4. Os hepatócitos foram estimulados com vasopressina, 100 nM (Sigma). Os dados foram plotados como fluorescência/fluorescência basal x 100, como descrito por ECHEVARRÍA *et al.*, 2003.

Sinalização de cálcio *in vivo*

Após os sete dias de tratamento, os animais do grupo controle e tratados com 5'-aza foram anestesiados utilizando uma mistura de cetamina (10%) e xilazina (5%) para realização de uma incisão na região abdominal. Após exposição do fígado, o lobo esquerdo foi embebido com solução contendo a sonda para cálcio, Fluo-4/AM, diluída em salina por 5 minutos. Em seguida os animais foram levados ao microscópio confocal e as células foram estimuladas com vasopressina 100 nM (Sigma) administrada por via endovenosa. Hepatócitos presentes na área abrangida por 2 vezes o valor do diâmetro da veia central foram considerados como hepatócitos da região pericentral. Os hepatócitos externos à essa área foram considerados como hepatócitos periportais. Os dados foram plotados como fluorescência/fluorescência basal x 100, como descrito por

ECHEVARRÍA *et al.*, 2003. Os sinais nucleares de cálcio foram avaliados como mostrado na FIGURA 3.

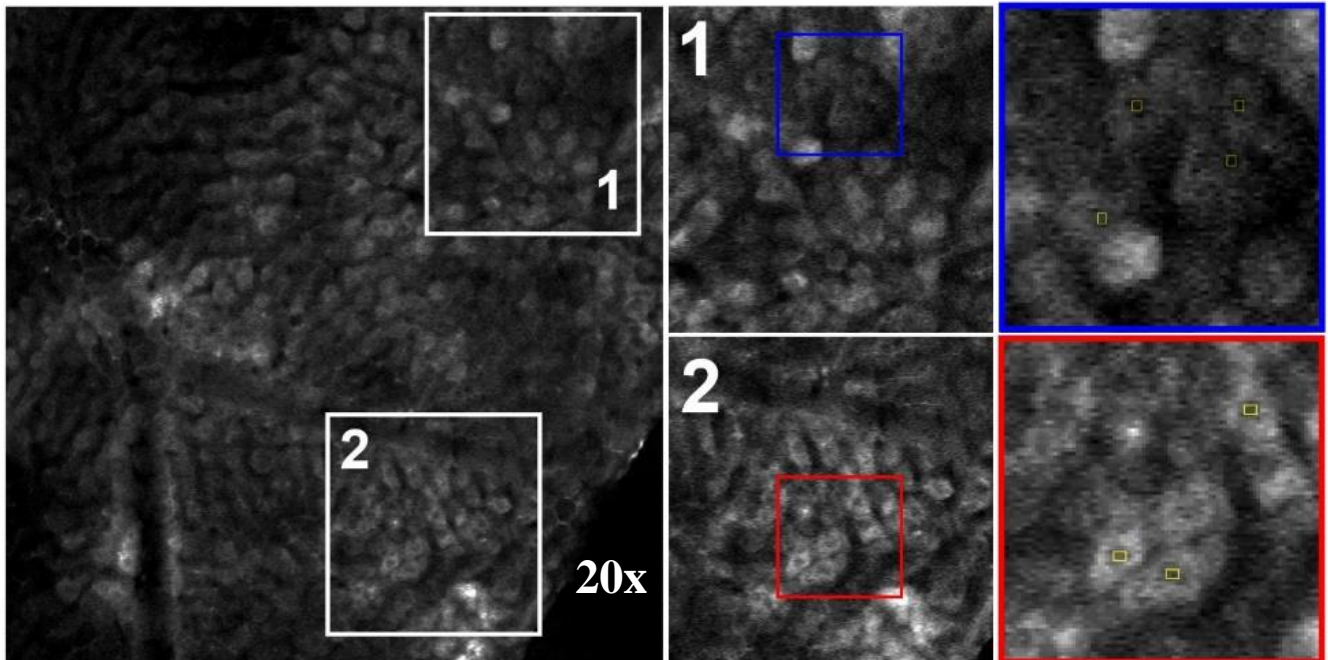


FIGURA 3. *Esquema de análise dos sinais nucleares de cálcio in vivo.* As análises de cálcio nucleares foram feitas utilizando os ROIs (quadrados amarelos) na região negativa da célula, correspondente ao núcleo das mesmas. As regiões 1 e 2 representam regiões periportais e pericentrais, respectivamente. A região delimitada pelo quadrado azul e vermelho representa uma amplificação das regiões delimitadas pela área 1 e 2.

Hepatectomia parcial

Os animais foram anestesiados utilizando uma mistura de cetamina (10%) e xilazina (5%) e aproximadamente 30% da massa hepática foi retirada. Como controle, animais do grupo Sham passaram por todo o processo cirúrgico sem qualquer retirada de partes do fígado. Os animais foram eutanasiados e pesados 24, 48 e 72 horas após a cirurgia. Os fígados desses animais também foram pesados e utilizados para imunomarcção de *Proliferating Cell Nuclear Antigen – PCNA*, a fim de verificar a taxa proliferativa, como anteriormente descrito. Hepatócitos presentes na área abrangida por

2 vezes o valor do diâmetro da veia central foi considerado como hepatócitos da região pericentral. Os hepatócitos externos à essa área foram considerados como hepatócitos periportais.

Células HepG2 *knockout* para ITPR3

O sistema disponível comercialmente CRISPR/Cas9 (Santa Cruz Biotechnology) foi usado para realizar o knockout do gene de ITPR3 em células HepG2 (células de linhagem de CHC humano). Resumidamente, as células foram co-transfectadas com duas construções de plasmídeo: uma contendo o RNA guia (gRNA) específico para ITPR3 e uma sequência que codifica mCherry (fluorescência vermelha), e um outro plasmídeo contendo a sequência que codifica a nuclease Cas9, juntamente com uma sequência que confere resistência à puromicina. Após 2 semanas, por meio de citometria de fluxo, as células foram submetidas a separação utilizando a marcação vermelha e mantidas em cultura sob seleção de puromicina (1 µg/mL). Após expansão da cultura a deleção do gene para ITPR3 foi confirmada por qPCR e *Western Blotting*. As células que expressam o ITPR3 (HepG2 WT) foram cultivadas em Dulbecco Modified Eagles Media (DMEM) suplementado com L-glutamina (1mM), soro fetal bovino (10% v/v) e Penicilina/Estreptomicina (100 Unidades/mL e 100 mg/mL) a 37 °C em atmosfera úmida contendo 5% de CO₂. As células que não expressam o ITPR3 (HepG2 ITPR3 KO) foram mantidas nas mesmas condições acrescidas de puromicina (1 µg/mL), como forma de seleção.

Apoptose

Células HepG2 WT ou ITPR3 KO foram tratadas com DMSO (controle), estaurosporina (5 μ M) ou etoposídeo (10, 25 e 50 μ M) por 16 horas seguida de avaliação de apoptose por atividade das caspases 3 e 7 e por marcação com Anexina V. Atividade de caspase 3/7 foi avaliada utilizando a quimiluminescência do kit Caspase-Glo 3/7 (Promega). As células controles e tratadas com estaurosporina foram marcadas com Anexina V conjugada com FITC e as células positivas para essa marcação foram contadas utilizando citometria de fluxo. O resultado está expresso como % de célula positiva em relação ao número total de célula.

Co-localização de ITPR3 e mitocôndria

Células HepG2 WT foram co-transfectadas com ITPR3-GFP e um marcador de membrana externa de mitocôndrias, mKO2-TOMM20. Imagens foram obtidas utilizando microscópio confocal (Zeiss) e a colocalização entre ITPR3 e mitocôndria foi calculada utilizando o software *Image J*.

Análise estatística dos dados

O software *GraphPad Prism* foi utilizado para a análise estatística dos dados. Os testes estatísticos utilizados foram o *t-Test* e *one-way ANOVA* seguido pelo pós-teste Bonferroni. $p < 0.05$ foi considerado como estatisticamente significativo.

RESULTADOS E DISCUSSÃO

RESULTADOS E DISCUSSÃO

O carcinoma hepatocelular (CHC) é a terceira causa de morte entre os tipos de câncer (JAMAL *et al.*, 2011). O CHC deriva de um contexto de doença hepática crônica, como por exemplos a infecção pelo vírus da hepatite C e o consumo crônico de álcool (EL-SERAG *et al.*, 2012). Assim, várias doenças hepáticas predis põem ao surgimento do CHC e várias vias moleculares vem sendo estudadas para propor a patogênese dessa doença, porém nenhuma via comum foi identificada. O íon cálcio (Ca^{2+}) regula várias funções celulares, incluindo várias etapas importantes para o crescimento do tumor, como a proliferação celular (RODRIGUES *et al.*, 2007 e GOMES *et al.*, 2008) e apoptose (BONONI *et al.*, 2017 e KUCHAY *et al.*, 2017). No fígado, os ITPRs são os únicos canais intracelulares de Ca^{2+} , sendo que nos hepatócitos saudáveis as únicas isoformas encontradas são as ITPR1 e ITPR2. O ITPR3 é expresso em quantidades insignificantes em condições fisiológicas, porém é expresso em linhagens de tumor hepático (Figura 4).

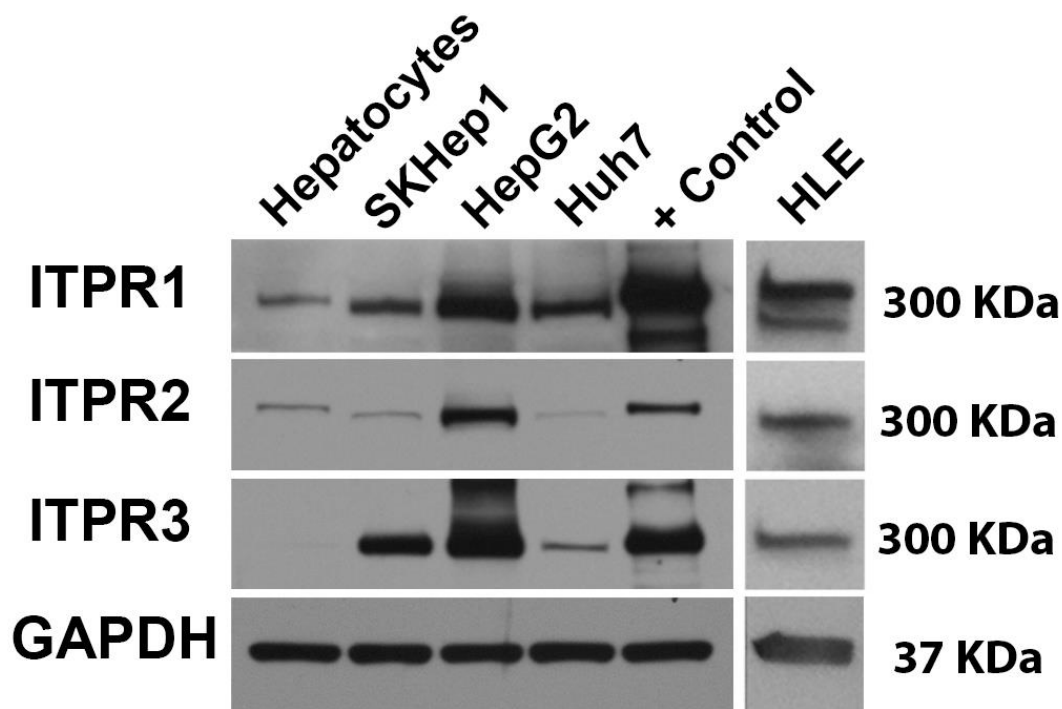


FIGURA 4. Expressão de receptores de Inositol 1,4,5-trifosfato em células hepáticas. Os receptores de Inositol 1,4,5-trifosfato (ITPR) são os únicos canais intracelulares de cálcio expresso no fígado. Em condições normais, os hepatócitos expressam a isoforma 1 (ITPR1) e isoforma 2 (ITPR2). A isoforma 3 (ITPR3) é expressa em quantidades insignificantes nos hepatócitos saudáveis e passam a ser expressos em linhagens celulares de carcinoma hepatocelular humano, como por exemplo SKHep1, HepG2, Huh7 e HLE. Proteína de cerebelo, células AR42J (pâncreas) e RINm5F (pâncreas) foram utilizadas como controle positivo para a detecção de ITPR1, ITPR2 e ITPR3, respectivamente. GAPDH foi utilizado como controle do loading de proteínas. Imagem representativa de três experimentos independentes.

Expressão de ITPR3 também foi observada em biópsias humanas de CHC proveniente de várias etiologias, como infecção pelo vírus HCB e HCV, consumo crônico de álcool e *non-alcoholic steatohepatitis* (NASH) (Figura 5a e 5b), e observa-se que a expressão desse canal de Ca^{2+} é restrita à área tumoral, não sendo expressa nos

hepatócitos da região não-tumoral (Figura 5c e 5d). A fim de se investigar qual a relevância clínica dessa expressão diferencial de um canal intracelular de Ca^{2+} , parâmetros clínicos foram correlacionados com a expressão de ITPR3. Observou-se que há uma relação entre sobrevida dos pacientes e os níveis de expressão de ITPR3, onde maiores níveis de expressão desse receptor nos tumores implicaram em uma menor sobrevida dos pacientes durante o período de cinco anos e também no período livre da doença (Figura 5e e 5f). Observou-se também, utilizando o sistema TNM de estadiamento dos tumores, sistema esse que leva em consideração o tamanhos dos tumores (T), o acometimento de linfonodos (N) e a presença de metástase (M), que a expressão de ITPR3 é maior nos estágios mais avançados da doença, não havendo diferença na expressão das outras isoformas normalmente encontradas no fígado, ITPR1 e ITPR2 (Figura 5g e 5h).

Para entender em qual momento da formação do CHC o ITPR3 passa a ser expresso, avaliou-se a expressão desse receptor em biopsias humanas em diferentes estágios prévios ao desenvolvimento da doença. Estágios fibróticos, estadiados de acordo com a classificação *METAVIR*, no qual são classificados como ausente (F0), leve (F1), moderada (F2) e severo (F3), cirrótico (F4), e amostras tumorais relacionadas à infecção pelo vírus HCV foram marcadas para ITPR3. Como grupo para comparação foram utilizados pacientes com glicogenose (*GSD – glycogen storage disease*), uma doença crônica que raramente progride para tumor (BAERTLING *et al.*, 2013). Observou-se que ITPR3 já é expresso em etapas que precedem o estabelecimento do tumor, e que essa expressão se mantém no tecido tumoral (Figura 5i e 5j). Não se observou uma relação entre a expressão de ITPR3 com a atividade inflamatória nas amostras utilizadas (Figura 5k).

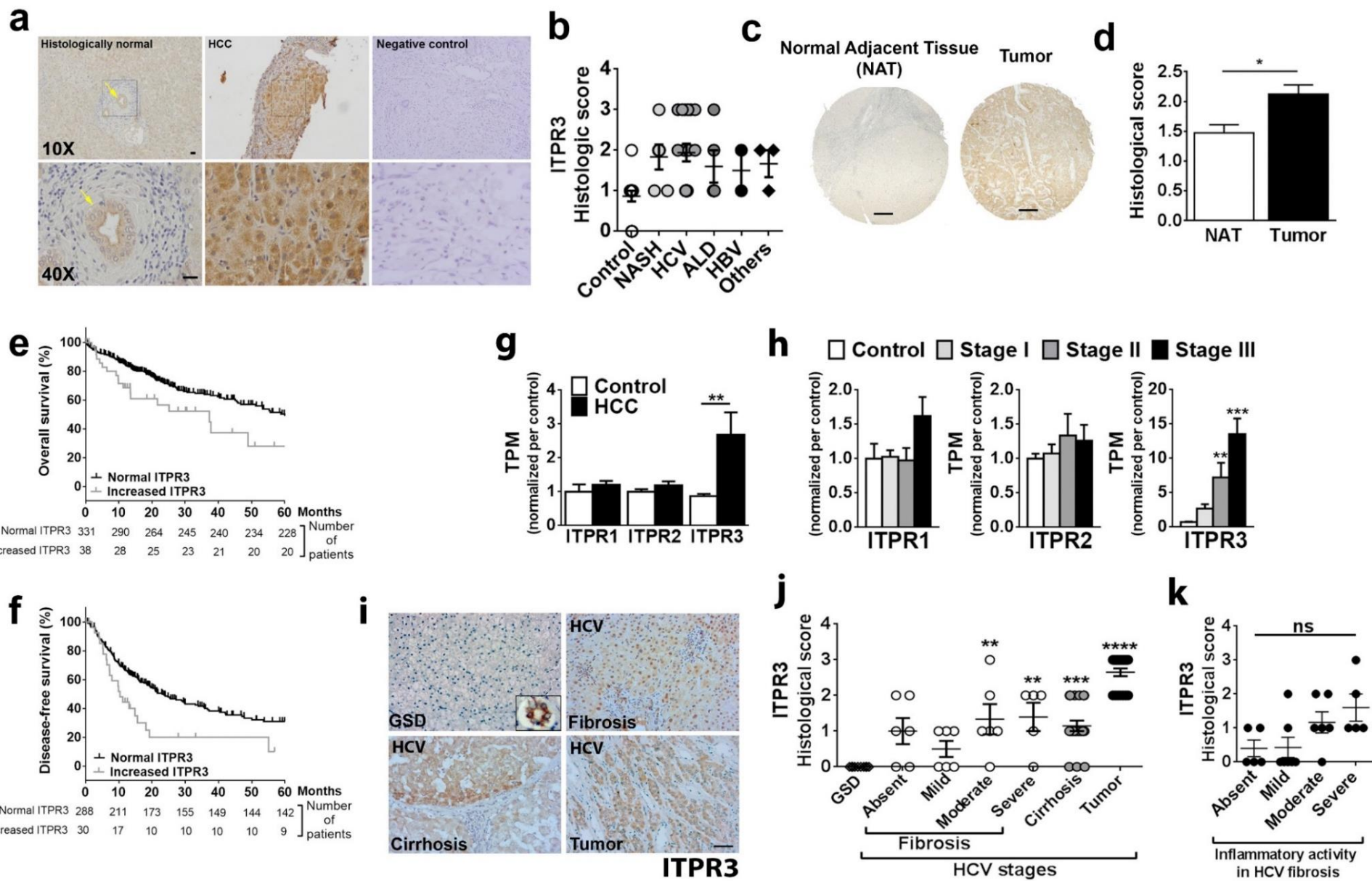


FIGURA 5. ITPR3 é expresso em carcinoma hepatocelular humano e está relacionado a um pior prognóstico. (a) Imunomarcção para ITPR3 em biópsias humanas de CHC de diferentes etiologias (infecção por HBV e HCV, NASH, DHA). Como controles da imunomarcção, tem-se a marcação de ITPR3 na região apical de colangiócitos e a não marcação quando se omite a utilização do anticorpo primário (negative control). Barra de escala: 20 μ m. (b) Quantificação da imunomarcção de ITPR3 nas biópsias de CHC. Score de número de células positivas: 0 (0-25% de células positivas), 1 (25-50% de células marcadas), 2 (50-75% de células marcadas) e 3 (75-100% de células marcadas) (n = 17 biópsias controle e 33 biópsias de CHC). (c) Marcação de ITPR3 na área tumoral e na área adjacente não tumoral (NAT), mostrando a especificidade da expressão deste canal de cálcio em hepatócitos tumorais. Barra de escala: 200 μ m. (d) Quantificação da imunomarcção de ITPR3 nas regiões tumorais e não tumorais (n = 20 biópsias em cada grupo). (e) Sobrevida em 5 anos de acompanhamento dos pacientes com CHC mostrou que uma maior expressão de ITPR3 se correlaciona com uma menor sobrevida do paciente. Pacientes com níveis normais de expressão de ITPR3 apresentaram em média 60,8 meses de sobrevida (n = 332 pacientes), enquanto pacientes com níveis de ITPR3 aumentados no tumor apresentaram sobrevida de 37,3 meses (n = 39 pacientes). (f) A sobrevida livre da doença apresenta perfil semelhante, paciente com níveis de ITPR3 normais apresentaram sobrevida de 23 meses e pacientes com níveis de ITPR3 aumentados, 10,4 meses de sobrevida. (g) Expressão dos ITPR em fígados controle e fígados tumorais. Os dados foram obtidos por meio do acesso ao banco de dados disponíveis em The Cancer Genome Atlas – TCGA. Há diferença de expressão entre os grupos somente na isoforma 3 do canal de cálcio ITPR (n = 23 controles e 72 pacientes com CHC). TPM: transcript per million. (h) Estratificação da expressão dos ITPRs de acordo com os estágios de classificação utilizando o sistema de estadiamento TNM. Esse sistema leva em consideração o tamanho dos tumores primários, acometimento de linfonodos e presença de metástase. Quanto maior o estágio, pior o prognóstico. Observa-se que o ITPR3 é mais expresso no estágio III, ou seja, o CHC com pior prognóstico. (i) Imunomarcção de ITPR3 em estágios antecedentes ao estabelecimento do CHC relacionado à infecção pelo vírus da Hepatite C: fibrose (n = 20 biópsias), cirrose (n = 20 biópsias) e tumor (n=20 biópsias). ITPR3 não foi detectado nas biópsias de GSD, mas a positividade da marcação nos colangiócitos (inserto) comprova a qualidade da técnica de marcação. Barra de escala: 50 μ m. (j) Quantificação de ITPR3 nos estágios de desenvolvimento do CHC em relação ao grau de fibrose presente nas amostras relacionadas à infecção pelo vírus da Hepatite C. (k) Quantificação de ITPR3 em relação à atividade inflamatória. Valores expressos como média \pm SD. * p<0.05.

Para validar os dados achados em amostras humanas, a expressão de ITPR3 foi avaliada em um modelo murino de desenvolvimento do CHC. Uma única dose de dietilnitrosamina (DEN), composto químico capaz de gerar mutações no DNA e assim produzir tumores hepáticos, foi administrada em camundongos machos às 2 semanas de idade (TOLBA et al., 2015). Seis meses após o tratamento, não se observou marcação positiva para ITPR3 no fígado desses animais, assim como nos fígados controles (Figura 6). No segundo tempo de avaliação, 9 meses após a injeção da droga, é possível observar uma alteração da arquitetura hepática com a presença de alguns hepatócitos positivos para ITPR3 (marcação em marrom). Contudo, nenhum nódulo tumoral foi encontrado. 12 meses após injeção única de DEN nódulos tumorais foram encontrados no fígado dos animais com marcação positiva para ITPR3 (Figura 6). Esses resultados corroboram em modelo experimental os achados que apontam que a expressão de ITPR3 é comum ao CHC humano e que sua expressão precede o estabelecimento do tumor, além de se correlacionar com um pior prognóstico da doença.

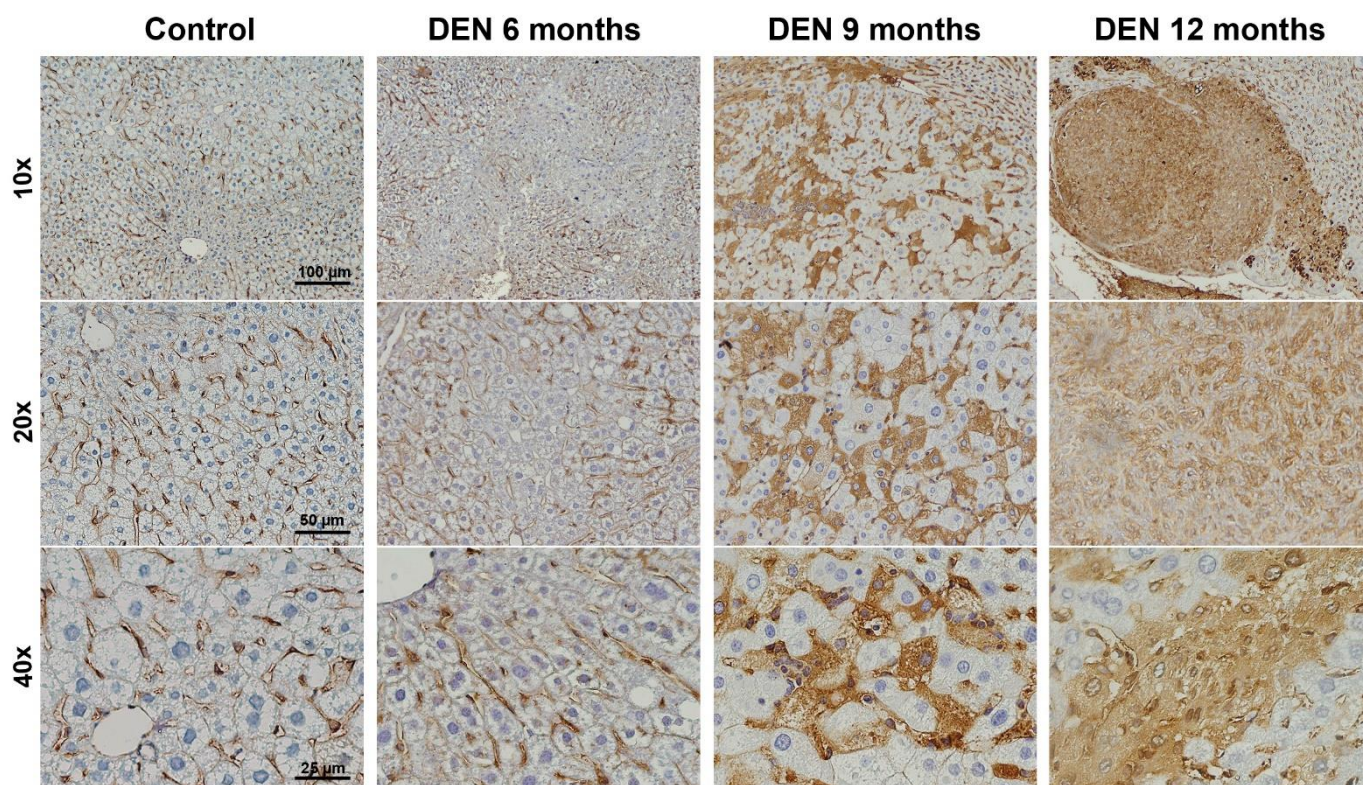


FIGURA 6. *Expressão de ITPR3 no desenvolvimento do carcinoma hepatocelular em modelo murino. Imunomarcação de ITPR3 em fígado de camundongo controle e fígados de animais tratados com uma única dose de DEN. É possível observar a ausência de marcação no fígado controle e 6 meses após o tratamento. Porém, 9 meses após a injeção da droga, é possível observar uma alteração da arquitetura hepática e o aparecimento de células positivas para ITPR3 (marcadas em marrom). Contudo, nenhum nódulo tumoral é observado nesse tempo de análise. Os nódulos tumorais surgem aos 12 meses após o tratamento com células positivas para ITPR3. As imagens estão em aumentos de 10x, 20x e 40x, como indicado na figura.*

A regulação da expressão de ITPR3 já foi alvo de vários estudos, sendo mostrado que fatores de transcrição como Nrf2 e NF- κ B, e o micro RNA 506 (miR-506) atuam regulando negativamente a expressão desse receptor em colangiócitos (WEERACHAYAPHORN *et al.*, 2015; FRANÇA e LIMA FILHO *et al.*, 2019 e

ANANTHANARAYANAN *et al.*, 2015). No entanto, não há estudos mostrando fatores que levariam ao aumento da expressão desse receptor. Sabe-se que, no processo de tumorigênese, alterações da expressão de genes podem ser causadas por modificações epigenéticas (JONES *et al.*, 1999; FEITELSON *et al.*, 2002; EHERLICH, 2002). Através de análise bioinformática foi possível verificar que a região promotora do gene *ITPR3* humano apresenta vários sítios de metilação do DNA, as chamadas ilhas CpG (Figura 7a). Sabendo então que o DNA da região promotora do *ITPR3* é passível de metilação e que a presença dessa regulação epigenética em promotores de gene pode suprimir a expressão do mesmo, avaliou-se os níveis de metilação do DNA em fígados controles e de pacientes com CHC. Utilizando os dados disponíveis no *The Cancer Genome Atlas – TCGA*, foram avaliados 16 domínios dentro da região promotora do gene *ITPR3* humano (Figura 7b). A análise mostra que os níveis de DNA metilado nos pacientes com CHC em sua maioria são menores nos diferentes domínios analisados quando comparado com grupo controle (Figura 7c). Essa diminuição da taxa de metilação do DNA só é observada para a isoforma 3 do ITPR, uma vez que as isoformas 1 e 2 do canal de Ca^{2+} são expressas nos hepatócitos em condições fisiológicas (Figura 7d e Figura complementar 1).

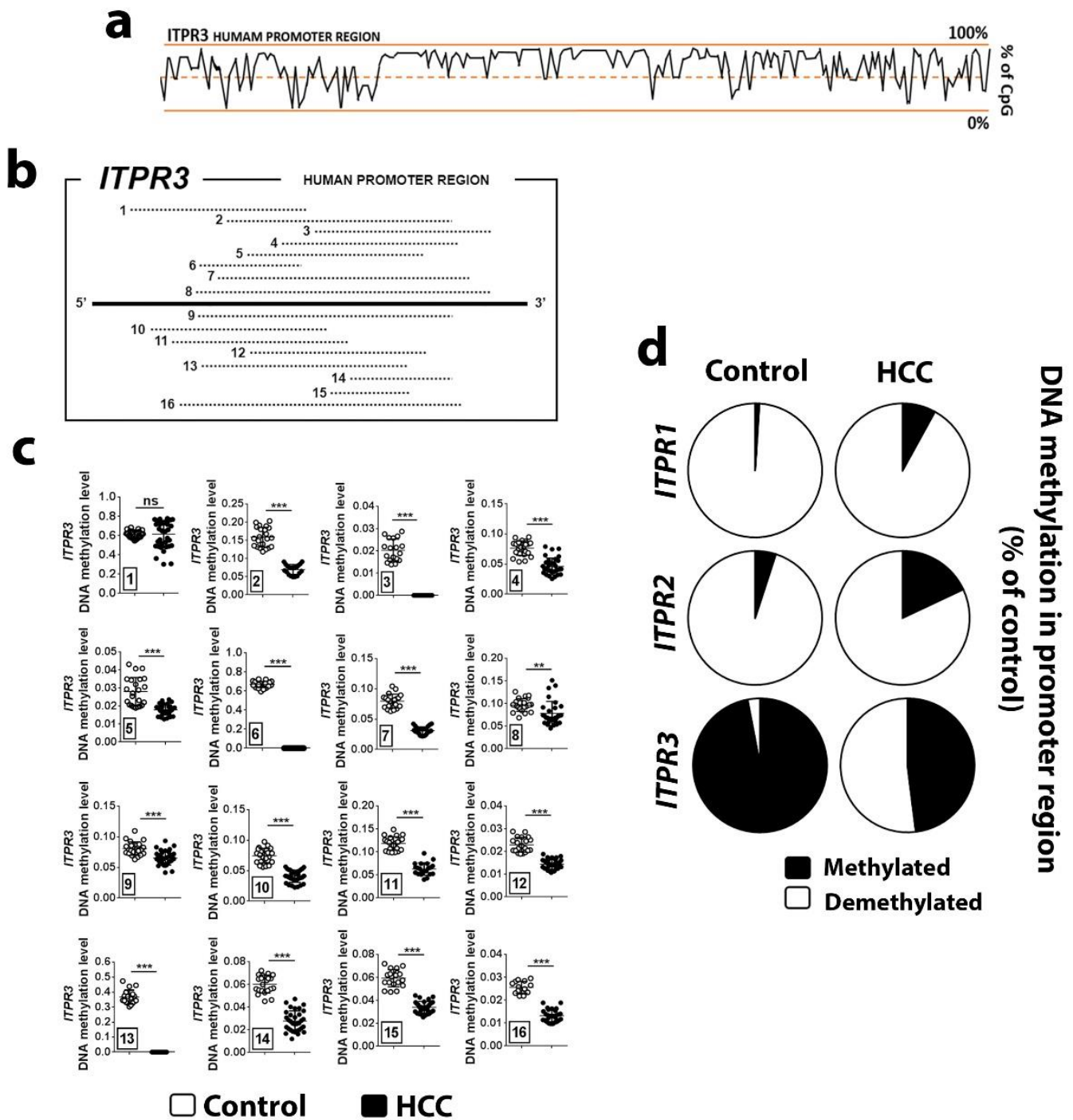


FIGURA 7. Metilação do DNA regula a expressão de ITPR3 em humanos. (a) Porcentagem de ilhas CpG na região promotora do ITPR3 em células humanas. A linha pontilhada representa 50% de chance de se encontrar uma ilha CpG na respectiva região do gene. As linhas superiores e inferiores representam, 100 e 0% de possibilidade de ilhas CpG, respectivamente. (b) Esquema

*representando as 16 posições dentro da região promotora do ITPR3 que foram utilizadas para avaliar os níveis de DNA metilado. (c) Níveis de metilação do DNA em fígados controles (pontos brancos, n = 23) são, em maioria, maiores que os encontrados nos fígados de pacientes com CHC (pontos pretos, n = 40), o que sugere que a expressão de ITPR3 é regulada pela metilação do DNA. (d) Níveis de metilação no DNA da região promotora das três isoformas do ITPR. Em condições fisiológicas, os hepatócitos expressam ITPR1 e ITPR2, por isso se observa nos controles um maior nível de DNA desmetilado para as regiões promotoras destes canais para Ca²⁺. Valores expressos como média ± SD. * p<0.05.*

A fim de se estabelecer a relação entre metilação do DNA e expressão do ITPR3 em hepatócitos e seu envolvimento na tumorigênese hepática, biópsias de diferentes estágios do desenvolvimento do CHC pela infecção crônica com HCV foram imunomarcadas para detecção de citosinas metiladas (5mC) nas ilhas CpG. Observou-se que o número de células marcadas para 5mC (núcleo marrom) diminui à medida que a doença progride (fibrose > cirrose/tumor) (Figura 8a e 8b). Interessantemente, a marcação de 5mC é inversamente proporcional à marcação de ITPR3. Nas amostras em que há uma maior marcação nuclear para o fator epigenético, GSD e fibrose, a imunomarcação de ITPR3 é ausente e/ou fraca. Já na cirrose e tumor, onde encontramos uma alta marcação de ITPR3 (Figura 5i e 5j), o número de núcleos positivos para 5mC é menor, evidenciando que os receptores de InsP₃ do tipo 3 podem ser regulados pela metilação do DNA. O mesmo evento é observado quando biópsias de cirrose e CHC relacionadas à outra etiologia, a doença alcoólica hepática (ALD) são imunomarcadas (Figura 8c e 8d).

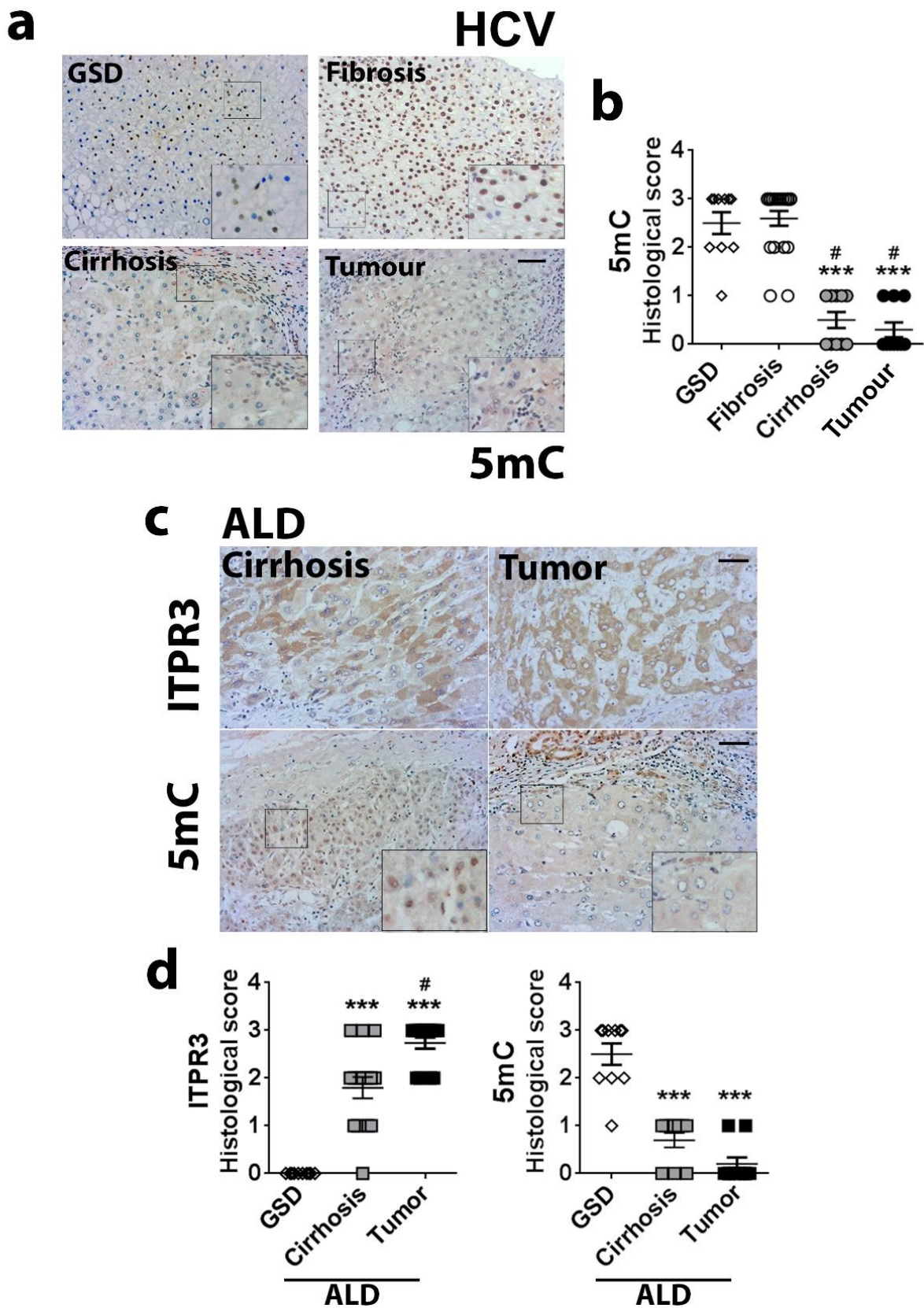


Figura 8. Análise da metilação do DNA em amostras de carcinoma hepatocelular. (a) Imunomarcagem de citosina metilada (5mC) em estágios anteriores ao estabelecimento do CHC relacionado à infecção pelo vírus da Hepatite C. Barra de escala: 50 μ m. (b) Quantificação do número de núcleos marcados nos estágios antecedentes e no CHC por infecção do vírus da

*Hepatite C. Score de número de células positivas: 0 (0-25% de células positivas), 1 (25-50% de células marcadas), 2 (50-75% de células marcadas) e 3 (75-100% de células marcadas). (c) Imunomarcção para ITPR3 e 5mC em cirrose e região tumoral relacionada à Doença Hepática Alcoólica (n = 15 amostras para cada estágio). Barra de escala: 50 μ . (d) Quantificação do número de células positivas. Como controle foi utilizado amostras de GSD, uma doença hepática que raramente evolui para CHC. Valores expressos como média \pm SD. * $p < 0.05$ (em comparação com GSD) e # < 0.05 (em comparação com fibrose).*

Para verificar a validade da relação entre desmetilação do DNA e expressão de ITPR3 observados nos achados da análise de bioinformática e das imunomarcações em humanos, camundongos Swiss foram tratados por 7 dias com 5'-azacitidina (5'-aza), uma droga sabidamente hipometilante do DNA por inibir covalentemente a DNA metiltransferase, enzima que transfere o grupo metil (CH₃) do S-adenosil-L-metionina (SAM) para o DNA (ABDULHAQ & JAMES, 2007; GANGAT *et al.*, 2016). O tratamento com 5'-aza não alterou o peso dos animais (Figura 9a), mas, por se tratar de um fármaco quimioterápico, atualmente utilizado no tratamento da leucemia, resultou em uma diminuição da contagem de leucócitos no sangue, processo esse conhecido como leucopenia (Figura 9b). Contudo, a função hepática, avaliada pela mensuração de enzimas hepáticas, e a arquitetura tecidual do parênquima hepático estavam normais (Figura 9c-9g). Esses resultados são importantes para mostrar que os achados futuros do trabalho são causados diretamente pela metilação, ou mais precisamente pela desmetilação do DNA, e não por fatores secundários ao protocolo de tratamento aqui estabelecido, que poderiam camuflar ou por em dúvida os resultados. O processo inflamatório seria um exemplo de interferente, uma vez que nesse evento biológico há uma alteração na expressão de genes devido a ação de fatores de transcrição (PLATANITIS & DECKER, 2018). O próprio ITPR3, em colangiócitos, tem sua expressão diminuída pela ação de Nrf2 e NF- κ B,

fatores de transcrição envolvidos no processo inflamatório (FRANÇA e LIMA FILHO *et al.*, 2019 e ANANTHANARAYANAN *et al.*, 2015; WARDYN *et al.*, 2015).

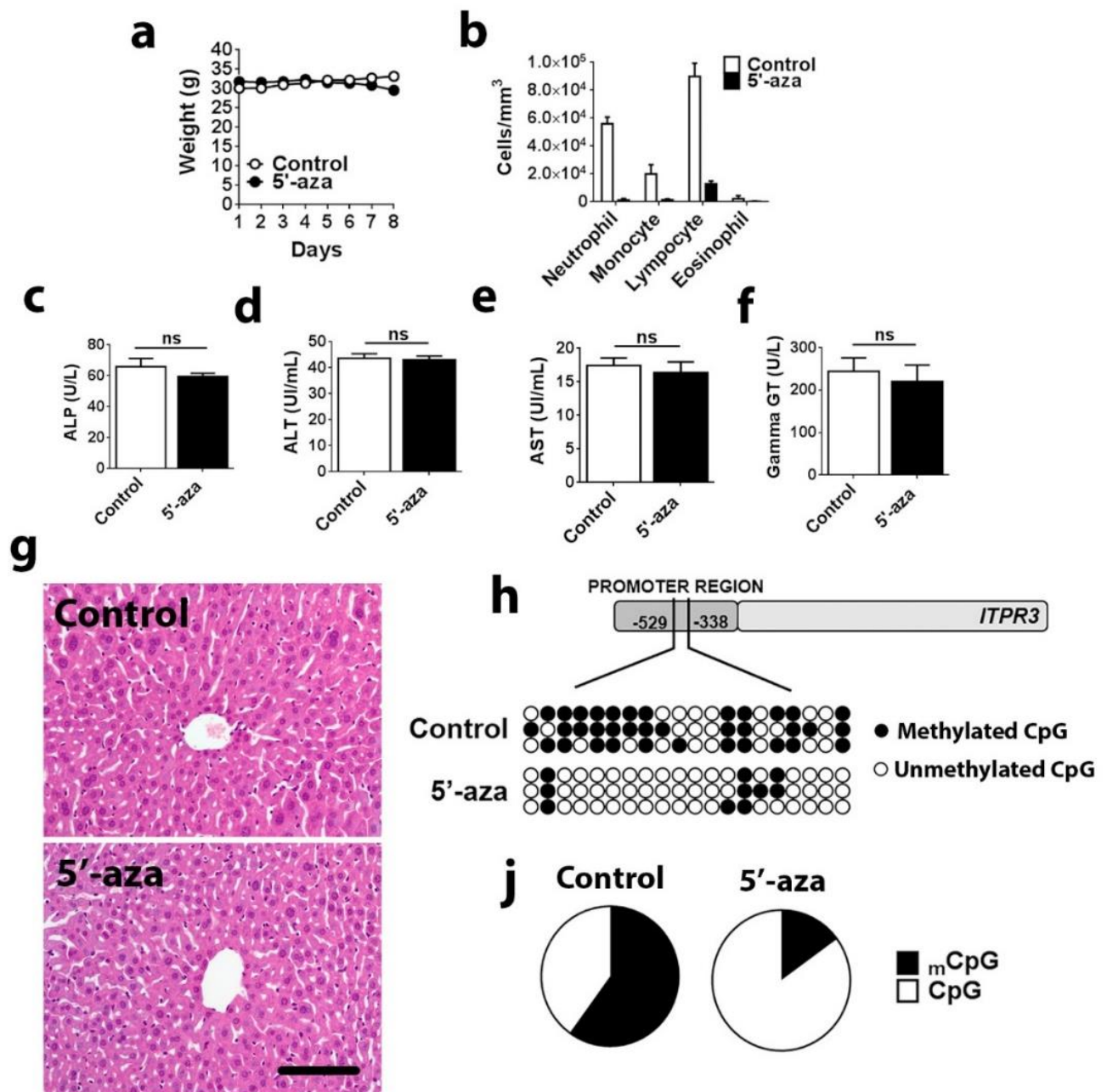


FIGURA 9. Tratamento com 5'-aza diminui a metilação do DNA na região promotora do gene para *ITPR3* em camundongos, sem causar dano hepático. (a) Acompanhamento do peso corpóreo dos animais durante o tratamento com 5'-aza. (b) 5'-aza é uma droga quimioterápica e desenvolve um quadro de leucopenia nos animais que receberam essa droga. Dosagem de enzimas hepáticas no soro dos animais mostrando que o tratamento com 5'-aza não causa danos hepáticos: (c) fosfatase alcalina – ALP, (d) alanina aminotransferase - ALT, (e) aspartato aminotransferase – AST e (f) gama glutiltransferase –GGT; n = 5 animais por grupo. (g) Avaliação do parênquima hepático utilizando a coloração pela hematoxilina e eosina. Pode-se observar a preservação dos cordões de hepatócitos e ausência de infiltrado inflamatório. Barra

de escala: 100 μm . (h) Avaliação da metilação do DNA na região promotora do *ITPR3* em camundongos. Após o tratamento com 5'-aza, observa-se, entre a posição -338 e -529 na região promotora do *ITPR3*, um aumento das ilhas CpG desmetiladas (círculos brancos). (i) Quantificação do número de ilhas CpG metiladas ($m\text{CpG}$) e ilhas CpG desmetiladas (CpG) na região promotora do *ITPR3* em hepatócitos de camundongos controle e tratados com 5'-aza ($n=3$ animais). Valores expressos como média \pm SEM.

Após o tratamento com 5'-aza, por meio de sequenciamento do DNA, avaliou-se a região promotora do *ITPR3* nos hepatócitos desses animais e constatou-se uma diminuição dos números de ilhas CpG metiladas em relação ao grupo tratado com salina (Figura 9h e 9i). Essa desmetilação do DNA na região promotora do *ITPR3* em hepatócitos de camundongos levou a um aumento dos níveis de RNA mensageiros (Figura 10a) e da expressão dessa proteína (Figura 10b), eventos observados em hepatócitos isolados. Observa-se um padrão de expressão de *ITPR3* perinuclear e reticular, padrão característico do retículo endoplasmático (Figura 10b). Separando as frações protéicas citoplasmáticas e nucleares das células hepáticas desses animais após o tratamento, é possível observar a presença de *ITPR3* em ambos os compartimentos celulares (Figura 10c e 10d), evidenciando que *ITPR3* é localizado, quando expresso, não somente no retículo endoplasmático, mas também no retículo nucleoplasmático. Já na análise da expressão de *ITPR3* no tecido hepático, é observado uma expressão concentrada nos hepatócitos próximos da veia central (Figura 10e). Isso pode ser explicado pela regionalização das funções hepáticas, ou seja, hepatócitos localizados na região pericentral são responsáveis pela metabolização de drogas devido a uma maior expressão de proteínas do citocromo P450. Já os hepatócitos periportais, estão envolvidos na produção e secreção de substâncias, como albumina e fatores de coagulação (HALPERN et al., 2017). A expressão de *ITPR3*, pós tratamento com 5'-aza, não alterou a expressão das outras isoformas do canal de Ca^{2+} , fisiologicamente expressas nos

hepatócitos (Figura 10f e 10g). Juntos, esses resultados demonstram que a expressão de ITPR3 é regulada por metilação do DNA em hepatócitos humanos e de camundongo.

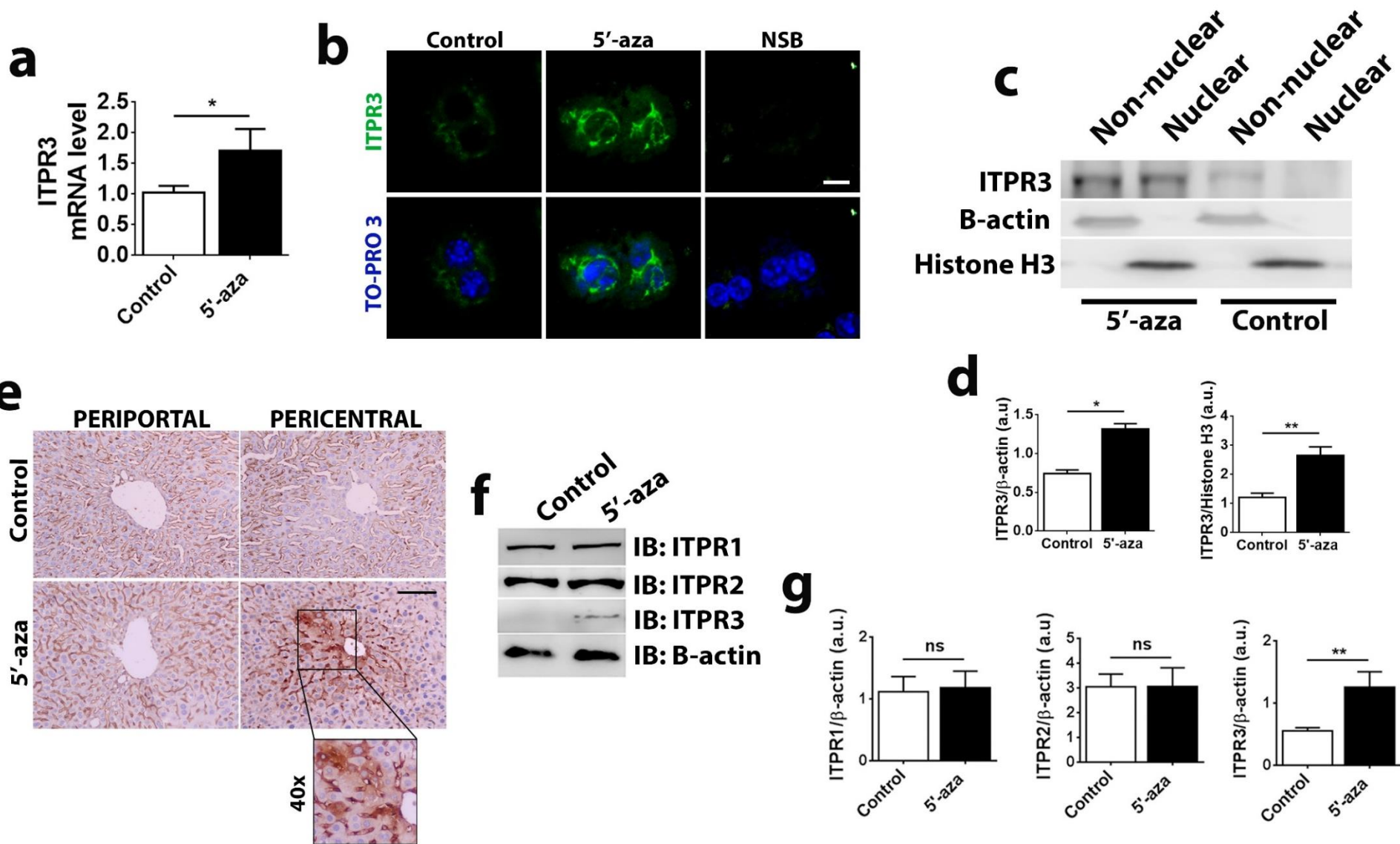


FIGURA 10. Desmetilação do DNA da região promotora do *ITPR3* libera sua expressão em hepatócitos. (a) Níveis de RNA mensageiro para *ITPR3* está aumentado após o tratamento com 5'-aza ($n = 5$ animais por grupo). (b) Expressão de *ITPR3* (verde) em hepatócitos isolados após tratamento com 5'-aza. O padrão de expressão desse canal de cálcio é perinuclear e reticulado, indicando a sua localização no retículo endoplasmático. A especificidade da ligação é dada pela não marcação no NSB. TO-PRO 3 (azul) foi utilizado para marcar o núcleo dos hepatócitos. Barra de escala: 10 μ m. (c) Western Blotting para *ITPR3* nas frações citoplasmáticas e nucleares de hepatócitos após o tratamento com a droga hipometilante do DNA. (d) Quantificação da expressão de *ITPR3* nas frações citoplasmáticas, validadas pela expressão de β -actina, e nas frações nucleares, representadas e validadas pela expressão de Histona H3 ($n = 3$ animais, ou seja, 3 frações citoplasmáticas e 3 frações nucleares de cada grupo). (e) Avaliação da expressão de *ITPR3* no lobo hepático. Observa-se expressão de *ITPR3* nos hepatócitos próximos à veia central, e isso pode ser justificado pelo fato de que hepatócitos dessa região são responsáveis pela metabolização de fármacos. Não se observa marcação para *ITPR3* evidente em hepatócitos próximos a veia porta. ($n = 5$ animais por grupo). (f) Western Blotting para os *ITPR* em hepatócitos isolados do grupo controle e tratados com 5'-aza. (g) Quantificação da expressão de *ITPR* em hepatócitos. Em situações fisiológicas hepatócitos expressam *ITPR1* e *ITPR2*. *ITPR3* só passa a ser expresso após desmetilação do DNA na região promotora promovido pela administração de 5'-aza ($n = 5$ animais por grupo). Valores expressos em média \pm SEM. * $p < 0.05$.

Por estar envolvida em várias funções celulares, a sinalização de Ca^{2+} em qualquer célula deve ser finamente modulada, para que não haja problemas. Exemplo dessa fina regulação foi descrita por Leite e colaboradores, onde os autores mostraram que a regulação do Ca^{2+} nuclear e citoplasmático se dá de maneira independente (LEITE *et al.*, 2003). Por isso, a junção entre quantidade, tempo, perfil e localização dos sinais de Ca^{2+} faz com que o mesmo íon regule funções diversas e seja considerado um segundo mensageiro celular (NEWTON *et al.*, 2016). No fígado, o Ca^{2+} regula funções como proliferação/regeneração e secreção de sais biliares e outros fluidos. Como a desmetilação do DNA na região promotora do *ITPR3* leva a expressão de um canal de Ca^{2+} adicional, foi feita a avaliação da sinalização de Ca^{2+} em hepatócitos isolado de fígado pós

tratamento com 5'-aza. Estimulando os hepatócitos com vasopressina (AVP), não foi possível observar diferença entre o sinal de Ca^{2+} de hepatócitos controle e tratados com 5'-aza (Figura 11). Sabidamente o fígado expressa receptores de vasopressina, V_{1a}R , receptores esses acoplados à proteína G e que quando estimulados pela ligação do seu agonista ativa a maquinaria intracelular de Ca^{2+} (AMAYA & NATHANSON, 2013).

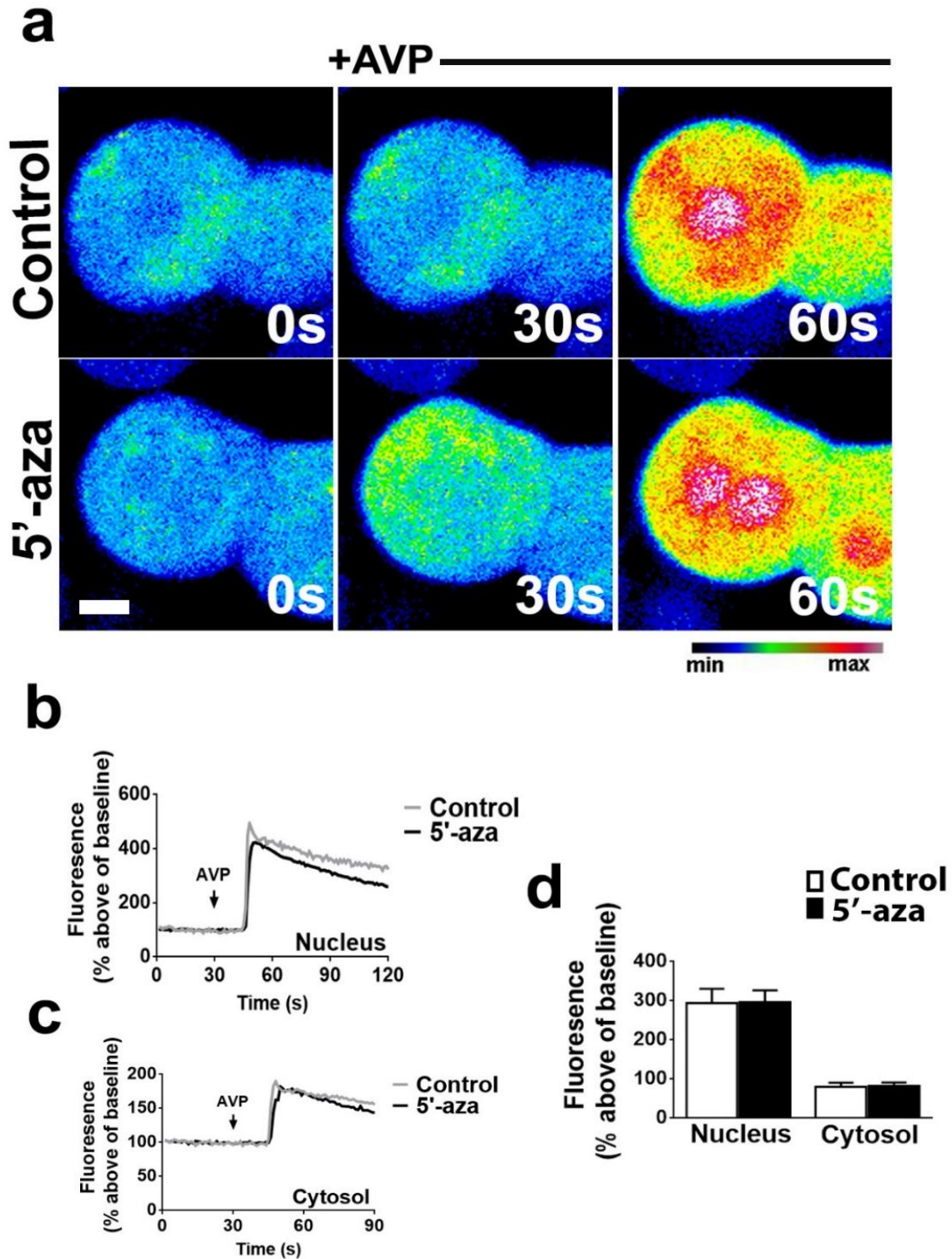
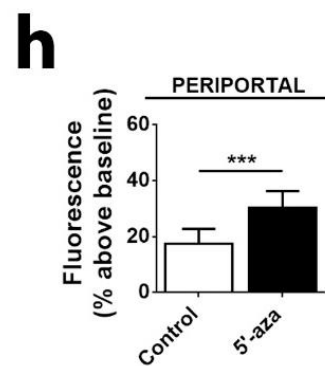
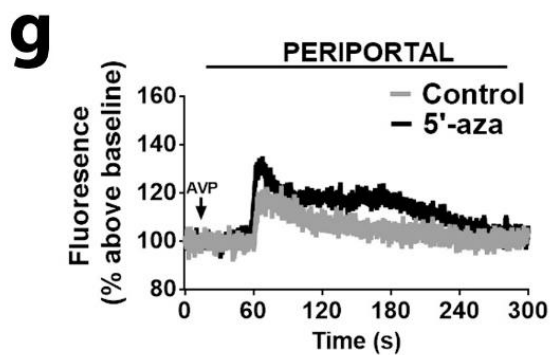
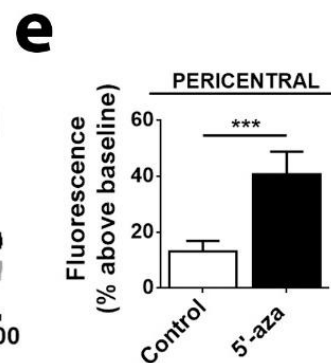
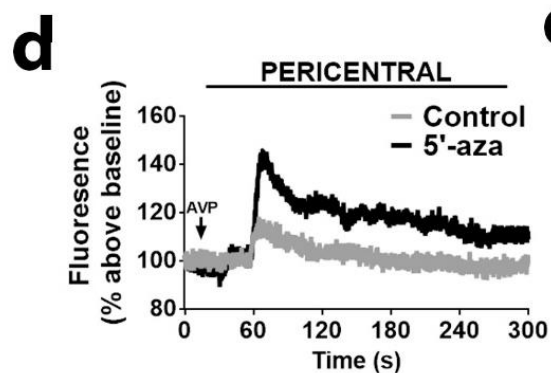
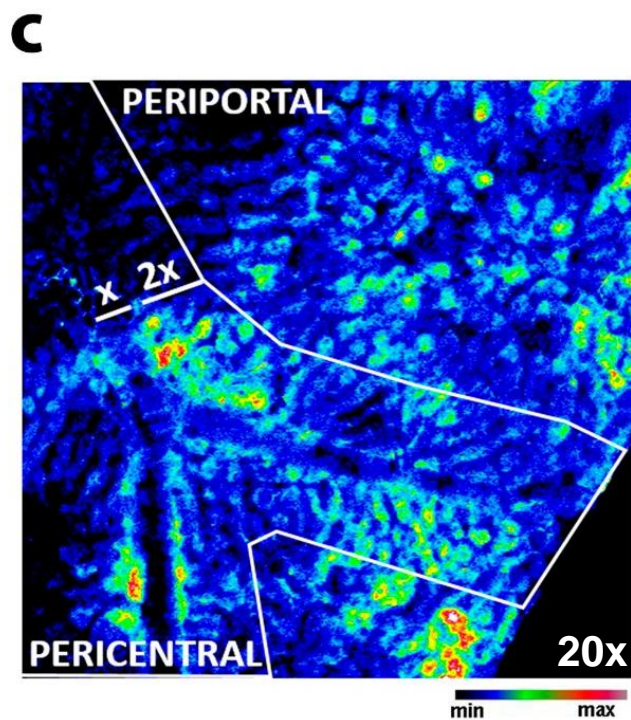
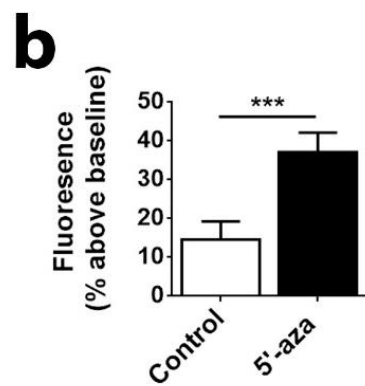
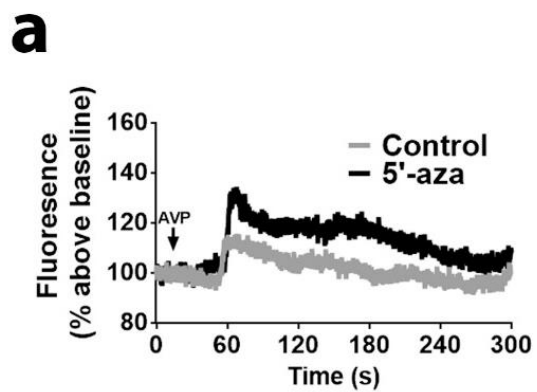


FIGURA 11. Sinalização de cálcio in vitro. (a) Imagens representativas do sinal de cálcio em hepatócitos isolados do fígado de animais controle e tratados com 5'-aza marcados com Fluo-4/AM e estimulados com vasopressina (100 ng/mL). Barra de escala: 10 μ m. Perfil de sinalização de cálcio no (b) núcleo e (c) citosol de hepatócitos isolados ($n = 40$ células). (d) Quantificação da amplitude dos sinais de cálcio no núcleo e citosol dos hepatócitos ($n = 40$ células por grupo). Valores expressos como média \pm SD.

Considerando que o ITPR3 é expresso em hepatócitos pericentrais (Figura 10e), no processo de isolamento se perde o local de origem da célula analisada durante o experimento. Assim, a saída encontrada para uma correta avaliação da sinalização de Ca^{2+} em hepatócitos pericentrais foi a realização do experimento *in vivo*, como realizada anteriormente por FONSECA *et al.*, 2018. Dessa forma, é possível analisar os sinais de Ca^{2+} nos hepatócitos da região pericentral e periportal separadamente. Os estudos de Ca^{2+} *in vivo* demonstraram um maior sinal quando os hepatócitos expressam ITPR3 após estimulação com AVP (Figura 12a e 12b). Esse aumento do sinal é devido à maior resposta dos hepatócitos presente na região pericentral, ou seja, que expressam ITPR3 (Figura 12c – 12e). É observado um pequeno aumento do sinal de Ca^{2+} nos hepatócitos periportais, mas não tão amplo quanto ao observado nos hepatócitos pericentrais (Figura 12c, 12g e 12h). Devido à expressão de ITPR3 no núcleo dos hepatócitos, os sinais de Ca^{2+} nesse compartimento celular também foram avaliados. Observou-se um aumento dos sinais de Ca^{2+} no núcleo das células que expressavam o ITPR3 tanto na região pericentral quanto na região periportal (Figura 12f e 12i). Esses resultados mostram que o receptor de InsP_3 do tipo 3, expressos em condições de desmetilação da região promotora do gene ITPR3, são funcionais e alteram a sinalização intracelular hepática de Ca^{2+} .



Nuclear calcium

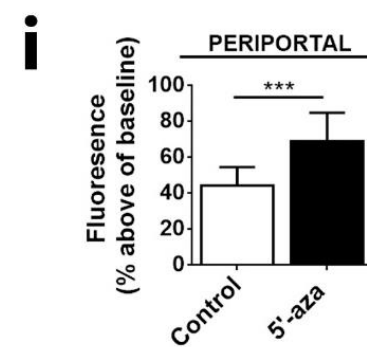
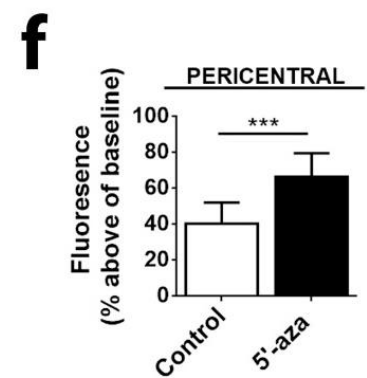
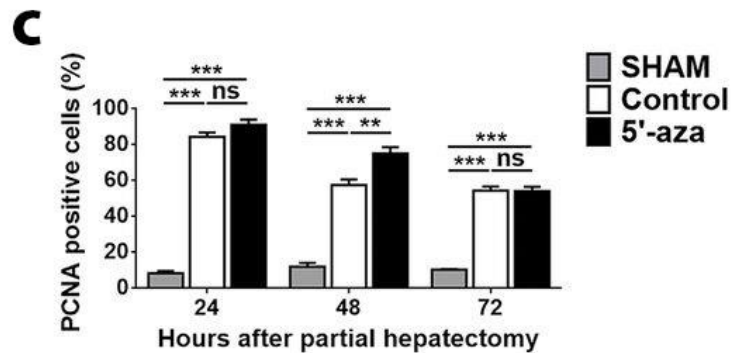
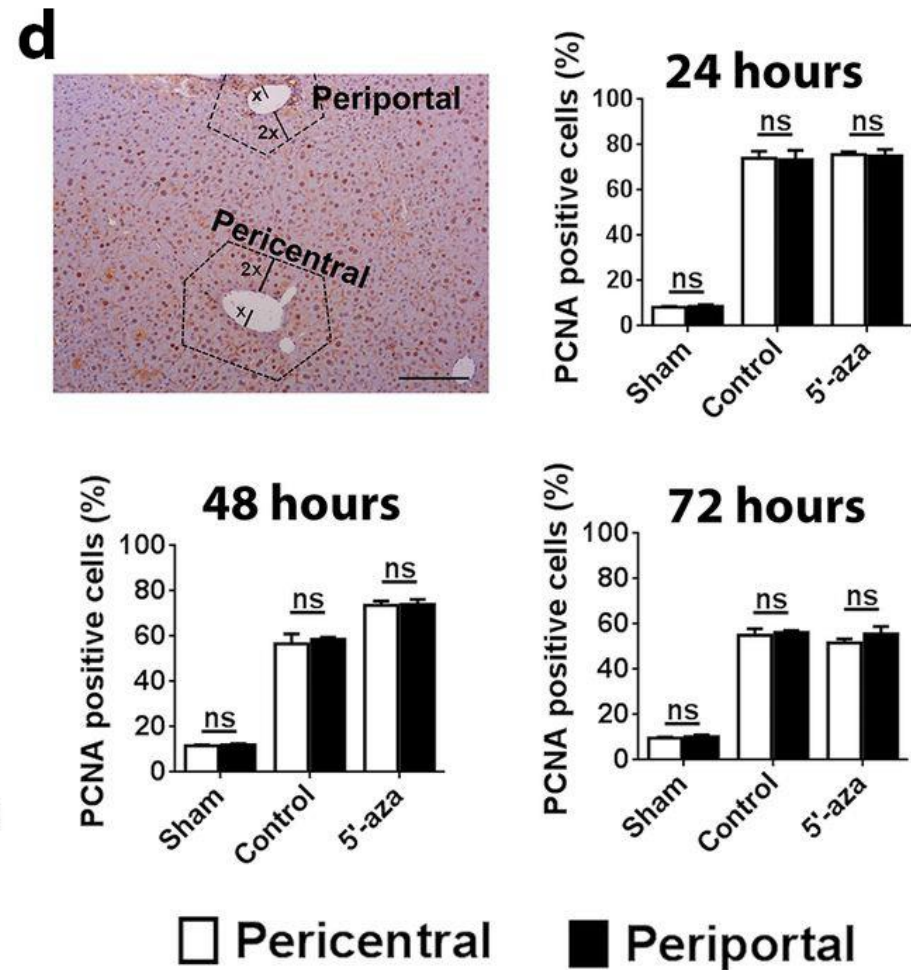
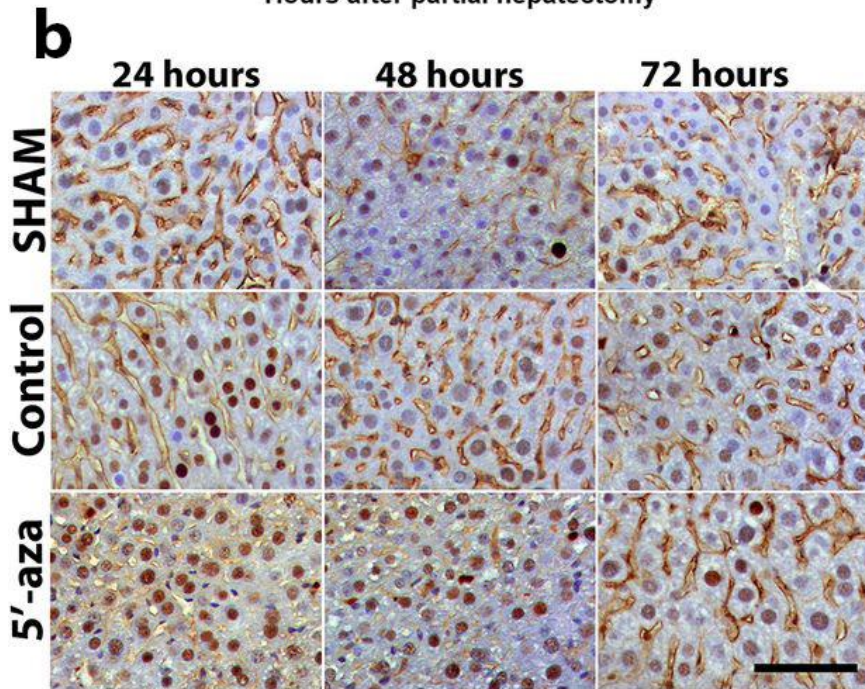
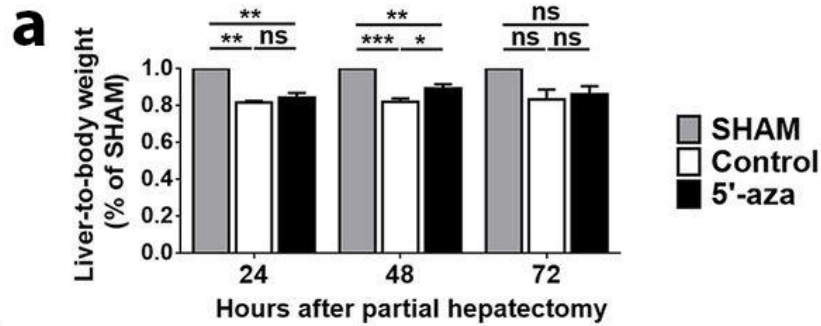


FIGURA 12. Sinalização de cálcio in vivo. (a) Perfil do sinal de cálcio em hepatócitos de animais controle e tratados com 5'-aza. As células foram marcadas com Fluo-4/AM e estimuladas com vasopressina (100 ng/mL). (b) Quantificação dos sinais de cálcio nos hepatócitos após estimulação com vasopressina. Observa-se um aumento da amplitude do sinal de cálcio nos animais que expressam ITPR3 (n = 5 animais por grupo). (c) Esquema demonstrando como foi feita a análise do sinal de Ca²⁺ nos hepatócitos localizados nas áreas pericentral e periportal. Os hepatócitos abrangidos por 2 vezes o valor do diâmetro da veia central foram considerados hepatócitos da área pericentral. Os hepatócitos excluídos dessa área foram considerados hepatócitos periportais. (d) Perfil do sinal de cálcio na região pericentral. (e) Quantificação da amplitude dos sinais de cálcio na região pericentral. Os hepatócitos que expressam ITPR3 apresentaram um sinal de cálcio significativamente maior do que hepatócitos controle (n = 5 animais). (f) Quantificação do sinal de cálcio no núcleo dos hepatócitos da região pericentral, mostrando um maior sinal de cálcio nuclear na presença de ITPR3. (g) Perfil do sinal de cálcio dos hepatócitos periportais após estímulo com vasopressina. (h) Quantificação do sinal de cálcio, após estímulo com vasopressina, nos hepatócitos periportais (n = 5 animais). (i) Quantificação do sinal de cálcio no núcleo dos hepatócitos da região periportal, mostrando um maior sinal de cálcio nuclear na presença de ITPR3. Valores expressos como média ± SEM. * p<0.05.

Sabendo que alterações na sinalização de Ca²⁺ podem alterar funções celulares, foram avaliados os efeitos fisiopatológicos da expressão de ITPR3 no hepatócito. Como já descrito, o Ca²⁺ nuclear regula a proliferação de hepatócitos (AMAYA *et al.*, 2014 e RODRIGUES *et al.*, 2007). Assim, avaliamos a capacidade regenerativa do fígado após expressão do ITPR3. Uma hepatectomia parcial (HP) de 30%, foi realizada nos animais após 7 dias de tratamento com o agente hipometilante do DNA ou salina. A capacidade regenerativa do fígado dos animais foi avaliada 24, 48 e 72 horas após o procedimento cirúrgico. Observou-se que 48 horas após a HP, o fígado dos animais que expressavam o canal de Ca²⁺ adicional apresentava uma maior regeneração hepática, medida pela relação entre o peso do fígado e o peso corpóreo (Figura 13a). Corroborando com esse achado, a imunomarcagem para *Proliferating Cell Nuclear Antigen* - PCNA, um marcador de

proliferação celular, mostrou-se aumentado no núcleo de hepatócitos que expressavam o ITPR3 após 48 horas da HP (Figura 13b e 13c). Como a expressão de ITPR3 e a sinalização de Ca^{2+} se mostraram concentradas na região pericentral, investigou-se se haveria uma maior proliferação dos hepatócitos nessa região. Porém, a proliferação dos hepatócitos, avaliada pela imunomarcagem de PCNA, se dá de maneira homogênea pelo lóbulo hepático (Figura 13d). A proliferação dos hepatócitos de forma irrestrita, independente da expressão de ITPR3 e de maiores sinais de Ca^{2+} totais e nucleares, pode ser explicada pelo fato de que os sinais de Ca^{2+} são originados em células específicas no fígado, como descrito por Leite *et al.*, em 2002. Reconhecidas como marca-passo hepáticos, algumas células apresentam uma expressão aumentada de receptores em sua membrana, como por exemplo, receptores de AVP (V_{1a}R), fazendo com que ativem a maquinaria de Ca^{2+} intracelular mais facilmente. O sinal de Ca^{2+} gerado nessas células são transmitidas às demais por meio de *gap junctions*, gerando um fenômeno de onda (LEITE *et al.*, 2002). Esse evento é importante não somente no fígado, onde regula funções como a secreção de glicose e bile, mas também no pâncreas, favorecendo a liberação de amilase (NATHANSON *et al.*, 1999; ELISEO *et al.*, 1998; CHANSON *et al.*, 1998). Assim, o maior sinal de Ca^{2+} nos hepatócitos da região periportal, devido à expressão de ITPR3, faz com haja uma proliferação celular aumentada em todo o lóbulo hepático devido ao espalhamento da sinalização de Ca^{2+} . Não houve variações na expressão das outras isoformas do ITPR que fisiologicamente são expressas nos hepatócitos, ITPR1 e ITPR2. (Figura 14). Magnino *et al.*, reportou um aumento na expressão de ITPR2 pós hepatectomia utilizado ratos como modelo (MAGNINO *et al.*, 2000). No presente estudo, como descrito, não houve variação na expressão da isoforma 2 do canal de Ca^{2+} , que pode ser explicado pela utilização de outra espécie animal na condução dos experimentos.



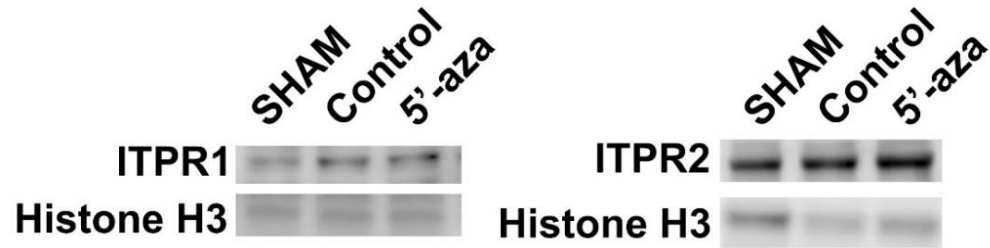
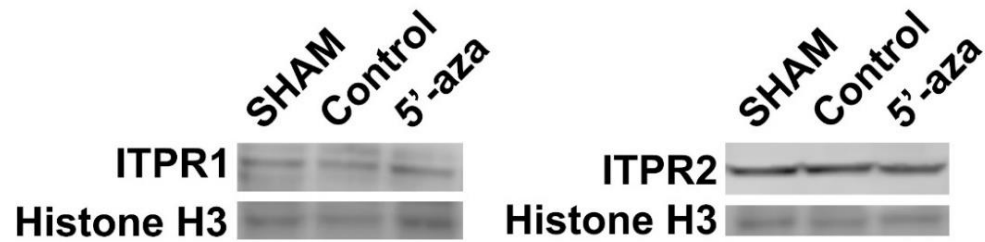
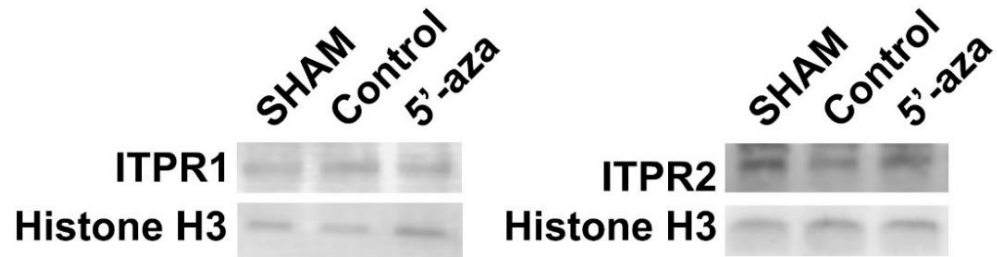
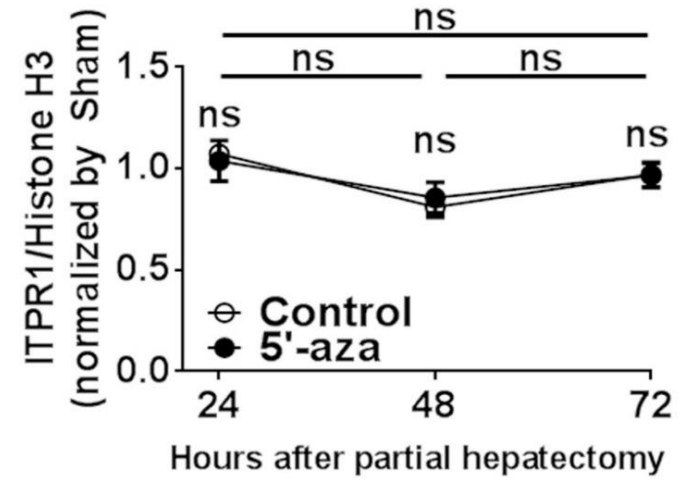
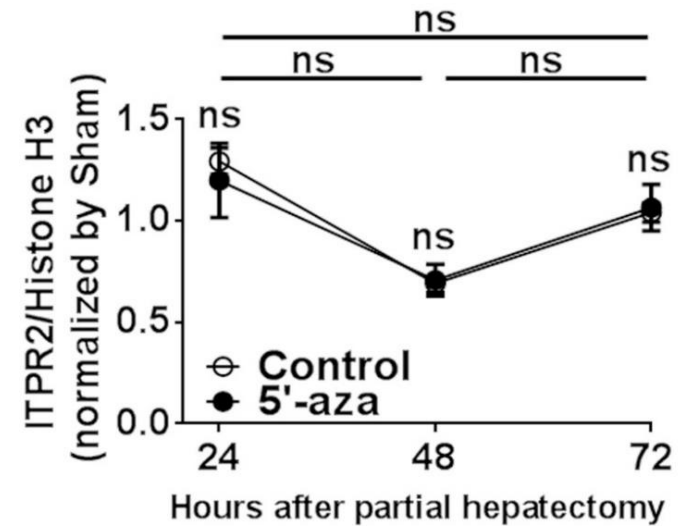
a**24 hours after partial hepatectomy****48 hours after partial hepatectomy****72 hours after partial hepatectomy****b****c**

FIGURA 13. Expressão de ITPR3 aumenta a capacidade proliferativa dos hepatócitos. (a) Relação peso do fígado pelo peso corpóreo dos animais 24, 48 e 72 horas após a cirurgia de remoção de 30% do fígado (HP). Observa-se que após 48 horas o fígado que expressa ITPR3 apresenta uma capacidade regenerativa aumentada ($n = 5$ animais por grupo/tempo). (b) Imunomarcação para Proliferating Cell Nuclear Antigen – PCNA. Barra de escala: 100 μm . (c) Quantificação da marcação nuclear de PCNA, mostrando que após 48 horas da HP há uma maior marcação nos hepatócitos que expressam ITPR3, explicando a maior regeneração nesse tempo. (d) Como ITPR3 é expresso na região pericentral, estratificou-se a quantificação de PCNA para as regiões pericentral e periportal. Porém não houve diferença na proliferação entre as regiões. Valores expressos como média \pm SEM. * $p < 0.05$.

Figura 14. Expressão de ITPR1 e ITPR2 após hepatectomia parcial. (a) Western Blotting para as isoformas 1 e 2 do ITPR3 em frações totais do fígado de camundongo SHAM, controle e tratados com 5'-aza, 24, 48 e 72 horas após hepatectomia parcial de 30%. (b) Quantificação da expressão de ITPR1 e ITPR2 após hepatectomia. Não houve variação da expressão dos canais de cálcio no fígado dos animais controle e tratados com 5'-aza quando comparados ao grupo SHAM.

A proliferação celular pode também ser regulada pela apoptose, tanto no processo de regeneração hepática (GUERRA *et al.*, 2011) quando no processo de crescimento tumoral (BONONI *et al.*, 2017 e KUCHAY *et al.*, 2017). Para avaliar o papel do ITPR3 no processo de apoptose, foi desenvolvida uma linhagem de CHC no qual o gene ITPR3 foi eliminado por meio da técnica CRISPR/Cas9 (ITPR3 KO). A eliminação da expressão de ITPR3 foi avaliada por meio de Western Blotting e por meio da expressão da proteína vermelha fluorescente (mCherry) acoplada ao cassete de direcionamento CRISPR (Figura 15a). A liberação de Ca^{2+} dependente de ITPR3 está relacionada à morte celular por apoptose (MENDES *et al.*, 2005), e esse evento foi avaliado na linhagem de CHC modificada, HepG2 ITPR3 KO. Primeiramente, a atividade de caspase3/7 foi avaliada tratando as células com estaurosporina (STA), onde foi observado um aumento da atividade de enzimas envolvidas no processo apoptótico nas células ITPR3 KO (Figura

15b). O mesmo resultado foi encontrado com a avaliação da porcentagem de células marcadas para anexina V, um marcador de apoptose (Figura 15c). A atividade de caspase 3/7 também é maior em células ITPR3 KO quando tratadas com etoposídeo, um outro agente que estimula a apoptose (Figura 15d). Esses resultados sugerem que a expressão de ITPR3 protege as células de CHC da morte celular por apoptose.

Buscando entender o mecanismo pelo qual o ITPR3 protege as células de CHC da apoptose, e sabendo que a transmissão de Ca^{2+} do retículo endoplasmático para a mitocôndria é capaz de modular a apoptose em vários tipos celulares (BONONI *et al.*, 2017 e KUCHAY *et al.*, 2017), além já ser descrito o papel de ITPR3 na transmissão de Ca^{2+} preferencialmente para a mitocôndria (MENDES *et al.*, 2005), avaliou-se a co-localização entre ITPR3 e mitocôndria. Utilizando plasmídeos específicos para facilitar a visualização de ITPR3 e mitocôndrias, foi possível verificar que a localização do ITPR3-GFP está distribuída pelo citosol em um padrão reticular, como o esperado pelo fato desse receptor ser expresso na membrana do retículo endoplasmático. Para identificar as mitocôndrias foi utilizado um marcador de membrana de mitocôndria, mKO2-TOMM20, que foi expresso em um padrão tubular, o que é comumente observado. Calculando a co-localização de ITPR3-GFP e o mKO2-TOMM20, foi possível identificar que há aproximadamente 15% de sobreposição, sugerindo que o ITPR3 está parcialmente localizado na interface do retículo endoplasmático com a mitocôndria (Figura 15e). Hepatócitos primários isolados do fígado dos animais controle e tratados com o agente hipometilante do DNA, foram desafiados a um estímulo apoptótico com estaurosporina. Observou-se que a expressão de ITPR3, por desmetilação do DNA na região promotora do gene, confere aos hepatócitos uma resistência a apoptose, evento medido pela clivagem de caspase 3 (Figura 15f e 15g). Com esse resultado, sugere-se que ITPR3

modula a apoptose quando expresso nos hepatócitos, regulando a transmissão de Ca^{2+} entre o retículo endoplasmático e a mitocôndria.

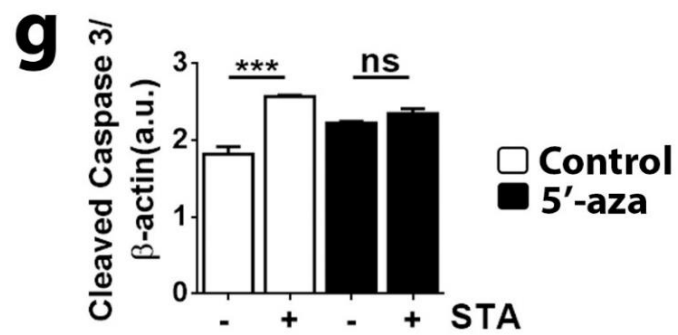
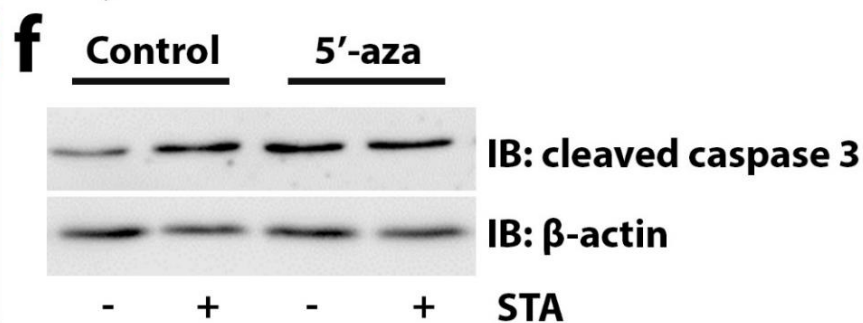
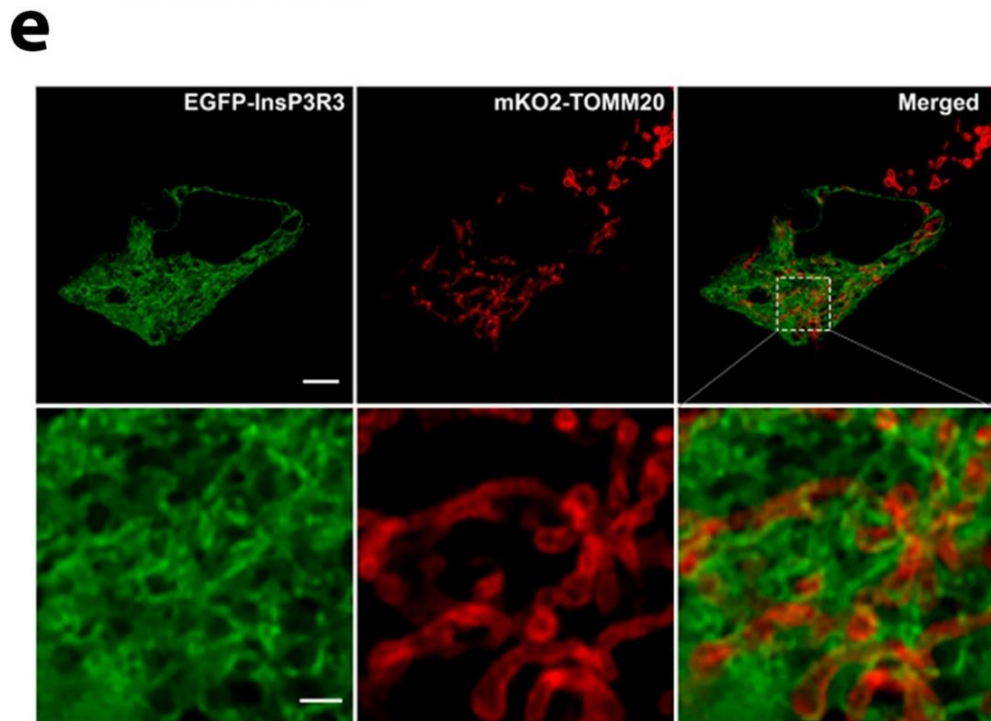
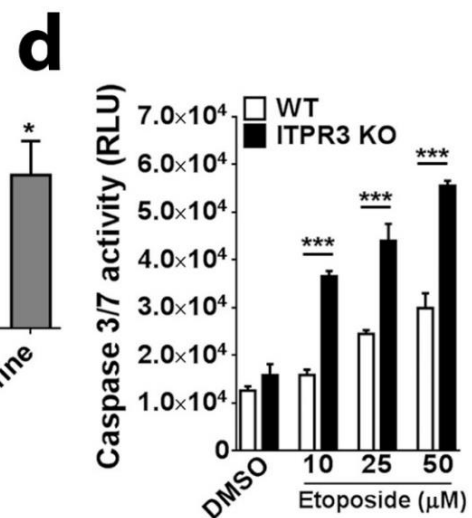
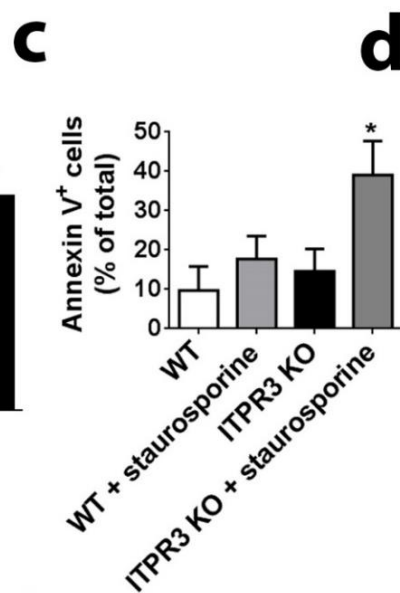
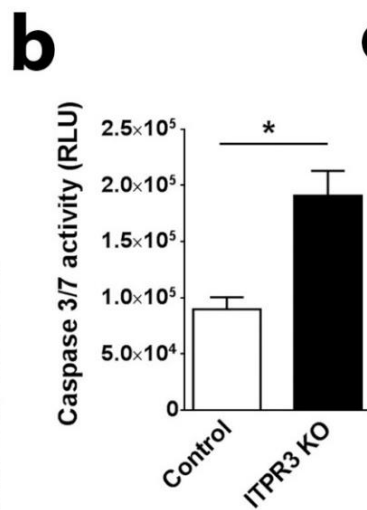
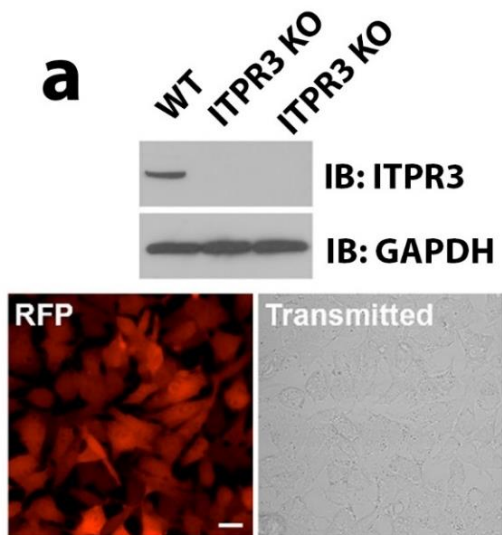


FIGURA 15. A expressão de ITPR3 torna as células de carcinoma hepatocelular resistentes a apoptose. (a) Western Blotting confirmando a deleção de ITPR3 nas células HepG2 e expressão de mCherry (proteína fluorescente vermelha) mostrando a eficiência da técnica de deleção de ITPR3 por CRISPR/Cas9. (b) Tratamento com estaurosporina aumentou a atividade de caspase 3/7 em células HepG2 ITPR3 KO (n = 9). (c) Número de células positivas para Anexina V, um marcador para apoptose, é maior nas células que não expressam o ITPR3 (n = 4). (d) Confirmando os resultados anteriores, a atividade de caspase 3/7 está aumentada nas células HepG2 ITPR3 KO quando tratadas com etoposídeo, um indutor de apoptose (n = 4). (e) Microscopia confocal mostrando a localização de expressão do ITPR3-GFP (verde) em células HepG2 WT. Houve co-localização entre ITPR3 e mitocôndria (vermelho) de aproximadamente 15%, mostrando que a expressão desse canal para cálcio pode regular a entrada do sinal apoptótico, tornando a célula mais resistente a esse evento de morte celular. Barra de escala superior: 5 μ m. Barra de escala inferior: 1 μ m. (f) Western Blotting da fração total de hepatócitos primários isolados de animais controle e que expressam ITPR3. Após o isolamento, as células foram tratadas com estaurosporina e os níveis de caspase 3 clivada foram avaliados (n = 3 animais por grupo). (g) Quantificação dos níveis de caspase 3 clivada após o desafio apoptótico por estaurosporina. Valores expressos como média \pm SEM. * $p < 0.05$.

A importância da apoptose mediada por ITPR3 está emergindo como um tema comum na biologia do câncer, embora o ITPR3 possa promover ou inibir a apoptose, dependendo do tipo de tumor (BONONI *et al.*, 2017; KUCHAY *et al.*, 2017 e SZALAI *et al.*, 1999). Já foi descrito que os ITPRs podem se ligar ao VDAC na membrana mitocondrial externa via grp75, que forma uma ‘sinapse’ facilitando a transmissão de Ca^{2+} do lúmen do retículo endoplasmático para a mitocôndria (BONONI *et al.*, 2017 e SZABADKAI *et al.*, 2006). O excesso de Ca^{2+} mitocondrial, por sua vez, desencadeia a abertura do poro de transição de permeabilidade (SZALAI *et al.*, 1999; ICHAS *et al.*, 1997 e GUERRA *et al.*, 2011), com vazamento de conteúdo mitocondrial para o citosol e posterior indução de apoptose via formação do apoptossoma (LI *et al.*, 1997). A isoforma do tipo 3 do ITPR é particularmente eficaz na modulação do Ca^{2+} mitocondrial e da apoptose (MENDES *et al.*, 2005). No entanto, existe uma variabilidade na forma

com que o ITPR3 é modulado e afeta a apoptose entre os diferentes tipos de tumor. Por exemplo, no melanoma, alterações na expressão do ITPR3 foram atribuídas à perda do supressor tumoral BAP1, que se liga e estabiliza o ITPR3. A perda de BAP1, portanto, leva à perda de ITPR3, que por sua vez reduz os sinais apoptóticos de Ca^{2+} mitocondrial (BONONI *et al.*, 2017). No câncer de próstata, a degradação do ITPR3 foi associada a mutações no PTEN, que normalmente competem com o FBXL2 para evitar que ele se ligue e que degrade o ITPR3. Na ausência de PTEN, ou na presença de certas formas mutantes, a degradação de ITPR3 é aumentada, o que leva à diminuição da apoptose (KUCHAY *et al.*, 2017). Um papel para o ITPR3 no câncer de cólon também foi demonstrado, e isso também tem sido relacionado ao efeito do ITPR3 na apoptose (SHIBAO *et al.*, 2010). Neste caso, o aumento da expressão de ITPR3 em amostras de câncer de cólon foi associado a um aumento de metástase e diminuição da sobrevivência do paciente. A super expressão de ITPR3 também foi associada à diminuição da apoptose em uma linhagem de câncer de cólon, enquanto o *knockdown* de ITPR3 levou ao aumento da apoptose (SHIBAO *et al.*, 2010).

Recentemente, o ITPR3 também foi relacionado à uma maior malignidade de colangiocarcinoma. Fisiologicamente, colangiócitos, células que compõem os ductos biliares e responsáveis pela diluição da bile, expressam todas as isoformas de ITPR, sendo a isoforma 3 a mais abundante (~80%) (SHIBAO *et al.*, 2003). O estudo mostra um aumento na expressão de ITPR3 tanto em biopsias humanas de colangiocarcinoma quanto em linhagens celulares deste tipo tumoral. Ao suprimir a expressão do canal de Ca^{2+} por meio de CRISPR/Cas9, foi observado uma diminuição da sinalização nuclear de Ca^{2+} induzida por ATP (UEASILAMONGKOL & KHAMPHAYA *et al.*, 2020). A participação do Ca^{2+} nuclear como um importante componente do desenvolvimento e progressão de tumores foi reportada anteriormente em um modelo de câncer de mama

triplo negativo. No estudo em questão, o bloqueio dos sinais nucleares de Ca^{2+} foi responsável por uma diminuição da proliferação das células tumorais e impedimento do crescimento do tumor por bloqueio da angiogênese, mediada pela liberação de CXCL-10. Além disso, etapas determinantes para a progressão do tumor e formação de metástases também foram diminuídas (GUIMARÃES *et al.*, 2017). Assim, como reportado no câncer de mama triplo negativo, a diminuição da sinalização nuclear de Ca^{2+} nas células de colangiocarcinoma, devido a supressão de ITPR3, reduziu a capacidade migratória e a invasividade celular, evidenciando uma maior malignidade às células que expressão ITPR3 (UEASILAMONGKOL & KHAMPHAYA *et al.*, 2020).

O presente trabalho encontrou resultados similares aos que já foram descritos na literatura a respeito de ITPR3: a expressão aumentada da isoforma 3 do ITPR no CHC está associada à diminuição da sobrevida do paciente e que a apoptose está aumentada quando o canal de Ca^{2+} é deletado. Não está claro por que ITPR3 promove a apoptose em certos tipos de malignidades, mas protege contra esse processo de morte celular em outros. Uma possível explicação é que os hepatócitos normalmente não expressam ITPR3, portanto, nessas células, os sinais de cálcio mitocondrial são devidos preferencialmente à isoforma ITPR1 (FERIOD *et al.*, 2017). Como ITPR3 tem uma afinidade menor do que ITPR1 para InsP_3 (TU *et al.*, 2005), é possível que a expressão *de novo* de ITPR3 permita que essa isoforma diminua a responsividade geral ao InsP_3 na junção retículo endoplasmático-mitocôndria, levando à diminuição da sinalização de Ca^{2+} mitocondrial e apoptose.

A real função de ITPR3 nos hepatócitos ainda não é muito esclarecido. O presente trabalho aponta o canal de Ca^{2+} como parte do complexo mecanismo de formação dos tumores hepáticos. Porém, estudos recentes demonstraram um papel protetor do ITPR3 nos hepatócitos infectados pelo vírus da Febre Amarela (LEMOS *et al.*, 2020). A

expressão de ITPR3 nos hepatócitos infectados pelo vírus da Febre Amarela resulta em efeitos biológicos idênticos ao descrito nesse trabalho; aumento da proliferação celular e diminuição de apoptose, além de reduzir o acúmulo de gordura nas células. Contudo, células *knockout* (KO) para ITPR3 apresentou maiores taxas de morte celular e maior acúmulo de gordura pós-infecção, demonstrando que a expressão de ITPR3 é benéfica e pode desempenhar um mecanismo protetivo aos danos agudos causados pelo vírus da Febre Amarela (LEMOS *et al.*, 2020). Em um modelo de injúria hepática por meio de isquemia e reperfusão, ITPR3 também passa a ser expresso nos hepatócitos e tem seu pico de expressão tempos antes da queda das enzimas hepáticas relacionadas a dano, como AST e ALT. O dano causado pela isquemia e reperfusão em animais ITPR3 KO fígado-específico são maiores quando comparado à animais selvagens, demonstrando em o papel protetivo de ITPR3 em modelo de doença hepática aguda (artigo em revisão). O próprio protocolo de indução de CHC por administração de DEN utilizado nesse projeto, quando realizado nos animais ITPR3 KO fígado específico, foi inviável devido a alta taxa de mortalidade dos animais quando comparado ao grupo WT (dado não publicado), evidenciando, em outro modelo experimental, a função protetora do ITPR3. Mais estudos precisam ser desenvolvidos para gerar um sólido conhecimento a respeito da biologia do ITPR3.

O atual trabalho identificou o ITPR3, um canal intracelular de Ca^{2+} , como parte do complexo processo de formação de tumores hepático, sendo uma via comum à várias etiologias. Esse receptor, que fisiologicamente não é expresso em hepatócitos saudáveis, passa a ser expresso após demestilação do DNA da região promotora do seu gene, regulando processos como proliferação celular e apoptose. O aparecimento de ITPR3 precede o estabelecimento do tumor hepático, já sendo expresso em estágios fibróticos finais e cirróticos. Assim, o ITPR3 surge como um possível biomarcador para a detecção

de carcinoma hepatocelular. Em um contexto clínico, ao se detectar a expressão de ITPR3 em biopsias hepáticas de pacientes cirróticos, cuidados deverão ser tomados uma vez que há indicativo para o surgimento do CHC. Consultas médicas menos espaçadas e exames clínicos mais rotineiros, podem ser ações a serem tomadas, a fim de se detectar precocemente o tumor hepático e dar início ao tratamento adequado.

A expressão de ITPR3 se mantém nas células tumorais e entender qual o seu papel nesse contexto se faz necessário para que novos conhecimentos básicos sobre a biologia do CHC possam ser gerados. Como o Ca^{2+} sabidamente regula o crescimento e desenvolvimento de tumores, além de etapas importantes para a formação de metástases, entender a relação do ITPR3 no contexto do câncer de fígado se faz necessários, para que se descubra novos alvos terapêuticos e vidas sejam salvas. Além disso, é descrito que as células tumorais apresentam uma perda da diferenciação, passando a expressar marcadores de pluripotência, como *octamer-binding transcription factor 4* (Oct4), *Sex Determining Region Y-Box 2* (Sox2), *Krüppel-like fator 4* (Klf4), c-Myc, Nanog e Lin28 (YIN *et al.*, 2012). A perda da diferenciação dos hepatócitos também pode ser explicada pela baixa expressão dos chamados *Liver-enriched transcription fator* (LETf), como o HNF4 α , evento que ocorre já nas etapas precedentes ao estabelecimento do tumor e responsável por uma piora clínica dos pacientes (LIU *et al.*, 2012; GUZMAN-LEPE *et al.*, 2018). Sabendo que uma das funções reguladas pela sinalização de Ca^{2+} , principalmente pelo Ca^{2+} nuclear, é a regulação da transcrição gênica e que células pluripotentes embrionárias humanas (hESC) e células pluripotentes induzidas (iPSC) apresentam uma alta expressão de ITPR3 (SYNNERGREN *et al.*, 2011; TAKEISHI *et al.*, 2020), entender se e como esse canal intracelular, assim como toda a maquinaria de Ca^{2+} contribui para a manutenção da expressão dos marcadores de pluripotência e/ou dos

LETF podem ajudar na identificação de alvos que futuramente poderão ser usados como terapia, além de contribuir para a geração de conhecimento básico.

CONCLUSÃO

CONCLUSÃO

Os resultados deste trabalho demonstram que a metilação do DNA na região promotora do gene, regula a expressão de ITPR3 em hepatócitos, e que a desregulação desse processo leva a expressão desse canal de cálcio. Essa expressão de ITPR3 é um evento comum observado em etapas anteriores ao desenvolvimento do CHC, independentemente da etiologia. Quando expresso, o ITPR3 gera um sinal nuclear de proliferação celular e um sinal citoplasmático de prevenção de apoptose, eventos celulares característicos de transformação celular e malignidade. Como resultado desses processos, há um aumento do número de células, que é visto no processo de formação do carcinoma hepatocelular e em outros tipos de tumor.

**REFERÊNCIAS
BIBLIOGRÁFICAS**

REFERÊNCIAS BIBLIOGRÁFICAS

ABDULHAQ, H. E ROSSETTI, J. M. The role of azacitidine in the treatment of myelodysplastic syndromes. **Expert Opinion on Investigational Drugs**. v. 16, p. 1967-1975, 2007.

AMAYA, M. J. e NATHANSON, M. H. Calcium Signaling in the Liver. **Compr Physiol**. v. 3, p. 515–539, 2013.

AMAYA, M. J.; OLIVEIRA, A. G.; GUIMARÃES, E. S.; NATHANSON, M. H. e LEITE, M. F. The insulin receptor translocates to the nucleus to regulate cell proliferation in liver. **Hepatology**. v. 59, p. 1–18, 2014.

ANANTHANARAYANAN, M. *et al.* Post-translational regulation of the type III inositol 1,4,5-trisphosphate receptor by miRNA-506. **Journal of Biological Chemistry**. v. 290, p. 184–196, 2015.

BAERTLING, F.; MAYATEPEK, E.; GERNER, P.; HIDEO, B. A.; FRANZEL, J.; SCHLUNE, A. E MEISSNER, T. Liver cirrhosis in glycogen storage disease Ib. **Molecular Genetics and Metabolism**. v. 108, p. 198-200, 2013.

BERRIDGE M. J.; BOOTMAN M. D. e RODERICK H. L. Calcium signaling: dynamics, homeostasis and remodeling. **Nature Reviews**. v. 4, p. 517-529, 2003.

BIRD, A. The Essentials of DNA Methylation. **Cell**. v. 70, p. 5-8, 1992.

BONONI, A.; GIORGI, C.; PATERGANI, S.; LARSON, D.; VERBRUGGEN, K. *et al.*
BAP1 regulates IP3R3-mediated Ca²⁺ flux to mitochondria suppressing cell transformation.
Nature. v. 546, p.549–553, 2017.

CHANSON, M.; FANJUL, M.; BOSCO, D.; NELLES, E.; SUTER, S.; WILLECKE, K. E
MEDA, P. Enhanced Secretion of Amylase from Exocrine Pancreas of Connexin32-deficient
Mice. **J. Cell Biol.** v.141, 1267–1275, 1998.

D’ALESSIO, A. C. e SZYF, M. Epigenetic tête-à-tête: the bilateral relationship between
chromatin modifications and DNA methylation. **Biochemistry and Cell Biology**. v. 84,
p.463-466, 2006.

DIMAURO, I., PEARSON, T.; CAPOROSSO, D. E JACKSON, M. J. A simple protocol for
the subcellular fractionation of skeletal muscle cells and tissue. **BMC Res Notes**. v. 5, p. 1-5,
2012.

EHRlich, M. DNA methylation in cancer: too much, but also too little. **Oncogene**. v. 21, p.
5400-5413, 2002.

EUGENIN, E. A.; GONZALEZ, H.; SAEZ, C. G. E SAEZ, J. C. Gap junctional
communication coordinates vasopressin-induced glycogenolysis in rat hepatocytes. **Am. J.**
Physiol. Gastrointest. Liver Physiol. v. 37, p. G1109–G1116, 1998.

EL-SERAG, H. e MASON, A. D. Rising Incidence of Hepatocellular Carcinoma in the United States. **The New England Journal of Medicine**. v. 340, p. 745-750, 1999.

EL-SERAG, H. B. Epidemiology of viral hepatitis and hepatocellular carcinoma. **Gastroenterology**. v 142, p. 1264–1273, 2012.

ESTELLER, M. DNA methylation and cancer therapy: new developments and expectations. **Current Opinion in Oncology**. v. 17, p. 55-60, 2005.

FRANÇA, A.; LIMA FILHO, ACM. *et al.* Effects of Endotoxin on Type 3 Inositol 1,4,5-Trisphosphate Receptor in Human Cholangiocytes. **Hepatology**. v 69, p. 817-830, 2019.

FARBER, E.; SOLT, D.; CAMERON, R.; LAISHES, B.; OGAWA, K. Newer insights into the pathogenesis of liver cancer. **The American Journal of Pathology**. v. 89, p. 477–482, 1977.

FEINBERG, A.P. Cancer epigenetics takes center stage. **PNAS**. v. 98, p. 392-392, 2001.

FEITELSON, M. A.; SUN, B.; TUFAN, N. L. S.; LIU, J.; PAN, J. e LIAN, Z. Genetic mechanisms of hepatocarcinogenesis. **Oncogene**. v. 21, p. 2593-2604, 2002.

FERIOD, C. N.; NGUYEN, L.; JURCZAK, M. J.; KRUGLOV, E. A.; NATHANSON, M. H.; SHULMAN, G. I.; BENNETT, A. M. *et al.* Inositol 1,4,5-trisphosphate receptor type II (InsP3R-II) is reduced in obese mice, but metabolic homeostasis is preserved in mice lacking

InsP3R-II. **American Journal of Physiology – Endocrinology and Metabolism**. v. 307, p. 1057-1064, 2014.

FERIOD, C. N.; OLIVEIRA, A. G.; GUERRA, M. T.; NGUYEN, L. M. et al. Hepatic inositol 1,4,5 trisphosphate receptor type 1 mediates fatty liver. **Hepatology Communications**. v. 00, p. 000, 2016.

FORNER, A.; REIG, M. e BRUIX, J. Hepatocellular carcinoma. **The Lancet**. v. 391, n. 03, p. 1301–1314, 2018.

FOSKETT, J. K. e MALK, D. O. Novel model of calcium and inositol 1,4,5-trisphosphate regulation of InsP3 receptor channel gating in native endoplasmic reticulum. **Biological Research**. v. 37, p.513-519, 2004.

NASEEMA GANGAT, N.; PATNAIK, M. M. E TEFFERI, A. Myelodysplastic syndromes: Contemporary review and how we treat. **American Journal of Hematology**. v. 91, p. 76-89, 2016.

GOMES, D. A.; RODRIGUES, M. A.; LEITE, M. F.; GOMEZ, M. V.; VARNAI, P.; BALLA, T.; BENNETT, A. M.; et al. c-Met must translocate to the nucleus to initiate calcium signals. **Journal of Biological Chemistry**. v. 283, p. 4344-4351, 2008.

GUERRA, M. T.; FONSECA, E. A.; MELO, F. M.; ANDRADE, V. A.; AGUIAR, C. J.; ANDRADE, L. M. et al. Mitochondrial calcium regulates rat liver regeneration through the modulation of apoptosis. **Hepatology**. v. 54, p. 296-306, 2011.

GUIMARÃES, E.; MACHADO, R.; FONSECA, M. C.; FRANÇA, A.; CARVALHO, C. et al. Inositol 1, 4, 5-trisphosphate-dependent nuclear calcium signals regulate angiogenesis and cell motility in triple negative breast cancer. **PLOS ONE**. v. 4, p. 1-22, 2017.

GUZMAN-LEPE, J.; CERVANTES-ALVAREZ, E.; COLLIN DE L'HORTET, A.; WANG, Y.; MARS, W. M.; ODA Y. *et al.* Liver-enriched transcription factor expression relates to chronic hepatic failure in humans. **Hepatology Communicatons**. v.2, p. 582-594, 2018.

HALPERN, B.; SHENHAV, R.; MATCOVITCH, O.; TOTH, B.; LEMZE, D. *et al.* Single-cell spatial reconstruction reveals global division of labour in the mammalian liver. **Nature**. v 542, p. 1–5, 2017.

HANDY, D. E.; CASTRO, R. e LOSCALZO, J. Epigenetic Modifications: Basic Mechanisms and Role in Cardiovascular Disease. **Circulation**. v. 123, p. 2145–2156, 2011.

HARDINGHAM G. E.; CHAWLA S.; JOHNSON C. M. e BADING H. Distinct functions of nuclear and cytoplasmic calcium in the control of gene expression. **Nature**. v. 385, p. 260-265, 1996.

HERNANDEZ, E.; LEITE, M. F.; GUERRA, M. T.; KRUGLOV, E. A. et al. The Spatial Distribution of Inositol 1,4,5-Trisphosphate Receptor Isoforms Shapes Ca²⁺ Waves. **Journal of Biological Chemistry**. v. 282, p.10057-10067, 2007.

HIRATA K.; PULS T.; O'NEILL A. F.; DRANOFF J. A. e NATHASON M. H. The type II Inositol 1,4,5-Trisphosphate Receptor Can trigger Ca²⁺ waves in rat hepatocytes. **Gastroenterology**. v. 122, p. 1088-1100, 2002.

ICHAS, F.; JOUAVILLE, L. S. & MATZAT, J.P. Mitochondria are excitable organelles capable of generating and conveying electric and calcium currents. **Cell**. v 89, p. 1145–1153, 1997.

JEMAL, A., BRAY, F. & FERLAY, J. Global Cancer Statistics: 2011. **CA: A Cancer Journal for Clinicians**. v 49, p.33-64, 2011.

JIANG, Q. X.; THROWER, E. C.; CHESTER, D. W.; EHRlich, B. E. E SIGWORTH, F. J. Three-dimensional structure of the type 1 inositol 1,4,5-trisphosphate receptor at 24 Å resolution. **THE EMBO JOURNAL**. v. 21, p. 3575-3581, 2002.

JONES, P. A. e LAIRD, P. W. Cancer-epigenetics comes of age. **Nature Genetics**. v. 21, p. 163-167, 1999.

KUCHAY, S.; GIORGI, C.; SIMONECHI, D.; PAGAN, J.; MISSIROLI, S. *et al.* PTEN counteracts FBXL2 to promote IP3R3- and Ca²⁺- mediated apoptosis limiting tumour growth. **Nature**. v 546, p. 554–558, 2017.

LAIRD, P. W. Cancer epigenetics. **Human Molecular Genetics**. v. 14, p. R65–R76, 2005.

LEITE M. F.; THROWER E. C.; ECHEVARRIA W.; KOULEN P.; HIRATA K. et al. Nuclear and cytosolic calcium are regulated independently. **PNAS**. v. 100, n. 5, p. 2975–2980, 2003.

LEMOS, F. O.; FRANÇA, A.; LIMA FILHO, A. C. M.; FLORENTINO, R. M.; SANTOS, M. L.; MISSIAGGIA, D. G.; RODRIGUES, G. O. L.; DIAS, F. F.; SOUZA PASSOS, I. B.; TEIXEIRA, M. M.; ANDRADE, A. M. F.; LIMA, C. X.; VIDIGAL, P. V. T.; COSTA, V. V.; FONSECA, M. C.; NATHANSON, M. H. e LEITE, M. F. Molecular Mechanism for Protection Against Liver Failure in Human Yellow Fever Infection. **Hepatology Communications**. v. 4, p. 657-669, 2020.

LI, P.; NIJHAWAN, D.; BUDIHARDJO, I.; SRINIVASULA, SM.; AHMAD, M.; ALNEMRI, ES.; E WANG, X. Cytochrome c and dATP-dependent formation of Apaf-1/caspase-9 complex initiates an apoptotic protease cascade. **Cell**. v 91, p. 479–489, 1997.

LIU, L.; YANNAM, G. R.; NISHIKAWA, T.; YAMAMOTO, T.; BASMA, H.; ITO, R. *et al.* The microenvironment in hepatocyte regeneration and function in rats with advanced cirrhosis. **Hepatology**. v. 55, p. 1529-1539, 2012.

LUND, A. H. e VAN LOHUIZEN, M. Epigenetics and cancer. **Genes & Development**. v. 18, p.2315-2335, 2004.

MAGNINO, F.; ST-PIERRE, M.; LÜTHI, M.; HILLY, M.; MAUGER, J. P. E DUFOUR, J. F. Expression of intracellular calcium channels and pumps after partial hepatectomy in rat. **Mol Cell Biol Res Commun**. v. 3, p. 374–379, 2000.

MENDES, C.; GOMES, D.; THOMPSON, M.; SOUTO, N. GOES, T. *et al.* The type III inositol 1,4,5-trisphosphate receptor preferentially transmits apoptotic Ca²⁺ signals into mitochondria. **Journal of Biological Chemistry**. v 280, p. 40892–40900, 2005.

MIKOSHIBA, K. IP₃ receptor/Ca²⁺ channel: from discovery to new signaling concepts. **Journal of Neurochemistry**. v. 102, p.1426-1446, 2007.

NATHANSON, M. H.; RIOS-VELEZ, L.; BURGSTÄHLER, A. D. E MENNONE, A. Communication via gap junctions modulates bile secretion in the isolated perfused rat liver. **Gastroenterology**. v. 116, p. 1176–1183, 1999.

NEWTON, A. C.; BOOTMAN, M. D. E SCOTT, J. D. Second Messengers. **Cold Spring Harbor Laboratory Press**. v. 8, p. 1-14, 2016.

NEWTON, C. L.; MIGNERY, G. A, e SUDHOF, T. C. Co-expression in vertebrate tissues and cell lines of multiple inositol 1,4,5-trisphosphate (InsP₃) receptors with distinct affinities for IP₃. **Journal of Biological Chemistry**. v.1, p.28613-28619, 1994.

OLIVEIRA, A. G.; GUIMARÃES, E. S.; ANDRADE, L. M.; MENEZES; G. B. e LEITE, M. F. Decoding Calcium Signaling Across the Nucleus. **Physiology (Bethesda)**. v. 29, p. 361-368, 2014.

PLATANITIS, J. e DECKER, T. Regulatory Networks Involving STATs, IRFs, and NFκB in Inflammation. **Frontiers in Immunology**. v. 9, p. 1-16, 2018.

RODRIGUES M. A.; GOMES D. A.; LEITE M. F. GRANT W. et al. Nucleoplasmic Calcium Is Required for Cell Proliferation. **Journal of Biological Chemistry**. v. 282, n. 23, p. 17061-17068, 2007.

ROTHHAMMER, T e BOSSERHOFF, A. K. Epigenetic events in malignant melanoma. **Pigment Cell Research**. v. 20, p. 99-111, 2007.

SCHUPPAN, D. e AFDHAL, H. N. Liver cirrhosis. **Lancet**. v. 371, n. 8, p. 838–851, 2008.

SHAH, S. Z. A.; ZHAO, D.; KHAN, S. H. E YANG, L. Regulatory Mechanisms of Endoplasmic Reticulum Resident IP3 Receptors. **J Mol Neurosci**. v.56, p. 938-948, 2015.

SHIBAO, K.; FIEDLER, MJ.; NAGATA, J.; MINAGAWA, N.; HIRATA, K.; NAKAYAMA, Y.; IWAKIRI, Y.; NATHANSON, MH. E YAMAGUCHI, K. The type III inositol 1,4,5-trisphosphate receptor is associated with aggressiveness of colorectal carcinoma. **Cell Calcium**. v. 48, p. 315–323, 2010.

SUBRAMANIAM, A.; SHANMUGAM, M.K.; PERUMAL, E.; LI, F.; NACHIYAPPAN, A.; DAI, X.; SWAMY, S.N.; AHN, K.S.; KUMAR, A.P.; TAN, B.K,H.; HUI, K.M.; SETHI, G. Potential role of signal transducer and activator of transcription (STAT)3 signaling pathway in inflammation, survival, proliferation and invasion of hepatocellular carcinoma. **Biochimica et Biophysica Acta**, v. 1835, p. 46-60, 2013.

SZABADKAI, G.; BIANCHI, K.; VARNAI, P.; DE STEPHANI, D. *et al.* Chaperone-mediated coupling of endoplasmic reticulum and mitochondrial Ca²⁺ channels. **Journal of Cell Biology**. V. 175, p. 901–911, 2006.

SZALAI, G., KRISHNAMURTHY, R. & HAJNÓCZKY, G. Apoptosis driven by IP₃-linked mitochondrial calcium signals. **EMBO Journal**. v. 18, p. 6349–6361, 1999.

SYNNEREGREN, J.; AMÉEN, C.; JANSSON, A. E SARTIPY, P. Global transcriptional profiling reveals similarities and differences between human stem cell-derived cardiomyocyte clusters and heart tissue. **Physiol Genomics**. v.44, p. 245–258, 2012.

TAKEISHI, K.; L'HORTET, A. C.; WANG, Y. *et al.* Assembly and Function of a Bioengineered Human Liver for Transplantation Generated Solely from Induced Pluripotent Stem Cells. **Cell Reports**. v. 31, p. 107711, 2020.

TANG, W. Y. e HO, S. M. Epigenetic reprogramming and imprinting in origins of disease. **Reviews In Endocrine And Metabolic Disorders**. v. 8, p.173-182, 2007.

TOLBA, R.; T KRAUS, T.; LIEDTKE, C.; SCHWARZ, M. E WEISKIRCHEN, R. Diethylnitrosamine (DEN)-induced carcinogenic liver injury in mice. **Laboratory Animals**. v. 49, p. 59-69, 2015.

TU, H.; WANG, Z.; NOSYREVA, E.; DE SMEDT, H. & BEZPROZVANNY, I. Functional characterization of mammalian inositol 1,4,5-trisphosphate receptor isoforms. **Biophysics Journal**. v. 88, p. 1046–1055, 2005.

UEASILAMONGKOL, P.; KHAMPHAYA, T.; GUERRA, M. T.; RODRIGUES, M. A.; GOMES, D. A.; KONG, Y.; WEI, W.; JAIN, D.; TRAMPERT, D. C.; ANANTHANARAYANAN, M.; BANALES, J. M.; ROBERTS, L. R.; FARSHIDFAR, F.; NATHANSON, M. H. e WEERACHAYAPHORN, J. Type 3 Inositol 1,4,5-Trisphosphate Receptor Is Increased and Enhances Malignant Properties in Cholangiocarcinoma. **Hepatology**. v. 71, p. 583-599, 2020.

WARDYN, J. D.; PONSFORD, A. H. E SANDERSON, C. M. Dissecting molecular cross-talk between Nrf2 and NF- κ B response pathways. **Biochem. Soc. Trans.** v. 43, p. 621–626, 2015.

WEERACHAYAPHORN, J.; AMAYA, M. J.; SPIRLI, C.; CHANSELA, P.; MITCHELL-RICHARDS, K. A.; ANANTHANARAYANAN, M. e NATHANSON, M. H. Nuclear Factor Erythroid 2-like 2 Regulates Expression of Inositol 1,4,5-trisphosphate Receptor, Type 3 and Calcium Signaling in Cholangiocytes. **Gastroenterology**. v 149, p. 211–222, 2015.

XIAO, M.; LI, J.; LI, W. *et al.* MicroRNAs activate gene transcription epigenetically as an enhancer trigger. **RNA Biol**. v. 4, p. 1326-1334, 2017.

YIN, X.; LI, Y. W.; JIN, J. J. et al. The clinical and prognostic implications of pluripotent stem cell gene expression in hepatocellular carcinoma. **Oncology Letters**. v. 5, p. 1155-1162, 2013

ZHANG, G.; WANG, Q. E XU, R. Therapeutics Based on microRNA: A New Approach for Liver Cancer. **Current Genomics**. v. 11, p. 311-325, 2010.

ANEXOS

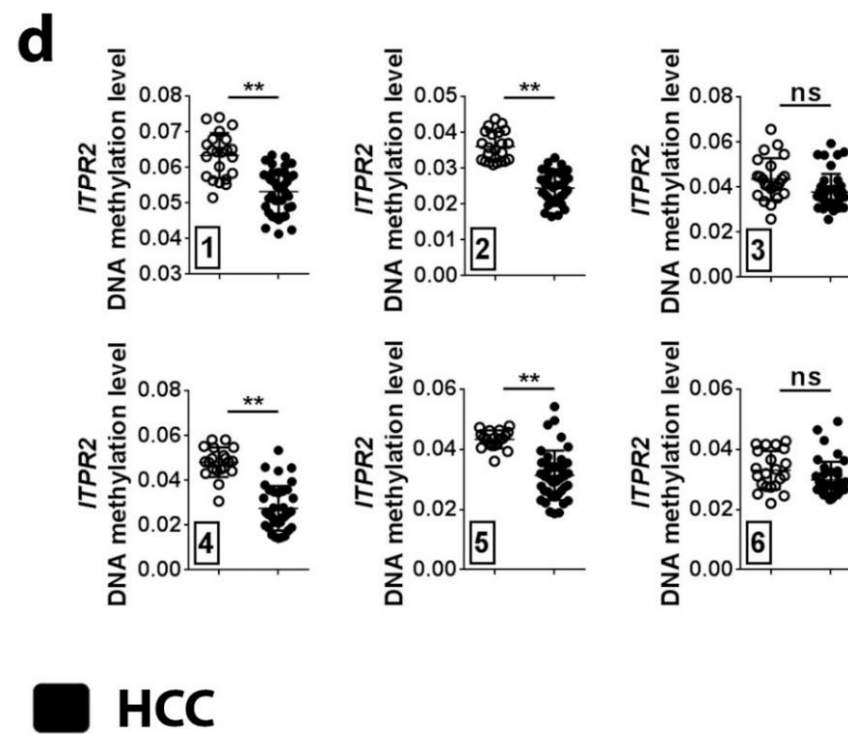
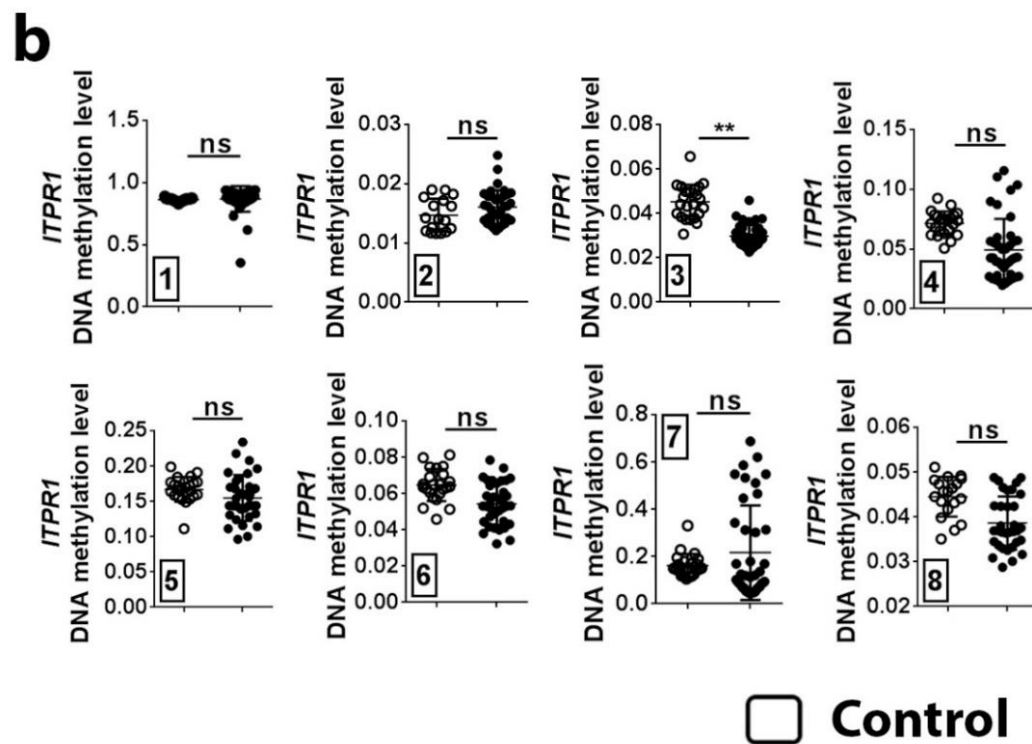
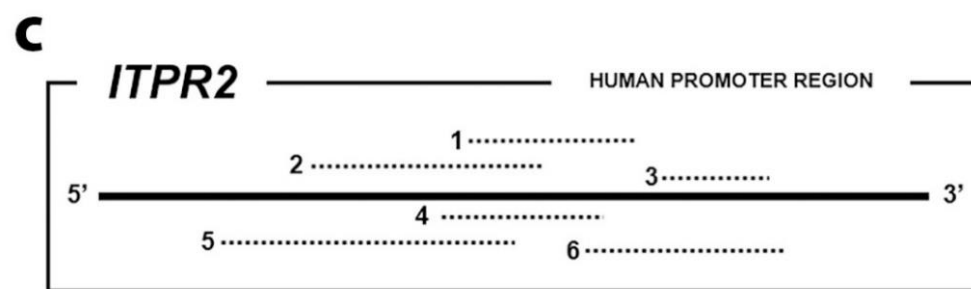
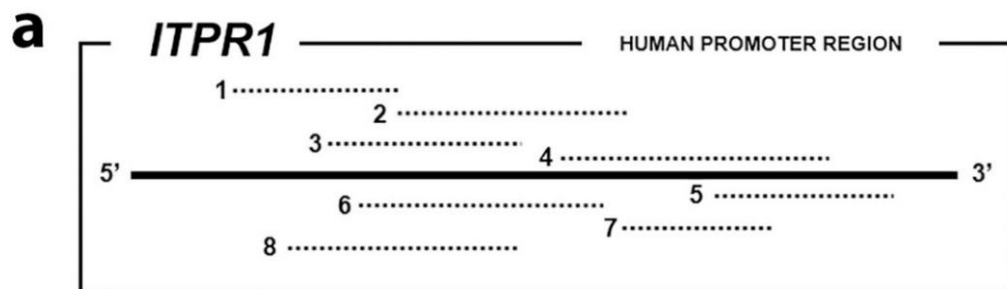


Figura complementar 1: Relacionada a Figura 7. Análise da metilação do DNA na região promotora do gene ITPR1 e ITPR2. (a) Esquema representando as 8 posições dentro da região promotora do ITPR1 que foram utilizadas para avaliar os níveis de DNA metilado. (b) Níveis de metilação do DNA em fígados controles (pontos brancos) e em fígado de pacientes com CHC (pontos pretos). (c) Esquema representando as 6 posições dentro da região promotora do ITPR2 que foram utilizadas para avaliar os níveis de DNA metilado. (d) Níveis de metilação do DNA em fígados controles (pontos brancos) e em fígado de pacientes com CHC (pontos pretos). Valores expressos como média \pm SD. * $p < 0.05$.

RESEARCH ARTICLE | *Liver and Biliary Tract Physiology/Pathophysiology*

Cholesterol-enriched membrane microdomains are needed for insulin signaling and proliferation in hepatic cells

Matheus de Castro Fonseca,^{1,2} Andressa França,^{2,3} Rodrigo Machado Florentino,² Roberta Cristelli Fonseca,^{2,4} Antônio Carlos Melo Lima Filho,² Paula Teixeira Vieira Vidigal,⁵ André Gustavo Oliveira,^{2,4} Laurent Dubuquoy,⁶ Michael H. Nathanson,⁷ and M. Fátima Leite²

¹Brazilian Biosciences National Laboratory, Brazilian Center for Research in Energy and Materials, Campinas, Sao Paulo, Brazil; ²Department of Physiology and Biophysics, Federal University of Minas Gerais, Belo Horizonte, Minas Gerais, Brazil; ³Department of Molecular Medicine, Federal University of Minas Gerais, Belo Horizonte, Brazil; ⁴Center for Gastrointestinal Biology, Federal University of Minas Gerais, Belo Horizonte, Minas Gerais, Brazil; ⁵Department of Pathological Anatomy and Forensic Medicine, Federal University of Minas Gerais, Belo Horizonte, Brazil; ⁶Lille Inflammation Research International Center–UMR995, INSERM, University of Lille, Lille, France; and ⁷Section of Digestive Diseases, Department of Internal Medicine, Yale University, New Haven, Connecticut

Submitted 9 January 2018; accepted in final form 14 February 2018

Fonseca MC, França A, Florentino RM, Fonseca RC, Lima Filho ACM, Vidigal PT, Oliveira AG, Dubuquoy L, Nathanson MH, Leite MF. Cholesterol-enriched membrane microdomains are needed for insulin signaling and proliferation in hepatic cells. *Am J Physiol Gastrointest Liver Physiol* 315: G80–G94, 2018. First published February 22, 2018; doi:10.1152/ajpgi.00008.2018.—Hepatocyte proliferation during liver regeneration is a well-coordinated process regulated by the activation of several growth factor receptors, including the insulin receptor (IR). The IR can be localized in part to cholesterol-enriched membrane microdomains, but the role of such domains in insulin-mediated events in hepatocytes is not known. We investigated whether partitioning of IRs into cholesterol-enriched membrane rafts is important for the mitogenic effects of insulin in the hepatic cells. IR and lipid rafts were labeled in HepG2 cells and primary rat hepatocytes. Membrane cholesterol was depleted *in vitro* with methyl- β -cyclodextrin (M β CD) and *in vivo* with lovastatin. Insulin-induced calcium (Ca²⁺) signals studies were examined in HepG2 cells and in freshly isolated rat hepatocytes as well as in whole liver *in vivo* by intravital confocal imaging. Liver regeneration was studied by 70% partial hepatectomy (PH), and hepatocyte proliferation was assessed by PCNA staining. A subpopulation of IR was found in membrane microdomains enriched in cholesterol. Depletion of cholesterol from plasma membrane resulted in redistribution of the IR along the cells, which was associated with impaired insulin-induced nuclear Ca²⁺ signals, a signaling event that regulates hepatocyte proliferation. Cholesterol depletion also led to ERK1/2 hyperphosphorylation. Lovastatin administration to rats decreased hepatic cholesterol content, disrupted lipid rafts and decreased insulin-induced Ca²⁺ signaling in hepatocytes, and delayed liver regeneration after PH. Therefore, membrane cholesterol content and lipid rafts integrity showed to be important for the proliferative effects of insulin in hepatic cells.

NEW & NOTEWORTHY One of insulin's actions is to stimulate liver regeneration. Here we show that a subpopulation of insulin receptors is in a specialized cholesterol-enriched region of the cell membrane and this subfraction is important for insulin's proliferative effects.

Address for reprint requests and other correspondence: M. Fatima Leite, Federal Univ. of Minas Gerais, Av. Antonio Carlos 6627, Belo Horizonte, MG-CEP 31270-901, Brazil (e-mail: leitemd@ufmg.br).

calcium signaling; hepatocytes; insulin signaling; lipid rafts; liver regeneration

INTRODUCTION

The process of cell proliferation during liver regeneration is mediated largely by several growth factors, which act through specific receptor tyrosine kinases (RTKs) to restore liver function after either liver damage or resection (13, 26). Insulin is one of such growth factors, but the mechanism by which it regulates cell proliferation is less well understood when compared with hepatocyte growth factor (HGF) and epidermal growth factor (EGF) (9). RTK-induced hepatocyte proliferation depends on increases in nucleoplasmic Ca²⁺ (44), which is mediated by inositol 1,4,5-trisphosphate (InsP₃). This pathway is activated when RTKs involved in cell proliferation translocate from the plasma membrane to the nucleus to locally generate InsP₃ and increase intracellular Ca²⁺ (2, 18, 44, 47).

The mechanism by which the RTKs translocate to the nucleus varies among the different growth factors. Translocation of the HGF receptor (c-met) to the nucleus depends on the adaptor protein Gab1 and importin β 1 (18). In contrast, EGF receptor (EGFR) internalization occurs in a dynamin/clathrin-dependent manner (9), while the insulin receptor (IR) reaches the nuclear compartment in a clathrin/caveolin-dependent event (2). Even though the internalization pathways differ among these receptors, at the plasma membrane each RTK is suggested to be differentially associated with cholesterol-enriched membrane microdomains known as lipid rafts (42, 53, 68). Lipid rafts are dynamic assemblies of cholesterol and sphingolipids in the lipid bilayer that can include or exclude proteins to variable extents, working as signaling scaffolds for a number of receptors (53). Association of IR to lipid rafts in the membrane has been described in preadipocytes in which these structures are essential for insulin-induced cell metabolism (48). In addition, caveolae, which are a subtype of lipid rafts, participate in the functioning and endocytosis of the IR (2, 12, 55). Moreover, depleting caveolin in hepatocytes, the major raft protein involved in the assembly of caveolae, sig-

nificantly reduces translocation of IR to the nucleus and cell proliferation (2). However, the effect of cholesterol depletion on insulin-mediated Ca^{2+} signaling and the importance of cell membrane integrity for liver regeneration and insulin signaling are so far unknown. Here we investigated the role of cholesterol-enriched membrane microdomains in hepatocyte insulin signaling and liver regeneration.

MATERIALS AND METHODS

Animals. Male Wistar rats (200 g) obtained from Centro de Bioterismo-Federal University of Minas Gerais (CEBIO-UFGM, Minas Gerais, Brazil) were used for all studies. Animals were maintained on a standard diet and housed under a 12-h light-dark cycle. All procedures were approved by the Ethics Committee in Animal Experimentation of UFGM and followed National Institutes of Health *Guidelines For The Care And Use Of Laboratory Animals*.

Cells and cell culture. The liver cancer cell line HepG2 was obtained from the American Type Culture Collection (ATCC HB-8065). Cells were cultured at 37°C in 5% CO_2 in DMEM (Invitrogen/Thermo Fisher Scientific, Carlsbad, CA) supplemented with 10% fetal bovine serum, 1 mM sodium pyruvate, 50 units/ml penicillin, and 50 mg/ml streptomycin. Rat hepatocytes were isolated from livers of male Wistar rats (200 g; CEBIO-UFGM). Briefly, livers from control and lovastatin-treated animals were perfused with Hank's A and then Hank's B medium containing 0.05% collagenase (Roche Applied Science, Indianapolis, IN) and passed through a 40- μ m nylon mesh filter. Primary hepatocytes were cultured at 37°C in 5% CO_2 -95% O_2 in Williams' medium E (Invitrogen/Thermo Fisher Scientific, Carlsbad, CA) containing 10% fetal bovine serum, 50 units/ml penicillin, and 50 g/ml streptomycin and plated on collagen-coated coverslips (50 μ g/ml; BD Biosciences, San Jose, CA). Hepatocytes were used 4–6 h after isolation, as previously described (14). The round shape of the cells is the proper and well-accepted morphology of this cell type to study calcium and other intracellular signaling events in hepatocytes in vitro. Hepatocytes viability was greater than 85% assessed by trypan blue exclusion test.

To disrupt the cholesterol-bearing lipid rafts in vitro, hepatocytes or HepG2 cells were incubated with 10 mM methyl- β -cyclodextrine (M β CD) or (2-hydroxypropyl)- γ -cyclodextrin (HYCD) for 45 min at 37°C (40, 46, 50). Control dishes were treated with culture medium alone.

Detection of Ca^{2+} signals. Cells were loaded with 6 μ M Fluo-4/AM (Invitrogen, Grand Island, NY) for 30 min at 37°C in 5% CO_2 . Then, coverslips containing the cells were transferred to a custom-built perfusion chamber on the stage of a Zeiss LSM 510 confocal microscope. Nuclear and cytosolic Ca^{2+} signals were monitored in individual cells during stimulation with 300 nM insulin, 100 nM AVP, 50 ng/ml EGF, or 100 ng/ml HGF (Sigma, St. Louis, MO) using a $\times 63$, 1.4 NA objective lens, as previously described (14, 17, 18). Changes in fluorescence were normalized by the initial fluorescence (F0) and were expressed as (F/F0) \times 100 (11, 29).

Imaging Ca^{2+} signaling in vivo. Control or lovastatin-treated rats were starved for 6–8 h and then submitted to a surgical procedure for in vivo liver imaging as previously described (32). All the experiments were performed according to the circadian timing of the animal. Then, livers were loaded with the Ca^{2+} probe Fluo-4/AM at 50 μ M in saline solution for 10 min by soaking the organ into a chamber containing the probe. Careful preparation of the Fluo-4 AM dye, as well as optimization of incubation time and temperature, were necessary to ensure an optimal labeling of the organ. Ca^{2+} signals were detected and measured by time-lapse confocal microscopy (Nikon A1). Insulin (600 nM) was injected intravenously during 2 min after 30 s of imaging, and changes in fluorescence were normalized by the initial fluorescence (F0) and expressed as (F/F0) \times 100. Another

control group was constituted of nontreated animals injected with saline instead of insulin (data not shown).

Immunoblotting. HepG2 cells and primary hepatocytes were harvested as described, and protein content was quantified according to Bradford protein assay. Whole cell protein lysate (25 μ g) was separated by 12% SDS-PAGE gel. For protein detection, specific primary antibodies against IR (rabbit, 1:1,000; Abcam, Cambridge, UK), β -actin (mouse, 1:1,000; Santa Cruz Biotechnology, Dallas, TX), Caveolin-1 (rabbit, 1:1,000; Santa Cruz Biotechnology, Dallas, TX), ERK1/2-pERK1/2 (mouse, 1:1,000; Abcam, Cambridge, UK) and AKT-p-AKT (rabbit, 1:1,000; Sigma-Aldrich) were used. The primary antibody incubation proceeded for 2 h at room temperature. After being washed, blots were incubated with horseradish peroxidase-conjugated specific secondary antibody (anti-mouse or anti-rabbit, 1:5,000; Sigma-Aldrich) at room temperature for 1 h. Immuno detection was carried out using enhanced chemiluminescence. Western blot digital images (8-bit) were used for densitometric analysis in ImageJ (National Institutes of Health, Bethesda, MD). In brief, the mean gray value, expressed in arbitrary units for each band, was calculated by subtracting the mean gray value of a region of interest in a background area from the mean gray value of individual ROIs of identical dimensions encompassing each individual band. To measure relative phosphorylation of ERK1/2, cell protein lysates (25 μ g/lane) were separated in parallel in two gels. The first gel was used to probe for the phosphorylated form of ERK1/2 (pERK1/2), and the second gel was used to detect total ERK1/2 (ERK total). The relative expression of pERK1/2 was then calculated by dividing the densitometric values of pERK1/2 by those of ERK total. Western blot analysis was performed with protein extracts from three independent experimental conditions.

Immunofluorescence. Confocal immunofluorescence was performed as previously described (11). To microscopically visualize membrane domains enriched with GM1, a marker of cholesterol-enriched microdomains, hepatocytes or HepG2 cells were plated onto coverslips and incubated for 10 min with CTxB-Alexa 555 (1 g/ml) (goat, 1:250; Cayman Chemical, Ann Harbor, MI), washed, and then incubated for 10 min with anti-CTxB antibody for the same time for patching. After being washed, cells were fixed with paraformaldehyde (4% in PBS) at 25°C for 20 min. Cells were then labeled with the specific primary antibodies against c-met (mouse, 1:250; Abcam), EGFR (rabbit, 1:250; Abcam), or IR (rabbit, 1:250; Abcam) and subsequently incubated with appropriate fluorescent secondary antibody conjugated to Alexa 488 (1:5,000) (Invitrogen, Grand Island, NY). For Cav-1 labeling in tissue, liver sections from control and lovastatin-treated animals were fixed in 10% neutral buffered formalin and embedded in paraffin. Five-micromolar tissue sections were dewaxed, and antigen retrieval was performed in citrate buffer containing 0.6% hydrogen peroxide. Then, sections were incubated overnight anti-Cav-1 (rabbit, 1:200; Santa Cruz Biotechnology, Dallas, TX) and subsequently incubated with a specific secondary antibody conjugated to Alexa 555 (Invitrogen, Grand Island, NY). Images were obtained using a Zeiss LSM 510 confocal microscope using a $\times 63$, 1.4 NA objective lens. Single slices were collected with a length of 0.2 μ m. Z-stacks were reconstructed from a 30-slice image. At least 20 slices from 30 cells of each group were individually analyzed in different regions of interest at the cell membrane. Fluorescence intensity of each slice and channel were quantified using ImageJ (National Institutes of Health).

MTT assay. MTT assay is widely used for measuring the metabolic activity of cells based on their reduction potential. Studies in mammalian cells showed that the reduced pyridine nucleotide cofactor NADH is responsible for most MTT reduction (4). Therefore, to perform the assay, 10^4 HepG2 cells were seeded per well in a 96-well plate with 200 μ l of DMEM containing 10% FBS, 1% antibiotic-antimitotic and kept for 24 h. Cultured cells were exposed to 10 mM M β CD or HYCD for 45 min. After the exposition period, the drugs were removed and 60 μ l of fresh medium were added in each well. Then, 50 μ l of 2H-tetrazolium (Thermo Fisher Scientific, Waltham,

MA) solution (5 mg/ml) were added and the cells were incubated for 4 h. Afterwards, 40 μ l of SDS solution/4% HCl were placed and incubated for 12 h. Absorbance was quantified at 595 nm in a spectrophotometer. For each experimental condition, four different measurements were taken.

Glucose quantification. Glucose content in the blood or media was measured using an enzymatic colorimetric assay method (Analisa, Belo Horizonte, Brazil), according to the manufacturer's instructions. Concentration was calculated through the equation: (standard concentration/standard absorbance) \times sample absorbance and expressed by percentage of control (2).

Measurement of bromodeoxyuridine incorporation. Cell proliferation was measured by bromodeoxyuridine (BrdU) incorporation using an enzyme linked immunosorbent assay (Roche Applied Science, Indianapolis, IN), according to the manufacturer's instructions. HepG2 cells were plated in 96-well culture plates, starved for 24 h after adhered, and then treated with M β CD or HyCD for 45 min. Cells were then treated with 10% serum or different concentrations of insulin (300, 600, 1,200 nM) for 15 min, washed with PBS, and subsequently incubated with BrdU labeling solution in serum-free medium. BrdU incorporation was measured with a multiplate reader after 16 h, as described previously (2).

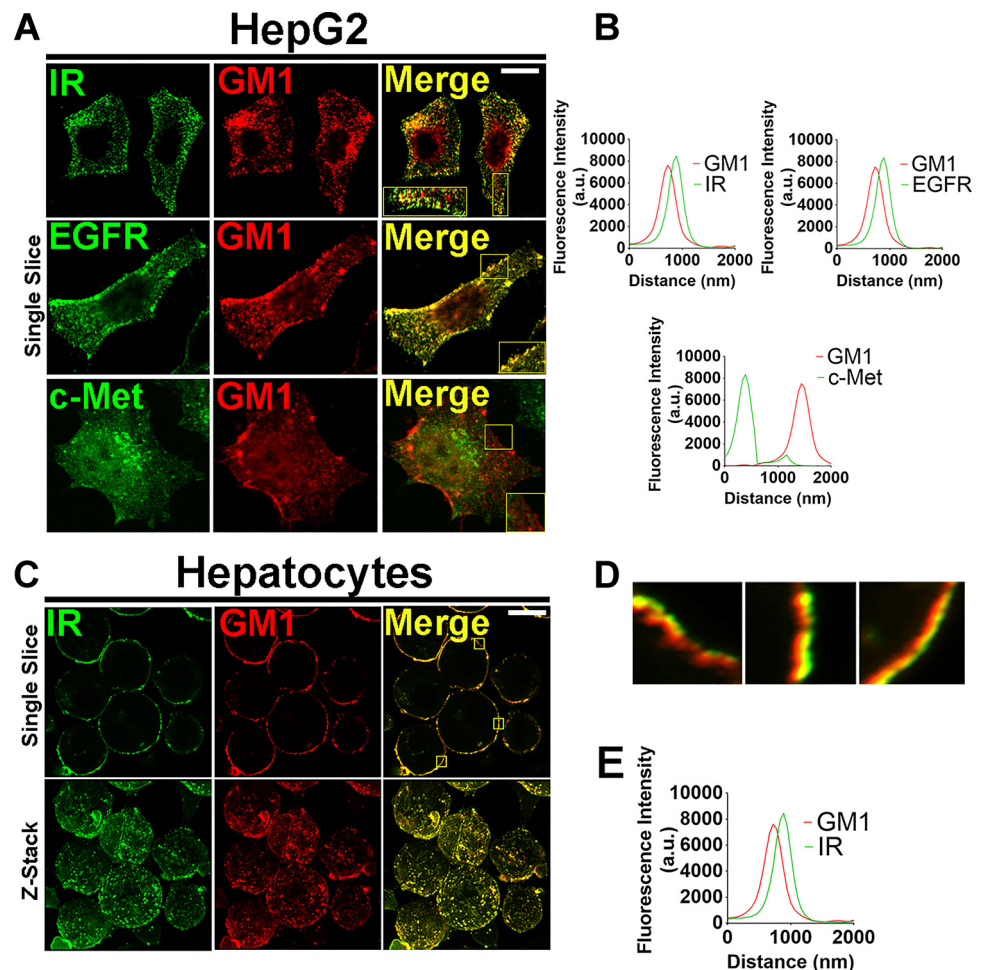
Lovastatin treatment and partial hepatectomy. Animals were treated intraperitoneally with saline solution or 15 mg \cdot kg $^{-1}\cdot$ day $^{-1}$ of lovastatin solution during 14 days before partial hepatectomy (PH) (5). The 70% PH was performed in adult male Wistar control and lovastatin-treated rats, as described (2, 23). Animals continued to be administrated with saline or lovastatin until the day of death. After 48 or 120 h of regeneration, livers were surgically removed and analyzed

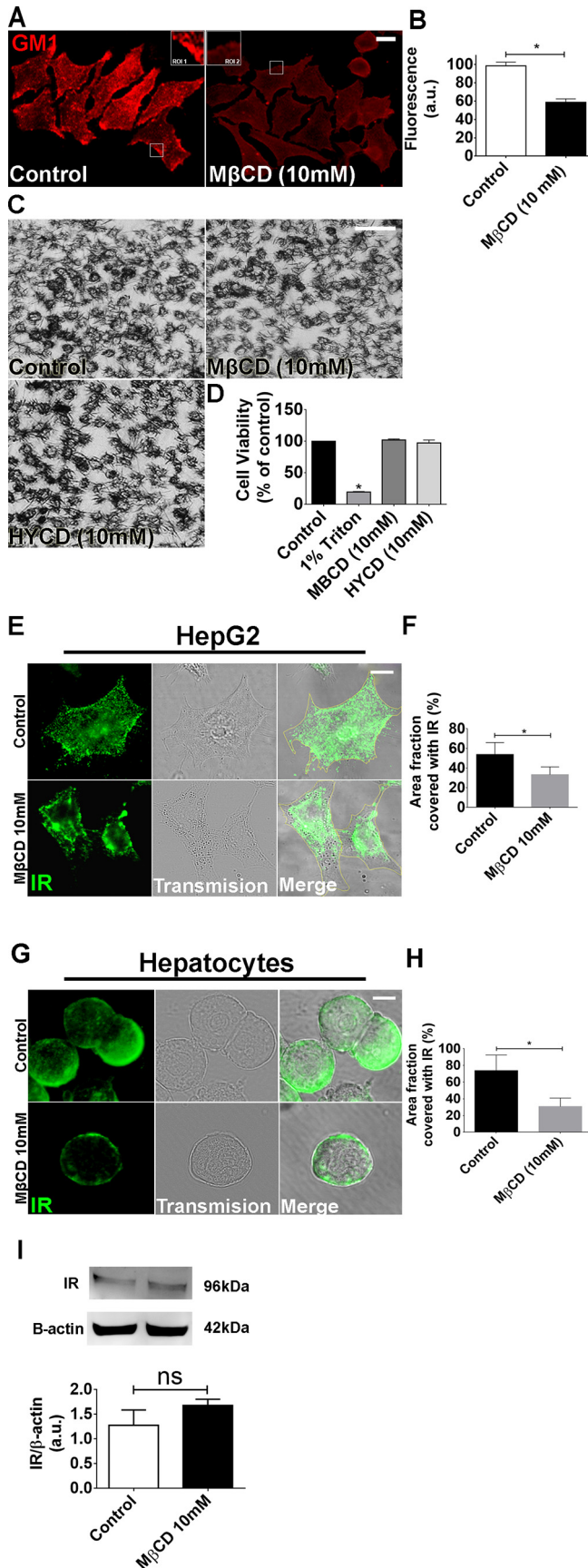
for measurement of liver/body weight ratio and cell proliferation index. Livers of nontreated and nonhepatectomized animals subjected to surgical stress (sham) were considered as controls.

Quantification of serum and liver cholesterol. Liver samples were collected during hepatectomy and submitted to lysis for 1.5 h in a 4°C ice-cold buffer solution containing 100 mM Tris-HCl (pH 8.0), 150 mM NaCl, 2 mM MgCl $_2$, 1% Triton X-100, 5 mM iodoacetamide, 0.025% NaN $_3$, 1 mM PMSF, 1 mM di-isopropylfluorophosphate, and 0.02 U/ml of aprotinin, with gentle stirring. Then, lysates were submitted to the Folch lipid extraction method, as described previously (14). For serum cholesterol analysis, blood samples were collected previously to the hepatectomy surgery, centrifuged and also submitted to Folch lipid extraction (14). Dried nonpolar lipids were subjected to cholesterol quantification using an Amplex Red Cholesterol Assay Kit (Invitrogen, Carlsbad, CA) according to the manufacturer's instructions.

Immunohistochemistry. Sections from sham, control, and lovastatin-treated animals' livers were fixed in 10% neutral buffered formalin and embedded in paraffin. Sections of 5 μ m were dewaxed and antigen retrieval was performed in citrate buffer containing 0.6% hydrogen peroxide. Nonspecific binding was blocked with 10% normal goat serum. Then, liver sections were immunostained with PCNA antibodies (1:50; DAKO Corporation, England, UK) or anti-insulin antibody (1:100, Abcam, Cambridge, UK) for 2 h at room temperature. After being washed in Tris-HCl buffer, sections were incubated for 30 min at room temperature with the biotinylated Link Universal Streptavidin-HRP (DAKO). The reactions were revealed by applying 3,3'-diaminobenzidine in chromogenic solution (DAKO). Sections were mounted in Hydromount (Fisher Scientific, Leicestershire, UK). Con-

Fig. 1. The insulin receptor (IR) is located in membrane microdomains enriched in cholesterol. **A:** representative confocal immunofluorescence of a single confocal slice of the IR, epidermal growth factor receptor (EGFR), and c-Met receptors (each receptor was labeled in green at left) and GM1 ganglioside labeled in red (middle) in HepG2 cells. Merged images show colocalization of IR and EGFR with GM1 but not c-Met with GM1 (right). **B:** quantification of fluorescence intensity on regions of interest, as represented by the tiny white squares in A. Superposition of the peaks indicates colocalization of green and red structures. (At least 20 slices from 30 cells of each group were individually analyzed). **C:** single confocal plane images of rat hepatocytes labeled for IR in green and GM1 in red (top) and z-stack images of the same cells (bottom). Merged images show colocalization of IR with GM1. **D:** high-resolution images of 3 regions of interest showing colocalization of green (IR) and red (GM1) structures. **E:** quantification of fluorescence intensity on delimited membrane regions of interest selected from several single slices of the merged images represented on D (representative small squares). Superposition of the peaks indicates colocalization of green and red structures. (At least 20 slices from 30 cells imaged of each group were individually analyzed). Scale bar = 10 μ M.





trols in which primary antibodies were omitted showed no specific staining. Histological images were obtained on a micro-camera (Olympus Q-color 5) coupled to a light microscope (Olympus BX43), captured with a plan-apochromatic objective ($\times 20$), and analyzed with Image-Pro Plus 4.5 (Media Cybernetics). To evaluate proliferation pattern, slice fields were randomly selected and a binary image was created to perform automatic quantification of positive PCNA nuclei.

Statistics. Results are expressed as mean values \pm SD. Prism (GraphPad, La Jolla, CA) was used for data analysis. Groups of data were compared using Student's *t*-test or one-way ANOVA (which was used because data sets included only one independent variable) followed by Bonferroni posttests, and $P < 0.05$ was taken to indicate statistical significance.

RESULTS

The IR resides in cholesterol-enriched membrane microdomains. Insulin regulates multiple effects in the liver, including metabolism and hepatocyte proliferation (2, 37). It has been suggested that membrane integrity and spatial localization of the IR in the plasma membrane are key regulators of insulin-mediated signaling events (63). Therefore, to investigate whether the IR is associated with cholesterol-enriched membrane domains, primary rat hepatocytes and HepG2 cells were stained for IR and the lipid raft marker GM1 and visualized by confocal microscopy. We observed that IR colocalizes with GM1 in both cell types (Fig. 1, A and C, top, and D). The peak of fluorescence emission intensity for IR and GM1, captured in a 0.2 μm -single-slice image, confirmed the close proximity of IR with GM1-enriched membrane microdomains (Fig. 1B, top left, and E). Besides insulin, other growth factors such as EGF and HGF are well known to regulate proliferation in hepatocytes (37). In addition, the EGF receptor is also localized to these membrane domains in different cancer cell lines (27, 30, 63, 67). However, less is known about the membrane location of EGFR and c-met in hepatocytes. We observed that, similar to the IR, EGFR colocalizes with GM1-enriched membrane area, while c-met does not (Fig. 1A, middle and bottom, and Fig. 1B, top right for EGFR and bottom for c-met). Therefore,

Fig. 2. Methyl- β -cyclodextrin (M β CD; 10 mM) treatment efficiently disrupts the lipid rafts without compromising cell viability. **A:** control and M β CD (10 mM)-treated HepG2 cells were labeled with CTxB to identify the lipid rafts. Regions of interest (ROI 1 and 2) show a zoom of the GM1 labeling in certain membrane areas. **B:** quantification of fluorescence intensity of A [control cells: 98.65 ± 4 arbitrary units (a.u.) vs. M β CD-treated cells: 58.8 ± 3.7 a.u.; $*P < 0.05$; $n = 159$ cells analyzed for each group]. **C:** bright-field images of MTT assay show cellular viability of control, M β CD, and (2-hydroxypropyl)- γ -cyclodextrin (HYCD)-treated cells. **D:** quantification of MTT assay in C. 1% Triton was used as a positive control of the technique (control: $100 \pm 0\%$; Triton-X: $19.63 \pm 0.4\%$; M β CD: $97.41 \pm 2.3\%$; HYCD: $102.2 \pm 0.7\%$; $*P < 0.05$; $n = 3$ individual experiments). **E:** Z-stack of control and M β CD-treated HepG2 cells immunostained for the insulin receptor (IR) (green). **F:** quantification of delimited (yellow traces) cell area covered with IR in HepG2 cells ($n = 55$ cells of 3 different experiments for each group were analyzed). **G:** Z-stack of control and M β CD-treated hepatocytes immunostained for IR (green). **H:** quantification of delimited (yellow traces) cell area covered with IR in hepatocytes ($n = 55$ cells of each 3 different experiments were analyzed; $*P < 0.05$; values expressed as means \pm SD). **I:** immunoblots for IR shows that there is no difference in the expression of IR between control and M β CD-treated HepG2 cells (control: 1.25 ± 0.27 vs. M β CD: 1.53 ± 0.11 ; $n = 3$ individual experiments). The values indicate the means \pm SD. $*P < 0.05$, difference between groups was statistically significant; ns, not significant. Data were analyzed by one-way ANOVA followed by Bonferroni posttests.

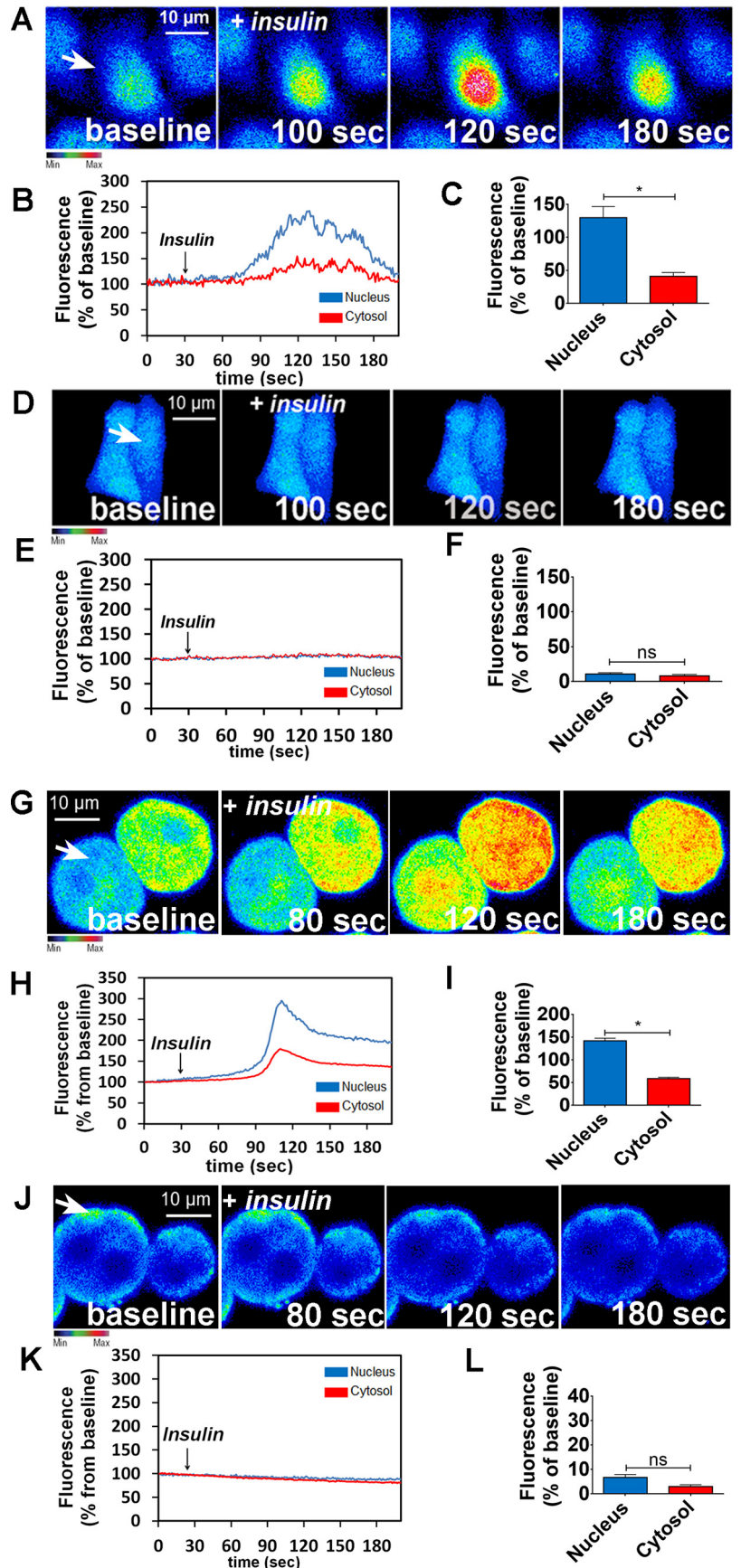


Fig. 3. Disruption of lipid rafts abolishes intracellular calcium signaling induced by insulin. *A*: confocal images of HepG2 cells loaded with Fluo-4/AM (6 μ M) and stimulated with insulin (300 nM). *A* and *D*: control (*A*) and methyl- β -cyclodextrin (M β CD)-treated cells (*D*) were analyzed. Images were pseudo-colored according to the scale shown at bottom. Scale bar = 10 μ m. *B* and *E*: observe that M β CD treatment nearly abolished the amplitude of Ca²⁺ signaling. Graphical representation of the fluorescence increase in the nucleus (blue traces) and cytosol (red traces) of a control (*B*) and an M β CD-treated cell (*E*), stimulated with insulin, pointed with an arrow. *C* and *F*: summary of insulin stimulation studies. *G* and *J*: confocal images of hepatocytes loaded with Fluo-4/AM (6 μ M) and stimulated with insulin (300 nM). Control (*G*) and M β CD-treated hepatocytes (*J*) were analyzed. *H* and *K*: Graphical representation of the fluorescence increase in the nucleus (blue traces) and cytosol (red traces) of a control (*H*) and an M β CD-treated cell (*K*) stimulated with insulin. *I* and *L*: summary of insulin stimulation studies (HepG2: control nucleus = 221.3 \pm 12%, control cytosol = 164 \pm 5%; *n* = at least 50 cells for each condition; hepatocytes: control nucleus = 142.3 \pm 2%, control cytosol = 58 \pm 2.2%; *n* = at least 50 cells for each condition). Values are means \pm SD of the peak Fluo-4 fluorescence acquired during the observation period, expressed as %baseline. **P* < 0.01, difference between groups was statistically significant; ns, not significant. Data were analyzed by one-way ANOVA followed by Bonferroni posttests.

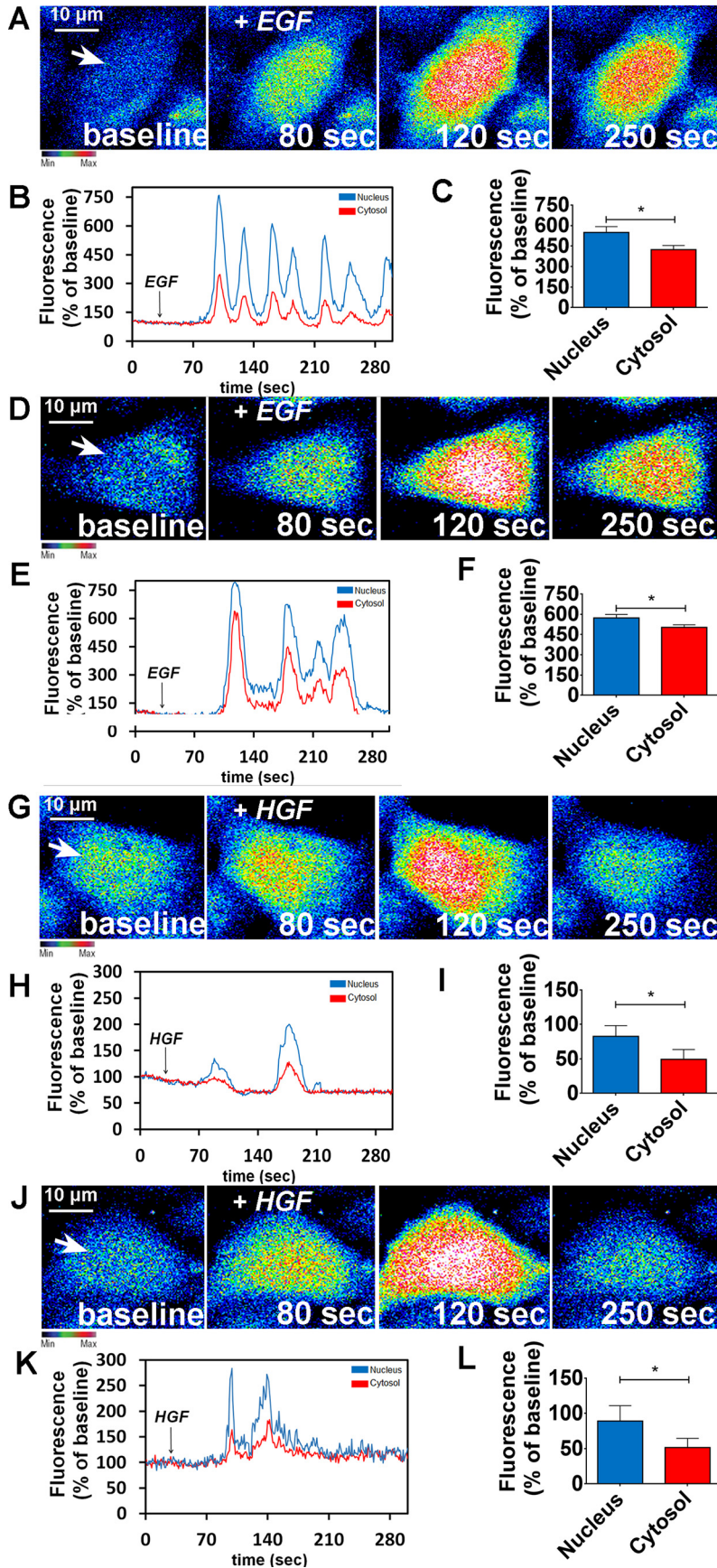


Fig. 4. Calcium signaling induced by epidemral growth factor (EGF) or hepatocyte growth factor (HGF) is not affected due lipid rafts disorganization. *A*: confocal images of HepG2 cells loaded with Fluo-4/AM (6 μM) and stimulated with EGF (50 ng/ml). *A* and *D*: control (*A*) and methyl- β -cyclodextrin (M β CD)-treated cells (*D*) were analyzed. Images were pseudocolored according to the scale shown at *bottom*. Scale bar = 10 μm . *B* and *E*: graphical representation of the fluorescence increase in the nucleus (blue traces) and cytosol (red traces) of a control (*B*) and an M β CD-treated cell stimulated with EGF (*E*), pointed with an arrow. *C* and *F*: summary of EGF stimulation studies. (control nucleus = $552.3 \pm 18\%$; control cytosol = $444 \pm 11\%$; $n =$ at least 50 cells for each condition). *G*: confocal images of HepG2 cells loaded with Fluo-4/AM (6 μM) and stimulated with HGF (100 ng/ml). *G* and *J*: control (*G*) and M β CD-treated cells (*J*) were analyzed. Images were pseudocolored according to the scale shown at *bottom*. Scale bar = 10 μm . *H* and *K*: graphical representation of the fluorescence increase in the nucleus (blue traces) and cytosol (red traces) of a control (*H*) and an M β CD-treated cell stimulated with HGF (*K*). *I* and *L*: summary of HGF stimulation studies (control nucleus = $589.3 \pm 11\%$; control cytosol = $498 \pm 6\%$; $n =$ at least 50 cells for each condition). Values are means \pm SD of the peak Fluo-4 fluorescence acquired during the observation period (expressed as % of baseline) and include the response from 55 control HepG2 cells and 55 M β CD-treated HepG2 cells, for each stimulus. The values indicate the means \pm SD. * $P < 0.01$, difference between groups was statistically significant; ns, not significant. Data were analyzed by one-way ANOVA followed by Bonferroni post tests.

the degree of association between RTKs and cholesterol-enriched domains at the plasma membrane varies among different receptors.

Disruption of lipid rafts redistributes the IR in hepatocytes and impairs insulin-induced Ca^{2+} signaling. IR activation in hepatocytes leads to $InsP_3$ -dependent nucleoplasmic Ca^{2+} signaling that induces proliferation (2, 47). In 3T3-L1 preadipocytes, inhibition of cholesterol biosynthesis disrupts lipid rafts, which affects IR activation (48). Thereby, we tested whether disruption of lipid rafts through cholesterol depletion would affect insulin signaling in the liver. Cells were treated

with 10 mM M β CD for 45 min. M β CD efficiently disrupted GM1-enriched microdomains, as expected (46), observed by the reduction of fluorescence intensity and change in the pattern of cholera toxin labeling (Fig. 2, A and B). M β CD treatment did not affect cell viability (Fig. 2, C and D). Triton-X treatment was used as a positive control and treatment with HYCD, an inactive analogue of M β CD (46), was used as negative control (Fig. 2, C and D). A reduction in the cell surface area labeled with IR was also observed (Fig. 2, E–H). To exclude the possibility of IR sequestration by M β CD, we performed Western blot of the cells after treatment with the

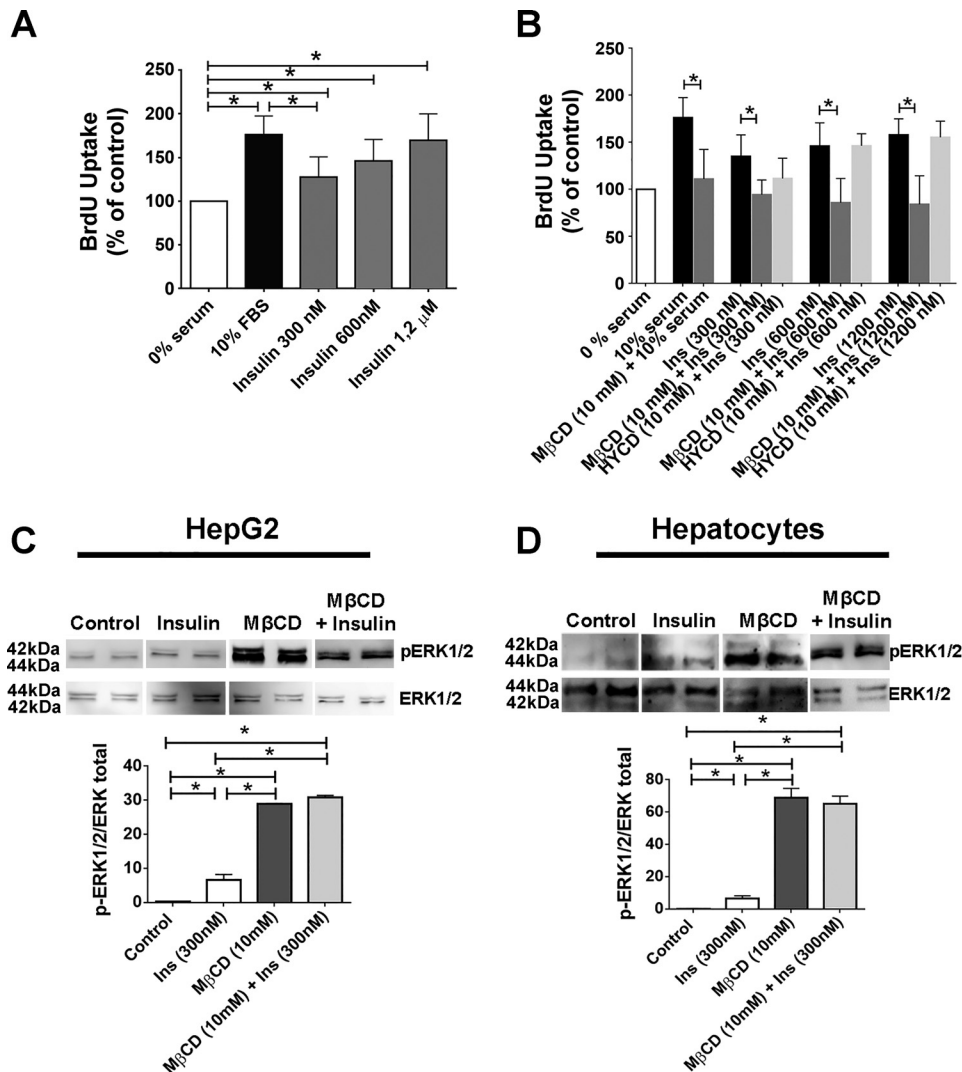


Fig. 5. Cell proliferation induced by insulin is reduced and pERK1/2 levels are increased when lipid rafts are disrupted. **A:** bromodeoxyuridine (BrdU) uptake in HepG2 cells before and after insulin (300, 600, and 1,200 nM, 14 h) stimulation. Ten percent of serum was used as additional positive control for cell proliferation [0% serum = 100%, 10% serum = 176 \pm 12%, insulin (300 nM) = 135 \pm 8%, insulin (600 nM) = 146 \pm 8%, insulin (1,200 nM) = 157 \pm 8%; n = at least 3 individual experiments in triplicate]. **B:** BrdU uptake in control and methyl- β -cyclodextrin (M β CD)-treated (45min) HepG2 cells before and after insulin (300, 600, and 1,200 nM, 14 h) stimulation. Ten percent serum and (2-hydroxypropyl)- γ -cyclodextrin (HYCD) was used as additional positive and negative controls, respectively, for cell proliferation [0% serum = 100%, 10% serum = 176 \pm 12%, M β CD + 10% serum = 110 \pm 11%, insulin (300 nM) = 135 \pm 8%, M β CD + insulin (300 nM) = 94.2 \pm 4.1%, insulin (600 nM) = 146 \pm 8%, M β CD + insulin (600 nM) = 85 \pm 6%, insulin (1,200 nM) = 157 \pm 8%, M β CD + insulin (1,200 nM) = 84 \pm 8%; n = 3 experiments in triplicate]. **C and D:** HepG2 cells (**C**) and rat hepatocytes (**D**) (control, insulin stimulated, M β CD treated) were stimulated with insulin and pERK1/2 levels were evaluated by immunoblot. M β CD + insulin samples shown in **C** and **D** were run on a separate gel. Densitometric analysis of the **C** and **D**, respectively, shows an increase on pERK1/2 levels in cells treated with M β CD [HepG2: control = 0.29 \pm 0.03 arbitrary units (a.u.), insulin (300 nM) = 6.61 \pm 1.6 a.u., M β CD + insulin = 30.7 \pm 0.5 a.u.; hepatocytes: control = 9.3 \pm 1.5 a.u., insulin (300 nM) = 31.19 \pm 0.8 a.u., M β CD + insulin = 66.33 \pm 9.4 a.u.; n = 3 independent experiments]. pERK and ERK blots shown in **C** and **D** are from the same experiments for each sample analyzed. The values indicate the means \pm SD. * P < 0.01, difference between groups was statistically significant; ns, not significant. Data were analyzed by one-way ANOVA followed by Bonferroni posttests.

drug. As observed, this IR reorganization was not due to a reduction of the total content IR in the cell, as demonstrated by Western blot (Fig. 2I).

To verify the relative importance of lipid raft integrity to insulin-induced Ca^{2+} signals, HepG2 cells and primary hepatocytes were treated with M β CD (10 mM) for 45 min and then stimulated with insulin (300 nM). HepG2 cells and primary hepatocytes loaded with the Ca^{2+} -sensitive dye Fluo-4/AM were examined by time-lapse confocal microscopy under control and M β CD-treated conditions. Nuclear and cytosolic Ca^{2+} signals were monitored. In control cells, insulin induced a transient Ca^{2+} response (Fig. 3, A–C, for HepG2 cells and Fig. 3, G–I, for hepatocytes). However, insulin-induced Ca^{2+} signaling was abolished in M β CD-treated cells (Fig. 3, D–F for HepG2 cells and Fig. 3, J–L, for hepatocytes). In contrast, cholesterol removal did not alter the pattern of Ca^{2+} signals induced by either EGF or HGF (Fig. 4). Together, these results provide evidence that lipid rafts are important for proper insulin-induced Ca^{2+} signaling in particular in hepatocytes.

Removal of membrane cholesterol impairs insulin-induced cell proliferation. The increase in nuclear Ca^{2+} triggered by insulin stimulates liver growth (2). Therefore, we investigated whether disruption of lipid rafts affects cell proliferation. HepG2 cells were synchronized in G0 by serum withdrawal and treated with M β CD for 45 min, and then, bromodeoxyuridine (BrdU) incorporation was measured. Insulin (300, 600, and 1,200 nM) and 10% fetal bovine serum each induced significant increases in BrdU uptake when compared with

unstimulated control cells, as expected (Fig. 5A). However, BrdU uptake was reduced in cholesterol-depleted cells, relative to insulin-stimulated control cells. HYCD was used as a negative control, showing the specificity of cholesterol removal for the reduction in insulin-induced cell proliferation (Fig. 5B). Additionally, ERK1/2, a MAPK kinase protein involved in the regulation of cell proliferation, was highly phosphorylated in HepG2 cells and primary hepatocytes pretreated with M β CD and then stimulated with insulin in comparison to control cells (Fig. 5, C and D). This finding is consistent with the previous observation that hyperphosphorylation of ERK1/2 inhibits cell proliferation (7, 38). Thus, cholesterol removal impairs the hepatic mitogenic effects of insulin. A role for lipid rafts in the more well-known metabolic effects of insulin has already been demonstrated (21, 59). For instance, in 3T3-L1 adipocytes in which lipid rafts were disrupted, insulin-induced glucose uptake was diminished due to reduced phosphatidylinositol 3-kinase (PI3K)-Akt/PKB activation, a pathway that takes part in cell metabolism (21, 59). We therefore evaluated whether glucose metabolism induced by insulin would also be affected by disrupting lipid rafts in hepatocytes. We observed a significant reduction in Akt phosphorylation in cells previously treated with M β CD (Fig. 6, A and B). In addition, M β CD-treated cells also exhibited diminished medium glucose uptake (Fig. 6, C and D). These data collectively provide evidence that membrane content of cholesterol plays a significant role for the proper regulation by insulin of glucose metabolism as well as cell proliferation in hepatocytes.

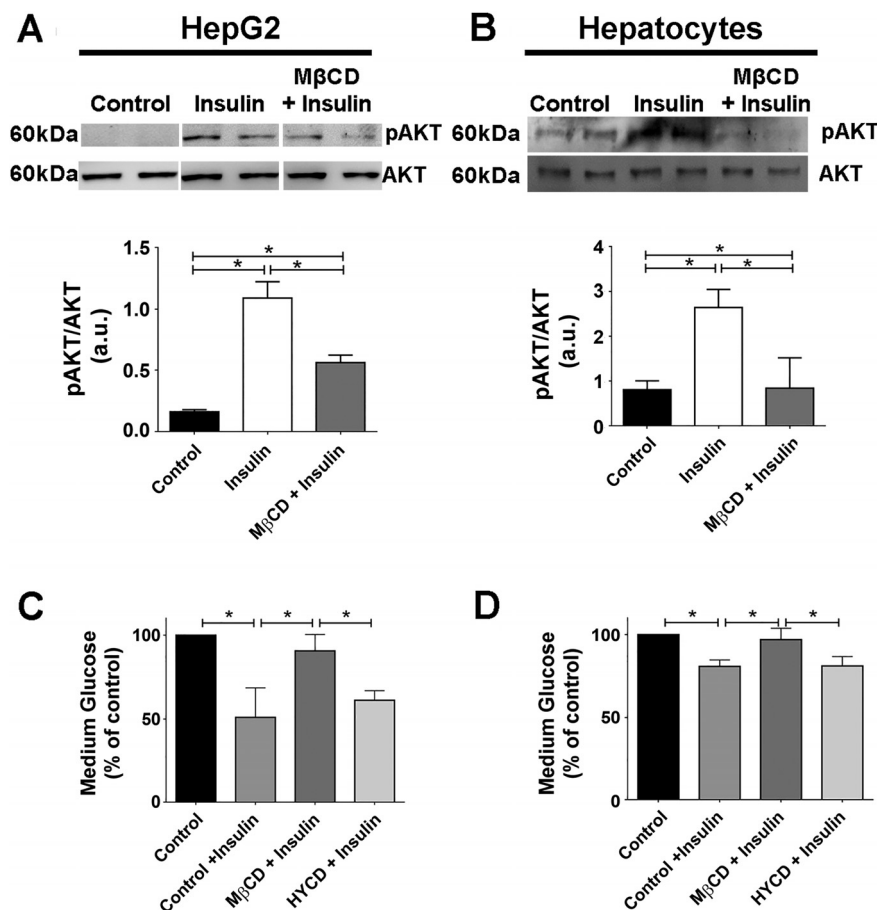


Fig. 6. The glucose uptake induced by insulin is reduced in cells treated with methyl- β -cyclodextrin (M β CD). *A* and *B*: HepG2 (*A*) and hepatocytes (*B*) (control, insulin stimulated, M β CD treated) were incubated with insulin for 15 min, and pAKT levels were evaluated by immunoblot. Densitometric analysis of the *A* and *B*, respectively, shows a decrease on pAKT levels in cells treated with M β CD [HepG2: control = 0.16 ± 0.01 arbitrary units (a.u.), insulin (300 nM) = 1.09 ± 0.13 a.u., M β CD + insulin = 0.56 ± 0.06 a.u.; hepatocytes: control = 0.80 ± 0.19 a.u., insulin (300 nM) = 2.6 ± 0.40 a.u., M β CD + insulin = 0.84 ± 0.6 a.u.; n = at least 3 individual experiments). All samples shown in *A* were run on the same gel but lanes were removed for final presentation. *C* and *D*: quantification of glucose uptake in the culture medium of HepG2 and hepatocytes for the control and M β CD-treated group. Incubation with (2-hydroxypropyl)- γ -cyclodextrin (HYCD) was used as a negative control [HepG2: control = 100%, control + insulin (300 nM) = $50.93 \pm 7.2\%$, M β CD + insulin = $83.15 \pm 8.4\%$, HYCD + insulin = $52.15 \pm 5.4\%$; hepatocytes: control = 100%, insulin (300 nM) = $80.91 \pm 2.25\%$, M β CD + insulin = $96.95 \pm 3.9\%$, HYCD + insulin = $81.22 \pm 3.2\%$; n = 3 individual experiments]. The values indicate the means \pm SD. * P < 0.01, difference between groups was statistically significant; ns, not significant. Data were analyzed by one-way ANOVA followed by Bonferroni posttests.

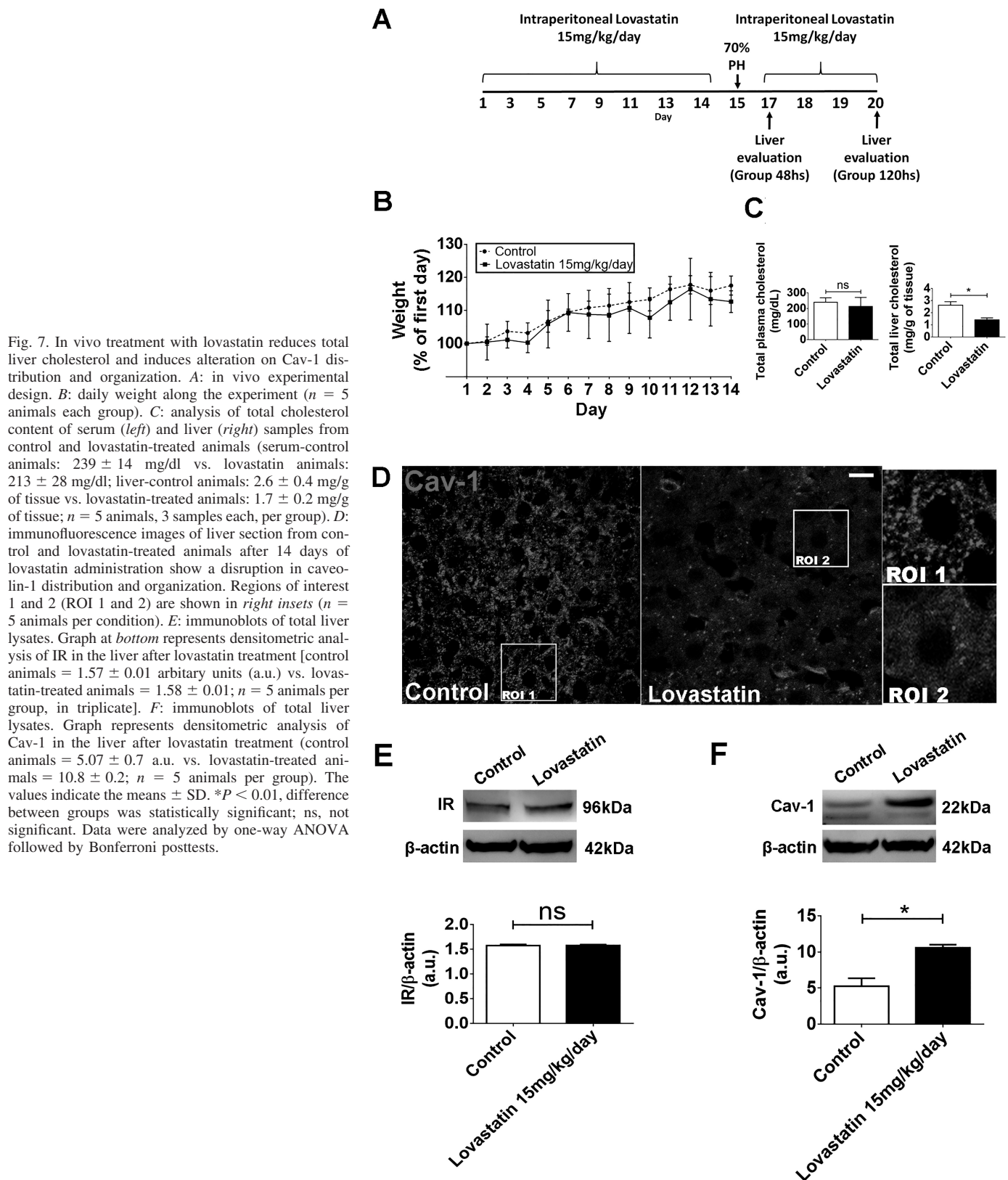


Fig. 7. In vivo treatment with lovastatin reduces total liver cholesterol and induces alteration on Cav-1 distribution and organization. *A*: in vivo experimental design. *B*: daily weight along the experiment ($n = 5$ animals each group). *C*: analysis of total cholesterol content of serum (*left*) and liver (*right*) samples from control and lovastatin-treated animals (serum-control animals: 239 ± 14 mg/dl vs. lovastatin animals: 213 ± 28 mg/dl; liver-control animals: 2.6 ± 0.4 mg/g of tissue vs. lovastatin-treated animals: 1.7 ± 0.2 mg/g of tissue; $n = 5$ animals, 3 samples each, per group). *D*: immunofluorescence images of liver section from control and lovastatin-treated animals after 14 days of lovastatin administration show a disruption in caveolin-1 distribution and organization. Regions of interest 1 and 2 (ROI 1 and 2) are shown in *right insets* ($n = 5$ animals per condition). *E*: immunoblots of total liver lysates. Graph at *bottom* represents densitometric analysis of IR in the liver after lovastatin treatment [control animals = 1.57 ± 0.01 arbitrary units (a.u.) vs. lovastatin-treated animals = 1.58 ± 0.01 ; $n = 5$ animals per group, in triplicate]. *F*: immunoblots of total liver lysates. Graph represents densitometric analysis of Cav-1 in the liver after lovastatin treatment (control animals = 5.07 ± 0.7 a.u. vs. lovastatin-treated animals = 10.8 ± 0.2 ; $n = 5$ animals per group). The values indicate the means \pm SD. * $P < 0.01$, difference between groups was statistically significant; ns, not significant. Data were analyzed by one-way ANOVA followed by Bonferroni posttests.

Lovastatin abolishes Ca^{2+} signaling induced by insulin and delays liver regeneration. To investigate the importance of lipid rafts for hepatic insulin signaling in vivo, we used lovastatin to inhibit HMG-CoA reductase, the major regulatory

enzyme in cholesterol biosynthesis (reviewed by Ref. 62). Rats treated with $15 \text{ mg} \cdot \text{kg}^{-1} \cdot \text{day}^{-1}$ of lovastatin for 14 days showed a reduction in total liver cholesterol with no significant changes in either their body weight or total serum cholesterol

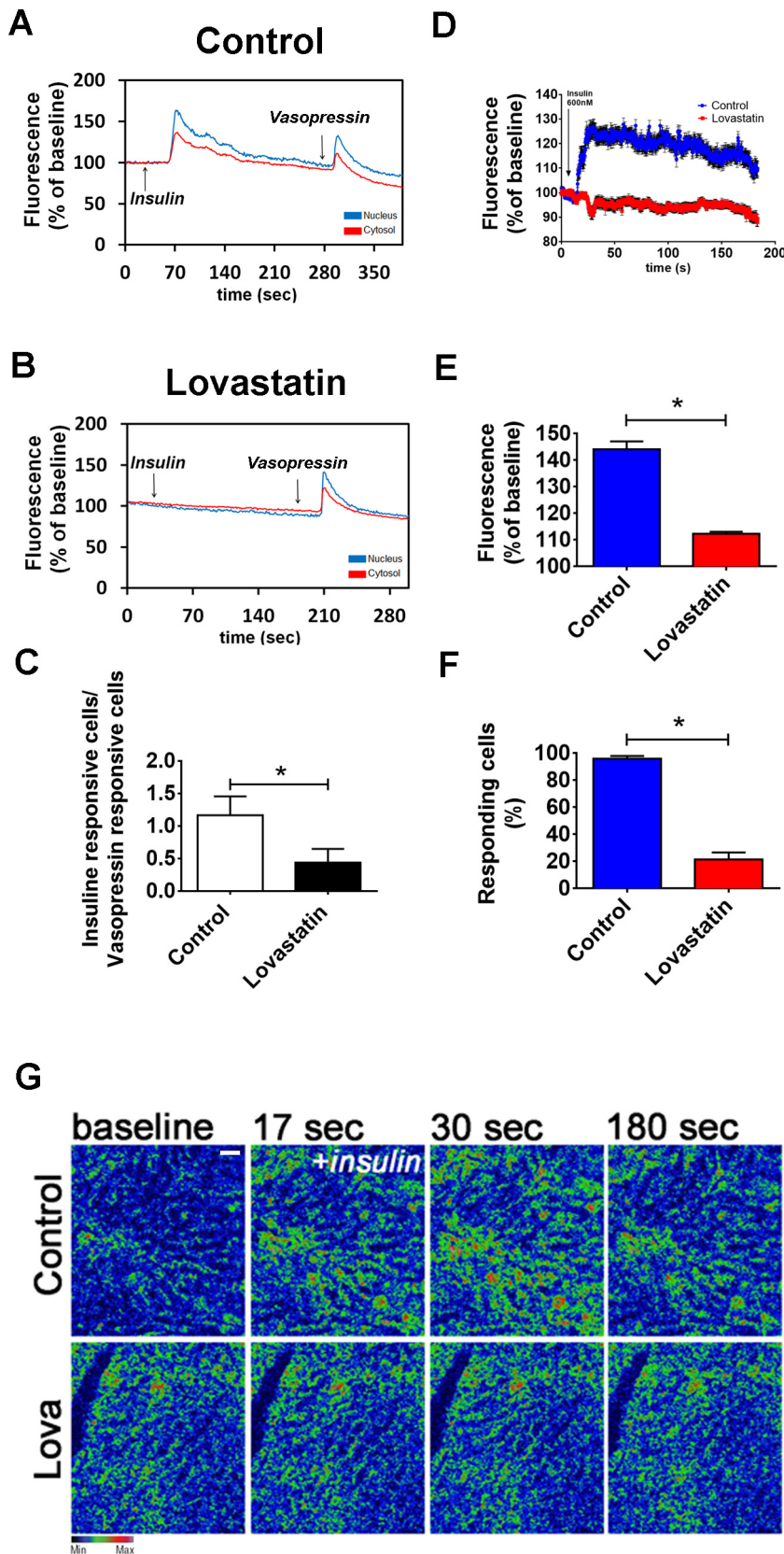


Fig. 8. In vivo treatment with lovastatin inhibits calcium signaling induced by insulin on rat hepatocytes and on in vivo intact liver. *A* and *B*: graphical representation of the fluorescence increase in the nucleus (blue traces) and cytosol (red traces) of a hepatocyte extracted from a control animal (*A*) and lovastatin-treated animal (*B*) stimulated with insulin (300 nM) and vasopressin (100 nM) (control nucleus = $165.3 \pm 2.5\%$; control cytosol = $124 \pm 1\%$; $n = 50$ cells from 3 animals per condition) (lovastatin nucleus = $102.3 \pm 3\%$; lovastatin cytosol = $124 \pm 2.6\%$; $n = 50$ cells from 3 animals per condition). *C*: graph showing the ratio of insulin responsive hepatocytes/vasopressin responsive hepatocytes from control and lovastatin-treated animals. Observe a reduced number of insulin responsive cells on the lovastatin group (control = 1.1 ± 0.3 cells vs. lovastatin = 0.44 ± 0.2 cells; $n = 5$ individual experiments per group, 50 cells for each group). *D*: graphical representation of the in vivo fluorescence increase of hepatocytes from the liver of control animals (blue traces) and lovastatin-treated animals (red traces) stimulated with insulin (600 nM) ($n = 4$ animals per group). *E*: summary of in vivo calcium studies in the liver induced by insulin (control = $143 \pm 3\%$ vs. lovastatin = $111 \pm 1\%$; $n = 5$ animals per group). *F*: graph showing the percentage of insulin-responsive cells of control and lovastatin-treated groups. Observe the reduced number of responsive hepatocytes of the liver from lovastatin-treated animals (control = $98 \pm 1\%$ vs. lovastatin = $20 \pm 4\%$; $n = 5$ animals and 5 fields analyzed per group). *G*: confocal images of livers loaded with Fluo-4/AM (6 μ M), stimulated with insulin (600 nM) and imaged in vivo. Images were pseudocolored according to the scale shown at the bottom. Scale bar = 40 μ M. Objective lens: $\times 20$. The values indicate the means \pm SD. * $P < 0.01$, difference between groups was statistically significant; ns, not significant. Data were analyzed by one-way ANOVA followed by Bonferroni posttests.

(Fig. 7, A–C). In addition, upon lovastatin treatment, Cav-1, a well-known component of the lipid rafts in hepatocytes (16, 22), changed its labeling pattern (Fig. 7D) as well as increased its expression level in the liver when compared with control saline-treated animals (Fig. 7F). These observed modifications were not accompanied by difference in the expression level of the insulin receptor (Fig. 7E).

To determine the effect of lovastatin on insulin-induced Ca^{2+} signals, hepatocytes from control and lovastatin-treated animals were isolated, loaded with Fluo-4/AM, and then examined by time-lapse confocal microscopy. Insulin-induced

Ca^{2+} signals were impaired in hepatocytes from the lovastatin-treated animals, while vasopressin-induced Ca^{2+} signals were not affected. To investigate whether lovastatin abolishment of the Ca^{2+} signaling induced by insulin was not due to the depletion of intracellular Ca^{2+} stores, vasopressin, another well-known intracellular Ca^{2+} mobilizing agonist in liver cells (41), was used to show the integrity of the intracellular Ca^{2+} store compartments. The ratio between insulin/vasopressin-responsive cells was also diminished in the lovastatin-treated group, when compared with the control group (Fig. 8C).

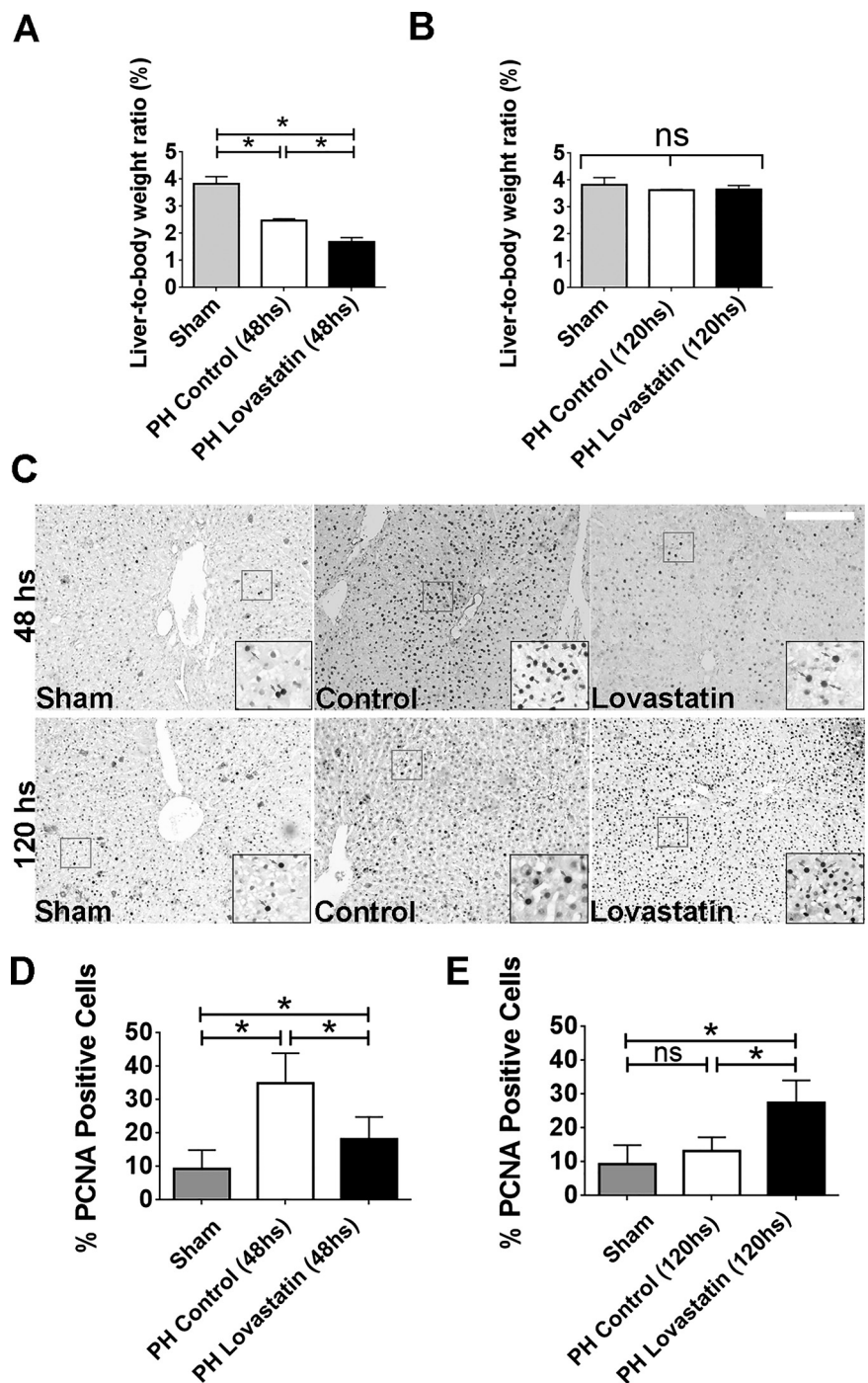


Fig. 9. In vivo treatment with lovastatin delays liver regeneration. **A** and **B**: liver/body weight ratio in control animals and subjected to lovastatin treatment after 48 h [sham = $3.82 \pm 0.15\%$, partial hepatectomy (PH) 48-h control = $2.6 \pm 0.14\%$ and PH 48-h lovastatin = $1.6 \pm 0.09\%$; **A**] and 120 h (sham = $3.82 \pm 0.16\%$, PH 120 h control = $3.6 \pm 0.01\%$ and PH 120 h lovastatin = $3.6 \pm 0.08\%$; **B**) of 70% partial hepatectomy ($n = 5$ animals per condition). **C**: immunohistochemistry images of liver section from control and lovastatin-treated animals 48 h (sham = $9.3 \pm 2.5\%$, PH 48-h control = $35 \pm 7\%$, PH 48-h lovastatin = $20 \pm 5\%$) and 120 h (sham = $9.3 \pm 2.5\%$, PH 120-h control = $13.2 \pm 1.6\%$, PH 120-h lovastatin = $27.4 \pm 3.2\%$) after PH ($n = 5$ slices per animal and 5 animals per group). PCNA staining in the nucleus (red arrows) allows identification of proliferation cells in each group. Scale bar = 50 μm . Objective lens: $\times 10$. **D** and **E**: quantification of PCNA-positive cells in control and lovastatin-treated animals after 48 h (**D**) and 120 h (**E**) of partial hepatectomy ($n = 5$ slices per animals and 5 animals per condition). * $P < 0.01$, difference between groups was statistically significant; ns, not significant. Data were analyzed by one-way ANOVA followed by Bonferroni posttests.

To determine whether lovastatin altered insulin-induced Ca^{2+} signals in vivo, Ca^{2+} was measured in hepatocytes in intact livers of control and lovastatin-treated rats. A prominent reduction in the Ca^{2+} signaling response to intravenous insulin (600 nM) was observed in the livers of lovastatin-treated animals (Fig. 8, D, E, and G; see also supplemental files S1 and S2; supplemental material for this article is available online at the Journal website). The number of insulin-responsive hepatocytes in the lovastatin group was also reduced (Fig. 8F). These findings show that disruption of lipid rafts decreases insulin-induced Ca^{2+} signaling in hepatocytes in vivo.

Hepatocytes have a unique capability to switch from a quiescent to a proliferative state in response to a reduction in cellular mass after surgical resection (13). The activation of certain membrane receptors is crucial for this process. To investigate the role of lipid rafts in liver regeneration, control and lovastatin-treated animals were subjected to 70% PH. Liver weight/body weight ratio was lower in lovastatin-treated animals than in controls, measured 48 h after PH (Fig. 9, A and B). No differences were observed between the groups 120 h after PH. To complement these observations, PCNA staining was performed in the liver slices of control and lovastatin-treated animals. The number of PCNA-positive cells was significantly greater in the control group than in the lovastatin-treated group, measured 48 h after PH (Fig. 9, C and D). In contrast, the opposite was observed 120 h after PH. Lovastatin-treated animals had a higher number of PCNA-positive cells when compared with the control group (Fig. 9, C and E). Since insulin acts mainly in the first hours during the process of liver regeneration (13, 37), we aimed to check the distribution of the IR after 48 h of PH in liver slices of both groups. Although not very striking, it can be noticed that the control group presents an increased accumulation of the IR in the nucleus, which stimulates cell proliferation (Fig. 10A). On the other hand, lovastatin-treated animals show IR mainly along the cell membrane (Fig. 10A). Taking together, these findings support the idea that cholesterol membrane reduction that might cause disruption of lipid rafts leads to impaired insulin signaling, resulting in delayed liver regeneration.

DISCUSSION

This work suggests that membrane cholesterol removal impairs insulin-induced Ca^{2+} signals, which in turn contributes to a reduced hepatic cell proliferation.

Liver regeneration after partial hepatectomy can be divided into several phases (13, 37, 66). In the first 2 h after injury, hepatocytes are activated to reenter cell cycle to proliferate. Thereby, an intense proliferation of hepatocytes leads to the restoration of much of the liver parenchyma during the following 48 h. Finally, the regeneration process finishes with replacement of liver mass occurring mainly because of proliferation of preexisting hepatocytes rather than by the activation of a progenitor cell compartment (10, 13). This entire process is coordinated by growth factors, cytokines, hormones, and factors from the extracellular matrix, a number of which have the ability to initiate and modulate the intracellular Ca^{2+} signals in hepatocytes (2, 20, 24), including insulin.

Since its discovery, insulin has been described as an anabolic hormone with a wide range of effects on cellular metabolism, inducing the uptake of glucose from the bloodstream, as

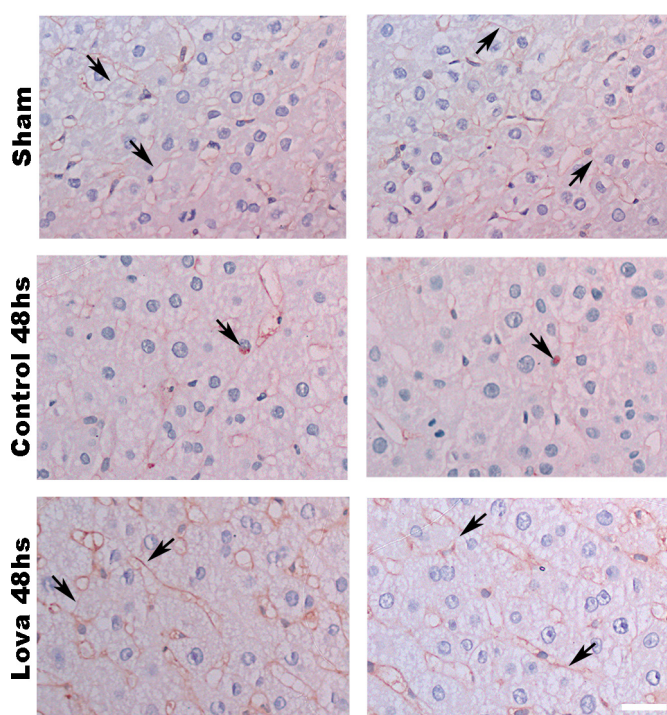


Fig. 10. Insulin receptor (IR) changes its distribution after lovastatin treatment followed by 70% hepatectomy. Immunohistochemistry images of liver sections from sham, control and lovastatin-treated animals 48 h after partial hepatectomy (PH). As can be seen immunohistochemistry, images never detect the IR in the hepatocyte nucleus in sham and lovastatin-treated group (observe the membrane concentration of IR) (top and bottom) but occasionally detect it in control animals (middle) 48 h after PH. Arrows: IR staining on cell membrane or in hepatocyte nuclei; scale bar = 40 μm . Objective lens: $\times 100$.

well as stimulating synthesis and inhibiting the degradation of glycogen, proteins, and lipids (57). In addition to these well-known effects on metabolism, insulin plays an important role in stimulating cell proliferation. Insulin-induced mitogenic effects were first described nearly 100 yr ago (17) by observation of the effects of insulin addition to chicken fibroblasts in culture. Multiple subsequent lines of evidence also point to insulin as a potent mitogen, including for 3T3 cells (25), rat hepatocytes, and hepatoma cells (2, 28), renal cell lines (60), and melanoma cells (33) among others (reviewed by Ref. 57). In the liver, insulin has strong metabolic (35, 49); revised by Ref. 1) and mitogenic effects (2, 23, 36), having significant functions during the process of hepatic regeneration through the activation of its receptor, located in the plasma membrane. Here we show that there is a close interaction between the IR and the cholesterol-enriched membrane microdomains in liver cells. As we clearly demonstrated here, HGF as well as EGF, other important growth factors also involved in liver regeneration, do not depend on membrane cholesterol integrity to trigger nuclear Ca^{2+} increase in hepatocytes and therefore cell proliferation. In addition, we also showed that cholesterol integrity at the plasma membrane level is important for the insulin/IR pathway that triggers signaling events that culminate in nuclear Ca^{2+} increase, known to be an absolute requirement for insulin to regulate hepatocyte proliferation (2).

The metabolic actions of insulin in the liver are mainly mediated by the PI3K-Akt/PKB pathway. Akt is activated at the plasma membrane upon IR-mediated phosphorylation of

PI3K (59). Previous studies have shown that when membrane cholesterol is depleted in 3T3-L1 adipocytes, AKT phosphorylation and glucose uptake are reduced (48). The current work extends this concept by providing evidence that disruption of cholesterol-enriched membrane microdomains due to cholesterol removal impairs the metabolic effects induced by insulin, as well as liver regeneration after PH.

Since its formulation more than 20 yr ago (6, 52, 54), the lipid raft theory became a turning point regarding cell signaling, especially with regards to membrane receptors. Treatment with M β CD, which disrupts rafts due to cholesterol removal (39, 40, 46), provides insights regarding how insulin signaling is affected once lipid content of liver cell membranes is modified. However, it is important to mention that although treatment of cells with this cyclodextrin leads to a selective extraction of cholesterol from the plasma membrane, hence disrupting the lipid rafts, it may also impair the formation of clathrin-coated endocytic vesicles (45). In addition, it was previously shown that acute cholesterol depletion specifically decreased the rate of internalization of transferrin receptor, nevertheless, receptor trafficking back to the cell surface was not affected (58). Thereby, the precise mechanism by which cholesterol depletion with M β CD impairs insulin signaling is still opened to further investigation.

It has been shown that a subpopulation of IR on the plasma membrane is associated with caveolin-enriched membrane domains (3, 15), but the functional significance of this has not been clear. We showed that lovastatin treatment rearranged caveolin organization on the cell membrane and led to an overexpression of this protein. This may be due to ERK activation, because there is a close cross talk between Cav-1 and ERK (19), in which phosphorylation of ERK leads to upregulation of Cav-1 in hepatocytes (34). A relevant increase in hepatic Cav-1 was also found in cirrhosis and chronic alcoholic fatty liver (51, 65), indicating its essential role for cholesterol trafficking and lipid homeostasis (43, 55). In addition, although ERK activation is closely related to cell proliferation, in the setting of chronically increased p-ERK, proliferative activity becomes inhibited due to accumulation of p21cip1, an inhibitor of cell cycle entry (7, 38). Therefore, besides contributing to Cav-1 overexpression, hyperactivation of ERK also led to arrest of hepatocytes in the cell cycle causing an impairment in cell proliferation.

Lovastatin is a potent inhibitor of HMG-CoA reductase, which decreases cholesterol biosynthesis (reviewed by Ref. 62). In fact, we observed that animals treated with lovastatin had a marked reduction in total cholesterol in the liver, without weight loss. It is suggested that lovastatin may induce cell cycle arrest in G₁ phase. This robust antiproliferative activity remains intact in many cancer cells (64). Lovastatin is a potent mitotic inhibitor in several cell types, including B-lymphocytes, glial cells, and mesangial cells (8, 56, 61). However, the precise mechanism by which this drug is able to induce cell arrest is not completely understood. Uptake of glucose in cells treated with statins is also significantly reduced, which may contribute to the antiproliferative effect of this drug (31). Regarding liver cell proliferation, lovastatin reduced the size and number of preneoplastic nodules in a model of chemical carcinogenesis in rat liver (5). In addition, Ca²⁺ signals induced by insulin, HGF, EGF, etc. in the liver are important for hepatocyte proliferation (18, 44, 47). The current work pro-

vides evidence that lovastatin impairs insulin-induced Ca²⁺ signaling in the liver, resulting in delayed liver regeneration. In our current work, we are not stating that statins are preventing liver regeneration, since after 120 h of hepatectomy both control and statin-treated animals presented the same level of regeneration. Hence, it is possible that the impairment in insulin-induced Ca²⁺ signaling affects hepatocyte reentry into cell cycle in the early phase of liver regeneration.

These findings provide the first in vivo evidence for the general importance of cholesterol membrane in liver regeneration. However, further studies are needed to unravel the importance of these membrane microdomains in each specific phase of liver regeneration, as well as their role in different liver cell types throughout the process of regeneration.

ACKNOWLEDGMENTS

We acknowledge the technical assistance of Gilson Nogueira, Conselho Nacional de Desenvolvimento Científico e Tecnológico, Fundação de Apoio a Pesquisa do Estado de Minas Gerais, Coordenação de Aperfeiçoamento de Pessoal de Nível Superior, National Institutes of Health, and National Institute on Alcohol Abuse and Alcoholism for funding this work. We also thank the Liver Center at Federal University of Minas Gerais for technical support.

GRANTS

This study was financially supported by Conselho Nacional de Desenvolvimento Científico e Tecnológico (CNPq); Fundação de Apoio a Pesquisa do Estado de Minas Gerais (FAPEMIG); Coordenação de Aperfeiçoamento de Pessoal de Nível Superior, and Instituto Nacional de Ciência e Tecnologia (Brazil); National Institute of Diabetes and Digestive and Kidney Diseases Grants P01-DK-57751, P30-DK-34989, R56-DK-99470, and R01-DK-45710; CNPq/Ministério da Ciência, Tecnologia, Inovações e Comunicações Grant 300990/201476; National Institute on Alcohol Abuse and Alcoholism Grant 1U01-AA-021908; and FAPEMIG/Région Hauts de France.

DISCLOSURES

No conflicts of interest, financial or otherwise, are declared by the authors.

AUTHOR CONTRIBUTIONS

M.d.C.F., A.G.O., and M.F.L. conceived and designed research; M.d.C.F., A.F., R.M.F., R.C.F., A.C.M., and P.T.V.V. performed experiments; M.d.C.F., A.F., A.G.O., and M.F.L. analyzed data; M.d.C.F., A.F., and M.F.L. interpreted results of experiments; M.d.C.F. prepared figures; M.d.C.F., A.G.O., and M.F.L. drafted manuscript; M.d.C.F., M.H.N., and M.F.L. edited and revised manuscript; M.d.C.F., P.T.V.V., A.G.O., L.D., M.H.N., and M.F.L. approved final version of manuscript.

REFERENCES

1. Agius L. Glucokinase and molecular aspects of liver glycogen metabolism. *Biochem J* 414: 1–18, 2008. doi:10.1042/BJ20080595.
2. Amaya MJ, Oliveira AG, Guimarães ES, Casteluber MC, Carvalho SM, Andrade LM, Pinto MC, Mennone A, Oliveira CA, Resende RR, Menezes GB, Nathanson MH, Leite MF. The insulin receptor translocates to the nucleus to regulate cell proliferation in liver. *Hepatology* 59: 274–283, 2014. doi:10.1002/hep.26609.
3. Balbis A, Baquiran G, Mounier C, Posner BI. Effect of insulin on caveolin-enriched membrane domains in rat liver. *J Biol Chem* 279: 39348–39357, 2004. doi:10.1074/jbc.M404282020.
4. Berridge MV, Tan AS. Characterization of the cellular reduction of 3-(4,5-dimethylthiazol-2-yl)-2,5-diphenyltetrazolium bromide (MTT): subcellular localization, substrate dependence, and involvement of mitochondrial electron transport in MTT reduction. *Arch Biochem Biophys* 303: 474–482, 1993. doi:10.1006/abbi.1993.1311.
5. Björkhem-Bergman L, Acimovic J, Torndal UB, Parini P, Eriksson LC. Lovastatin prevents carcinogenesis in a rat model for liver cancer. Effects of ubiquinone supplementation. *Anticancer Res* 30: 1105–1112, 2010.


6. Brown DA, London E. Functions of lipid rafts in biological membranes. *Annu Rev Cell Dev Biol* 14: 111–136, 1998. doi:10.1146/annurev.cellbio.14.1.111.
7. Chambard JC, Lefloch R, Pouyssegur J, Lenormand P. ERK implication in cell cycle regulation. *Biochim Biophys Acta* 1773: 1299–1310, 2007. doi:10.1016/j.bbamcr.2006.11.010.
8. Choi JW, Jung SE. Lovastatin-induced proliferation inhibition and apoptosis in C6 glial cells. *J Pharmacol Exp Ther* 289: 572–579, 1999.
9. De Angelis Campos AC, Rodrigues MA, de Andrade C, de Goes AM, Nathanson MH, Gomes DA. Epidermal growth factor receptors destined for the nucleus are internalized via a clathrin-dependent pathway. *Biochem Biophys Res Commun* 412: 341–346, 2011. doi:10.1016/j.bbrc.2011.07.100.
10. Duncan AW, Dorrell C, Grompe M. Stem cells and liver regeneration. *Gastroenterology* 137: 466–481, 2009. doi:10.1053/j.gastro.2009.05.044.
11. Echevarria W, Leite MF, Guerra MT, Zipfel WR, Nathanson MH. Regulation of calcium signals in the nucleus by a nucleoplasmic reticulum. *Nat Cell Biol* 5: 440–446, 2003. doi:10.1038/ncb980.
12. Fagerholm S, Ortegren U, Karlsson M, Ruishalme I, Strålfors P. Rapid insulin-dependent endocytosis of the insulin receptor by caveolae in primary adipocytes. *PLoS One* 4: e5985, 2009. doi:10.1371/journal.pone.0005985.
13. Fausto N, Campbell JS, Riehle KJ. Liver regeneration. *Hepatology* 43, Suppl 1: S45–S53, 2006. doi:10.1002/hep.20969.
14. Folch J, Lees M, Sloane Stanley GH. A simple method for the isolation and purification of total lipides from animal tissues. *J Biol Chem* 226: 497–509, 1957.
15. Foti M, Porcheron G, Fournier M, Maeder C, Carpentier JL. The neck of caveolae is a distinct plasma membrane subdomain that concentrates insulin receptors in 3T3-L1 adipocytes. *Proc Natl Acad Sci USA* 104: 1242–1247, 2007. doi:10.1073/pnas.0610523104.
16. Garg A, Agarwal AK. Caveolin-1: a new locus for human lipodystrophy. *J Clin Endocrinol Metab* 93: 1183–1185, 2008. doi:10.1210/jc.2008-0426.
17. Gey GT, Thalheimer W. Observations on the effects of insulin introduced into the medium of tissue cultures. *JAMA* 82: 1609–1609, 1924. doi:10.1001/jama.1924.26520460003014d.
18. Gomes DA, Rodrigues MA, Leite MF, Gomez MV, Varnai P, Balla T, Bennett AM, Nathanson MH. c-Met must translocate to the nucleus to initiate calcium signals. *J Biol Chem* 283: 4344–4351, 2008. doi:10.1074/jbc.M706550200.
19. Gortazar AR, Martin-Millan M, Bravo B, Plotkin LI, Bellido T. Crosstalk between caveolin-1/extracellular signal-regulated kinase (ERK) and β -catenin survival pathways in osteocyte mechanotransduction. *J Biol Chem* 288: 8168–8175, 2013. doi:10.1074/jbc.M112.437921.
20. Guerra MT, Fonseca EA, Melo FM, Andrade VA, Aguiar CJ, Andrade LM, Pinheiro AC, Casteluber MC, Resende RR, Pinto MC, Fernandes SO, Cardoso VN, Souza-Fagundes EM, Menezes GB, de Paula AM, Nathanson MH, Leite MF. Mitochondrial calcium regulates rat liver regeneration through the modulation of apoptosis. *Hepatology* 54: 296–306, 2011. doi:10.1002/hep.24367.
21. Gustavsson J, Parpal S, Strålfors P. Insulin-stimulated glucose uptake involves the transition of glucose transporters to a caveolae-rich fraction within the plasma membrane: implications for type II diabetes. *Mol Med* 2: 367–372, 1996.
22. Hayashi YK, Matsuda C, Ogawa M, Goto K, Tominaga K, Mitsuhashi S, Park YE, Nonaka I, Hino-Fukuyo N, Haginoya K, Sugano H, Nishino I. Human PTRF mutations cause secondary deficiency of caveolins resulting in muscular dystrophy with generalized lipodystrophy. *J Clin Invest* 119: 2623–2633, 2009. doi:10.1172/JCI38660.
23. Higgins GM, Anderson RM. Experimental pathology of the liver—restoration of the liver of the white rat following partial surgical removal. *Arch Patol* 12: 186–202, 1931.
24. Hirata K, Puhl T, O'Neill AF, Dranoff JA, Nathanson MH. The type II inositol 1,4,5-trisphosphate receptor can trigger Ca^{2+} waves in rat hepatocytes. *Gastroenterology* 122: 1088–1100, 2002. doi:10.1053/gast.2002.32363.
25. Holley RW, Kiernan JA. Control of the initiation of DNA synthesis in 3T3 cells: low-molecular weight nutrients. *Proc Natl Acad Sci USA* 71: 2942–2945, 1974. doi:10.1073/pnas.71.8.2942.
26. Huang W, Ma K, Zhang J, Qatanani M, Cuvillier J, Liu J, Dong B, Huang X, Moore DD. Nuclear receptor-dependent bile acid signaling is required for normal liver regeneration. *Science* 312: 233–236, 2006. doi:10.1126/science.1121435.
27. Irwin ME, Bohin N, Boerner JL. Src family kinases mediate epidermal growth factor receptor signaling from lipid rafts in breast cancer cells. *Cancer Biol Ther* 12: 718–726, 2011. doi:10.4161/cbt.12.8.16907.
28. Leffert H. Glucagon, insulin and their hepatic receptors: an endocrine pattern characterizing hepatoproliferative transitions in the rat. In: *Glucagon: Its Role in Physiology and Clinical Medicine*. New York, Springer, 1977.
29. Leite MF, Thrower EC, Echevarria W, Koulen P, Hirata K, Bennett AM, Ehrlich BE, Nathanson MH. Nuclear and cytosolic calcium are regulated independently. *Proc Natl Acad Sci USA* 100: 2975–2980, 2003. doi:10.1073/pnas.0536590100.
30. Liu L, Brown D, McKee M, Lebrasseur NK, Yang D, Albrecht KH, Ravid K, Pilch PF. Deletion of Cavin/PTRF causes global loss of caveolae, dyslipidemia, and glucose intolerance. *Cell Metab* 8: 310–317, 2008. doi:10.1016/j.cmet.2008.07.008.
31. Malenda A, Skrobanska A, Issat T, Winiarska M, Bil J, Oleszczak B, Sinski M, Firczuk M, Bujnicki JM, Chlebowska J, Staruch AD, Glodkowska-Mrowka E, Kunikowska J, Krolicki L, Szablewski L, Gacjong Z, Koziak K, Jakobisiak M, Golab J, Nowis DA. Statins impair glucose uptake in tumor cells. *Neoplasia* 14: 311–323, 2012. doi:10.1593/neo.12444.
32. Marques PE, Antunes MM, David BA, Pereira RV, Teixeira MM, Menezes GB. Imaging liver biology in vivo using conventional confocal microscopy. *Nat Protoc* 10: 258–268, 2015. doi:10.1038/nprot.2015.006.
33. Mather JP, Sato GH. The growth of mouse melanoma cells in hormone-supplemented, serum-free medium. *Exp Cell Res* 120: 191–200, 1979. doi:10.1016/0014-4827(79)90549-4.
34. Meyer C, Dzieran J, Liu Y, Schindler F, Munker S, Müller A, Coulouarn C, Dooley S. Distinct dedifferentiation processes affect caveolin-1 expression in hepatocytes. *Cell Commun Signal* 11: 6, 2013. doi:10.1186/1478-811X-11-6.
35. Michael MD, Kulkarni RN, Postic C, Previs SF, Shulman GI, Magnuson MA, Kahn CR. Loss of insulin signaling in hepatocytes leads to severe insulin resistance and progressive hepatic dysfunction. *Mol Cell* 6: 87–97, 2000. doi:10.1016/S1097-2765(05)00015-8.
36. Michalopoulos G, Pitot HC. Primary culture of parenchymal liver cells on collagen membranes. Morphological and biochemical observations. *Exp Cell Res* 94: 70–78, 1975. doi:10.1016/0014-4827(75)90532-7.
37. Michalopoulos GK, DeFrances MC. Liver regeneration. *Science* 276: 60–66, 1997. doi:10.1126/science.276.5309.60.
38. Mirza AM, Gysin S, Malek N, Nakayama K, Roberts JM, McMahon M. Cooperative regulation of the cell division cycle by the protein kinases RAF and AKT. *Mol Cell Biol* 24: 10868–10881, 2004. doi:10.1128/MCB.24.24.10868-10881.2004.
39. Munro S. Lipid rafts: elusive or illusive? *Cell* 115: 377–388, 2003. doi:10.1016/S0092-8674(03)00882-1.
40. Nagata J, Guerra MT, Shugrue CA, Gomes DA, Nagata N, Nathanson MH. Lipid rafts establish calcium waves in hepatocytes. *Gastroenterology* 133: 256–267, 2007. doi:10.1053/j.gastro.2007.03.115.
41. Nicou A, Serrière V, Prigent S, Boucherie S, Combettes L, Guillon G, Alonso G, Tordjmann T. Hypothalamic vasopressin release and hepatocyte Ca^{2+} signaling during liver regeneration: an interplay stimulating liver growth and bile flow. *FASEB J* 17: 1901–1903, 2003. doi:10.1096/fj.03-0082fje.
42. Pike LJ. Growth factor receptors, lipid rafts and caveolae: an evolving story. *Biochim Biophys Acta* 1746: 260–273, 2005. doi:10.1016/j.bbamcr.2005.05.005.
43. Pol A, Luetterforst R, Lindsay M, Heino S, Ikonen E, Parton RG. A caveolin dominant negative mutant associates with lipid bodies and induces intracellular cholesterol imbalance. *J Cell Biol* 152: 1057–1070, 2001. doi:10.1083/jcb.152.5.1057.
44. Resende RR, Andrade LM, Oliveira AG, Guimarães ES, Guatimosim S, Leite MF. Nucleoplasmic calcium signaling and cell proliferation: calcium signaling in the nucleus. *Cell Commun Signal* 11: 14, 2013. doi:10.1186/1478-811X-11-14.
45. Rodal SK, Skretting G, Garred O, Vilhardt F, van Deurs B, Sandvig K. Extraction of cholesterol with methyl-beta-cyclodextrin perturbs formation of clathrin-coated endocytic vesicles. *Mol Biol Cell* 10: 961–974, 1999. doi:10.1091/mbc.10.4.961.
46. Rodrigues HA, Lima RF, Fonseca MC, Amaral EA, Martinelli PM, Naves LA, Gomez MV, Kushmerick C, Prado MA, Guatimosim C. Membrane cholesterol regulates different modes of synaptic vesicle release and retrieval at the frog neuromuscular junction. *Eur J Neurosci* 38: 2978–2987, 2013.

47. **Rodrigues MA, Gomes DA, Andrade VA, Leite MF, Nathanson MH.** Insulin induces calcium signals in the nucleus of rat hepatocytes. *Hepatology* 48: 1621–1631, 2008. doi:10.1002/hep.22424.
48. **Sánchez-Wandelmer J, Dávalos A, Herrera E, Giera M, Cano S, de la Peña G, Lasunción MA, Busto R.** Inhibition of cholesterol biosynthesis disrupts lipid raft/caveolae and affects insulin receptor activation in 3T3-L1 preadipocytes. *Biochim Biophys Acta* 1788: 1731–1739, 2009. doi:10.1016/j.bbame.2009.05.002.
49. **Sanger F.** Fractionation of oxidized insulin. *Biochem J* 44: 126–128, 1949. doi:10.1042/bj0440126.
50. **Sarnataro D, Campana V, Paladino S, Stornaiuolo M, Nitsch L, Zurzolo C.** PrP(C) association with lipid rafts in the early secretory pathway stabilizes its cellular conformation. *Mol Biol Cell* 15: 4031–4042, 2004. doi:10.1091/mbc.e03-05-0271.
51. **Shah V, Toruner M, Haddad F, Cadelina G, Papapetropoulos A, Choo K, Sessa WC, Groszmann RJ.** Impaired endothelial nitric oxide synthase activity associated with enhanced caveolin binding in experimental cirrhosis in the rat. *Gastroenterology* 117: 1222–1228, 1999. doi:10.1016/S0016-5085(99)70408-7.
52. **Simons K, Ikonen E.** Functional rafts in cell membranes. *Nature* 387: 569–572, 1997. doi:10.1038/42408.
53. **Simons K, Toomre D.** Lipid rafts and signal transduction. *Nat Rev Mol Cell Biol* 1: 31–39, 2000. doi:10.1038/35036052.
54. **Simons K, van Meer G.** Lipid sorting in epithelial cells. *Biochemistry* 27: 6197–6202, 1988. doi:10.1021/bi00417a001.
55. **Smart EJ, Ying Y, Donzell WC, Anderson RG.** A role for caveolin in transport of cholesterol from endoplasmic reticulum to plasma membrane. *J Biol Chem* 271: 29427–29435, 1996. doi:10.1074/jbc.271.46.29427.
56. **Song X, Liu BC, Lu XY, Yang LL, Zhai YJ, Eaton AF, Thai TL, Eaton DC, Ma HP, Shen BZ.** Lovastatin inhibits human B lymphoma cell proliferation by reducing intracellular ROS and TRPC6 expression. *Biochim Biophys Acta* 1843: 894–901, 2014. doi:10.1016/j.bbamcr.2014.02.002.
57. **Straus DS.** Effects of insulin on cellular growth and proliferation. *Life Sci* 29: 2131–2139, 1981. doi:10.1016/0024-3205(81)90482-3.
58. **Subtil A, Gaidarov I, Kobylarz K, Lampson MA, Keen JH, McGraw TE.** Acute cholesterol depletion inhibits clathrin-coated pit budding. *Proc Natl Acad Sci USA* 96: 6775–6780, 1999. doi:10.1073/pnas.96.12.6775.
59. **Taniguchi CM, Emanuelli B, Kahn CR.** Critical nodes in signalling pathways: insights into insulin action. *Nat Rev Mol Cell Biol* 7: 85–96, 2006. doi:10.1038/nrm1837.
60. **Taub M, Chuman L, Saier MH Jr, Sato G.** Growth of Madin-Darby canine kidney epithelial cell (MDCK) line in hormone-supplemented, serum-free medium. *Proc Natl Acad Sci USA* 76: 3338–3342, 1979. doi:10.1073/pnas.76.7.3338.
61. **Terada Y, Inoshita S, Nakashima O, Yamada T, Kuwahara M, Sasaki S, Marumo F.** Lovastatin inhibits mesangial cell proliferation via p27Kip1. *J Am Soc Nephrol* 9: 2235–2243, 1998.
62. **Tobert JA.** Lovastatin and beyond: the history of the HMG-CoA reductase inhibitors. *Nat Rev Drug Discov* 2: 517–526, 2003. doi:10.1038/nrd1112.
63. **Vainio S, Heino S, Mansson JE, Fredman P, Kuismanen E, Vaarala O, Ikonen E.** Dynamic association of human insulin receptor with lipid rafts in cells lacking caveolae. *EMBO Rep* 3: 95–100, 2002. doi:10.1093/embo-reports/kvf010.
64. **Vosper J, Masuccio A, Kullmann M, Ploner C, Geley S, Hengst L.** Statin-induced depletion of geranylgeranyl pyrophosphate inhibits cell proliferation by a novel pathway of Skp2 degradation. *Oncotarget* 6: 2889–2902, 2015. doi:10.18632/oncotarget.3068.
65. **Wang X, Abdel-Rahman AA.** Effect of chronic ethanol administration on hepatic eNOS activity and its association with caveolin-1 and calmodulin in female rats. *Am J Physiol Gastrointest Liver Physiol* 289: G579–G585, 2005. doi:10.1152/ajpgi.00282.2004.
66. **Xu C, Chen X, Chang C, Wang G, Wang W, Zhang L, Zhu Q, Wang L, Zhang F.** Transcriptome analysis of hepatocytes after partial hepatectomy in rats. *Dev Genes Evol* 220: 263–274, 2010. doi:10.1007/s00427-010-0345-1.
67. **Zhang Z, Wang L, Du J, Li Y, Yang H, Li C, Li H, Hu H.** Lipid raft localization of epidermal growth factor receptor alters matrix metalloproteinase-1 expression in SiHa cells via the MAPK/ERK signaling pathway. *Oncol Lett* 12: 4991–4998, 2016. doi:10.3892/ol.2016.5307.
68. **Zundel W, Swiersz LM, Giaccia A.** Caveolin 1-mediated regulation of receptor tyrosine kinase-associated phosphatidylinositol 3-kinase activity by ceramide. *Mol Cell Biol* 20: 1507–1514, 2000. doi:10.1128/MCB.20.5.1507-1514.2000.



Article

Polymorphism in the Promoter Region of NFE2L2 Gene Is a Genetic Marker of Susceptibility to Cirrhosis Associated with Alcohol Abuse

Kemper Nunes dos Santos ^{1,†}, Rodrigo M. Florentino ^{1,†}, Andressa França ¹, Antônio Carlos Melo Lima Filho ¹, Marcone Loiola dos Santos ¹, Dabny Missiaggia ¹, Matheus de Castro Fonseca ² , Igor Brasil Costa ³, Paula Vieira Teixeira Vidigal ¹, Michael H. Nathanson ⁴, Fernanda de Oliveira Lemos ^{1,*} and M. Fatima Leite ¹

¹ Universidade Federal de Minas Gerais, Belo Horizonte, MG 31270-901, Brazil

² Laboratório Nacional de Biotecnologia (LNBio), Centro de Pesquisa em Energia e Materiais (CNPEM), Campinas, SP 13083-970, Brazil

³ Instituto de Pesquisas Evandro Chagas – IEC, Ananindeua, PA 67030-000, Brazil

⁴ Section of Digestive Diseases, Yale University School of Medicine, New Haven, CT 06510, USA

* Correspondence: folemos@hotmail.com

† These authors contributed equally to this work.

Received: 19 June 2019; Accepted: 15 July 2019; Published: 23 July 2019



Abstract: Alcoholic liver disease (ALD) is a highly prevalent spectrum of pathologies caused by alcohol overconsumption. Morbidity and mortality related to ALD are increasing worldwide, thereby demanding strategies for early diagnosis and detection of ALD predisposition. A potential candidate as a marker for ALD susceptibility is the transcription factor nuclear factor erythroid-related factor 2 (Nrf2), codified by the nuclear factor erythroid 2-related factor 2 gene (NFE2L2). Nrf2 regulates expression of proteins that protect against oxidative stress and inflammation caused by alcohol overconsumption. Here, we assessed genetic variants of NFE2L2 for association with ALD. Specimens from patients diagnosed with cirrhosis caused by ALD were genotyped for three NFE2L2 single nucleotide polymorphisms (SNP) (SNPs: rs35652124, rs4893819, and rs6721961). Hematoxylin & eosin and immunohistochemistry were performed to determine the inflammatory score and Nrf2 expression, respectively. SNPs rs4893819 and rs6721961 were not specifically associated with ALD, but analysis of SNP rs35652124 suggested that this polymorphism predisposes to ALD. Furthermore, SNP rs35652124 was associated with a lower level of Nrf2 expression. Moreover, liver samples from ALD patients with this polymorphism displayed more severe inflammatory activity. Together, these findings provide evidence that the SNP rs35652124 variation in the Nrf2-encoding gene NFE2L2 is a potential genetic marker for susceptibility to ALD.

Keywords: Alcoholic liver disease; Nrf2; Polymorphism; NFE2L2 gene

1. Introduction

Alcoholic liver disease (ALD), a spectrum of pathologies that include fatty liver disease, alcoholic hepatitis, and cirrhosis caused by alcohol overconsumption [1,2], is a global public health issue. Approximately 2.4 billion people consume alcohol worldwide, and 75 million people are at risk of alcohol-associated liver disease [3]. It is estimated that 2 million people die of liver disease each year, and up to 50% of these cases are due in part to alcoholic cirrhosis [1]. ALD, as with other chronic liver diseases, may not be clinically apparent early in the disease process. This highlights the importance of early diagnosis for management and treatment to prevent cirrhosis-related morbidity and mortality, as well as to detect ALD susceptibility.

Ethanol metabolism generates reactive oxygen species (ROS), causing oxidative stress and inflammation, the main pathogenic events involved in ALD [4,5]. Therefore, preventing the increase in ROS is a potential mechanism to protect the liver tissue from the damage caused by alcohol consumption. An endogenous mechanism of hepatoprotection is mediated by the nuclear erythroid-related factor 2 (Nrf2). Nrf2 is a basic leucine zipper transcription factor that controls the expression of the antioxidant response element (ARE)—dependent genes, leading to the expression of cytoprotective and anti-inflammatory proteins [6,7]. Dysregulation of Nrf2 activity correlates with the development of several chronic inflammatory diseases [7–10]. For instance, knock-out (KO) mice for Nrf2 displayed aggravated liver injury after alcohol ingestion [11,12].

Progression and prognosis of alcohol-related liver disease is influenced by multiple factors, including genetics [2]. The most common type of genetic variation is the single nucleotide polymorphism (SNP), which represents a nucleotide substitution in the genome that is associated with altered vulnerability to disease [13,14]. SNPs in the promoter region of the Nuclear factor erythroid 2-related factor 2 gene (NFE2L2) have been associated with disease susceptibility and other inherited phenotypes, especially conditions characterized by increased levels of oxidative stress [15]. However, SNPs in NFE2L2 have not yet been related to ALD. Here we investigated whether polymorphisms in the promoter region of the NFE2L2 gene are associated with worse prognosis in a cohort of ALD patients. For comparison, we examined the specificity of NFE2L2 SNPs for ALD by comparing the occurrence of these SNPs in patients with chronic hepatitis C virus (HCV) infection. Our findings suggest SNP rs35652124 is a specific genetic marker for susceptibility to the development of ALD.

2. Results

2.1. Single Nucleotide Polymorphism at -274 of the NFE2L2 Promoter Region Is a Genetic Marker for ALD Susceptibility

Two of the three analyzed polymorphisms in the promoter region of NFE2L2, the gene that encodes Nrf2 (Figure 1), showed clinical significance in ALD samples.

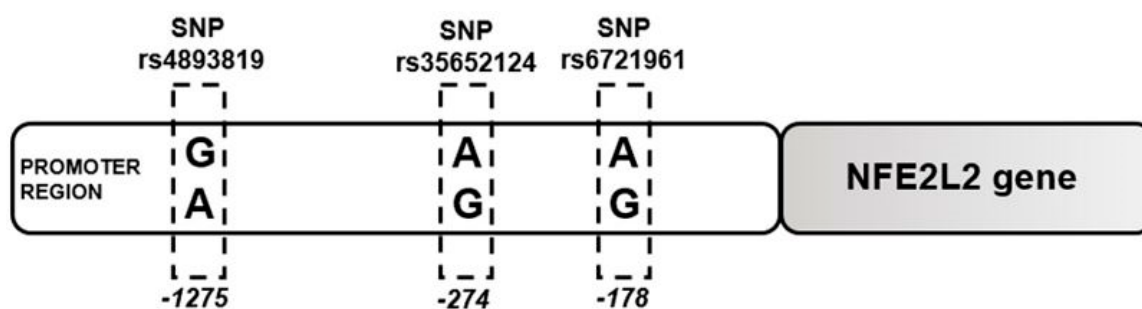


Figure 1. Schematic position of the selected polymorphisms in nuclear factor erythroid 2-related factor 2 gene (NFE2L2). The three polymorphisms studied in this work are localized in promoter region of NFE2L2 gene. Single Nucleotide Polymorphism (SNP) rs6721961 is located at position -178, where can be present an adenine (A) or guanine (G). SNP rs35652124 is in position -274 in the promoter region, and the variation is the same of the first. Lastly, SNP rs4893819 is localized in position -1275 in the promoter region of NFE2L2 gene. In this position, the variation occurs between G and A. All these positions are considering the position in relation 3' → 5'.

The SNP rs35652124 analysis showed the polymorphism -274 adenine (A) in the promoter region of NFE2L2 gene in most ALD patients ($n = 55$ patients (59.8%)), while the variant -274 guanine (G) was also present but less frequently in the same group ($n = 37$ patients (40.2%)). Conversely, control group showed the variant -274G in most of the samples ($n = 25$ patients (59.5%)), whereas the polymorphism -274A was less frequent in normal tissue ($n = 17$ patients (40.5%)) (Table 1). We also performed the SNP rs35652124 analysis in patients with cirrhosis caused by HCV to evaluate the specificity of this polymorphism for ALD. In contrast to what was observed in ALD, most patients with cirrhosis caused

by HCV had the variant -274G (n = 19 patients - 67.9%) instead of -274A (n = 9 patients—32.1%) (Table 2). The comparison between HCV and control liver samples did not show any significant difference regarding the frequency of the variant -274A or -274G (Table 3). These observations are consistent with the idea that the presence of an A in SNP rs35652124 is associated with ALD development, while the presence of a G may be a protective factor.

Table 1. Allele Frequencies Compared to Alcoholic liver disease (ALD)/Control Groups—SNP rs35652124 (-214 A > G).

Allele	ALD n (%)		Control n (%)		p Value
A/A	18	39.1	5	23.8	0.1457
G/G	9	19.6	9	42.9	
A/G	19	41.3	7	33.3	
Total	46	100.0	21	100	
A/A	18	39.1	5	23.8	0.2192
G/G_A/G	28	60.9	16	76.2	
Total	46	100.0	21	100	
A/A_A/G	37	80.4	12	57.1	0.0460
G/G	9	19.6	9	42.9	
Total	46	100.0	21	100	
A	55	59.8	17	40.5	0.0387
G	37	40.2	25	59.5	
Total	92	100.0	42	100	

Table 2. Allele Frequencies Compared to Alcoholic liver disease (ALD)/hepatitis C virus (HCV) Groups—SNP rs35652124 (-214 A > G).

Allele	ALD n (%)		HCV n (%)		p Value
A/A	18	39.1	2	14.3	0.0668
G/G	9	19.6	7	50.0	
A/G	19	41.3	5	35.7	
Total	46	100.0	14	100.0	
A/A	18	39.1	2	14.3	0.0746
G/G_A/G	28	60.9	12	85.7	
Total	46	100.0	14	100.0	
A/A_A/G	37	80.4	7	50.0	0.0345
G/G	9	19.6	7	50.0	
Total	46	100.0	14	100.0	
A	55	59.8	9	32.1	0.0106
G	37	40.2	19	67.9	
Total	92	100.0	28	100.0	

Table 3. Allele Frequencies Compared to hepatitis C virus (HCV)/Control Groups—SNP rs35652124 (-214 A > G).

Allele	HCV n (%)		Control n (%)		p Value
A/A	2	14.3	5	23.81	0.7898
G/G	7	50.0	9	42.86	
A/G	5	35.7	7	33.33	
Total	14	100.0	21	100	
A/A	2	14.3	5	23.81	0.4995
G/G_A/G	12	85.7	16	76.19	
Total	14	100.0	21	100	
A/A_A/G	7	50.0	12	57.14	0.6846
G/G	7	50.0	9	42.86	
Total	14	100.0	21	100	
A	9	32.1	17	40.48	0.4832
G	19	67.9	25	59.52	
Total	28	100.0	42	100	

The second polymorphism with clinical importance was the SNP rs6721961, located at position -178 in the promoter region of the NFE2L2 gene. The frequency of -178A and -178G in the samples from ALD patients was not different when we compared them to HCV samples (HCV—A: n = 22 patients—61.1%; and G: n = 14 patients—38.9%/ ALD A: n = 38 patients—41.3%; and G: n = 54 patients—58.7%) (Table 4). However, the frequency of the alleles A/A and A/G was lower in the ALD group (allele A/A: n = 27 patients—58.7%; and allele G/G: n = 19 patients—41.3%) than in the HCV group (alleles A/A and A/G: n = 16 patients—88.9%; allele G/G: n = 2 patients—11.1%) (Table 4). Together, these results suggest that the presence of the nucleotide A in the position -178 of the promoter region of NFE2L2 is associated with cirrhotic liver disease, since both ALD and HCV samples preferentially showed this polymorphism.

Table 4. Allele Frequencies Compared to Alcoholic liver disease (ALD)/hepatitis C virus (HCV) Groups—SNP rs6721961 (-178 A > G).

Allele	ALD n (%)		HCV n (%)		p Value
A/G	16	34.8	10	55.6	0.0531
A/A	11	23.9	6	33.3	
G/G	19	41.3	2	11.1	
Total	46	100.0	18	100.0	
A/A	11	23.9	6	33.3	0.6510
A/G_G/G	35	76.1	12	66.7	
Total	46	100.0	18	100.0	
A/A_A/G	27	58.7	16	88.9	0.0360
G/G	19	41.3	2	11.1	
Total	46	100.0	18	100.0	
A	38	41.3	22	61.1	0.0685
G	54	58.7	14	38.9	
Total	92	100.0	36	100.0	

The third polymorphism analyzed was the SNP rs4893819, in the position -1275 of the promoter region of NFE2L2 gene. The comparison between ALD and HCV liver samples did not show any significant difference regarding the frequency of the variant -1275A or -1275G (Table 5).

Table 5. Allele Frequencies Compared to Alcoholic liver disease (ALD)/hepatitis C virus (HCV) Groups—SNP rs4893819 (-1275 G > A).

Allele	ALD n (%)		HCV n (%)		p Value
A/A	10	22.7	4	28.6	0.8715
G/G	22	50.0	7	50.0	
G/A	12	27.3	3	21.4	
Total	44	100.0	14	100.0	
A/A	10	22.7	4	28.6	0.7245
G/G_G/A	34	77.3	10	71.4	
Total	44	100.0	14	100.0	
A/A_G/A	22	50.0	7	50.0	1.000
G/G	22	50.0	7	50.0	
Total	44	100.0	14	100.0	
A	32	36.4	11	39.3	0.9568
G	56	63.6	17	60.7	
Total	88	100.0	28	100.0	

Together, these results are consistent with the idea that the polymorphism -274A in the promoter region of NFE2L2 predisposes to ALD while the polymorphism at -178A might be associated with susceptibility to develop cirrhosis from ALD plus other causes as well.

2.2. Single Nucleotide Polymorphism Rs35652124 in the NFE2L2 Gene Correlates With Inflammatory Score in ALD

In light of the protective effect of Nrf2 against oxidative stress caused by alcohol consumption, we aimed to assess whether polymorphisms in the promoter region of NFE2L2 directly correlate with expression of Nrf2 in the liver. To address this question, immunohistochemistry was performed in the ALD and HCV samples after Nrf2 antibody optimization, using liver specimens from healthy patients (negative control—nonspecific binding), and specimens from patients with extrahepatic biliary atresia (positive control for Nrf2 nuclear translocation) [16] (Figure S1). Although Nrf2 staining was not nuclear in most ALD specimens analyzed, Nrf2 was localized throughout the cytoplasm in the ALD samples, and preferentially in the perinuclear region (Figure 2). This altered distribution could be due to the fact that ALD specimens used here were from patients with at least six months of alcohol abstinence before liver transplantation. Therefore, the absence of the acute alcohol stimuli could contribute to the lower nuclear translocation of Nrf2 observed in these ALD samples. In addition to the Nrf2 nuclear translocation, the de novo synthesis of this transcription factor is also involved in the mechanism of cell protection after exposure to reactive oxygen species [17,18]. This is in agreement with our findings that in SNP rs35652124 polymorphisms, Nrf2 expression was higher in samples exhibiting the -274G/G allele than in samples with the -274A/A or -274A/G alleles (G/G = 183.1 ± 3.9 ; A/A = 170.1 ± 2.9 ; A/G = 70.3 ± 1.9), (Figure 2A,B). The expression of superoxide dismutase 1 (SOD1), a gene which transcription is targeted for a variety of transcription factors, including Nrf2 [19], was also observed in most ALD samples (Figure S2), suggesting some level of Nrf2 activation. These results support the observation that the presence of -274A in SNP rs35652124, both in homozygosity (A/A) or heterozygosity (A/G), may be a risk factor for ALD, while the -274G/G allele is a protective factor.

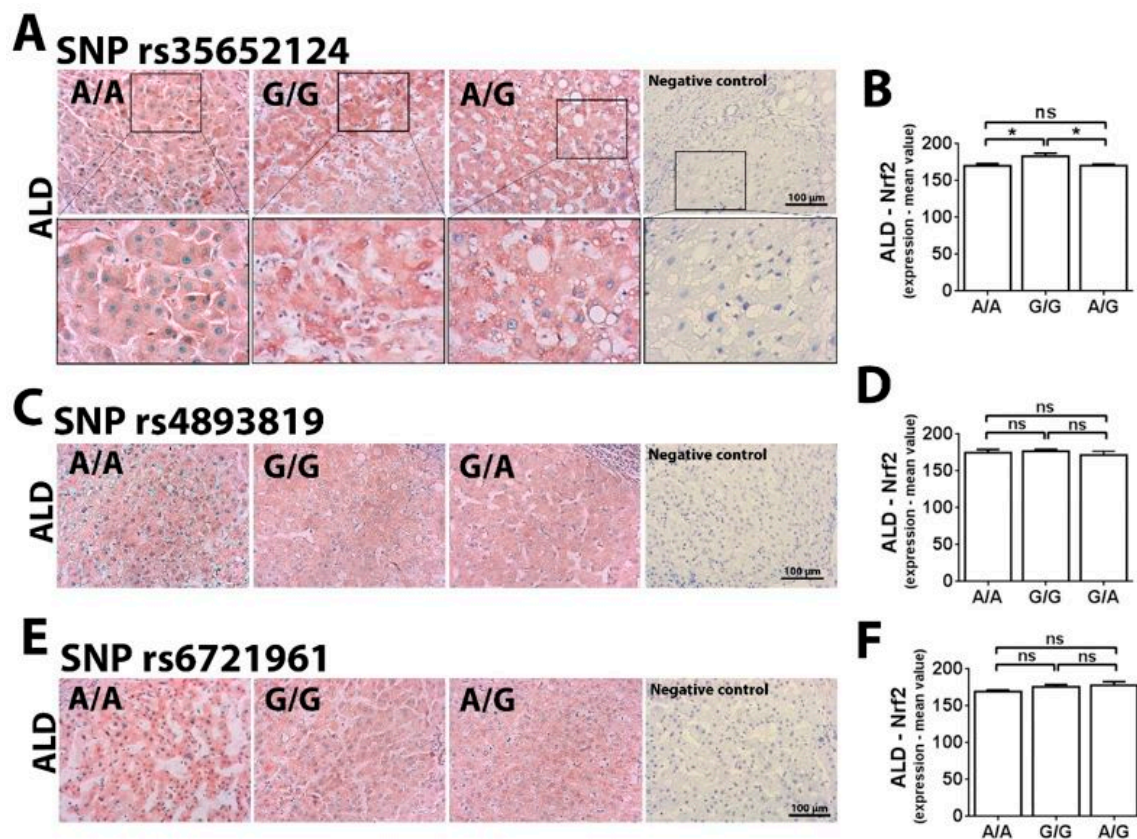


Figure 2. Nrf2 expression in the different polymorphisms of NFE2L2 gene in patients with ALD-associated cirrhosis. (A) Immunohistochemistry for Nrf2 in the SNP rs35652124 genotypes. (B) Quantification of Nrf2 expression (mean value) in the different genotypes of SNP rs35652124. (C) Immunohistochemistry for Nrf2 in the SNP rs4893819 genotypes. (D) Quantification of Nrf2 expression (mean value) in the different genotypes of SNP rs4893819. (E) Immunohistochemistry for Nrf2 in the SNP rs6721961 genotypes. (F) Quantification of Nrf2 expression (mean value) in different genotypes of SNP rs6721961 (n = 15 patients with ALD-associated cirrhosis; and n = 5 patients in each genotype. * $p < 0.05$. Values are expressed as mean \pm SEM).

When it comes to the SNP rs4893819 (Figure 2C,D) and SNP rs6721961 (Figure 2E,F) polymorphisms, no correlation was observed regarding Nrf2 expression and the alleles A/A, A/G or G/G. Moreover, Nrf2 expression was not associated with the presence of any specific allele in SNP rs35652124, SNP rs4893819 or SNP rs6721961 in HCV samples (Figure S3).

There was no correlation between the polymorphism in the promoter region of NFE2L2 and the biochemical data of patients with either ALD (Table 6) or HCV (Tables S2–S4). These results might reflect the end-stage nature of the ALD and HCV cases, because all these patients had cirrhosis and required liver transplantation.

Table 6. Allele frequencies compared clinical data to Alcoholic liver disease (ALD) SNPs.

Allele	ALD - SNP rs35652124 (-214 A > G)															
	M %	F %	Age	MELD	ALT	AST	GGT	TB	DB	IB	ALP	LDH	ALB	INR	UR	CR
A/A	94.45	5.55	53.61 (2.057)	16.54 (1.101)	46.25 (11.02)	76.91 (19.03)	114.75 (21.65)	3.26 (0.3964)	1.20 (0.2407)	2.05 (0.3092)	214.2 (39.73)	460.23 (48.82)	3.12 (0.1612)	1.68 (0.0984)	27.77 (2.699)	1.04 (0.183)
G/G	100	0	55.25 (3.304)	16 (0.7559)	51.71 (4.46)	77.34 (13.1)	212 (56.35)	3.43 (0.5941)	1.68 (0.505)	1.79 (0.1932)	191.3 (51.58)	468.6 (57.1)	3.07 (0.1686)	1.48 (0.085)	34.72 (4.387)	0.95 (0.112)
A/G	100	0	52.21 (2.924)	17 (1.075)	30.47 (5.188)	39.93 (4.364)	88.34 (27.72)	3.36 (0.5608)	1.42 (0.4408)	2.04 (0.2102)	125.63 (16.44)	421.02 (46.45)	3.25 (0.1566)	1.82 (0.1526)	38.04 (3.144)	0.99 (0.068)
<i>p</i> value	-	-	0.7761	0.8396	0.2224	0.1226	0.0514	0.9742	0.6619	0.7853	0.1928	0.8082	0.7287	0.2295	0.0643	0.9129
Allele	ALD - SNP rs4893819 (-1275 G > A)															
	M %	F %	Age	MELD	ALT	AST	GGT	TB	DB	IB	ALP	LDH	ALB	INR	UR	CR
A/A	88.89	11.11	48.33 (2.809)	16.66 (0.8028)	46.2 (5.275)	60.05 (11.8)	112.63 (39.07)	3.26 (0.439)	1.3 (0.2762)	2 (0.2608)	159.2 (23.81)	421.44 (40.07)	3.01 (0.04)	1.56 (0.0898)	26.76 (5.056)	1.36 (0.321)
G/G	100	0	53 (2.282)	16.71 (1.029)	44.87 (8.916)	70.73 (15.51)	118.7 (20.65)	3.24 (0.417)	1.2 (0.2856)	2.03 (0.2483)	151.06 (18.09)	468.6 (47.46)	3.10 (0.149)	1.81 (0.1171)	29.85 (3.431)	0.9 (0.074)
G/A	100	0	59 (2.967)	16.86 (1.487)	36 (10.75)	55.67 (15.92)	180 (79.48)	3.71 (0.5114)	1.63 (0.4826)	1.89 (0.3667)	268.3 (79.75)	443.6 (75.63)	3.47 (0.2327)	1.56 (0.1429)	35.45 (5.895)	1.51 (0.107)
<i>p</i> value	-	-	0.0563	0.9946	0.7944	0.8009	0.5107	0.7671	0.7181	0.9516	0.1054	0.8480	0.2425	0.2825	0.6952	0.1259
Allele	ALD - SNP rs6721961 (-178 A > G)															
	M %	F %	Age	MELD	ALT	AST	GGT	TB	DB	IB	ALP	LDH	ALB	INR	UR	CR
A/A	90	10	56.5 (3.212)	16.63 (1.101)	39.5 (7.058)	72.75 (10.37)	158.71 (60.2)	3.64 (0.3599)	1.63 (0.3632)	2.03 (0.3692)	267.62 (68.49)	381.42 (58.18)	3.3 (0.184)	1.5 (0.1257)	37 (4.687)	1.32 (0.269)
G/G	100	0	49.71 (1.957)	15 (0.7977)	40.18 (5.564)	58.94 (8.13)	115.7 (21.53)	2.63 (0.3742)	0.93 (0.1771)	1.87 (0.2752)	146.1 (16.06)	471.01 (49.53)	3.07 (0.1274)	1.7 (0.107)	32.04 (3.942)	0.84 (0.051)
A/G	100	0	57.14 (2.344)	17.36 (1.002)	43.73 (11.83)	59.85 (21.59)	120.5 (33.98)	3.74 (0.5585)	1.69 (0.4554)	1.92 (0.181)	126.5 (19.45)	470.8 (47.57)	3.18 (0.198)	1.68 (1.1344)	34.19 (2.451)	0.97 (0.086)
<i>p</i> value	-	-	0.0482	0.1959	0.9359	0.7991	0.7017	0.1677	0.2381	0.9141	0.0235	0.4332	0.6492	0.5050	0.6612	0.0623

M: male; F: female; MELD: Model for End-Stage Liver Disease; ALT: alanine transaminase; AST: aspartate transaminase; GGT: Gamma-glutamyltransferase; TB: total bilirubin; DB: direct bilirubin; IB: indirect bilirubin; ALP: alkaline phosphatase; LDH: lactate dehydrogenase; ALB: albumin; INR: international normalized ratio; UR: urea; CR: creatinine.

Finally, the association between histological findings and polymorphisms in the promoter region of NFE2L2 was evaluated after histological analysis of the hematoxylin and eosin (H&E)-stained ALD samples. Chronic liver disease can be divided in different stages of fibrosis levels and inflammatory activity [20]. All the ALD and HCV liver samples showed higher level of fibrosis, in such a way that just the inflammatory activity was scored (Figure 3A). For the SNP rs35652124 in the ALD samples (Figure 3B), we observed higher inflammatory activity for the alleles -274A/A and -274A/G (A/A: absent = 1 case; mild = 6 cases; moderate = 5 cases; severe = 1 case. A/G: absent = 3 cases; mild = 6 cases; moderate = 5 cases; severe = 3 cases). On the other hand, most of the samples with -274G/G allele showed attenuated inflammatory activity (G/G: absent = 1 case; mild = 3 cases; moderate = 2 cases; severe = 1 case). For the SNP rs6721961 -178A allele as a risk factor for liver damage, no difference was observed in the inflammatory activity (A/A: absent = 1 case; mild = 3 cases; moderate = 3 cases; severe = 2 case. A/G: absent = 2 cases; mild = 7 cases; moderate = 3 cases; severe = 1 cases. G/G: absent = 1 case; mild = 7 cases; moderate = 5 cases; severe = 2 case) (Figure 3C). The absence of correlation between the polymorphism and inflammatory activity was also observed for the SNP rs4893819 (A/A: absent = 0 case; mild = 5 cases; moderate = 2 cases; severe = 1 case. G/A: absent = 1 cases; mild = 4 cases; moderate = 4 cases; severe = 1 cases. G/G: absent = 2 case; mild = 6 cases; moderate = 6 cases; severe = 2 cases) (Figure 3D).

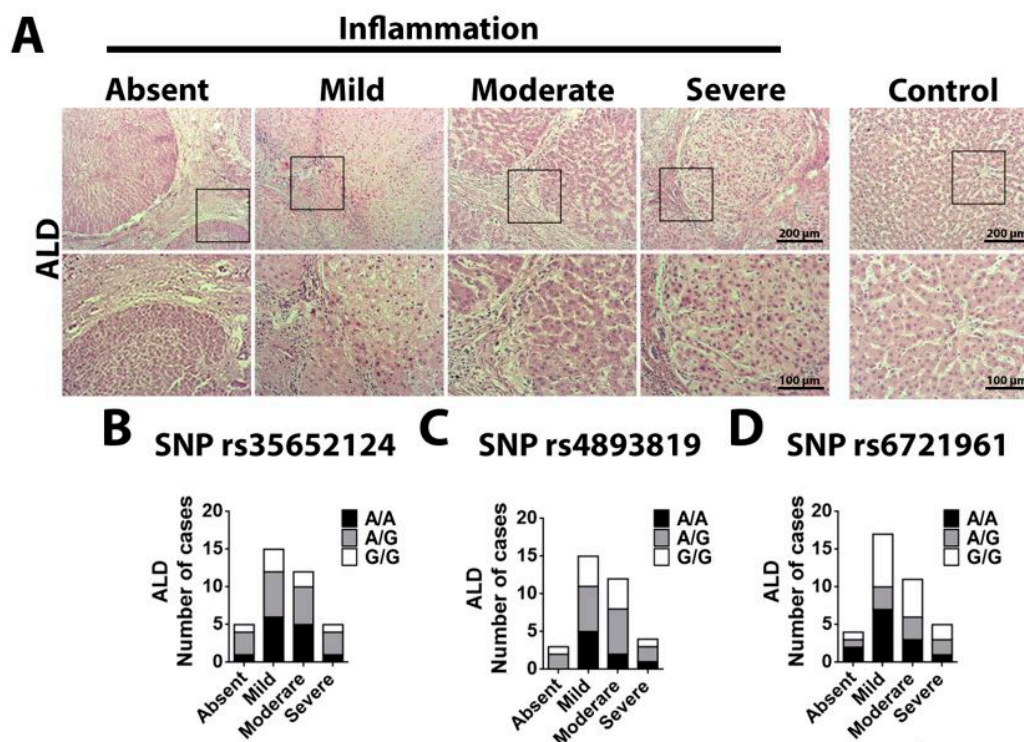


Figure 3. Inflammation score in the different polymorphism of NFE2L2 gene in patients with cirrhosis from ALD. (A) HE from ALD patients showing the score of inflammation. The METAVIR parameters are considered: A0 mean no inflammation activity; A1 means mild inflammatory activity; A2 means moderate inflammatory activity and A3 means intense inflammatory activity. (B) Number of cases in each inflammatory score considering the polymorphism SNP rs35652124. (C) Number of cases in each inflammatory score considering the polymorphism SNP rs4893819. (D) Number of cases in each inflammatory score considering the polymorphism SNP rs6721961 (n = 37 patients for SNP rs35652124; n = 37 patients for SNP rs6721961; and n = 34 patients for SNP rs4893819).

Together, these results suggest that polymorphism -274A in the promoter region of NFE2L2 gene is associated with worse inflammatory activity in ALD samples.

3. Discussion

Single nucleotide polymorphisms are the most common type of polymorphisms and occur at a frequency of approximately 1 in 1000 base pairs [21] throughout the genome (coding sequences, intronic sequences, and promoter region).

In this study, we established, for the first time, a specific and functional association between a SNP in the promoter region of the NFE2L2 gene and susceptibility to ALD. ALD can lead to cirrhosis, liver cancer, and liver failure, and is the most frequent indication for orthotopic liver transplantation in some populations [22]. Although the pathogenesis of ALD has not yet been fully elucidated, an interaction among behavioral, environmental and genetic factors is appreciated [22,23]. Most studies of the genetic predisposition to ALD have focused on genes related to cell metabolism and detoxifying enzymes [24–26]. Recently, genes for patatin-like phospholipase domain-containing protein 3 (PNPLA3), transmembrane 6 superfamily member 2 (TM6SF2) and membrane-bound O-acyltransferase domain-containing 7 (MBOAT7) have emerged as potential markers of susceptibility to develop alcohol-related liver injury [27]. These three proteins are involved in lipid metabolism, and therefore may also participate in the pathogenesis of ALD, because steatosis is the initial histological finding from alcohol overconsumption [27]. For example, PNPLA3 is expressed in hepatocytes, and functions as a lipase, catalyzing the hydrolysis of triglycerides [28]. SNP rs738409 in the PNPLA3 gene is strongly associated with the alcoholic hepatitis [29,30], alcoholic cirrhosis [31,32], hepatocellular carcinoma (HCC) and reduced transplantation-free survival [32–34], as well as non-alcoholic fatty liver disease (NAFLD) [27,35]. TM6SF2 is involved in very low-density lipoprotein (VLDL) secretion, and the rs58542926 variant has been associated with ALD cirrhosis [31], HCC [34], and NAFLD [36,37]. SNP rs10401969 of the TM6SF2 gene also correlates with ALD cirrhosis [31]. MBOAT7 catalyzes the transfer of fatty acids between phospholipids and lysophospholipids, and the SNP rs641738 is associated with higher risk of NAFLD [38] and inflammation and fibrosis in chronic hepatitis B [39], while rs626283 is correlated with ALD cirrhosis [31].

Generation of ROS is a common consequence of alcohol metabolism [23,40], which is counteracted by the Nrf2/ARE axis [41]. Nrf2 is a switch for the endogenous antioxidant response by activating its downstream target genes responsible for regulating oxidative stress and inactivating toxic chemicals and proteins [9,42–44]. Although a decline in Nrf2 expression has already been observed in older rodents [45] and in age-related neurodegenerative disorder in humans [46], which can contribute to the susceptibility to various diseases, the specimens selected for the current work were from patients with similar ages. Several endogenous mechanisms are responsible for reducing cellular oxidative stress through expression of antioxidant genes, such as glutathione-S-transferase (GST), coenzyme Q10 (Q10), NAD(P)H:quinone oxidoreductase (QR), and superoxide dismutase 1 (SOD1) which have the common promoter element called the antioxidant response element [47]. Activation of Nrf2 as a response to cell injury has already been described in different liver cells and several liver diseases, such as cholestatic liver injury [16], viral hepatitis, drug-induced hepatitis, liver fibrosis, and cirrhosis, HCC, and alcoholic and non-alcoholic steatohepatitis [44]. For instance, impairment of acetaldehyde detoxification, aggravation of inflammatory response, and liver failure are key common events observed in ethanol-fed Nrf2 knock-out mice, confirming the importance of this transcriptional factor to prevent liver injury [12].

Several SNPs in the encoding region of the NFE2L2 gene, have already been associated with diseases characterized by oxidative stress and inflammation, including acute lung injury [48], chronic gastritis [49], gastric ulcer [50], ulcerative colitis [51], chronic obstructive pulmonary disease [52], and type 2 diabetes mellitus [15]. Our findings suggest that a variant of the NFE2L2 gene specifically correlates with ALD cirrhosis. Our findings show that the variant -274A in SNP rs35652124 correlates with the occurrence of ALD cirrhosis but not with HCV-associated cirrhosis. Additionally, we observed that this variant associates with reduced expression of Nrf2, followed by a more severe inflammatory condition, which is in agreement with previous studies showing that Nrf2-deficient mice exhibit worst liver damage induced by alcohol intake [12]. This polymorphism of NFE2L2 has also been implicated

in other diseases, such as Parkinson's disease (PD) [53], hypertension, and cardiovascular disease [54]. In PD, for example, 10 SNPs within the NFE2L2 gene, including 3 exonic SNPs, 2 intronic SNPs, 3 promoter SNPs, and 2 SNPs in 3' region of NFE2L2 gene were found [55].

In conclusion, our findings provide evidence that single nucleotide variations in the promoter region of NFE2L2, specifically the variant -274A of SNP rs35652124, might contribute to the pathogenesis of cirrhosis from ALD. In addition, the lower Nrf2 expression and severe inflammatory activity observed in patients carrying the -274A allele, suggest the potential relevance of this polymorphism in ALD susceptibility and in the progression of this disease

4. Materials and Methods

4.1. Human Specimens

Human liver tissue specimens and clinical data from 49 patients with ALD in the cirrhotic phase were collected from patients, with alcohol abstinence for at least 6 months, who underwent liver transplantation at Hospital das Clínicas, Federal University of Minas Gerais (UFMG), from 1998 to 2015. Eighteen liver specimens from patients with HCV and 21 liver biopsies from liver organ donors, from 2012 to 2017, were used for comparison to the ALD group (Table S1). The average age of the patients used in this study were similar among the groups (control: 49.5, ALD: 53.6, and HCV: 57.9; $p > 0.05$ one-way analysis of variance (ANOVA)). The study was approved on 31st may 2017 by the Research Ethics Committee of UFMG, CAAE 67814117.6.0000.5149. Written informed consent was obtained from all subjects.

4.2. Genotyping

SNP analysis of the variants present in the promoter region of NFE2L2 gene was performed in the liver specimens of ALD, HCV, and healthy groups. SNPs rs35652124 (-214 A > G), rs4893819 (-1275 G > A) and rs6721961 (-178 A > G) were analyzed in approximately 25 mg of paraffin-embedded hepatic tissues. Genomic DNA was extracted and purified with the DNeasy Blood & Tissue kit (Qiagen®, Hilden, North Rhine-Westphalia, Germany), in accordance with the manufacturer's instruction. For genotyping, the genomic DNA was incubated with rhAmp™ Genotyping Master Mix and rhAmp™ Reporter Mix and the primers (rhAmp™ SNP Assay) for the SNPs rs35652124, rs4893819, and rs6721961, according to the guidelines (Integrated DNA Technologies—IDT®, Coralville, Iowa, USA). The polymerase chain reaction (PCR) amplification was performed in the 7500 real-time PCR system (Thermo Fisher Scientific, Foster City, California, USA) under the following conditions: 95 °C for 10 minutes (1 cycle), 40 cycles at 95 °C for 10 sec., 60 °C for 30 sec., and 68 °C for 20 sec. The assay model was the rhAmp™ SNP Genotyping System, for qPCR-SNP (IDT®, Coralville, Iowa, USA).

4.3. Histopathological Analysis

Formalin-fixed, paraffin-embedded human liver specimens were sectioned at 4 µm thicknesses and stained with hematoxylin and eosin (H&E). The slides were evaluated under a light microscope (CX4; Olympus, Shinjuku, Tokyo, Japan) and the inflammatory cell infiltrate, polymorphonuclear leukocytes and mononuclear cells, in the epithelial and connective tissues was graded as absent—no inflammation activity; mild inflammatory activity; moderate inflammatory activity; and intense inflammatory activity, by an experienced pathologist, in a blinded fashion [20].

4.4. Immunohistochemistry

Immunohistochemistry was performed using formalin-fixed, paraffin-embedded human liver specimens with the Novolink Polymer Detection Kit (Leica Biosystems, Benton Lane, Newcastle, UK). Four µm-thick sections were dewaxed, and antigen retrieval was performed in citrate buffer 1 mM (pH 6.0). Following peroxidase and protein block, specimens were incubated with anti-Nfr2 (Abcam, Cambridge, MA, USA) and anti-SOD1 (Santa Cruz, Dallas, TX, USA) antibody overnight at room temperature. Reactions were revealed by applying 3,3'-diaminobenzidine (DAB). To compare Nfr2 expression in ALD,

HCV, and healthy groups, images were converted to 8-bit. Regions of interest were selected and pixel intensity (0-255, grayscale) was measured in Image J software (Bethesda, Maryland, USA) [56].

4.5. Statistical Analysis

Results are presented as mean \pm SEM. Data were analyzed using GraphPad Prism software (version 7; GraphPad Software, La Jolla, CA, USA). Differences among experimental groups were assessed for significance $p < 0.05$, using the Student's t-test or one-way ANOVA followed by Bonferroni post-test.

Supplementary Materials: Supplementary materials can be found at <http://www.mdpi.com/1422-0067/20/14/3589/s1>.

Author Contributions: K.N.d.S., R.M.F. and M.F.L. conceived the project. K.N.d.S., R.M.F., A.F., A.C.M.L.F., M.L.d.S., D.M., M.d.C.F. and F.d.O.L. conducted experiments. K.N.d.S., R.M.F., A.F., A.C.M.L.F., M.L.d.S. and D.M. analyzed data. I.B.C., P.V.T.V., M.H.N and M.F.L. contributed with reagents/materials/analysis tools. F.d.O.L. and M.d.C.F. wrote the first draft of the manuscript. M.d.C.F., M.H.N, F.d.O.L. and M.F.L. edited the manuscript. All authors agreed to the final version of the manuscript.

Funding: This research was funded by Conselho Nacional de Desenvolvimento Científico e Tecnológico (CNPq 159892/2018-0), Fundação de Amparo à Pesquisa de Minas Gerais (FAPEMIG), Coordenação de Aperfeiçoamento de Pessoal (CAPES), Fundação de Amparo à Pesquisa do Estado de São Paulo (FAPESP 2018/20014-0), Liver Center at UFMG, NIH (DK57751, DK34989, DK114041, and DK112797 to MHN). This work also was supported by the Gladys Phillips Crofoot Professorship.

Conflicts of Interest: The authors declare no conflict of interest.

Abbreviations

ALD	Alcoholic Liver Disease
ROS	Reactive Oxygen Species
Nrf2	Nuclear erythroid-related factor 2
SNP	Single Nucleotide Polymorphism
NFE2L2	Nuclear erythroid-related factor 2 gene
HCV	Hepatitis C virus
A	Adenine
G	Guanine
PNPLA3	Patatin-like phospholipase domain-containing protein 3
TM6SF2	Transmembrane 6 superfamily member 2
MBOAT7	Membrane-bound O-acyltransferase domain-containing 7
HCC	Hepatocellular carcinoma
NAFLD	Non-alcoholic fatty liver disease
VLDL	Very low-density lipoprotein
ARE	Antioxidant response element
GST	Glutathione-S-transferase
Q10	Coenzyme Q10
QR	NAD(P)Hiquinone oxidoreductase
SOD1	Superoxide dismutase 1
PD	Parkinson's disease
M	Male
F	Female
MELD	Model for End-Stage Liver Disease
ALT	Alanine transaminase
AST	Aspartate transaminase
GGT	Gamma-glutamyltransferase
TB	Total bilirubin
DB	Direct bilirubin
IB	Indirect bilirubin
ALP	Alkaline phosphatase
LDH	Lactate dehydrogenase
ALB	Albumin
INR	International normalized ratio
UR	Urea
CR	Creatinine

References

1. Singal, A.K.; Bataller, R.; Ahn, J.; Kamath, P.S.; Shah, V.H. ACG clinical guideline: Alcoholic liver disease. *Am. J. Gastroenterol.* **2018**, *113*, 175–194. [[CrossRef](#)] [[PubMed](#)]
2. Thursz, M.; Kamath, P.S.; Mathurin, P.; Szabo, G.; Shah, V.H.; Szabo, G.; Kamath, P.S.; Shah, V.H.; Thursz, M.; Mathurin, P.; et al. Alcohol-related liver disease: Areas of consensus, unmet needs and opportunities for further study. *J. Hepatol.* **2019**, *70*, 521–530. [[CrossRef](#)] [[PubMed](#)]
3. Asrani, S.K.; Devarbhavi, H.; Eaton, J.; Kamath, P.S. Burden of liver diseases in the world. *J. Hepatol.* **2019**, *70*, 151–171. [[CrossRef](#)] [[PubMed](#)]
4. Ceni, E.; Mello, T.; Galli, A. Pathogenesis of alcoholic liver disease: Role of oxidative metabolism. *World J. Gastroenterol.* **2014**, *20*, 17756–17772. [[CrossRef](#)] [[PubMed](#)]
5. Gao, B.; Tsukamoto, H. Inflammation in alcoholic and nonalcoholic fatty liver disease: Friend or foe? *Gastroenterology* **2016**, *150*, 1704–1709. [[CrossRef](#)] [[PubMed](#)]
6. Iranshahy, M.; Iranshahi, M.; Abtahi, S.R.; Karimi, G. The role of nuclear factor erythroid 2–related factor 2 in hepatoprotective activity of natural products: A review. *Food Chem. Toxicol.* **2018**, *120*, 261–276. [[CrossRef](#)] [[PubMed](#)]
7. Vomund, S.; Schafer, A.; Parnham, M.J.; Brune, B.; von Knethen, A. Nrf2, the master regulator of anti-oxidative responses. *Int. J. Mol. Sci.* **2017**, *18*, 2772. [[CrossRef](#)] [[PubMed](#)]
8. Bellezza, I. Oxidative stress in age-related macular degeneration: Nrf2 as therapeutic target. *Front. Pharmacol.* **2018**, *9*, 1280. [[CrossRef](#)]
9. Hennig, P.; Garstkiewicz, M.; Grossi, S.; Di Filippo, M.; French, L.E.; Beer, H.D. The crosstalk between Nrf2 and inflammasomes. *Int. J. Mol. Sci.* **2018**, *19*, 562. [[CrossRef](#)]
10. Li, N.; Nel, A.E. Role of the Nrf2-mediated signaling pathway as a negative regulator of inflammation: Implications for the impact of particulate pollutants on asthma. *Antioxid Redox Signal* **2006**, *8*, 88–98. [[CrossRef](#)]
11. Lu, C.; Xu, W.; Zhang, F.; Shao, J.; Zheng, S. Nrf2 knockdown disrupts the protective effect of curcumin on alcohol-induced hepatocyte necroptosis. *Mol. Pharm.* **2016**, *13*, 4043–4053. [[CrossRef](#)] [[PubMed](#)]
12. Lamle, J.; Marhenke, S.; Borlak, J.; von Wasielewski, R.; Eriksson, C.J.; Geffers, R.; Manns, M.P.; Yamamoto, M.; Vogel, A. Nuclear factor-erythroid 2-related factor 2 prevents alcohol-induced fulminant liver injury. *Gastroenterology* **2008**, *134*, 1159–1168. [[CrossRef](#)] [[PubMed](#)]
13. Kim, S.S.; Eun, J.W.; Cho, H.J.; Lee, H.Y.; Seo, C.W.; Noh, C.K.; Shin, S.J.; Lee, K.M.; Cho, S.W.; Cheong, J.Y. Effect of fibroblast growth factor-2 and its receptor gene polymorphisms on the survival of patients with hepatitis B virus-associated hepatocellular carcinoma. *Anticancer Res.* **2019**, *39*, 2217–2226. [[CrossRef](#)] [[PubMed](#)]
14. Zhang, Y.; Gong, X.; Yin, Z.; Cui, L.; Yang, J.; Wang, P.; Zhou, Y.; Jiang, X.; Wei, S.; Wang, F.; et al. Association between NRG1 gene polymorphism and resting-state hippocampal functional connectivity in schizophrenia. *BMC Psychiatry* **2019**, *19*, 108. [[CrossRef](#)] [[PubMed](#)]
15. Wang, X.; Chen, H.; Liu, J.; Ouyang, Y.; Wang, D.; Bao, W.; Liu, L. Association between the NF-E2 related factor 2 gene polymorphism and oxidative stress, anti-oxidative status, and newly-diagnosed type 2 diabetes mellitus in a chinese population. *Int. J. Mol. Sci.* **2015**, *16*, 16483–16496. [[CrossRef](#)] [[PubMed](#)]
16. Weerachayaphorn, J.; Amaya, M.J.; Spirli, C.; Chansela, P.; Mitchell-Richards, K.A.; Ananthanarayanan, M.; Nathanson, M.H. Nuclear factor, Erythroid 2-Like 2 regulates expression of type 3 Inositol 1,4,5-trisphosphate receptor and calcium signaling in cholangiocytes. *Gastroenterology* **2015**, *149*, 211–222.e10. [[CrossRef](#)] [[PubMed](#)]
17. Purdom-Dickinson, S.E.; Sheveleva, E.V.; Sun, H.; Chen, Q.M. Translational control of nrf2 protein in activation of antioxidant response by oxidants. *Mol. Pharmacol.* **2007**, *72*, 1074–1081. [[CrossRef](#)] [[PubMed](#)]
18. Covas, G.; Marinho, H.S.; Cyrne, L.; Antunes, F. Activation of Nrf2 by H₂O₂: De Novo Synthesis Versus Nuclear Translocation. In *Methods in Enzymology*; Academic Press: Cambridge, MA, USA, 2013; Volume 528, pp. 157–171.
19. Milani, P.; Gagliardi, S.; Cova, E.; Cereda, C. SOD1 transcriptional and posttranscriptional regulation and its potential implications in ALS. *Neurol. Res. Int.* **2011**, *2011*, 458427. [[CrossRef](#)]

20. Shasthry, S.M.; Rastogi, A.; Bihari, C.; Vijayaraghavan, R.; Arora, V.; Sharma, M.K.; Sarin, S.K. Histological activity score on baseline liver biopsy can predict non-response to steroids in patients with severe alcoholic hepatitis. *Virchows Arch.* **2018**, *472*, 667–675. [[CrossRef](#)]
21. Brookes, A.J. The essence of SNPs. *Gene* **1999**, *234*, 177–186. [[CrossRef](#)]
22. Stickel, F.; Datz, C.; Hampe, J.; Bataller, R. Pathophysiology and management of alcoholic liver disease: Update 2016. *Gut Liver* **2017**, *11*, 173–188. [[CrossRef](#)] [[PubMed](#)]
23. Magdaleno, F.; Blajszczak, C.C.; Nieto, N. Key events participating in the pathogenesis of alcoholic liver disease. *Biomolecules* **2017**, *7*, 9. [[CrossRef](#)] [[PubMed](#)]
24. Reed, T.; Page, W.F.; Viken, R.J.; Christian, J.C. Genetic predisposition to organ-specific endpoints of alcoholism. *Alcohol. Clin. Exp. Res.* **1996**, *20*, 1528–1533. [[CrossRef](#)] [[PubMed](#)]
25. Toth, R.; Fiatal, S.; Petrovski, B.; McKee, M.; Adany, R. Combined effect of ADH1B RS1229984, RS2066702 and ADH1C RS1693482/RS698 alleles on alcoholism and chronic liver diseases. *Dis. Markers* **2011**, *31*, 267–277. [[CrossRef](#)] [[PubMed](#)]
26. Zhang, Y.; Guo, T.; Yang, F.; Mao, Y.; Li, L.; Liu, C.; Sun, Q.; Li, Y.; Huang, J. Single-nucleotide rs738409 polymorphisms in the PNPLA3 gene are strongly associated with alcoholic liver disease in Han Chinese males. *Hepatol. Int.* **2018**, *12*, 429–437. [[CrossRef](#)] [[PubMed](#)]
27. Anstee, Q.M.; Daly, A.K.; Day, C.P. Genetics of alcoholic liver disease. *Semin. Liver Dis.* **2015**, *35*, 361–374. [[PubMed](#)]
28. BasuRay, S.; Wang, Y.; Smagris, E.; Cohen, J.C.; Hobbs, H.H. Accumulation of PNPLA3 on lipid droplets is the basis of associated hepatic steatosis. *Proc. Natl. Acad. Sci. USA* **2019**, *116*, 9521–9526. [[CrossRef](#)] [[PubMed](#)]
29. Liangpunsakul, S.; Puri, P.; Shah, V.H.; Kamath, P.; Sanyal, A.; Urban, T.; Ren, X.; Katz, B.; Radaeva, S.; Chalasani, N.; et al. Effects of age, sex, body weight, and quantity of alcohol consumption on occurrence and severity of alcoholic hepatitis. *Clin. Gastroenterol. Hepatol.* **2016**, *14*, 1831–1838.e3. [[CrossRef](#)]
30. Atkinson, S.R.; Way, M.J.; McQuillin, A.; Morgan, M.Y.; Thursz, M.R. Homozygosity for rs738409:G in PNPLA3 is associated with increased mortality following an episode of severe alcoholic hepatitis. *J. Hepatol.* **2017**, *67*, 120–127. [[CrossRef](#)] [[PubMed](#)]
31. Buch, S.; Stickel, F.; Trépo, E.; Way, M.; Herrmann, A.; Nischalke, H.D.; Brosch, M.; Rosendahl, J.; Berg, T.; Ridinger, M.; et al. A genome-wide association study confirms PNPLA3 and identifies TM6SF2 and MBOAT7 as risk loci for alcohol-related cirrhosis. *Nat. Genet.* **2015**, *47*, 1443. [[CrossRef](#)] [[PubMed](#)]
32. Salameh, H.; Raff, E.; Erwin, A.; Seth, D.; Nischalke, H.D.; Falletti, E.; Burza, M.A.; Leathert, J.; Romeo, S.; Molinaro, A.; et al. PNPLA3 gene polymorphism is associated with predisposition to and severity of alcoholic liver disease. *Am. J. Gastroenterology* **2015**, *110*, 846–856. [[CrossRef](#)] [[PubMed](#)]
33. Friedrich, K.; Wannhoff, A.; Kattner, S.; Brune, M.; Hov, J.R.; Weiss, K.H.; Antoni, C.; Dollinger, M.; Neumann-Haefelin, C.; Seufferlein, T.; et al. PNPLA3 in end-stage liver disease: Alcohol consumption, hepatocellular carcinoma development, and transplantation-free survival. *J. Gastroenterol. Hepatol.* **2014**, *29*, 1477–1484. [[CrossRef](#)] [[PubMed](#)]
34. Falletti, E.; Cussigh, A.; Cmet, S.; Fabris, C.; Toniutto, P. PNPLA3 rs738409 and TM6SF2 rs58542926 variants increase the risk of hepatocellular carcinoma in alcoholic cirrhosis. *Dig. Liver Dis.* **2016**, *48*, 69–75. [[CrossRef](#)] [[PubMed](#)]
35. Goossens, N.; Hoshida, Y. Is hepatocellular cancer the same disease in alcoholic and nonalcoholic fatty liver diseases? *Gastroenterology* **2016**, *150*, 1710–1717. [[CrossRef](#)] [[PubMed](#)]
36. Sookoian, S.; Castano, G.O.; Scian, R.; Mallardi, P.; Fernandez Gianotti, T.; Burgueno, A.L.; San Martino, J.; Pirola, C.J. Genetic variation in transmembrane 6 superfamily member 2 and the risk of nonalcoholic fatty liver disease and histological disease severity. *Hepatology* **2015**, *61*, 515–525. [[CrossRef](#)] [[PubMed](#)]
37. Goffredo, M.; Caprio, S.; Feldstein, A.E.; D’Adamo, E.; Shaw, M.M.; Pierpont, B.; Savoye, M.; Zhao, H.; Bale, A.E.; Santoro, N. Role of TM6SF2 rs58542926 in the pathogenesis of nonalcoholic pediatric fatty liver disease: A multiethnic study. *Hepatology* **2016**, *63*, 117–125. [[CrossRef](#)] [[PubMed](#)]
38. Mancina, R.M.; Dongiovanni, P.; Petta, S.; Pingitore, P.; Meroni, M.; Rametta, R.; Boren, J.; Montalcini, T.; Pujia, A.; Wiklund, O.; et al. The MBOAT7-TMC4 variant rs641738 increases risk of nonalcoholic fatty liver disease in individuals of European descent. *Gastroenterology* **2016**, *150*, 1219–1230. [[CrossRef](#)] [[PubMed](#)]
39. Thabet, K.; Chan, H.L.Y.; Petta, S.; Mangia, A.; Berg, T.; Boonstra, A.; Brouwer, W.P.; Abate, M.L.; Wong, V.W.; Nazmy, M.; et al. The membrane-bound O-acyltransferase domain-containing 7 variant rs641738 increases inflammation and fibrosis in chronic hepatitis B. *Hepatology* **2017**, *65*, 1840–1850. [[CrossRef](#)] [[PubMed](#)]

40. Meroni, M.; Longo, M.; Rametta, R.; Dongiovanni, P. Genetic and epigenetic modifiers of alcoholic liver disease. *Int. J. Mol. Sci.* **2018**, *19*, 3857. [[CrossRef](#)] [[PubMed](#)]
41. Bataille, A.M.; Manautou, J.E. Nrf2: A potential target for new therapeutics in liver disease. *Clin. Pharmacol. Ther.* **2012**, *92*, 340–348. [[CrossRef](#)] [[PubMed](#)]
42. Xu, D.; Xu, M.; Jeong, S.; Qian, Y.; Wu, H.; Xia, Q.; Kong, X. The role of Nrf2 in liver disease: Novel molecular mechanisms and therapeutic approaches. *Front. Pharmacol.* **2018**, *9*, 1428. [[CrossRef](#)] [[PubMed](#)]
43. Zhao, N.; Guo, F.F.; Xie, K.Q.; Zeng, T. Targeting Nrf-2 is a promising intervention approach for the prevention of ethanol-induced liver disease. *Cell. Mol. Life Sci.* **2018**, *75*, 3143–3157. [[CrossRef](#)] [[PubMed](#)]
44. Shin, S.M.; Yang, J.H.; Ki, S.H. Role of the Nrf2-ARE pathway in liver diseases. *Oxid. Med. Cell. Longev.* **2013**, *2013*, 763257. [[CrossRef](#)] [[PubMed](#)]
45. Suh, J.H.; Shenvi, S.V.; Dixon, B.M.; Liu, H.; Jaiswal, A.K.; Liu, R.M.; Hagen, T.M. Decline in transcriptional activity of Nrf2 causes age-related loss of glutathione synthesis, which is reversible with lipoic acid. *Proc. Natl. Acad. Sci. USA* **2004**, *101*, 3381–3386. [[CrossRef](#)] [[PubMed](#)]
46. Niedzielska, E.; Smaga, I.; Gawlik, M.; Moniczewski, A.; Stankowicz, P.; Pera, J.; Filip, M. Oxidative stress in neurodegenerative diseases. *Mol. Neurobiol.* **2016**, *53*, 4094–4125. [[CrossRef](#)] [[PubMed](#)]
47. Kensler, T.W.; Wakabayashi, N.; Biswal, S. Cell survival responses to environmental stresses via the Keap1-Nrf2-ARE pathway. *Annu. Rev. Pharmacol. Toxicol.* **2007**, *47*, 89–116. [[CrossRef](#)]
48. Marzec, J.M.; Christie, J.D.; Reddy, S.P.; Jedlicka, A.E.; Vuong, H.; Lanken, P.N.; Aplenc, R.; Yamamoto, T.; Yamamoto, M.; Cho, H.Y.; et al. Functional polymorphisms in the transcription factor NRF2 in humans increase the risk of acute lung injury. *FASEB J.* **2007**, *21*, 2237–2246. [[CrossRef](#)] [[PubMed](#)]
49. Arisawa, T.; Tahara, T.; Shibata, T.; Nagasaka, M.; Nakamura, M.; Kamiya, Y.; Fujita, H.; Hasegawa, S.; Takagi, T.; Wang, F.Y.; et al. The relationship between Helicobacter pylori infection and promoter polymorphism of the Nrf2 gene in chronic gastritis. *Int. J. Mol. Med.* **2007**, *19*, 143–148. [[CrossRef](#)] [[PubMed](#)]
50. Arisawa, T.; Tahara, T.; Shibata, T.; Nagasaka, M.; Nakamura, M.; Kamiya, Y.; Fujita, H.; Yoshioka, D.; Arima, Y.; Okubo, M.; et al. Association between promoter polymorphisms of nuclear factor-erythroid 2-related factor 2 gene and peptic ulcer diseases. *Int. J. Mol. Med.* **2007**, *20*, 849–853. [[CrossRef](#)] [[PubMed](#)]
51. Arisawa, T.; Tahara, T.; Shibata, T.; Nagasaka, M.; Nakamura, M.; Kamiya, Y.; Fujita, H.; Yoshioka, D.; Okubo, M.; Sakata, M.; et al. Nrf2 gene promoter polymorphism is associated with ulcerative colitis in a Japanese population. *Hepato-gastroenterology* **2008**, *55*, 394–397.
52. Hua, C.C.; Chang, L.C.; Tseng, J.C.; Chu, C.M.; Liu, Y.C.; Shieh, W.B. Functional haplotypes in the promoter region of transcription factor Nrf2 in chronic obstructive pulmonary disease. *Dis. Markers* **2010**, *28*, 185–193. [[CrossRef](#)] [[PubMed](#)]
53. Von Otter, M.; Bergstrom, P.; Quattrone, A.; De Marco, E.V.; Annesi, G.; Soderkvist, P.; Wettinger, S.B.; Drozdik, M.; Bialecka, M.; Nissbrandt, H.; et al. Genetic associations of Nrf2-encoding NFE2L2 variants with Parkinson's disease—A multicenter study. *BMC Med. Genet.* **2014**, *15*, 131. [[CrossRef](#)] [[PubMed](#)]
54. Shimoyama, Y.; Mitsuda, Y.; Tsuruta, Y.; Hamajima, N.; Niwa, T. Polymorphism of Nrf2, an antioxidative gene, is associated with blood pressure and cardiovascular mortality in hemodialysis patients. *Int. J. Med. Sci.* **2014**, *11*, 726–731. [[CrossRef](#)] [[PubMed](#)]
55. Gui, Y.; Zhang, L.; Lv, W.; Zhang, W.; Zhao, J.; Hu, X. NFE2L2 variations reduce antioxidant response in patients with Parkinson disease. *Oncotarget* **2016**, *7*, 10756–10764. [[CrossRef](#)] [[PubMed](#)]
56. Camp, R.L.; Chung, G.G.; Rimm, D.L. Automated subcellular localization and quantification of protein expression in tissue microarrays. *Nat. Med.* **2002**, *8*, 1323–1328. [[CrossRef](#)] [[PubMed](#)]



Expression of the type 3 InsP₃ receptor is a final common event in the development of hepatocellular carcinoma

Mateus T Guerra,¹ Rodrigo M Florentino,² Andressa Franca,² Antonio C Lima Filho,² Marcione L dos Santos,² Roberta C Fonseca,² Fernanda O Lemos,² Matheus C Fonseca,³ Emma Kruglov,¹ Albert Mennone,¹ Basile Njei,¹ Joanna Gibson,⁴ Fulan Guan,⁵ Yung-Chi Cheng,⁵ Meenakshisundaram Ananthanarayanan,¹ Jianlei Gu,^{6,7} Jianping Jiang,^{6,7} Hongyu Zhao,⁶ Cristiano X Lima,⁸ Paula T Vidigal,⁹ Andre G Oliveira,² Michael H Nathanson,¹ Maria Fatima Leite²

► Additional material is published online only. To view please visit the journal online (<http://dx.doi.org/10.1136/gutjnl-2018-317811>).

For numbered affiliations see end of article.

Correspondence to

Dr Michael H Nathanson, Internal Medicine, Section of Digestive Diseases, Yale University School of Medicine, New Haven, CT 06519, USA; michael.nathanson@yale.edu

MTG and RMF contributed equally.
MHN and MFL contributed equally.

Received 26 October 2018
Revised 25 June 2019
Accepted 30 June 2019
Published Online First 17 July 2019



© Author(s) (or their employer(s)) 2019. No commercial re-use. See rights and permissions. Published by BMJ.

To cite: Guerra MT, Florentino RM, Franca A, et al. *Gut* 2019;**68**:1676–1687.

ABSTRACT

Background & objectives Hepatocellular carcinoma (HCC) is the second leading cause of cancer death worldwide. Several types of chronic liver disease predispose to HCC, and several different signalling pathways have been implicated in its pathogenesis, but no common molecular event has been identified. Ca²⁺ signalling regulates the proliferation of both normal hepatocytes and liver cancer cells, so we investigated the role of intracellular Ca²⁺ release channels in HCC.

Design Expression analyses of the type 3 isoform of the inositol 1, 4, 5-trisphosphate receptor (ITPR3) in human liver samples, liver cancer cells and mouse liver were combined with an evaluation of DNA methylation profiles of ITPR3 promoter in HCC and characterisation of the effects of ITPR3 expression on cellular proliferation and apoptosis. The effects of *de novo* ITPR3 expression on hepatocyte calcium signalling and liver growth were evaluated in mice.

Results ITPR3 was absent or expressed in low amounts in hepatocytes from normal liver, but was expressed in HCC specimens from three independent patient cohorts, regardless of the underlying cause of chronic liver disease, and its increased expression level was associated with poorer survival. The *ITPR3* gene was heavily methylated in control liver specimens but was demethylated at multiple sites in specimens of patient with HCC. Administration of a demethylating agent in a mouse model resulted in ITPR3 expression in discrete areas of the liver, and Ca²⁺ signalling was enhanced in these regions. In addition, cell proliferation and liver regeneration were enhanced in the mouse model, and deletion of *ITPR3* from human HCC cells enhanced apoptosis.

Conclusions These results provide evidence that *de novo* expression of ITPR3 typically occurs in HCC and may play a role in its pathogenesis.

INTRODUCTION

Hepatocellular carcinoma (HCC) is distinguished from most types of malignancy in several ways. First, its incidence is rising,¹ which has been attributed

Significance of this study

What is already known on this subject?

► Liver cancer is the second most common cause of cancer death worldwide. Although a few non-overlapping signalling pathways contribute to its pathogenesis, no final common pathway to the development of this cancer is known. Calcium signalling mediated by intracellular calcium channels of the inositol 1, 4, 5-trisphosphate receptor (ITPR) family controls the balance between cellular proliferation and cell death in other types of malignancies but its role in liver cancer has not been explored.

What are the new findings?

► The intracellular calcium channel type 3 isoform of the ITPR (ITPR3), which is nearly absent in healthy liver, becomes expressed during the development of liver cancer in multiple cohorts of patients with liver cancer and in a mouse model.
► This new expression of ITPR3 is due to demethylation of its promoter and results in enhanced calcium signalling and less apoptosis, as well as impaired patient survival.

How might it impact on clinical practice in the foreseeable future?

► These findings suggest that expression of ITPR3 in hepatocytes may be part of a final common pathway in the development of liver cancer and its expression and downstream subcellular calcium signals may be novel targets for therapeutic intervention.

in part to the widespread occurrence of hepatitis B and C worldwide, plus the increasing frequency of non-alcoholic fatty liver disease (NAFLD). Second, the 5-year survival rate has not increased significantly during the past 30 years and remains in the 12%–15% range. Third, tissue biopsy generally is neither required nor obtained to diagnose HCC,² so

molecular profiling of this type of malignancy is not part of most standard treatment strategies. However, there is growing recognition of the fact that there is the variability of behaviour among HCCs and that a better understanding of what governs this behaviour could lead to more effective targeted treatment strategies.³ Ca²⁺ signalling regulates processes important for tumour growth, including cell proliferation^{4,5} and apoptosis,^{6,7} and several studies have implicated Ca²⁺ signalling pathways in HCC in particular. Inositol 1, 4, 5-trisphosphate receptors (ITPRs) are the intracellular Ca²⁺ channels expressed in hepatocytes.⁸ ITPR2 is the dominant isoform and localises to the apical region where it regulates secretion,^{9,10} whereas ITPR1 is localised to the endoplasmic reticulum (ER)–mitochondrial interface where it regulates lipid metabolism.¹¹ ITPR3 is absent or expressed at low levels in normal hepatocytes,⁸ but alterations in its expression are thought to play a causal role in a number of other types of malignancies including colon cancer,¹² melanoma,⁷ mesothelioma and prostate cancer.⁶ Here we investigated whether and how ITPR3 is involved in the pathogenesis of HCC.

METHODS

DNA methylation profile analysis

Publicly available data banks were used for bioinformatics analysis of DNA methylation levels in the promoter region of human *ITPR* genes. Control individuals were selected from the Gene Expression Omnibus and comprised individuals between 33 and 57 years of age, 47% women and 53% men (n=23) with no history of liver inflammation or fibrosis. For patients with liver cancer, a subset of 40 patients were chosen at random from The Cancer Genome Atlas (TCGA) database. Their demographics (mean age 59 years, 65% men, 48% stage I disease) were similar to that of the entire database. In both data banks, the levels of DNA methylation (beta value) were accessed using genomic DNA from the total liver and the Illumina Human Methylation 450 method. CpG islands within the promoter of each *ITPR* gene were selected based on the following ID_REF sequences: *ITPR1* (cg24699271; cg03918306; cg04251662; cg06716686; cg09407429; cg14643330; cg21024916; cg21858376), *ITPR2* (cg02569086; cg03966406; cg16175911; cg18238734; cg24082826; cg25960567) and *ITPR3* (cg02066343; cg02084729; cg02478409; cg03489495; cg05234888; cg08355863; cg09209803; cg12650926; cg12913957; cg14639225; cg16400825; cg19889152; cg20706766; cg22065976; cg24603235; cg27193704). The percentage of CpG islands in the *ITPR3* promoter region was obtained using the Ensembl genome browser.

Analysis of survival data of patients with HCC

Data generated from the TCGA Research Network (<http://cancergenome.nih.gov/>) were used to divide patients into two groups based on *ITPR3* mRNA expression levels. The first group consisted of 39 out of 370 patients (10.5%) with elevated *ITPR3* expression ($z > 1.0$ as the cut-off). The remaining 331 patients ($z < 1.0$) were grouped as normal *ITPR3* expression. Overall and disease-free 5-year survival curves for each group were plotted in GraphPad Prism.

Animal studies

Swiss male mice (8–10 weeks old) were used for the treatments with the DNA methylation inhibitor 5'-azacytidine (5'-aza). Animals were housed under a 12-hour light–dark cycle, with *ad libitum* access to standard diet and water. The treatment group received daily i.p. injection of 5'-aza (2 mg/kg of body weight)

for 7 days. Control mice were injected with sterile saline. Body weight was monitored daily and animals were sacrificed on day 8 for collection of liver tissue and blood samples. Similarly, male Floxed ITPR3 (FloxR3), kindly provided by Dr Ju Chen (University of California, San Diego, California, USA)¹³ and liver-specific ITPR3 knock out (LSKO3) mice on C57/BL6 background were subjected to the same 5'-aza treatment prior to partial hepatectomy (PH). LSKO3 were generated by crossing FloxR3 mice with Albumin Cre (Jackson Laboratories, Bar Harbor, Maine, USA) as reported previously.¹¹ For the induction of HCC, 2-week-old male C57/BL6 mice (Jackson Laboratories) were injected with a single intraperitoneal dose of diethylnitrosamine (50 mg/kg of body weight). Control animals were injected with sterile saline. Animals were killed at 6, 9 and 12 months after the injection for tissue collection and analysis.

Four-week-old NCR nude female mice (average body weight, 20 g) were obtained from Charles River (Worcester, Massachusetts, USA) and acclimated to laboratory conditions 1 week before tumour implantation. Nude mice were maintained in accordance with the Institutional Animal Care and Use Committee procedures and guidelines. HepG2 tumour xenografts were established by subcutaneous injection of 5×10^6 HepG2 cells/site (wild type (WT) or ITPR3KO) in each mouse. Starting at 14 days postinjection, HepG2 tumours were measured daily using a calliper and the body weights of the mice were monitored as well.

Culture of primary hepatocytes

Mouse hepatocytes were isolated from livers of male Swiss mice after 5'-aza treatment. Briefly, livers were perfused with Hanks A and then Hanks B medium containing 0.05% collagenase (Roche Applied Science) and passed through a 40 μ m nylon mesh filter to yield primary hepatocytes in suspension. Hepatocytes were then plated on collagen-I-coated coverslips at 37°C in 5% CO₂/95% O₂ in Williams' medium E (Thermo Fisher Scientific) containing 10% fetal bovine serum, 50 units/mL penicillin and 50 g/mL streptomycin. Hepatocytes were used 4–6 hours after isolation, as previously described.¹⁴

Serum chemistries

Mouse serum was obtained by centrifugation of total blood and used to assess liver function through the following panel of serological tests: alkaline phosphatase (Bioclin, Brazil), alanine aminotransferase (Labtest, Brazil), aspartate aminotransferase (Labtest, Brazil) and gamma-glutamyl transferase (Labtest, Brazil), as previously described.¹⁵

Immunoblotting

Western blots of hepatocyte and liver cancer cell lysates were performed as previously described.¹⁶

DNA methylation of the mouse *ITPR3* promoter region

Genomic DNA was extracted from isolated hepatocytes using DNeasy Blood & Tissue Kit (QUIAGEN) according to the manufacturer's instruction. A total of 1 μ g of genomic DNA was treated with bisulfite using the EZ DNA Methylation Kit (Zymo Research), as reported,¹⁷ which converts unmethylated cytosines into uracil. The promoter region of *ITPR3* was amplified by conventional PCR using the forward primer 5'-AAGCCGCTA-GAGAACGCCC-3' and reverse primer 5'-CCACACACATG-CAAATCCCG-3'. The efficiency of DNA amplification was monitored using a 1% agarose gel electrophoresis followed by capillary electrophoresis sequencing in an ABI3730 apparatus

using POP7 polymer and BigDye V.3.1. Sequencing data were analysed using Sequence Scanner Software (Applied Biosystems).

Real-time PCR

Total mRNA of isolated hepatocytes was extracted using Trizol reagent (Sigma Aldrich) according to the instructions of the user manual. cDNAs were generated from 1 µg RNA using the High-Capacity cDNA Reverse Transcription Kit (Life Technologies). Real-time PCR analyses were carried out with SYBR Green PCR Supermix (Bio-Rad) using PCR primers on a CFX96 Real-Time PCR system (Bio-Rad). Mouse *ITPR3* primers were used and the relative mRNA expression was determined by the comparative Ct method using Bio-Rad software (Bio-Rad) with beta-actin as the reference gene.

RNA sequencing and enrichment analysis

Total RNA was isolated from WT and *ITPR3*KO HepG2 cells (five biological replicates/each) using the RNeasy kit (Qiagen, Germantown, Maryland, USA). RNA integrity number was determined by Agilent Bioanalyzer 2100 (Agilent Technologies). On average, 30 million sequencing reads (100 bp paired-end) of each sample were obtained using an Illumina 6000 Sequencer and the reads were mapped to the University of California Santa Cruz hg19 human genome by STAR (2.5.4b-foss-2016b),¹⁸ 87.77% of which were uniquely aligned to the reference. The raw read counts of genes were counted using subread (1.6.4)¹⁹ based on National Center for Biotechnology Information RefSeq annotation. Within R Bioconductor, edgeR package was applied to normalise raw read counts, and log₂ transformed counts per million represent the relative expression level of individual genes.²⁰ The limma package was used to detect differential expression between the groups;²¹ linear modelling was applied with subsequent empirical Bayesian analysis p-value adjustment for multiple testing. Pathways enrichment of significant differentially expressed genes ($p \leq 0.05$) in different gene subsets was determined by IPA (Ingenuity Pathway Analysis, QIAGEN). The apoptosis (GO:0006915, 2764 genes)-related genes were defined by QuickGO (<https://www.ebi.ac.uk/QuickGO/>).

Immunofluorescence

Isolated hepatocytes were plated onto six-well plates containing glass coverslips treated with collagen type I solution (Sigma) and 4–6 hours later cells were fixed with 4% paraformaldehyde (Electron Microscopy Science) and permeabilised with 0.5% Triton X-100 (Sigma). After washing in phosphate buffered saline (PBS), unspecific binding was blocked using PBS, 10% BSA, Triton X-100 0.05% and 5% goat serum for 1 hour at room temperature. Immunolabelling with primary *ITPR3* monoclonal antibody (1:100; Millipore) was performed for 1 hour at room temperature, followed by 1-hour incubation at room temperature with goat antimouse secondary antibody conjugated with Alexa Fluor 488 (1:200; Life Technologies) and TO-PRO3 (1:1000; Thermo Fisher Scientific) as nuclear staining. Controls in which primary antibodies were omitted showed no specific staining. Images were collected on a Zeiss LSM 510 confocal microscope, as previously described.¹⁶

Immunohistochemistry

Formalin-fixed and paraffin-embedded mouse and human liver tissue sections were de-waxed and antigen retrieval was performed in citrate buffer (10 mM) containing 0.6% hydrogen peroxide. The Novolink Polymer Detection System (Leica Biosystems, Germany) was used in the subsequent steps as described

previously.¹⁵ Primary antibodies against *ITPR3* (1:100; Sigma), proliferating cell nuclear antigen (PCNA) (1:100; Abcam) and 5'-methylcytosine (5mC) (1:400; Zymo Research) were incubated overnight at room temperature followed by incubation with detection polymer for 40 min at room temperature. DAB was used for signal detection. Images were obtained using an optical microscope (Zeiss, Germany) at with a 20× objective. Human liver tissue samples were from three independent cohorts of liver specimens obtained from: (1) Hospital das Clínicas, UFMG; (2) Department of Pathology – Yale New Haven Hospital on approval by the respective human investigation committees; (3) a 40-patient tissue array purchased from US Biomax (Derwood, MD). For quantification purposes of all histological staining, fields of view were chosen by a blinded investigator and the quantification was performed by a different investigator to minimise bias.

In vivo calcium measurements

Animals were anaesthetised with a mixture of ketamine (10%) and xylazine (5%). Livers were loaded with the Ca²⁺ indicator dye Fluo-4/AM (Thermo Fisher Scientific) for 10 min at room temperature and placed onto the stage of a Nikon A1 confocal microscope, as described previously.¹⁵ Arginine vasopressin (AVP), a known InsP3-dependent Ca²⁺ release agonist,^{22,23} was injected IV at a concentration of 100 ng/mL to trigger InsP3-dependent Ca²⁺ release. Data are expressed as fluorescence/baseline fluorescence × 100%. Hepatocytes surrounding the central vein and within a radius of two times the average size of individual hepatocytes were defined as pericentral (PC). The remaining hepatocytes were classified as belonging to the periportal (PP) region.

Partial hepatectomy

PH was carried out as described.²⁴ At 48 hours postsurgery, livers were removed and fixed in 10% neutral buffered formalin and embedded in paraffin for PCNA staining. For quantification of the zonal distribution of PCNA staining, PP and PC zones were defined as areas of twice the radius of the nearby portal and central veins, respectively.

Knockout of *ITPR3* by CRISPR/Cas9 in human cells

A commercially available CRISPR/Cas9 system was used to knock out *ITPR3* in HepG2 liver cancer cells (Santa Cruz Biotechnology). Briefly, cells were cotransfected with a plasmid containing the *ITPR3*-specific guide RNA and the sequence encoding the Cas9 nuclease alongside a plasmid which promotes the insertion of red fluorescent protein (RFP) and puromycin resistance sequences via homology-directed repair within the deleted loci in the *ITPR3* gene. After 2 weeks, cells were subjected to fluorescence-activated cell sorting and red fluorescent cells were sorted and cultured under puromycin (1 µg/mL) selection following a limited dilution protocol. On expansion, RFP-positive clones were subjected to Western blot analysis of *ITPR3* to verify successful knock out. Successful deletion of exon 3 of the *ITPR3* gene and correct integration of the sequences coding for RFP and puromycin resistance were confirmed by PCR amplification followed by automated DNA sequencing. Control HepG2 cells are referred to as WT and correspond to non-transfected cells cultured in media without Puromycin. Cells depleted of *ITPR3* are referred to as *ITPR3*KO. Cells were grown in Dulbecco Modified Eagles Media supplemented with L-glutamine (1 mM), fetal bovine serum (10% v/v) and penicillin/

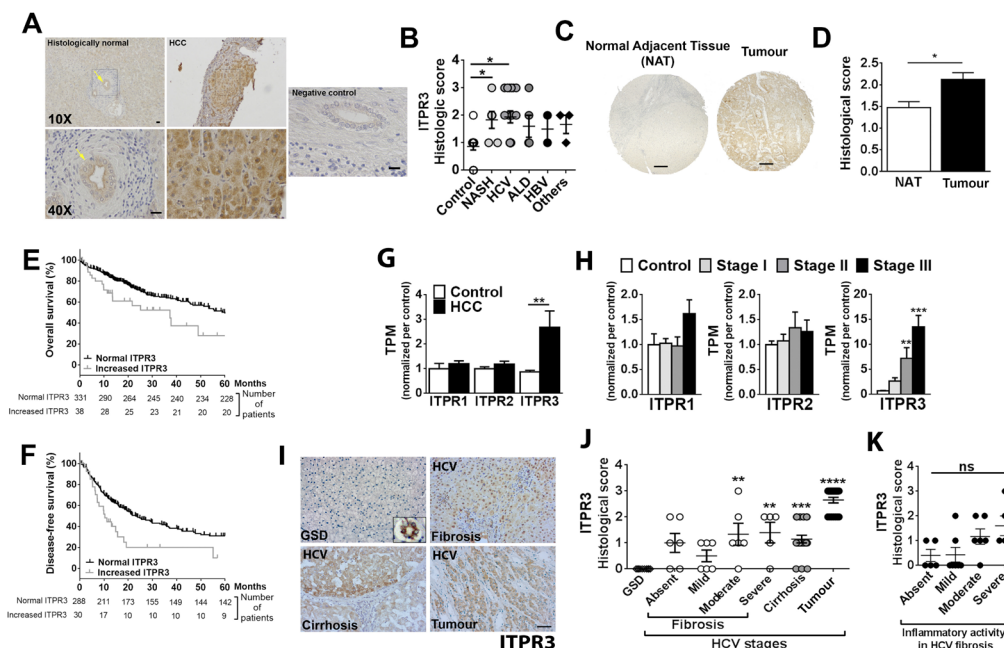


Figure 1 ITPR3 is expressed in human HCC and is associated with poorer survival. (A) ITPR3 expression in a histologically normal liver biopsy (top left) and an HCC specimen (top middle). Bottom row showing a magnified view of the regions marked with the black square in the top row. Bottom left showing ITPR3 expressed in the apical region of a bile duct in the normal liver specimen (arrow) but is minimal in surrounding hepatocytes. Bottom middle showing that there is diffuse cytosolic staining of ITPR3 in HCC hepatocytes. Top and bottom right showing a negative control (scale bar, 20 μ m). (B) Quantification of ITPR3 staining showing that labelling is significantly increased in HCC specimens from patients with NASH and HCV ($p < 0.05$, $n = 15$ and $p < 0.01$, $n = 6$, respectively by ANOVA with Dunnett's post-test) relative to control specimens ($n = 17$). The remaining samples were: alcoholic liver disease ($n = 5$) and HBV infection ($n = 2$); additionally, two specimens were from patients in which two of these liver diseases were present. (C) ITPR3 staining in HCC (tumour) and NAT in a representative image from a commercially obtained tissue microarray (scale bar, 200 μ m). (D) ITPR3 staining of HCC was significantly increased relative to the correspondent NATs. ($n = 40$, $p < 0.01$ by paired t test). (E) Five-year survival is reduced in patients with HCC with ITPR3 mRNA expression with $z > 1$ above the mean (median = 37.3 months, $n = 39$) in comparison to all other patients with HCC (median = 60.8 months, $n = 332$; $p < 0.01$ by log-rank test). (F) Disease-free survival is also decreased in patients with HCC with higher ITPR3 expression (median = 10.4 months in high ITPR3 versus median = 23.0 months in other patients with HCC; $p < 0.004$ by log-rank test). (G) mRNA expression of ITPR1–3 in control ($n = 26$) and patients with HCC ($n = 89$). ITPR1 and ITPR2, which are physiologically expressed in hepatocytes, are not altered in HCC, but ITPR3 expression is significantly increased in HCC ($p < 0.05$, Bonferroni post-tests). (H) mRNA expression of ITPR3 correlates with the clinical stage of HCC. mRNA levels of ITPR1 and ITPR2 are similar in clinical stages I–III. However, mRNA of ITPR3 is significantly increased in stage II and stage III compared with control (** $p < 0.05$ and *** $p < 0.001$, Bonferroni post-tests, respectively). (I) Representative images of ITPR3 staining in specimens collected from Universidade Federal de Minas Gerais diagnosed with GSD ($n = 10$), and different stages of the of HCV infection, such as fibrosis ($n = 20$), cirrhosis ($n = 20$) and tumour ($n = 20$). ITPR3 was not detected in GSD hepatocytes, even though it was expressed in cholangiocytes (inset) (scale bar, 50 μ m). (J) Quantification of ITPR3 staining according to the degree of fibrosis showing that ITPR3 starts to be expressed as early as in moderate fibrosis and remains elevated until the tumour stage in specimens from HCV-infected patients (** $p < 0.05$, *** $p < 0.01$ and **** $p < 0.001$). (K) ITPR3 expression is not correlated to inflammatory activity in HCV infection specimens. ALD, alcoholic liver disease; ANOVA, analysis of variance; GSD, glycogen storage disease; HBV, hepatitis B virus; HCC, hepatocellular carcinoma; HCV, hepatitis C virus; ITPR1, type 1 isoform of the inositol 1, 4, 5-trisphosphate receptor; ITPR2, type 2 isoform of the inositol 1, 4, 5-trisphosphate receptor; ITPR3, type 3 isoform of the inositol 1, 4, 5-trisphosphate receptor; NASH, non-alcoholic steatohepatitis; NAT, non-tumour adjacent tissue.

streptomycin (100 units/mL and 100 mg/mL) at 37°C in a humidified atmosphere containing 5% CO₂.

Apoptosis

WT and ITPR3KO cells were treated with dimethyl sulfoxide (vehicle control), staurosporine (STA, 5 μ M) or etoposide (10, 25 and 50 μ M) for 16 hours followed by luminescence measurements of Caspase 3/7 activity using the Caspase-Glo 3/7 assay (Promega, Madison, Wisconsin, USA) according to the manufacturer's instructions, in a BioTek Synergy 2 plate reader. Additionally, control and STA-treated cells were stained with Annexin V-FITC conjugated antibody and counted in fluorescence-activated cell sorter (FACS; BD LSR II). Results are expressed as percentage of Annexin V positive cells relative to total cell count. HepG2 cells were mock-transfected or transfected with

a mCherry-tagged rat ITPR3 plasmid, a gift from David Yule (University of Rochester Medical Center, Rochester, New York, USA). One day after transfection, cells were treated with STA (5 M for 6 hours) followed by incubation with Yo-Pro-1 and imaged on a Zeiss Axio Observer Z1 epifluorescence microscope with a 20 \times objective to detect apoptotic cell death. The number of Yo-Pro-1-positive cells in 8–14 fields was counted in Image J and is expressed as the percentage of total cells. Primary hepatocytes isolated from control and 5'-aza-treated animals were exposed to vehicle or STA. Cleaved caspase 3 expression was then evaluated in total cell lysates as a marker of apoptosis.

Colocalisation of ITPR3 and mitochondria in HepG2 cells

HepG2 cells were cotransfected with enhanced green fluorescent protein (EGFP)-ITPR3 (a gift from Colin W. Taylor, University

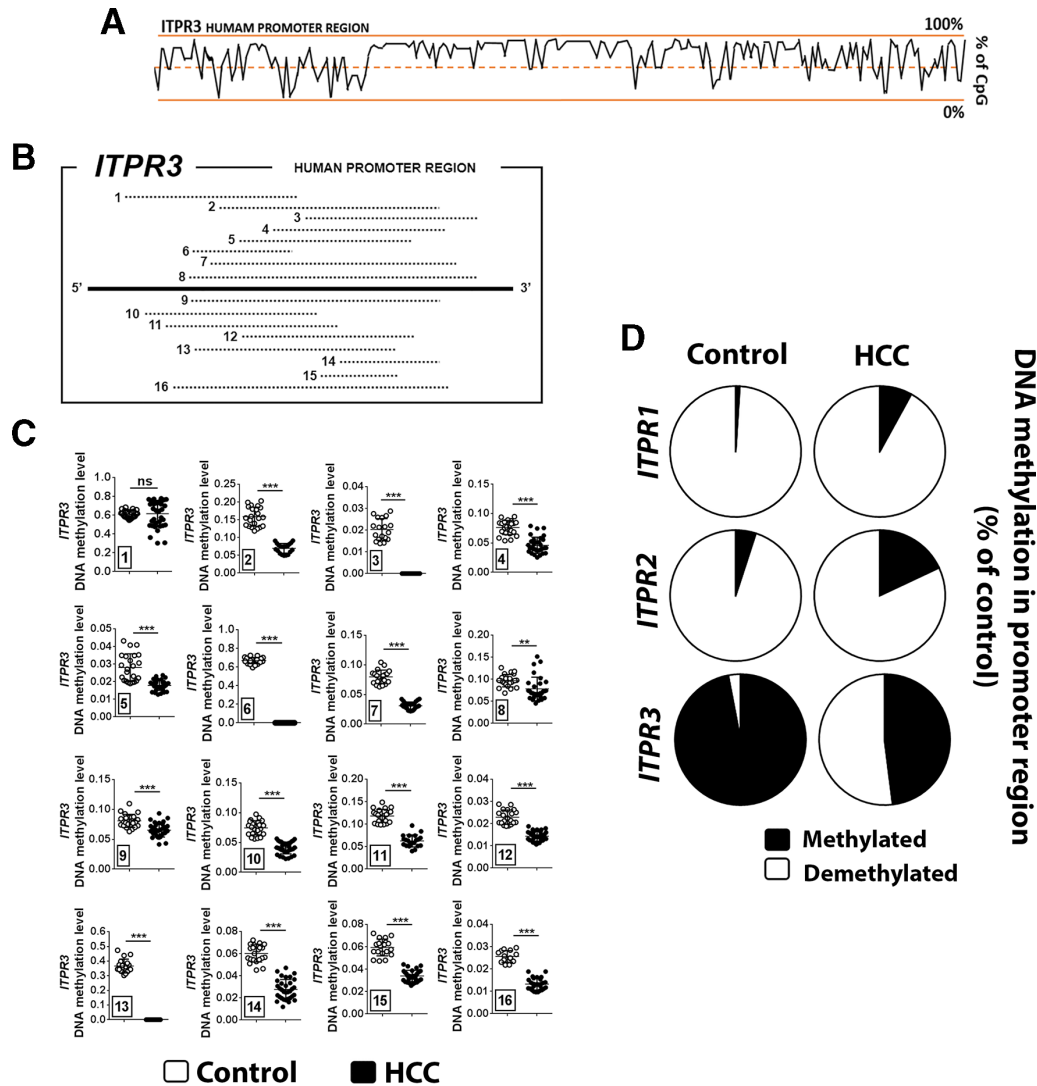


Figure 2 The promoter of human *ITPR3* is demethylated in HCC. (A) CpG islands in the promoter region of the human *ITPR3* gene. The lower line indicates 0% likelihood of a CpG island and the upper line indicates 100% likelihood. (B) Schematic representation of 16 methylated regions in the *ITPR3* promoter, analysed by bioinformatics using GEO data for control patients and TCGA data for patients with HCC. (C) Methylation of the *ITPR3* promoter from patients with HCC ($n=40$) is lower than in control patients ($n=23$) at 16 different sites ($*p<0.05$, Bonferroni post-tests). (D) Percentage methylation of the promoter region of the human *ITPR1*, *ITPR2* and *ITPR3* genes. HCC values are relative to that observed in controls. GEO, Gene Expression Omnibus; HCC, hepatocellular cancer; TCGA, The Cancer Genome Atlas.

of Cambridge, UK)²⁵ and the outer mitochondrial membrane marker mKO2-TOMM20 (a gift from Michael Davidson to Addgene—plasmid # 57899). The cells were imaged on a Zeiss LSM 880 AiryScan Fast Confocal (Zeiss Microscopy, Thornwood, New York, USA) with a 63X/1.4NA objective and excitation of 488 nm and 561 nm for EGFP and KO₂, respectively. The emission signals were collected between 495 and 550 nm (EGFP) and >570 nm (KO₂) on the AiryScan detector and processed for improved (~140 nm) resolution using the built-in super-resolution algorithm in ZEN Black software. Mander's coefficient of colocalisation between EGFP and KO₂ was calculated with the Coloc2 plug-in in ImageJ (National Institutes of Health) in a total of 25 cells from 3 independent transfections.

Statistical analysis

Data are presented as arithmetic mean \pm SD unless otherwise indicated. For statistical analysis, means between two groups were compared by *t*-test or Mann-Whitney non-parametric test as specified in the online supplementary figure legends.

Comparison of multiple groups was performed by one-way analysis of variance with Bonferroni post-tests. A *p*-value of ≤ 0.05 was taken to indicate statistical significance.

RESULTS

ITPR3 was absent in normal human hepatocytes (online supplementary figure 1), but was present in samples of patient with HCC (figure 1A) and cell lines (online supplementary figure 1). *ITPR3* was present regardless of whether the underlying liver disease was hepatitis B virus, hepatitis C virus (HCV), NAFLD or alcoholic liver disease (ALD), which are the four most common predisposing factors to the development of HCC.²⁶ Histological scoring of *ITPR3* staining was significantly increased in HCC specimens from patients with non-alcoholic steatohepatitis and HCV relative to non-HCC controls (figure 1B). In the second cohort, *ITPR3* staining was significantly increased in the tumour area, relative to non-tumour adjacent tissue (NAT; figure 1C,D). To begin to investigate the clinical relevance of this de novo expression, the relationship between *ITPR3* expression

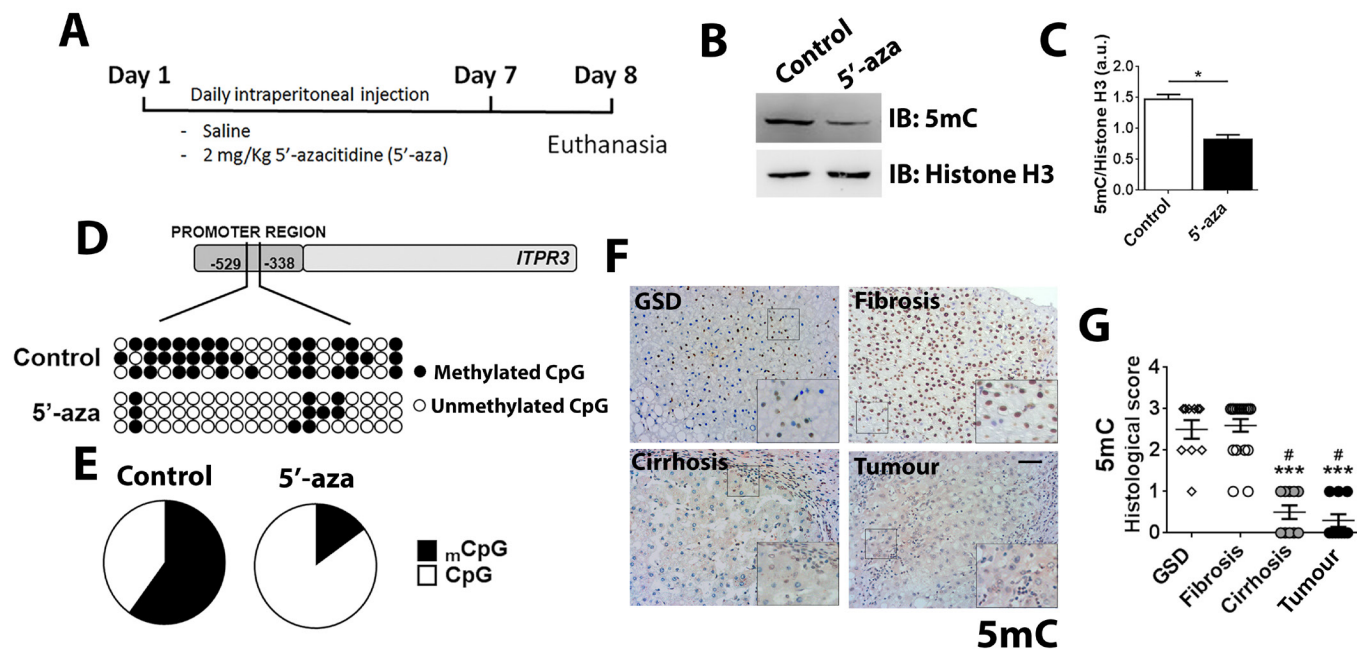


Figure 3 DNA methylation levels are decreased in HCC and in mice treated with 5'-aza. (A) Experimental protocol of 5'-aza treatment in mice. (B) Immunoblot of hepatocyte lysates demonstrating reduction of total methylated cytosine (5mC) after treatment with 5'-aza. (C) Densitometric analysis showing ~50% reduction in methylation after 5'-aza treatment (n=3, *p<0.05, Bonferroni post-test). (D) Demethylation sites of CpG islands in the mouse *ITPR3* promoter region after 5'-aza treatment. Black dots represent methylated sites and white dots represent demethylated sites (n=3 animals for each condition). (E) Percentage of methylated CpG (mCpG, black) and demethylated CpG (white) in the promoter region of the mouse *ITPR3* gene. (F) Representative images of immunostaining for 5mC in livers from patients with GSD (n=10), and different stages of HCV infection, including fibrosis (n=20), cirrhosis (n=20) and tumour (n=20) (scale bar, 50 μ m). (G) Quantification of nuclear 5mC staining showing that methylation is markedly decreased in HCV-related cirrhosis and tumour compared with GSD and HCV-related fibrosis (**p<0.01 and #p<0.001, Bonferroni post-tests). 5'-aza, 5'-azacitidine; GSD, glycogen storage disease; HCC, hepatocellular carcinoma; HCV, hepatitis C virus; *ITPR3*, type 3 isoform of the inositol 1, 4, 5-trisphosphate receptor.

in HCC and patient survival was examined using data from TCGA. *ITPR3* expression was >1z above the mean for patients with HCC in 11% (39 of 371) of the samples, and both 5-year overall and disease-free survival were significantly reduced in this patient group (figure 1E,F). Because normal hepatocytes express *ITPR1* and *ITPR2* and low to undetectable levels of *ITPR3*,⁸ the expressions of all three *ITPRs* were compared between normal and HCC samples from the TCGA repository. *ITPR3* mRNA expression was significantly increased in HCC relative to control specimens, whereas *ITPR1* and *ITPR2* expressions were similar between the two groups (figure 1G). Also, the increased *ITPR3* expression in HCC was more pronounced in disease stages II and III, according to the TNM criteria (figure 1H). To understand whether *ITPR3* expression precedes HCC, expression was examined in liver specimens from the third cohort of patients, with chronic liver disease from HCV or ALD. With either disease, nearly half of the specimens from patients with cirrhosis without HCC expressed *ITPR3*, whereas nearly all specimens from patients with HCC expressed *ITPR3*. In contrast, *ITPR3* was not expressed in patients with glycogen storage disease (GSD), a chronic liver disease that does not typically predispose to HCC in the absence of cirrhosis, such as the patients studied here²⁷ (figure 1I and online supplementary figures 2A, B). Moreover, expression of *ITPR3* increased with the degree of fibrosis (figure 1J), although it did not correlate with inflammatory activity in the same specimens (figure 1K). Additionally, *ITPR3* expression preceded tumour formation in a mouse model of HCC (online supplementary figure 3A). These findings collectively suggest that de novo expression of *ITPR3*

is a common feature of human HCC, precedes its development, and is associated with the degree of fibrosis and with a poorer disease outcome.

To study the role of *ITPR3* on tumour growth in vivo, a HepG2 HCC cell line was developed in which the *ITPR3* gene was deleted using CRISPR/Cas-9 (*ITPR3KO*). Loss of *ITPR3* was confirmed by western blot and by expression of red fluorescent protein (RFP) that was inserted in the genome alongside the CRISPR targeting cassette on successful recombination. WT or *ITPR3KO* HepG2 cells were implanted subcutaneously in nude mice and tumour growth was assessed over time. Tumour growth was monitored over a 1-week period, once all implanted tumours became visible (42 days). During the week in which HCC growth was monitored, five of six WT tumours grew, whereas only three of eight *ITPR3KO* tumours grew. Total tumour volume was significantly lower in animals implanted with *ITPR3KO* cells when compared with mice bearing WT HepG2 cells (online supplementary figure 3B).

Both transcription factors and miRNAs that decrease *ITPR3* expression have been identified,^{28–30} but factors that increase *ITPR3* are not known. Bioinformatic analysis showed that the *ITPR3* promoter region has a number of CpG islands (figure 2A), which are potential methylation sites capable of suppressing gene expression.³¹ In most of the 16 regions analysed (figure 2B), DNA methylation levels were lower in hepatocytes from patients with HCC than in normal controls (figure 2C). In contrast, the promoter regions of *ITPR1* and *ITPR2* were already demethylated in hepatocytes from normal control individuals (figure 2D and online supplementary figure

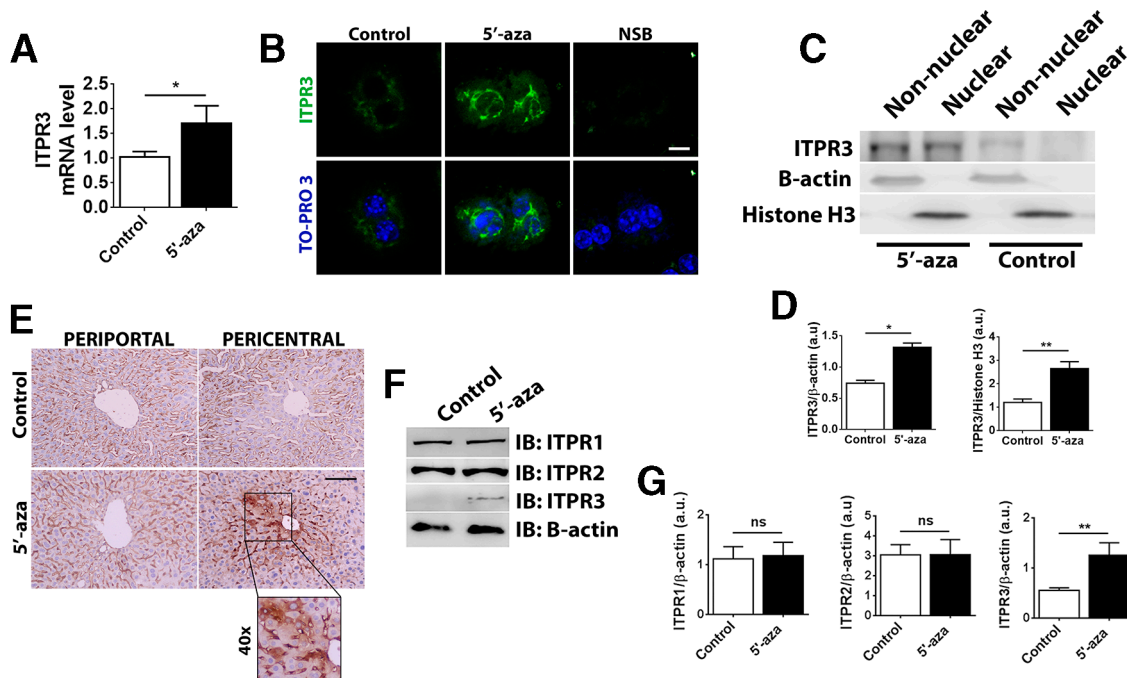


Figure 4 Demethylation induces ITPR3 expression in hepatocytes in vivo. (A) ITPR3 mRNA expression in isolated hepatocytes is significantly increased after 5'-aza treatment, relative to controls (n=5 in each group, *p<0.05, Bonferroni post-tests). (B) ITPR3 staining (green) in isolated mouse hepatocytes from control liver and after 5'-aza treatment demonstrating the subcellular pattern of ITPR3 expression. Nuclei are shown in blue. (scale bar, 10 μ m). (C) Immunoblot of liver lysates showing the presence of ITPR3 in the nuclei of hepatocytes after the demethylation treatment. (D) Densitometric analysis showing cytosolic and nuclear expression of ITPR3 in hepatocytes in 5'-aza-treated hepatocyte lysate (*p<0.05 and **p<0.01, Bonferroni post-tests). (E) Immunohistochemistry for ITPR3 in liver sections showing that expression after 5'-aza treatment is mostly concentrated in the region of the central venule (scale bar, 100 μ m). (F) Representative immunoblot of hepatocyte lysates demonstrating that 5'-aza treatment increases ITPR3 expression relative to control. ITPR1 and ITPR2 expressions are unchanged by 5'-aza. (G) Densitometric analyses showing that ITPR3 is the only ITPR isoform with increased expression after 5'-aza treatment (n=3, **p<0.01, by Student *t*-test). 5'-aza, 5'-azacitidine; ITPR1, type 1 isoform of the inositol 1, 4, 5-trisphosphate receptor; ITPR2, type 2 isoform of the inositol 1, 4, 5-trisphosphate receptor; ITPR3, type 3 isoform of the inositol 1, 4, 5-trisphosphate receptor; NSB, non-specific binding control.

4), consistent with the observation that ITPR1 and ITPR2 are normally expressed in hepatocytes.^{8–10} To investigate more directly the role of DNA methylation in hepatic ITPR3 expression, 5'-aza was used to inhibit DNA methyltransferases in vivo (figure 3A).³² This protocol decreased DNA methylation levels, reflected by a decrease in 5mC staining (figure 3B,C) as well as demethylation of specific CpG islands in the ITPR3 promoter (Figure 3D; Figure 3E), and without evidence for non-specific liver damage (online supplementary figure 5). Similarly, 5mC levels were decreased in HCC specimens when compared with non-cirrhotic GSD controls (Figure 3F; Figure 3G). Together, these results indicated that inhibition of DNA methyltransferase efficiently demethylates ITPR3 promoter and that 5mC levels are decreased in HCC.

Hepatocyte ITPR3 mRNA was increased in response to 5'-aza (figure 4A), and the newly expressed Ca²⁺ channel was localised in part in a perinuclear distribution (figure 4B). Moreover, ITPR3 was present in both nuclear and non-nuclear fractions of hepatocytes isolated from mice treated with 5'-aza (figure 4C,D). ITPR3 was furthermore concentrated in hepatocytes near the central venule (figure 4E), perhaps reflecting the higher capacity of PC hepatocytes to metabolise 5'-aza into its active metabolite.³³ De novo expression of ITPR3 in this model was not associated with altered expression of ITPR1 or ITPR2 (figure 4F,G). The regional difference in ITPR3 expression in an animal model provided the opportunity to examine whether there were corresponding regional differences in Ca²⁺ signalling. Livers were loaded with the Ca²⁺-sensitive fluorescent

dye Fluo-4/AM, then time-lapse confocal imaging was used to monitor hepatocyte Ca²⁺ signalling in vivo. The peak response to the hepatocyte Ca²⁺ agonist AVP was higher in animals treated with 5'-aza (figure 5A,B). This increased response was primarily due to the PC, ITPR3-expressing hepatocytes (figure 5C–E), as a less pronounced increase in Ca²⁺ signalling was seen in PP hepatocytes relative to untreated controls (figure 5F). Also, the time to peak for Ca²⁺ signals was increased in PC, but not in PP hepatocytes, of 5'-aza-treated mice when compared with control, which may reflect the lower sensitivity of ITPR3 to InsP₃ (figure 5G). The amplitude of Ca²⁺ signals in the nucleus also was increased in the PC, ITPR3-expressing hepatocytes (figure 5H and online supplementary figure 6) and PP hepatocytes (figure 5H). However, these regional differences in Ca²⁺ signalling were not observed in hepatocytes isolated from control and 5'-aza-treated mice, likely due to the high concentration of AVP used to trigger Ca²⁺ release (online supplementary figure 7). Nonetheless, the changes in nuclear Ca²⁺ observed in vivo are of potential importance because both normal liver regeneration and growth of liver tumours depend on nuclear Ca²⁺ signals.^{4,5,34}

Finally, several functional effects were examined to understand the pathophysiological significance of expression of ITPR3 in hepatocytes. Because nuclear Ca²⁺ regulates hepatocyte proliferation,^{4,34} liver regeneration following PH was studied. Both liver-to-body weight and nuclear PCNA staining were significantly increased in 5'-aza-treated animals relative to controls at 48 hours after PH (figure 6A–C). PCNA staining was uniformly

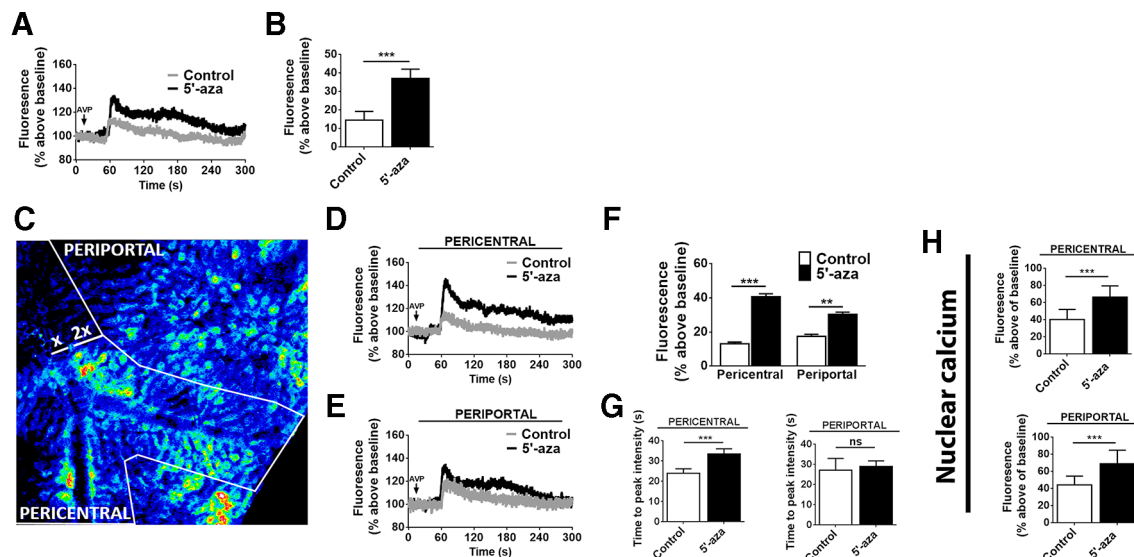


Figure 5 Demethylation enhances calcium signalling in hepatocytes in vivo. (A) Representative time course of hepatocyte Ca^{2+} signals following stimulation by intravenous infusion of AVP (100 ng/mL), monitored by in vivo time-lapse confocal imaging of livers in animals treated with 5'-aza and controls. Fluorescence of the Ca^{2+} dye Fluo-4 is expressed as a percentage of basal fluorescence. (B) Peak fluorescence after AVP stimulation is more than doubled in animals treated with 5'-aza ($n=3$ animals per group, $***p<0.001$). (C) Representative pseudocoloured confocal fluorescence image showing identification of PC and PP regions. (D) Representative time course of Fluo-4 fluorescence levels in hepatocytes near the central venule (PC region), where ITPR3 expression is increased by 5'-aza. Note the increase is greater than is seen by imaging the whole liver. (E) Representative time course of Fluo-4 fluorescence levels in hepatocytes near the portal venule (PP region), where little to no ITPR3 expression is induced by 5'-aza. Note the increase is smaller than that observed in the whole liver. (F) Fluorescence peak after AVP stimulation is higher in PC hepatocytes from animals treated with 5'-aza ($***p<0.001$) than in PP hepatocytes from the same group ($**p<0.01$). (G) Time to the maximal peak of Ca^{2+} in PC hepatocytes is higher in PC hepatocytes from 5'-aza-treated animals ($***p<0.01$). (H) Fluorescence peaks in PC and PP hepatocyte nuclei are significantly increased in animals treated with 5'-aza compared with controls. Fluorescence is expressed as a percentage of basal fluorescence ($n=20$ nuclei were monitored per animal in 3 animals per group, $***p<0.001$). AVP, arginine vasopressin; 5'-aza, 5'-azacitidine; ITPR3, type 3 isoform of the inositol 1, 4, 5-trisphosphate receptor; PC, pericentral; PP, periportal.

distributed across the liver lobule (figure 6D). Also, expressions of ITPR1 and ITPR2, the two main ITPR isoforms in quiescent hepatocytes, did not change at all three time points (24, 48 and 72 hours) post-hepatectomy (online supplementary figure 8). This is in contrast to previous results showing a significant increase of ITPR2 protein expression 48 hours after PH, which may reflect species differences.³⁵

To more directly evaluate the role of ITPR3 in hepatocyte proliferation in vivo, liver regeneration was compared between FloxedR3 (Control) and AlbCreR3KO (LSKO3) mice treated with 5'-aza. After 48 hours, liver-to-body weight ratios were significantly higher in LSKO3 mice when compared with controls (online supplementary figure 9A), but PCNA staining was significantly decreased in LSKO3 mice compared with control (online supplementary figure 9B). ITPR3 expression was detected in control mice around the central veins and occasionally elsewhere throughout the liver lobule, whereas ITPR3 was mostly absent in LSKO3 livers (online supplementary figure 9C). Therefore, hepatocyte proliferation after PH as measured by PCNA labelling is increased when ITPR3 expression is induced and decreased when it is knocked out. It is unclear why liver-to-body weight is increased despite lower PCNA labelling in LSKO3 mice. This may reflect hypertrophy to compensate for impaired proliferation, or else some other chronic compensatory effects, especially in light of previous reports that ITPR3 remains undetectable in hepatocytes after PH in rats.³⁵

Cell proliferation can also be regulated by apoptosis, both in liver regeneration²⁴ and tumour growth.^{6,7} ITPR3-dependent Ca^{2+} release is involved in apoptotic cell death,³⁶ so apoptosis was evaluated in WT and ITPR3KO cells (figure 7A) in several ways.

Caspase 3/7 activity following STA treatment was significantly increased in ITPR3KO cells, relative to WT cells (figure 7B). No difference in baseline caspase activity was detected between the two groups. Similar results were obtained by FACS analysis of Annexin V positive cells (figure 7C). Caspase 3/7 activity also was greater in ITPR3KO cells than in WT when apoptosis was induced with etoposide rather than STA (figure 7D). These results are consistent with the idea that ITPR3 protects HCC cells from cell death via inhibition of apoptosis. Because the transfer of Ca^{2+} from the ER to mitochondria modulates apoptosis in multiple cell types^{6,7} and because ITPR3 preferentially transmits Ca^{2+} to mitochondria,³⁶ colocalisation of a green fluorescent protein (GFP)-tagged ITPR3 and mKO2-TOMM20, a marker of the outer mitochondrial membrane, was evaluated in HepG2 cells using super-resolution microscopy. GFP-ITPR3 distributed throughout the cytosol in a reticular pattern, consistent with it being localised to the ER, and mKO2-TOMM20 was found in tubular structures resembling mitochondria. The colocalisation analysis revealed that a fraction of the GFP-ITPR3 (~15%) overlapped with mKO2-TOMM20 (figure 7E), suggesting that ITPR3 is partially located at the interface between ER and mitochondria. This is consistent with the idea that, when present in hepatocytes, ITPR3 might modulate apoptosis by controlling the transmission of Ca^{2+} between these two organelles.

Apoptosis was also analysed in primary hepatocytes isolated from control and 5'-aza-treated mice in the presence of STA. Cleaved caspase 3 expression was increased in cells treated with STA compared with non-treated controls. In contrast, there was a trend towards increased cleaved caspase 3 expression in cells from 5'-aza-treated mice, and this was not further increased by

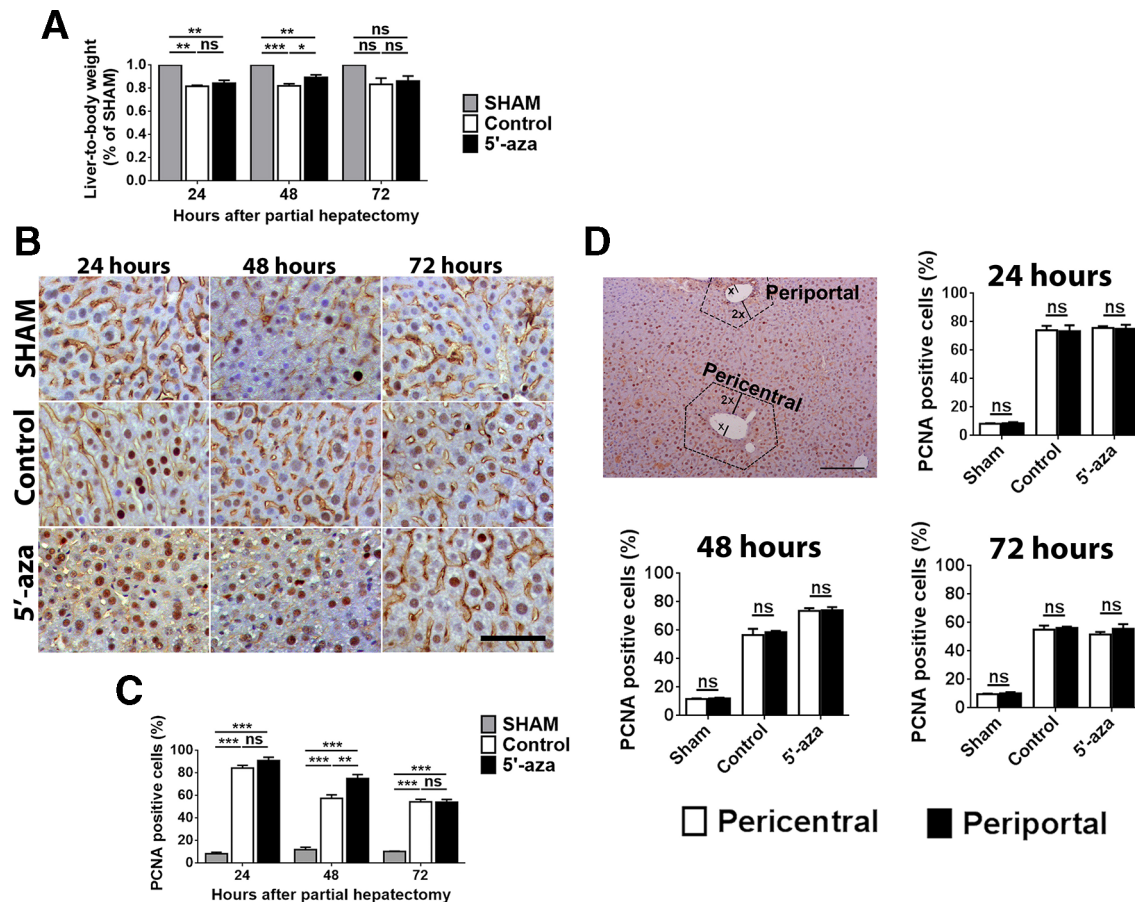


Figure 6 Demethylation accelerates liver regeneration in mice. (A) Liver-to-body weight ratio at 24, 48 and 72 hours after PH showing increased ratio in 5'-aza-treated group, relative to controls (n=5 animals per group, *p<0.05; **p<0.01; ***p<0.001, Bonferroni post-test). (B) Immunohistochemistry for PCNA in liver sections after PH (scale bar, 100 μ m). (C) Quantification of PCNA-positive cells 24, 48 and 72 hours after PH, demonstrating that 5'-aza treatment increases hepatocyte proliferation (n=5 animals per group, **p<0.01; ***p<0.001). (D) Quantification of PCNA-positive cells in PC and PP regions 24, 48 and 72 hours after PH. Dotted regions on the micrograph illustrate PC and PP areas used for quantification as defined in the methods section. 5'-aza, 5'-azacitidine; PC, pericentral; PH; partial hepatectomy; PP, periportal.

STA (figure 7F,G). Similarly, transient overexpression of mCherry-tagged ITPR3 induced apoptosis in HepG2 cells, whereas treatment of these cells with STA did not further increase apoptotic cell death (figure 7H). Together these results suggest that de novo expression of ITPR3 may induce apoptosis in either hepatocytes or HCC cells, but in both cases, the surviving cells become resistant to cell death induced by apoptotic stimuli.

Because ITPR-dependent Ca^{2+} signalling triggers store-operated Ca^{2+} entry (SOCE) that shapes the overall intracellular Ca^{2+} response, the expression of the main components of SOCE was investigated in WT and ITPR3KO cells. Expressions of all SOCE-related genes (ORA1, ORAI2, ORAI3, STIM1 and STIM2) were similar in WT and ITPR3KO, suggesting that alterations in SOCE do not contribute to the effects of ITPR3 on liver cancer development (online supplementary table 1).

To understand the mechanism by which ITPR3 might protect rather than induce apoptotic cell death, RNA sequencing was performed to compare global gene expression between WT and ITPR3KO HepG2 cells. This analysis revealed that the presence of ITPR3 in a liver cancer cell is associated with changes in multiple apoptosis-related genes. Two of these genes, POU4F1 and SIAH2, were the most upregulated and downregulated genes, respectively, in WT cells relative to ITPR3KO (figure 7I). POU4F1 is a transcription factor that is upregulated in acute myeloid leukaemia³⁷ and it triggers an antiapoptotic and prosurvival response in sensory

neurons.³⁸ SIAH2 is a ubiquitin E3-ligase that promotes breast cancer growth by remodelling of the tumour microenvironment.³⁹ These results suggest that chronic ITPR3 expression might trigger an antiapoptotic response in liver cancer through modulation of gene expression and proteasome activity.

DISCUSSION

The importance of ITPR3-mediated apoptosis is emerging as a common theme in cancer biology,^{6,7,40} although ITPR3 can either promote or inhibit apoptosis, depending on the type of tumour. ITPRs can link to VDAC in the outer mitochondrial membrane via grp75, which forms a 'quasi-synapse' that facilitates the transmission of calcium from the lumen of the ER directly into mitochondria.⁴¹ Excessive mitochondrial calcium, in turn, triggers the opening of the permeability transition pore,^{40,42} with leakage of mitochondrial contents into the cytosol and then induction of apoptosis via formation of the apoptosome.⁴³ ITPR3 is particularly effective at modulating mitochondrial calcium and apoptosis.³⁶ However, there is variability in the way that ITPR3 is modulated and affects apoptosis among different tumour types. For example, in both melanoma and mesothelioma, changes in ITPR3 expression have been attributed to the loss of the tumour suppressor BAP1, which binds to and stabilises ITPR3. Loss of BAP1, therefore, leads to loss of ITPR3, which in turn reduces apoptotic mitochondrial calcium signals.⁶ In prostate cancer,

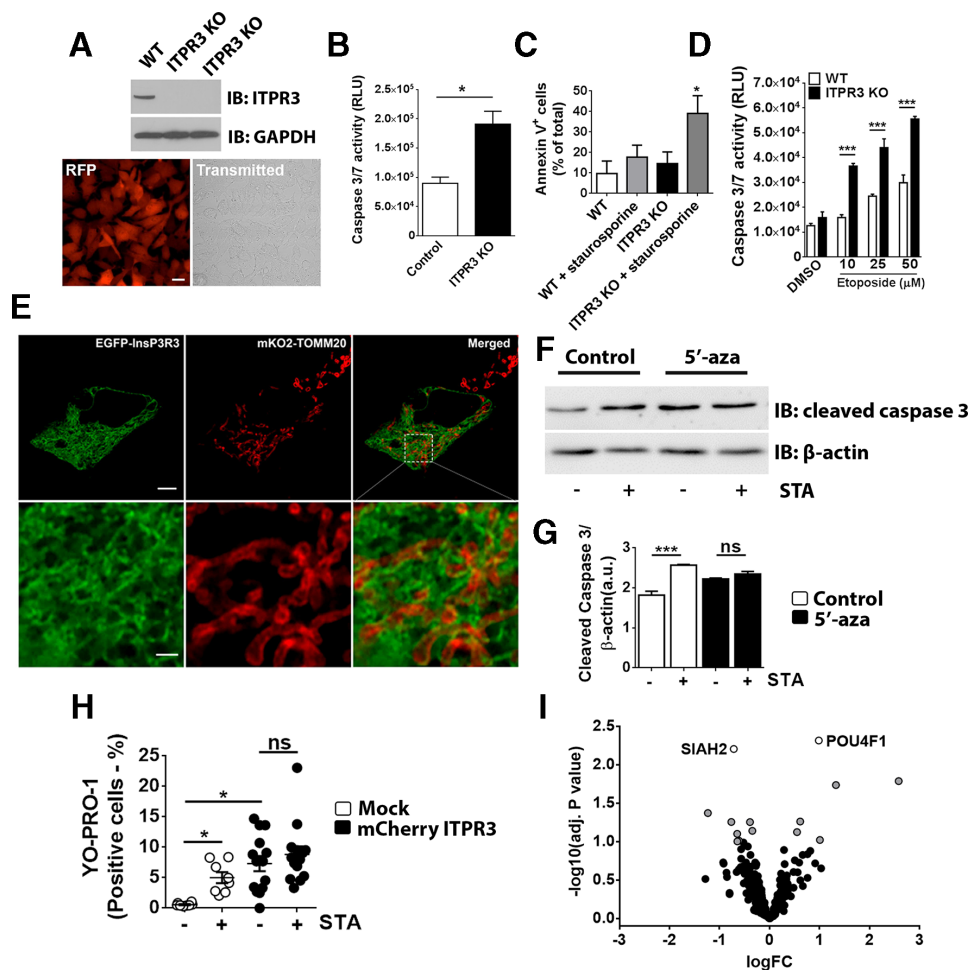


Figure 7 Knockout of ITPR3 sensitises liver cancer cells to apoptosis (A) Representative western blot showing efficient elimination of ITPR3 expression in HepG2 cells by CRISPR-Cas9 in two separate clones. Expression of RFP as a marker for successful integration of the knockout cassette in the genome of HepG2 cells (scale bar, 20 μ m). (B) Caspase 3/7 activity after treatment of HepG2 cells with STA is increased in ITPR3KO relative to WT cells (values are mean \pm SEM, n=9 in each group, *p<0.01). (C) Similarly, the percentage of Annexin 5-positive cells is increased in ITPR3KO cells when compared with WT cells on overnight treatment with STA (values are mean \pm SEM, n=4 in each group; *p<0.01). (D) ITPR3KO cells have increased Caspase 3/7 activity when treated with Etoposide (values are mean \pm SEM, n=3 in each group; p<0.001). (E) Super-resolution image of a representative HepG2 cell coexpressing EGFP-ITPR3 and mKO2-TOMM20 (mitochondrial marker). Top row: scale bar, 5 μ m. Bottom row: scale bar, 1 μ m. (F) Representative immunoblot for cleaved caspase 3 in hepatocyte lysates from control and 5'-aza-treated mice after STA treatment. (G) Densitometric analysis showing that 5'-aza treatment prevents the increase of cleaved caspase 3 in hepatocytes (**p<0.01). (H) Percentage of YO-PRO-1 - positive cells in HepG2 WT after STA treatment. The over expression of ITPR3 in HepG2 cells prevents apoptosis induced by STA. (I) Volcano plot showing the expression of apoptotic genes in HepG2 WT cells compared with HepG2 ITPR3KO cells. Genes to the left of zero are downregulated and the ones to the right of zero are upregulated in WT versus ITPR3KO. The genes represented by open symbols, SIAH2 and POU4F1, showed the highest adjusted p-value. Grey symbols show genes with adjusted p-value >1.0. Black symbols represent the remaining genes. 5' -aza, 5' -azacitine; DMSO, dimethyl sulfoxide; GAPDH, glyceraldehyde 3-phosphate dehydrogenase; ITPR3, type 3 isoform of the inositol 1, 4, 5-trisphosphate receptor; KO, knockout; RFP, red fluorescent protein; RLU, relative light units; STA, staurosporine; WT, wild type.

ITPR3 degradation has instead been linked to mutations in phosphatase and tensin homolog (PTEN), which normally competes with FBXL2 to prevent it from binding to and degrading ITPR3. In the absence of PTEN, or in the presence of certain mutant forms, degradation of ITPR3 is increased, which leads to decreased apoptosis.⁷ A role for ITPR3 in colon cancer has been demonstrated as well, and this also has been related to the effect of ITPR3 on apoptosis.¹² In this case, increased ITPR3 expression in colon cancer resection specimens was associated with increased metastasis and decreased patient survival. Overexpression of ITPR3 also was associated with decreased apoptosis in a colon cancer cell line, whereas knockdown of ITPR3 led to increased apoptosis.¹² The current work similarly found that increased ITPR3 expression in HCC is associated with decreased

patient survival and that susceptibility to apoptosis is increased when ITPR3 is deleted.

Our work also provides evidence that promoter demethylation is responsible for controlling de novo expression of ITPR3 in HCC. Although DNA hypomethylation is a common feature of multiple cancers,⁴⁴ our results suggest that promoter methylation of the *ITPR3* gene is a more specific event, because the closely related genes *ITPR1* and *ITPR2* did not display changes in methylation or expression in HCC. Thus, *ITPR3* expression might follow a similar pattern to that of oncogenes such as *c-jun* and *c-myc*, whose expression is similarly controlled by DNA methylation.⁴⁵

It is unclear why ITPR3 promotes apoptosis in certain types of malignancies but protects against it in others. One possible explanation suggested by our findings is that overexpression of ITPR3

initially promotes cell death, likely due to increased transfer of calcium to nearby mitochondria, but surviving cells compensate by developing an antiapoptotic gene expression programme. Another possible explanation is that hepatocytes do not normally express ITPR3,^{8–10} so in these cells, mitochondrial calcium signals normally are due entirely to ITPR1.¹¹ Because ITPR3 has a lower affinity than ITPR1 for InsP₃,⁴⁶ it is possible that de novo expression of ITPR3 enables this isoform to decrease the overall responsiveness to InsP₃ in the ER–mitochondrial junction, leading to decreased mitochondrial calcium signalling and apoptosis. A final explanation relates to the recent observation that mitochondria in cancer cells become ‘addicted’ to calcium so that loss or inhibition of ITPR’s can lead to cell death,⁴⁷ although this is thought to result in necrosis rather than apoptosis.

Of additional relevance to cancer biology is that calcium signals in the nucleoplasm are necessary for tumour growth.⁴ In the liver, nucleoplasmic calcium signals can be selectively generated by activation of receptor tyrosine kinases (RTKs). This occurs when specific growth factors bind to their cognate RTKs, which then translocate from the plasma membrane to the nucleus in order to locally activate PLC, which then increases nucleoplasmic InsP₃ that binds to nuclear ITPRs. This signalling pathway has been demonstrated for the hepatocyte growth factor receptor c-met,⁵ the EGF receptor,⁴⁸ and the insulin receptor,^{14 34} each of which may play a role in the development of HCC.^{49 50} Furthermore, ITPR3 is expressed not only in the ER but also in the nuclear fraction in liver cancer cell lines, and nuclear ITPRs are more sensitive than non-nuclear ITPRs to InsP₃ in these cells.⁵¹ This raises the possibility that expression of ITPR3 in the liver leads to enhanced calcium signalling in the nucleus as a contributing factor to the development of HCC, consistent with what we observed in 5′-aza-treated livers stimulated with vasopressin, a known stimulator of liver growth.⁵² How our findings regarding ITPR3 expression and its contribution to normal liver regeneration translate to cancer biology remains to be determined. Although similar Ca²⁺-inducing agonists promote hepatocyte proliferation after PH and tumour growth in HCC, it is not known whether the underlying proliferative mechanisms involve ITPR3 in similar ways. Additional work will be needed to determine whether and why there is an absolute requirement for de novo expression of ITPR3 in the pathogenesis of HCC, as well as whether it is a rational target for therapy.

Author affiliations

¹Department of Internal Medicine, Section of Digestive Diseases, Yale University School of Medicine, New Haven, Connecticut, USA

²Department of Physiology and Biophysics, Universidade Federal de Minas Gerais, Belo Horizonte, Brazil

³Centro Nacional de Pesquisa em Energia e Materiais, Campinas, Brazil

⁴Department of Pathology, Yale University School of Medicine, New Haven, Connecticut, USA

⁵Department of Pharmacology, Yale University School of Medicine, New Haven, Connecticut, USA

⁶Department of Biostatistics, Yale University School of Medicine, New Haven, Connecticut, USA

⁷Department of Bioinformatics and Biostatistics, SJTU-Yale Joint Center for Biostatistics, School of Life Science and Biotechnology, Shanghai Jiao Tong University, China

⁸Department of Surgery, School of Medicine, Universidade Federal de Minas Gerais, Belo Horizonte, Brazil

⁹Department of Pathological Anatomy and Forensic Medicine, School of Medicine, Universidade Federal de Minas Gerais, Belo Horizonte, Brazil

Acknowledgements The authors thank Kathy Harry and Masahiro Takeuchi for help with mouse tissue isolation (Yale Liver Center). They also acknowledge the support of the UFMG Liver Center.

Contributors MTG and RMF: designed and performed experiments, analysed data and help to write the manuscript. AF, ACMLF, RCF, FOL and MCF: performed in vivo

experiments and analyse data related to 5′-azacitidine treatments. MLS: performed immunohistochemistry in human tissues and analysed clinical data. EK: performed experiments and analysed data related to the ITPR3KO HepG2 cells. AM: processed DEN tissue samples and graded histological scores in HCC specimens. FG and YCC: designed and performed xenograft tumor assays in nude mice. MA: generated liver-specific ITPR3 knock out mice. JG, JJ and HZ: analysed RNA sequencing data. BN, JAG, CXL and PTV: identified and diagnosed human HCC specimens. AGO: performed in vivo calcium imaging experiments. MHN and MFL: supervised the project, formulated the hypothesis, designed experiments and edited the manuscript.

Funding This work was supported by grants from NIH (DK57751, DK34989, DK114041, DK112797 and OD20142 to MHN, and DK07356 to MHN and BN) and CNPq (300990/20147 to MFL). This work also was supported by the Gladys Phillips Crofoot Professorship.

Competing interests None declared.

Ethics approval All studies employing archived human liver specimens were approved by the local Human Investigation Committee at UFMG – Protocol # 71206617.8.0000.5149 and Yale University – Protocol # 1304011763). Animal studies were approved by the Institutional Animal Care and Use Committees at UFMG – Protocol #169/2014 and Yale University – Protocol # 2012-07602.

Provenance and peer review Not commissioned; externally peer reviewed.

REFERENCES

- 1 El-Serag HB, Kanwal F. Epidemiology of hepatocellular carcinoma in the United States: where are we? Where do we go? *Hepatology* 2014;60:1767–75.
- 2 Heimbach J, Kulik LM, Finn R, et al. Aasld guidelines for the treatment of hepatocellular carcinoma. *Hepatology* 2017.
- 3 Llovet JM, Zucman-Rossi J, Pikarsky E, et al. Hepatocellular carcinoma. *Nat Rev Dis Primers* 2016;2:16018.
- 4 Rodrigues MA, Gomes DA, Leite MF, et al. Nucleoplasmic calcium is required for cell proliferation. *J Biol Chem* 2007;282:17061–8.
- 5 Gomes DA, Rodrigues MA, Leite MF, et al. c-Met must translocate to the nucleus to initiate calcium signals. *J Biol Chem* 2008;283:4344–51.
- 6 Bononi A, Giorgi C, Patergnani S, et al. BAP1 regulates IP3R3-mediated Ca²⁺ flux to mitochondria suppressing cell transformation. *Nature* 2017;546:549–53.
- 7 Kuchay S, Giorgi C, Simoneschi D, et al. PTEN counteracts FBXL2 to promote IP3R3- and Ca²⁺-mediated apoptosis limiting tumour growth. *Nature* 2017;546:554–8.
- 8 Hirata K, Puls T, O’Neill AF, et al. The type II inositol 1,4,5-trisphosphate receptor can trigger Ca²⁺ waves in rat hepatocytes. *Gastroenterology* 2002;122:1088–100.
- 9 Kruglov EA, Gautam S, Guerra MT, et al. Type 2 inositol 1,4,5-trisphosphate receptor modulates bile salt export pump activity in rat hepatocytes. *Hepatology* 2011;54:1790–9.
- 10 Cruz LN, Guerra MT, Kruglov E, et al. Regulation of multidrug resistance-associated protein 2 by calcium signaling in mouse liver. *Hepatology* 2010;52:327–37.
- 11 Ferioli CN, Oliveira AG, Guerra MT, et al. Hepatic Inositol 1,4,5 Trisphosphate Receptor Type 1 Mediates Fatty Liver. *Hepatol Commun* 2017;1:23–35.
- 12 Shibao K, Fiedler MJ, Nagata J, et al. The type III inositol 1,4,5-trisphosphate receptor is associated with aggressiveness of colorectal carcinoma. *Cell Calcium* 2010;48:315–23.
- 13 Ouyang K, Leandro Gomez-Amaro R, Stachura DL, et al. Loss of IP3R-dependent Ca²⁺ signalling in thymocytes leads to aberrant development and acute lymphoblastic leukemia. *Nat Commun* 2014;5:4814.
- 14 Rodrigues MA, Gomes DA, Andrade VA, et al. Insulin induces calcium signals in the nucleus of rat hepatocytes. *Hepatology* 2008;48:1621–31.
- 15 Fonseca MC, França A, Florentino RM, et al. Cholesterol-enriched membrane microdomains are needed for insulin signaling and proliferation in hepatic cells. *Am J Physiol Gastrointest Liver Physiol* 2018;315:G80–G94.
- 16 Guimarães E, Machado R, Fonseca MC, et al. Inositol 1,4,5-trisphosphate-dependent nuclear calcium signals regulate angiogenesis and cell motility in triple negative breast cancer. *PLoS One* 2017;12:e0175041.
- 17 Xia L, Ma S, Zhang Y, et al. Daily variation in global and local DNA methylation in mouse livers. *PLoS One* 2015;10:e0118101.
- 18 Dobin A, Davis CA, Schlesinger F, et al. STAR: ultrafast universal RNA-seq aligner. *Bioinformatics* 2013;29:15–21.
- 19 Liao Y, Smyth GK, Shi W. The R package Rsubread is easier, faster, cheaper and better for alignment and quantification of RNA sequencing reads. *Nucleic Acids Res* 2019;47:e47.
- 20 Robinson MD, McCarthy DJ, Smyth GK. edgeR: a Bioconductor package for differential expression analysis of digital gene expression data. *Bioinformatics* 2010;26:139–40.
- 21 Ritchie ME, Phipson B, Wu D, et al. limma powers differential expression analyses for RNA-sequencing and microarray studies. *Nucleic Acids Res* 2015;43:e47.
- 22 Morel A, O’Carroll AM, Brownstein MJ, et al. Molecular cloning and expression of a rat V1a arginine vasopressin receptor. *Nature* 1992;356:523–6.
- 23 Nathanson MH, Moyer MS, Burgstahler AD, et al. Mechanisms of subcellular cytosolic Ca²⁺ signaling evoked by stimulation of the vasopressin V1a receptor. *J Biol Chem* 1992;267:23282–9.

- 24 Guerra MT, Fonseca EA, Melo FM, *et al.* Mitochondrial calcium regulates rat liver regeneration through the modulation of apoptosis. *Hepatology* 2011;54:296–306.
- 25 Pantazaka E, Taylor CW. Differential distribution, clustering, and lateral diffusion of subtypes of the inositol 1,4,5-trisphosphate receptor. *J Biol Chem* 2011;286:23378–87.
- 26 El-Serag HB. Epidemiology of viral hepatitis and hepatocellular carcinoma. *Gastroenterology* 2012;142:1264–73.
- 27 Baertling F, Mayatepek E, Gerner P, *et al.* Liver cirrhosis in glycogen storage disease Ib. *Mol Genet Metab* 2013;108:198–200.
- 28 Ananthanarayanan M, Banales JM, Guerra MT, *et al.* Post-translational regulation of the type III inositol 1,4,5-trisphosphate receptor by miRNA-506. *J Biol Chem* 2015;290:184–96.
- 29 Franca A, Carlos Melo Lima Filho A, Guerra MT, *et al.* Effects of Endotoxin on Type 3 Inositol 1,4,5-Trisphosphate Receptor in Human Cholangiocytes. *Hepatology* 2019;69:817–30.
- 30 Weerachayaphorn J, Amaya MJ, Spirli C, *et al.* Nuclear Factor, Erythroid 2-Like 2 Regulates Expression of Type 3 Inositol 1,4,5-Trisphosphate Receptor and Calcium Signaling in Cholangiocytes. *Gastroenterology* 2015;149:211–22.
- 31 Chen ZX, Riggs AD. DNA methylation and demethylation in mammals. *J Biol Chem* 2011;286:18347–53.
- 32 Christman JK. 5-Azacytidine and 5-aza-2'-deoxycytidine as inhibitors of DNA methylation: mechanistic studies and their implications for cancer therapy. *Oncogene* 2002;21:5483–95.
- 33 Halpern KB, Shenhav R, Matcovitch-Natan O, *et al.* Single-cell spatial reconstruction reveals global division of labour in the mammalian liver. *Nature* 2017;542:352–6.
- 34 Amaya MJ, Oliveira AG, Guimarães ES, *et al.* The insulin receptor translocates to the nucleus to regulate cell proliferation in liver. *Hepatology* 2014;59:274–83.
- 35 Magnino F, St-Pierre M, Lüthi M, *et al.* Expression of intracellular calcium channels and pumps after partial hepatectomy in rat. *Mol Cell Biol Res Commun* 2000;3:374–9.
- 36 Mendes CC, Gomes DA, Thompson M, *et al.* The type III inositol 1,4,5-trisphosphate receptor preferentially transmits apoptotic Ca²⁺ signals into mitochondria. *J Biol Chem* 2005;280:40892–900.
- 37 Dunne J, Gascoyne DM, Lister TA, *et al.* AML1/ETO proteins control POU4F1/BRN3A expression and function in t(8;21) acute myeloid leukemia. *Cancer Res* 2010;70:3985–95.
- 38 Hudson CD, Morris PJ, Latchman DS, *et al.* Brn-3a transcription factor blocks p53-mediated activation of proapoptotic target genes Noxa and Bax in vitro and in vivo to determine cell fate. *J Biol Chem* 2005;280:11851–8.
- 39 Ma B, Cheng H, Mu C, *et al.* The SIAH2-NRF1 axis spatially regulates tumor microenvironment remodeling for tumor progression. *Nat Commun* 2019;10:1034.
- 40 Szalai G, Krishnamurthy R, Hajnóczky G. Apoptosis driven by IP(3)-linked mitochondrial calcium signals. *Embo J* 1999;18:6349–61.
- 41 Szabadkai G, Bianchi K, Várnai P, *et al.* Chaperone-mediated coupling of endoplasmic reticulum and mitochondrial Ca²⁺ channels. *J Cell Biol* 2006;175:901–11.
- 42 Ichas F, Jouaville LS, Mazat JP. Mitochondria are excitable organelles capable of generating and conveying electrical and calcium signals. *Cell* 1997;89:1145–53.
- 43 Li P, Nijhawan D, Budihardjo I, *et al.* Cytochrome c and dATP-dependent formation of Apaf-1/caspase-9 complex initiates an apoptotic protease cascade. *Cell* 1997;91:479–89.
- 44 Klutstein M, Nejman D, Greenfield R, *et al.* DNA Methylation in Cancer and Aging. *Cancer Res* 2016;76:3446–50.
- 45 Tao L, Yang S, Xie M, *et al.* Hypomethylation and overexpression of c-jun and c-myc protooncogenes and increased DNA methyltransferase activity in dichloroacetic and trichloroacetic acid-promoted mouse liver tumors. *Cancer Lett* 2000;158:185–93.
- 46 Tu H, Wang Z, Nosyreva E, *et al.* Functional characterization of mammalian inositol 1,4,5-trisphosphate receptor isoforms. *Biophys J* 2005;88:1046–55.
- 47 Cárdenas C, Müller M, McNeal A, *et al.* Selective Vulnerability of Cancer Cells by Inhibition of Ca(2+) Transfer from Endoplasmic Reticulum to Mitochondria. *Cell Rep* 2016;14:2313–24.
- 48 De Angelis Campos AC, Rodrigues MA, de Andrade C, *et al.* Epidermal growth factor receptors destined for the nucleus are internalized via a clathrin-dependent pathway. *Biochem Biophys Res Commun* 2011;412:341–6.
- 49 Ueki T, Fujimoto J, Suzuki T, *et al.* Expression of hepatocyte growth factor and its receptor c-met proto-oncogene in hepatocellular carcinoma. *Hepatology* 1997;25:862–6.
- 50 Ito Y, Takeda T, Sakon M, *et al.* Expression and clinical significance of erb-B receptor family in hepatocellular carcinoma. *Br J Cancer* 2001;84:1377–83.
- 51 Leite MF, Thrower EC, Echevarria W, *et al.* Nuclear and cytosolic calcium are regulated independently. *Proc Natl Acad Sci U S A* 2003;100:2975–80.
- 52 Nicou A, Serrière V, Prigent S, *et al.* Hypothalamic vasopressin release and hepatocyte Ca²⁺ signaling during liver regeneration: an interplay stimulating liver growth and bile flow. *Faseb J* 2003;17:1901–3.

Correction: *Expression of the type 3 InsP_3 receptor is a final common event in the development of hepatocellular carcinoma*

Guerra MT, Florentino RM, Franca A, *et al.* Expression of the type 3 InsP_3 receptor is a final common event in the development of hepatocellular carcinoma. *Gut* 2019;68:1676-87. doi:10.1136/gutjnl-2018-317811.

The fifteenth author's name should be Meenakshisundaram Ananthanarayanan.

© Author(s) (or their employer(s)) 2020. No commercial re-use. See rights and permissions. Published by BMJ.

Gut 2020;69:e1. doi:10.1136/gutjnl-2018-317811corr1



Inositol 1,4,5-trisphosphate receptor in the liver: Expression and function

Fernanda de Oliveira Lemos, Rodrigo M Florentino, Antônio Carlos Melo Lima Filho, Marcone Loiola dos Santos, M Fatima Leite

ORCID number: Fernanda de Oliveira Lemos (0000-0002-7070-4412); Rodrigo M Florentino (0000-0001-7033-176X); Antônio Carlos Melo Lima Filho (0000-0002-8185-669X); Marcone Loiola dos Santos (0000-0001-8835-2104); M Fatima Leite (0000-0001-9709-8865).

Author contributions: All authors contributed to this paper with literature review and analysis, drafting and critical revision and editing, and approval of the final version.

Conflict-of-interest statement: No potential conflicts of interest. No financial support.

Open-Access: This article is an open-access article which was selected by an in-house editor and fully peer-reviewed by external reviewers. It is distributed in accordance with the Creative Commons Attribution Non Commercial (CC BY-NC 4.0) license, which permits others to distribute, remix, adapt, build upon this work non-commercially, and license their derivative works on different terms, provided the original work is properly cited and the use is non-commercial. See: <http://creativecommons.org/licenses/by-nc/4.0/>

Manuscript source: Unsolicited manuscript

Received: August 18, 2019

Peer-review started: August 18, 2019

First decision: October 14, 2019

Fernanda de Oliveira Lemos, Rodrigo M Florentino, Antônio Carlos Melo Lima Filho, M Fatima Leite, Department of Physiology and Biophysics, Universidade Federal de Minas Gerais, Belo Horizonte, Minas Gerais 31270-901, Brazil

Marcone Loiola dos Santos, Department of Cell Biology, Universidade Federal de Minas Gerais, Belo Horizonte, Minas Gerais 31270-901, Brazil

Corresponding author: M Fatima Leite, PhD, Full Professor, Department of Physiology and Biophysics, Federal University of Minas Gerais, Av. Antônio Carlos 6627, Belo Horizonte, Minas Gerais 31270-901, Brazil. leitemd@ufmg.br

Telephone: +55-31-34092518

Fax: +55-31-34092947

Abstract

The liver is a complex organ that performs several functions to maintain homeostasis. These functions are modulated by calcium, a second messenger that regulates several intracellular events. In hepatocytes and cholangiocytes, which are the epithelial cell types in the liver, inositol 1,4,5-trisphosphate (InsP₃) receptors (ITPR) are the only intracellular calcium release channels. Three isoforms of the ITPR have been described, named type 1, type 2 and type 3. These ITPR isoforms are differentially expressed in liver cells where they regulate distinct physiological functions. Changes in the expression level of these receptors correlate with several liver diseases and hepatic dysfunctions. In this review, we highlight how the expression level, modulation, and localization of ITPR isoforms in hepatocytes and cholangiocytes play a role in hepatic homeostasis and liver pathology.

Key words: Inositol 1,4,5-trisphosphate receptor; Liver; Calcium signaling; Hepatocytes and cholangiocytes

©The Author(s) 2019. Published by Baishideng Publishing Group Inc. All rights reserved.

Core tip: Calcium regulates a variety of functions in our body. In the liver, inositol 1,4,5-trisphosphate receptors (ITPR) are the only expressed intracellular calcium release channels. ITPR regulates liver functions under healthy situation, but they can also be involved in liver diseases, depending for instance, in which isoform is expressed in a specific cell type, level of expression and where inside the cell each isoform is expressed. In this review, we discuss about ITPR roles in hepatic cells in physiological

Revised: October 22, 2019**Accepted:** November 13, 2019**Article in press:** November 13, 2019**Published online:** November 28, 2019**P-Reviewer:** Morales-González JA, Sun XT**S-Editor:** Wang J**L-Editor:** A**E-Editor:** Zhang YL

and pathological conditions.

Citation: Lemos FO, Florentino RM, Lima Filho ACM, Santos MLD, Leite MF. Inositol 1,4,5-trisphosphate receptor in the liver: Expression and function. *World J Gastroenterol* 2019; 25(44): 6483-6494

URL: <https://www.wjgnet.com/1007-9327/full/v25/i44/6483.htm>

DOI: <https://dx.doi.org/10.3748/wjg.v25.i44.6483>

INTRODUCTION

The liver is an important and vital organ that regulates several functions, ranging from drug and macronutrient metabolism to immune system support^[1-3]. Essentially all liver functions are at some point regulated by intracellular calcium (Ca²⁺). In hepatocytes and cholangiocytes, the principal epithelial cell types of the liver, inositol 1,4,5-trisphosphate (InsP₃) receptors (ITPR) are the only intracellular Ca²⁺ release channels^[6,7]. There are three types of ITPR: type 1 (ITPR1), type 2 (ITPR2) and type 3 (ITPR3)^[8,9], and these receptors are expressed mainly along the endoplasmic and nucleoplasmic reticulum^[10,11].

Dysregulation in the expression of ITPR can be a cause of several liver disorders, or can be involved in the development of diseases, such as cholestasis^[12] and non-alcoholic fatty liver disease (NAFLD)^[13]. In this review, we will discuss the expression and the physiological functions of each isoform of ITPR present in liver hepatocytes and cholangiocytes as well as their role in disease (Table 1).

LIVER

The liver is the largest internal organ^[5] and is responsible for drug metabolism, albumin production, glycogen storage, cholesterol synthesis, bile secretion, and many other functions^[14]. The liver is mostly composed of hepatocytes, which account for 80% of all cells in this organ^[15]. The remaining 20% is composed mostly of cholangiocytes, Kupffer cells, stellate cells and liver sinusoidal endothelial cells^[15]. Macroscopically, the liver is divided in four anatomic lobes, called the left, right, caudate and quadrate lobe^[16,17]. In each lobe the cells are organized in a specific conformation, constituting a microscopic functional and structural unit, the lobule^[14,18] (Figure 1). In the lobule, the hepatocytes are arranged in cords, connecting the portal triad to the central vein. In the space formed among the hepatocyte cords are the liver sinusoidal endothelial cells, the Kupffer cells, which are the resident macrophages in the liver, and the stellate cells, a cell type that stores vitamin A in its cytosol and secretes hepatocyte growth factor (HGF)^[14,19,20].

As an epithelial cell, the hepatocyte is polarized, with a basolateral membrane in contact with the sinusoids and an apical side forming the biliary canaliculus. The biliary canaliculus is a virtual space between two hepatocytes, into which hepatocytes secrete bile acids^[4]. The biliary canaliculi join to form the bile duct, which is lined by cholangiocytes, specialized cells that secrete electrolytes and fluids into the bile, altering bile composition and viscosity. The bile duct conducts the bile to the gallbladder, where it is stored until its content are needed to help lipid digestion^[21,22].

Blood from the portal vein passes throughout the sinusoids and drains into the central vein^[14,23]. Near the portal vein there are two other important structures: the hepatic artery and the bile duct. Together, these structures form the portal triad. The hepatocytes around this area are more highly oxygenated than those that are closer to the central vein, because the blood reaches the portal triad first^[14]. This region in the lobule is called zone 1, while zone 2 is the transitional zone, and zone 3 is the region near the central vein^[24,25] (Figure 2). It has been shown that based on their zonal position, hepatocytes regulate specific liver functions. For example, hepatocytes in zone 1 are more involved in producing albumin and proteins of both the complement system and coagulation pathway, while hepatocytes from zone 3 are more important for drug metabolism and bile production^[26].

Due to the key role of the liver in metabolism, hepatic tissue is continuously exposed to insults from xenobiotics, toxic metabolites and infectious agents^[2]. As result of this, the liver has a remarkable capacity for regeneration. In mice, liver functions are restored within days of removing two-thirds of the organ. This capacity

Table 1 Functions of inositol 1,4,5-trisphosphate receptor isoforms in hepatocytes and cholangiocytes

IIPR isoform	Cell type	Function	Ref.
IIPR1	Hepatocytes	Glucose secretion	[64]
		Lipid metabolism	[63,65]
		Liver regeneration	[66,67]
IIPR2	Cholangiocytes	Bicarbonate secretion	[12,61]
	Hepatocytes	Organic anion secretion	[6,62,69]
IIPR3	Cholangiocytes	Liver regeneration	[13,71]
		bicarbonate secretion	[12,61]
	Hepatocytes	Physiologically absent	[6]
IIPR3	Hepatocytes	Proliferation and survival of hepatocellular carcinoma	[74]
		Bicarbonate secretion	[12,61]
		Proliferation, migration, and survival of cholangiocarcinoma	[82]

IIPR: Inositol 1,4,5-trisphosphate receptor; IIPR1: IIPR isoform 1; IIPR2: IIPR isoform 2; IIPR3: IIPR isoform 3.

is also observed in humans for which liver function after partial hepatectomy is reestablished within a few weeks^[27]. In many cases of liver disease, for which partial hepatectomy is indicated as a treatment, a small piece of healthy liver is implanted to drive hepatic tissue regeneration^[27,28]. The path to regeneration depends on the extent of liver loss. When 1/3 of the liver is removed, the primary response is hepatocyte cellular hypertrophy, *i.e.*, an increase in cell size. When liver loss reaches 2/3, hepatocyte hyperplasia, an increase of the number of hepatocytes occurs to reestablish liver function. When 80-90 % of the liver is removed, the biliary epithelial cells (BEC) turn into progenitor cells, which differentiate into hepatocytes or BEC^[28] that are able to regenerate the tissue. Liver regeneration is a complex process and the mechanism by which the hepatocytes stop proliferating after reestablishment of liver function is poorly understood. It is important to highlight that Ca²⁺ signaling, and consequently the IIPR isoforms, play an essential role in liver regeneration, as discussed below.

CALCIUM SIGNALING AND IIPRS

Many biological functions are regulated by intracellular Ca²⁺. These include cell proliferation, gene expression, secretion, motility and cell death, among others^[29-33]. As in other tissues, Ca²⁺ signaling in the liver starts with the binding of an agonist to a receptor, which may be a G protein-coupled receptor (GPCR) (Figure 3) or a tyrosine kinase receptor (RTK). Upon agonist-receptor binding, phospholipase C (PLC) is activated (typically isoform PLC β when GPCR is activated or isoform PLC γ after RTK activation), causing breakdown of the membrane phospholipid phosphatidylinositol 4,5-bisphosphate (PIP₂), that generates diacylglycerol (DAG) and InsP₃. DAG remains at the plasma membrane while InsP₃ diffuses into the cytoplasm where it can bind to the InsP₃ receptor (IIPR) localized along the endoplasmic reticulum membrane, nuclear envelope or nucleoplasmic reticulum. InsP₃-IIPR binding causes a conformational change in the IIPR, leading to the release of internal Ca²⁺ stores^[32,34]. InsP₃ is inactivated either after conversion to inositol 1,2-bisphosphate (InsP₂) by type I inositol polyphosphate 5-phosphatase or by InsP₃-kinase mediated phosphorylation, forming inositol 1,3,4,5-tetrakisphosphate (InsP₄)^[35,36].

Because of the toxic effect of high concentrations of Ca²⁺ to the cells, this ion is promptly removed from the cytosol after its release. Different mechanisms are involved in this process, including the activation of plasma membrane Ca²⁺-ATPase or Na⁺/Ca²⁺ exchanger that exports Ca²⁺ out of the cell, while sarco-/endoplasmic Ca²⁺-ATPase (SERCA) and mitochondrial Ca²⁺ uptake 1 (MCU1) move Ca²⁺ into the endoplasmic reticulum and mitochondria, respectively^[37,38].

The IIPRs are formed by approximately 2700 amino acids^[39,40] and are organized in three domains: a N-terminal domain, which includes the InsP₃-binding region, a C-terminal domain, which forms the channel pore, and a regulatory domain between the other regions (Figure 4). IIPR is an intrinsic membrane protein, with 6 transmembrane segments^[41,42]. There are some sites along the IIPR structure that regulate the activity of the receptor, or determine its localization by posttranslational modifications (phosphorylation, ubiquitination, oxidation, and proteolytic frag-

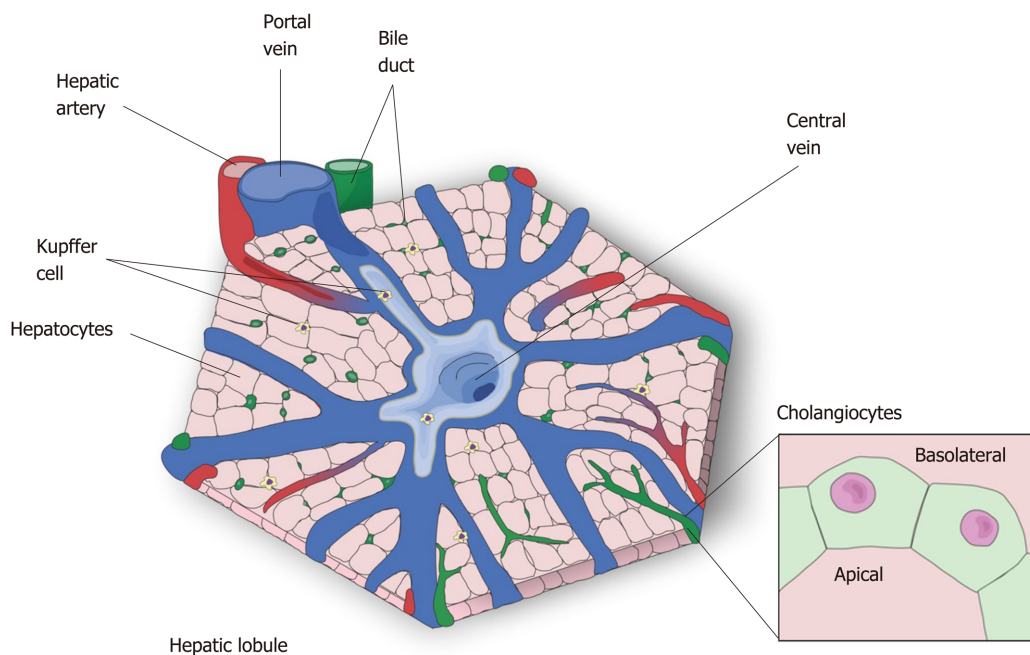


Figure 1 The hepatic lobule—the microscopic functional structure of the liver. The hepatocytes are arranged in cord, connecting the central vein to the portal triad, which is formed by a hepatic artery, a portal vein and a bile duct. The other represented cell types are: *Kupffer cell*, resident macrophages responsible for the immunologic response in the liver, and *cholangiocytes* which form the bile duct that transport bile to the gallbladder.

mentation) or by interaction with modulatory proteins, such as chromogranin A and B, neuronal Ca^{2+} sensor 1, cytochrome c, and antiapoptotic Bcl-2 family members^[43-46]. There are three isoforms of ITPR: type 1 (ITPR1), type 2 (ITPR2) and type 3 (ITPR3)^[8,9]. They share 70% homology^[47], however each isoform of ITPR displays a distinct affinity to $InsP_3$: ITPR2 has the highest affinity, ITPR1 has an intermediate affinity, and ITPR3 has the lowest affinity^[48,49]. In order to open the Ca^{2+} channel, four $InsP_3$ molecules need to bind to ITPR^[50]. Moreover, Ca^{2+} ions directly modulate the open probability of the channel^[51,52]. ITPR1 displays what is called a “bell shape” open probability curve, in other words, at lower concentrations of Ca^{2+} the ITPR1 releases Ca^{2+} , while higher Ca^{2+} concentrations inhibit the channel^[53,54]. For ITPR3, the open probability of the channel increases with increased Ca^{2+} concentration^[52,55], and the ITPR2 dependence on Ca^{2+} concentration remains controversial. While single-channel studies show that ITPR2 displays the same configuration as observed for ITPR3, studies with whole cells exhibit similarity with ITPR1^[51,56,57], suggesting an effect of the modulatory proteins on the ITPRs channel activity.

ITPRs are widely expressed, sometimes with the prevalence of a single ITPR isoform in a specific tissue. For example, in the central nervous the main ITPR isoform is ITPR1, regulating neurite formation among other functions^[58]. ITPR2 is the isoform mainly expressed in cardiomyocytes, participating in heart rate and in the action potential duration^[59]. In pancreatic tissue, ITPR2 and ITPR3 are involved in the exocytosis of zymogen granules^[60].

In the liver, hepatocytes express ITPR1 and ITPR2^[6], whereas all three isoforms are expressed in cholangiocytes^[12]. Below, we discuss separately about the ITPR isoforms in hepatic cells, focusing on hepatocytes and cholangiocytes, while indicating their main function and expression pattern in normal condition and in liver disease.

ITPR1: Metabolism and electrolyte secretion

ITPR1 is expressed in both hepatocytes and cholangiocytes, corresponding to approximately 20% of the total ITPRs present in these cells. It is localized along the endoplasmic reticulum, throughout the cytoplasm and near the nucleus^[6,61-63].

In normal liver tissue, ITPR1 regulates metabolism in hepatocytes^[63-65]. After exposure to glucagon, mouse hepatocytes display an increase in ITPR1 phosphorylation by the activity of protein kinase A (PKA), raising intracellular Ca^{2+} concentration that leads to glucose secretion^[64]. More evidence of the ITPR1 function in liver metabolism was shown in obese (ob/ob) and high fat diet (HFD) mouse models. Ob/ob mice and mice maintained on a high-fat diet (HFD) overexpress ITPR1, increasing the amount of these Ca^{2+} channels in close proximity to the mitochondria^[65]. In accordance with the increase in ITPR expression, cytoplasmic and

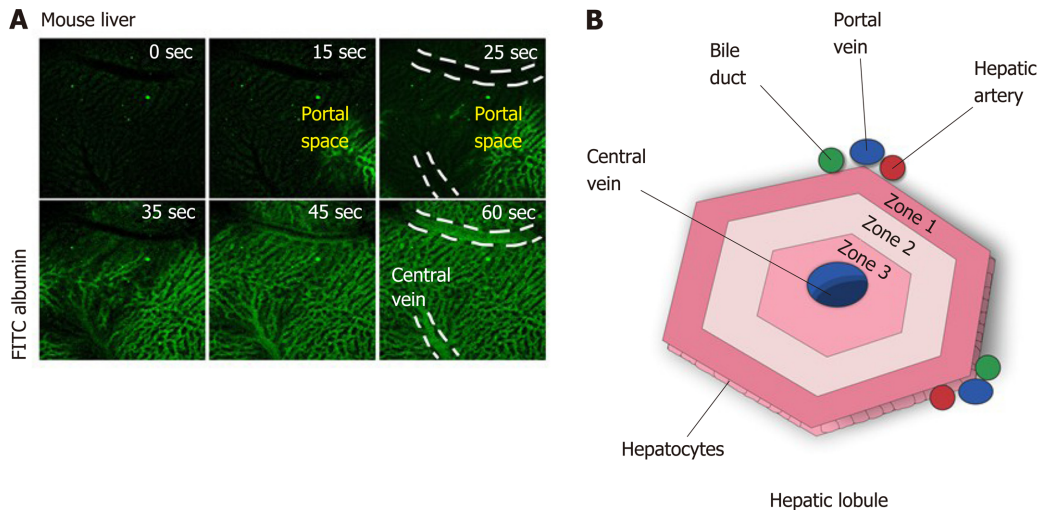


Figure 2 The microenvironment in the hepatic lobules. A: Perfusion with fluorescein isothiocyanate albumin shows that the blood flow arrives in the liver by portal vein, passes throughout the sinusoidal space, and drains into the central vein; B: Due to this blood flux, different zones of oxygenation are observed: zone 1, closer to portal vein, is the most highly oxygenated and zone 3 is the least oxygenated. zone 2 is intermediary. The direction of bile flux is opposite to that of blood flow. The bile acids excreted by the hepatocytes go to the bile duct through the biliary canaliculus.

mitochondrial Ca^{2+} concentration is increased in obese mice, causing mitochondrial dysfunction and impairment of metabolic homeostasis^[65]. Conversely, the reduction of ITPR1 expression in the mouse liver, by short hairpin RNA technique, improved glucose tolerance and mitochondrial metabolism^[65]. These results were validated in ITPR1 liver-specific knockout mice (ITPR1 LSKO). ITPR1 LSKO mice are leaner and display less hepatic steatosis after HFD, and also have reduced levels of triglycerides and lipogenic gene expression. These metabolic alterations are in accordance with the lower mitochondrial Ca^{2+} signal observed in isolated hepatocytes from ITPR1 LSKO mice^[63]. Translational studies corroborate these findings by showing that liver specimens from non-alcoholic steatohepatitis (NASH) donors display increased hepatic ITPR1 expression which is concentrated closer to mitochondria. Based on these observations, it has been suggested that ITPR1 plays a role in steatosis in human fatty liver diseases^[63].

Another function of ITPR1 in hepatocytes is related to the liver regeneration. Knocking down ITPR1 in rat with small interfering RNA (siRNA), attenuates Ca^{2+} signaling, and results in an impairment of hepatocytes proliferation after partial hepatectomy, measured by proliferating cell nuclear antigen staining positive cells. Consequently, the liver growth is diminished at the early phase (up to 48 h) of liver regeneration^[66]. The involvement of ITPR1 in the beginning of the liver regeneration process is supported by the normal expression of this isoform immediately after the partial hepatectomy, followed by a downregulation of ITPR1 afterwards^[67].

In cholangiocytes, ITPR1, together with the ITPR2, are responsible for releasing bicarbonate after the activation of type 3 muscarine receptor by acetylcholine. These findings were observed by using intrahepatic bile duct units isolated from rat liver tissue, previously transfected with ITPR1 and ITPR2 siRNA, and then by measuring the luminal pH after acetylcholine exposition. It was shown that the bicarbonate secretion was reduced in ITPR1 and ITPR2 knockdown cells^[61]. Moreover, in cholestasis, which is a disorder that causes bile accumulation, the expression of ITPR1 is decreased, similarly to what occur to the other ITPR isoforms^[12]. These observations suggest that the downregulation of ITPRs is an early event in the pathogenesis of cholestasis. As a consequence of the decrease of ITPR1 expression in a rat model of bile duct ligation, the Ca^{2+} signal is reduced and the biliary bicarbonate secretion is impaired in isolated cholangiocytes^[12]. Together, these findings show that ITPR1 isoform plays a crucial role in hepatocyte metabolism and proliferation, as well as in cholangiocyte secretory activity, which are essential functions for normal liver.

ITPR2: Bile acid /electrolyte secretion and liver regeneration

ITPR2 is considered the principal intracellular Ca^{2+} release channel expressed in human and rodent hepatocytes^[6,68]. This isoform is mostly concentrated in the canalicular membrane (apical region) of hepatocytes^[62,69], and due to its localization and high affinity for InsP_3 ^[48,49], ITPR2 plays an essential role in bile formation^[6,69]. ITPR2 modulates the multidrug resistance associated protein 2 (Mrp2), which is

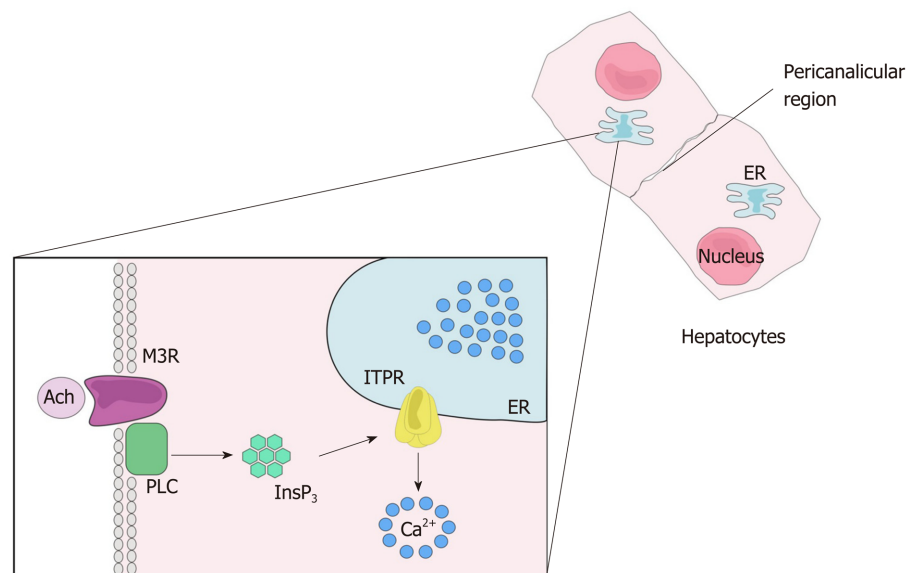


Figure 3 Calcium signaling. After the ligation of an agonist to its receptor, here represent by the ligation of acetylcholine to muscarinic acetylcholine receptor, phospholipase C is activated and produces 1,4,5 inositol triphosphate. The inositol 1,4,5-trisphosphate binds its receptor, inositol 1,4,5-trisphosphate receptor, that is expressed mainly along the endoplasmic reticulum, leading to Ca^{2+} release into the cytosol. Ach: Acetylcholine; M3R: Muscarinic acetylcholine receptor; PLC: Phospholipase C; InsP_3 : Inositol 1,4,5-trisphosphate; ITPR: Inositol 1,4,5-trisphosphate receptor; ER: Endoplasmic reticulum.

responsible for organic anion secretion into bile, such as bilirubin, glutathione S-conjugates, and oxidized glutathione. Impairment of intracellular Ca^{2+} signal inhibits the insertion of the Mrp2 into the apical plasma membrane in hepatocytes and reduces organic ion secretion. Similarly, hepatocytes isolated from ITPR2 knockout mice also presented decreased intracellular Ca^{2+} signaling, as well as impaired organic ion secretion^[69].

Another bile salt transporter regulated by ITPR2 activity is the bile salt export pump (Bsep), an important protein normally positioned along the canalicular membrane of the hepatocyte. In a three-dimensional culture system of rat hepatocytes, siRNA against ITPR2 significantly reduced bile salt secretion, correlating with the downregulation and mislocalization of Bsep. Reduced bile secretion was also observed when the pericanalicular localization of ITPR2 was disrupted by methyl- β -cyclodextrin to disturb lipid rafts^[62]. Confirming the importance of ITPR2 to the correct bile salt transporter localization and secretory activity, immunohistochemistry analysis of hepatocytes from lipopolysaccharides (LPS) and estrogen cholestasis rat models showed a reduction of ITPR2 expression level and its diffuse distribution, different from its normal localization to the apical membrane^[62]. Conversely, fasting causes a physiological upregulation of ITPR2 expression level^[70]. It was shown that overnight fasting raises the mRNA and protein levels of ITPR2 in rat hepatocytes. It happens by the activation of cAMP signaling caused by a fast-dependent increase of serum glucagon levels^[70].

The correct expression level of ITPR2 is also important for hepatocyte proliferation. Downregulation of ITPR2 was observed in obese mice^[71], a condition that compromises liver regeneration^[72]. ITPR2 downregulation was also observed in human liver specimens of patients diagnosed with steatosis and NAFLD, common liver diseases associated with obesity^[13]. Recently, the connection between lower expression of ITPR2 and impairment of liver regeneration in some liver diseases was clarified^[13]. In both human biopsies of steatosis and NAFLD, as well as in a high fructose diet induced rat model of NAFLD, the transcriptional factor c-Jun activates a pro-inflammatory environment that negatively regulates ITPR2 expression in hepatocytes^[13]. As consequence of downregulation of ITPR2, a delay of liver regeneration was observed. Similarly, ITPR2 knockout mice subjected to partial hepatectomy showed more liver damage and decreased proliferation of hepatocytes^[13]. This was a consequence of decreased nuclear Ca^{2+} signaling, a fundamental event for cell proliferation^[10,66]. ITPR2-knockout cells markedly reduced nucleoplasmic Ca^{2+} and proliferation rates compared to WT cells^[13].

In cholangiocytes, ITPR2 represents about 10% of total ITPR, and is distributed diffusely throughout the endoplasmic reticulum membrane in the cytosol^[12].

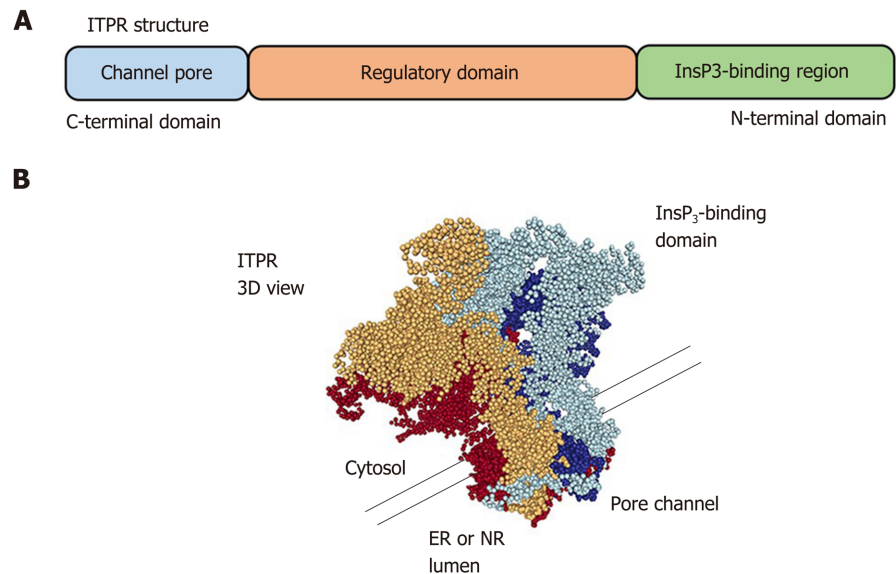


Figure 4 Inositol 1,4,5-trisphosphate receptor structure. A: Linear structure of inositol 1,4,5-trisphosphate receptor (ITPR). The inositol 1,4,5-trisphosphate (InsP₃)-binding domain is located on the N-terminal region and the pore channel is on the C-terminal region. The receptor spans organelle membrane six times; B: Tridimensional view of ITPR showing that the receptor is formed by a 4 single chain. It is necessary that four InsP₃ molecules bind to the receptor to lead the calcium releases by a pore of the channel. The tridimensional structure was adapted from Molecular Modeling Database (National Center for Biotechnology Information). ER: Endoplasmic reticulum; ITPR: Inositol 1,4,5-trisphosphate receptor; NR: Nucleoplasmic reticulum.

Functional studies showed that ITPR2 participates in the bicarbonate secretion by cholangiocytes. As discussed above, ITPR1 and ITPR2 knockdown cholangiocytes show a decrease in Ca²⁺ signal, and a reduction in Ca²⁺-dependent bicarbonate secretion when stimulated by acetylcholine^[61]. Similar observations have been made in some cholestatic human diseases. The expression of ITPR2 is dramatically reduced in cholangiocytes from samples of patients with bile duct obstruction and primary biliary cirrhosis^[12]. In summary, the ITPR2 displays an essential function in the liver, regulating bile formation and bicarbonate secretion, as well as regenerating hepatocytes.

ITPR3: Cell proliferation and electrolyte secretion

In normal conditions, hepatocytes express ITPR1 and ITPR2 isoforms, but not the ITPR3^[6]. However, ITPR3 is present in several hepatocellular carcinoma (HCC) cell lines^[73,74], as well as in NASH-related HCC^[75]. The mechanism of the “de novo” ITPR3 expression in hepatocytes in the context of HCC has been partially described and involves epigenetic modification^[74], which represents changes in the genome structure that do not alter the nucleotide sequence. Examples include DNA methylation and histone modification^[76]. Recently, bioinformatics analysis showed that the ITPR3 promoter region has a large number of CpG islands^[74] that can be methylated by DNA methyltransferases, resulting in suppression of the gene^[76,77]. Due to high level of DNA methylation at the ITPR3 promoter region, ITPR3 expression is repressed in hepatocytes under normal conditions. However, the referred methylation level is decreased in patients with HCC, allowing the expression of ITPR3 to be increased under hepatocellular disease conditions^[74]. The expression of ITPR3 drives cell proliferation besides preventing the apoptotic cascade activation^[74], events closely related to tumor development. Together, these findings put the ITPR3 Ca²⁺ channel as an essential factor that contributes to the pathogenesis of HCC.

Contrary to the normal hepatocytes, cholangiocytes constitutively express all three isoforms of ITPR^[7], with the ITPR3 being the most widely expressed, constituting approximately 80% of ITPRs in this cell type. ITPR3 mainly localizes to the apical region of the cholangiocytes in rodents and humans^[7]. This apical localization of ITPR3 in cholangiocytes is important for its physiological function of secreting bicarbonate^[78]. It was shown that downregulation of ITPR3 selectively disturbs the cAMP-induced bicarbonate secretion^[61]. Different from ITPR1 and ITPR2, in which the bicarbonate secretion is dependent on activation of muscarinic acetylcholine receptors, ITPR3 leads to bicarbonate secretion by a cAMP-dependent cascade, wherein activation of secretin receptor indirectly stimulates InsP₃ production and Ca²⁺

release via ITPR3^[61].

As described above to the other ITPR isoforms, the ITPR3 expression is progressively decreased in bile duct ligation cholestasis rat model. Downregulation of ITPR3 was also observed after acute cholestasis, such as the endotoxin mouse model, as well as in chronic cholestatic disease in human, *e.g.*, bile duct obstruction, biliary atresia, primary biliary cirrhosis, sclerosing cholangitis, and autoimmune cholestatic^[12].

Several intracellular mechanisms have already been elucidated as being responsible for the loss of ITPR3 in cholangiocytes under pathological conditions. It was demonstrated for instance that LPS inoculation activates Toll like receptor 4 in cholangiocytes and, consequently, the transcription factor NF- κ B. NF- κ B then associates to the ITPR3 promoter region, inhibiting its expression in cholangiocytes. This mechanism is responsible for the loss of ITPR3 in patients affected by cholestasis due to sepsis or severe alcoholic hepatitis^[79]. In cholangiopathies under oxidative stress conditions, including sclerosing cholangitis, primary biliary cholangitis, primary biliary obstruction and biliary atresia, the nuclear erythroid 2-like transcription factor 2 (Nrf2) is activated, acting negatively on ITPR3 expression^[80]. Finally, the ITPR3 expression is also negatively regulated by the microRNA miR-506 in patients with primary biliary cholangitis^[81].

Conversely to the downregulation of ITPR3 in cholangiopathies and cholestasis, this Ca²⁺ channel becomes over-expressed in cholangiocarcinoma^[82]. ITPR3 accumulates in ER-mitochondrial junctions in cholangiocarcinoma cell lines, increasing mitochondrial Ca²⁺ signaling. Moreover, ITPR3 increases nuclear Ca²⁺ signaling in cholangiocarcinoma, which contributes to cell proliferation, migration, and survival^[82].

Together, these findings show that ITPR3 is absent in healthy hepatocytes but is expressed in HCC and indicates that it may be a target to understand liver cancer and its clinical implications. On the other hand, in cholangiocytes, ITPR3 is crucial to bile formation and the decrease in its expression causes cholestasis, observed in many liver diseases, while it is over-expressed in cholangiocarcinoma, contributing to malignant features, such as cell proliferation, migration and survival.

CONCLUSION

In this review, we described several evidences of the role of the Ca²⁺ signaling, and consequently the activity of ITPRs, in normal liver functions. Mislocalization and/or change in expression level of these Ca²⁺ channels have been directly related to some liver disease (summarized in **Figure 5**). The alterations in ITPR expression and localization point these Ca²⁺ channels as a valuable biomarker for prediction and prognosis of hepatic disease. In addition to diagnosis for liver diseases, ITPR would be a rational target for these pathological conditions. Epigenetic modification, pro-inflammatory transcription factors and miRNA have already been associated to the modulation of ITPR expression in pathological conditions. However, this field remains to be better explored to elucidate the upstream cascade that drives ITPR expression alterations. Better understanding of this pathway could open the perspective of developing pharmacological strategies for liver diseases, specifically targeting each ITPR isoforms.

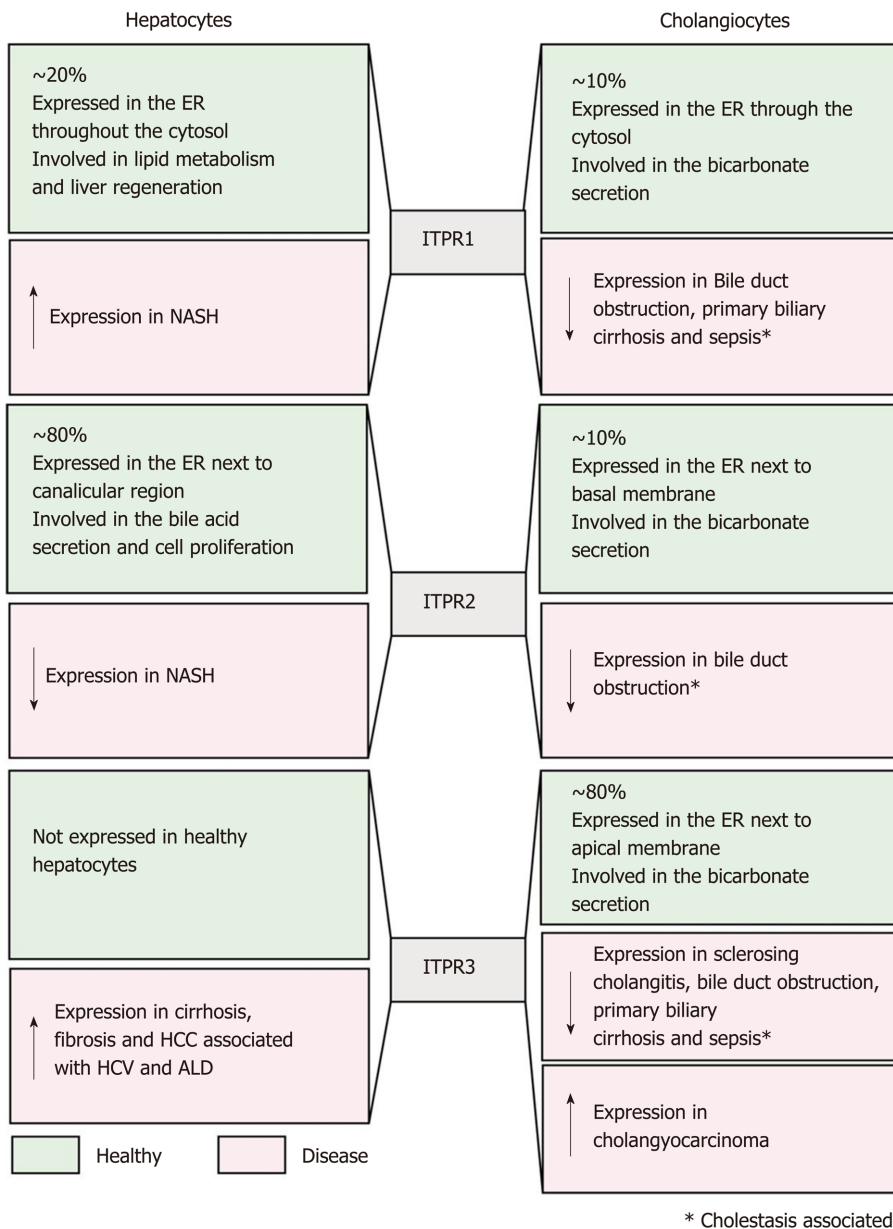


Figure 5 Inositol 1,4,5-trisphosphate receptors in the liver: Expression and functions. This figure summarizes, in green, Inositol 1,4,5-trisphosphate receptor (ITPR) isoform expression in hepatocytes and cholangiocytes under physiological condition, and in red the expression level and function of each ITPR isoform in liver diseases. ITPR1: ITPR isoform 1; ITPR2: ITPR isoform 2; ITPR3: ITPR isoform 3; ER: Endoplasmic reticulum; NAFLD: Non-alcoholic fatty liver disease; HCC: Hepatocellular carcinoma.

ACKNOWLEDGEMENTS

We thank Dr Christopher Kushmerick (Universidade Federal de Minas Gerais), Mr Sriram Amirneni (University of Pittsburgh) and Dr Michael Nathanson (Yale University) for generously providing many useful suggestions and comments on the manuscript. Fellowship and scholarships are acknowledged from Conselho Nacional de Desenvolvimento Científico e Tecnológico and Coordenação de Aperfeiçoamento de Pessoal.

REFERENCES


- 1 **Han HS**, Kang G, Kim JS, Choi BH, Koo SH. Regulation of glucose metabolism from a liver-centric perspective. *Exp Mol Med* 2016; **48**: e218 [PMID: 26964834 DOI: 10.1038/emm.2015.122]
- 2 **Robinson MW**, Harmon C, O'Farrelly C. Liver immunology and its role in inflammation and homeostasis. *Cell Mol Immunol* 2016; **13**: 267-276 [PMID: 27063467 DOI: 10.1038/cmi.2016.3]
- 3 **Bechmann LP**, Hannivoort RA, Gerken G, Hotamisligil GS, Trauner M, Canbay A. The interaction of

- hepatic lipid and glucose metabolism in liver diseases. *J Hepatol* 2012; **56**: 952-964 [PMID: [22173168](#) DOI: [10.1016/j.jhep.2011.08.025](#)]
- 4 **Chiang JYL**, Ferrell JM. Bile Acid Metabolism in Liver Pathobiology. *Gene Expr* 2018; **18**: 71-87 [PMID: [29325602](#) DOI: [10.3727/105221618X15156018385515](#)]
 - 5 **Bhatia SN**, Underhill GH, Zaret KS, Fox IJ. Cell and tissue engineering for liver disease. *Sci Transl Med* 2014; **6**: 245sr2 [PMID: [25031271](#) DOI: [10.1126/scitranslmed.3005975](#)]
 - 6 **Hirata K**, Pusi T, O'Neill AF, Dranoff JA, Nathanson MH. The type II inositol 1,4,5-trisphosphate receptor can trigger Ca²⁺ waves in rat hepatocytes. *Gastroenterology* 2002; **122**: 1088-1100 [PMID: [11910359](#) DOI: [10.1053/gast.2002.32363](#)]
 - 7 **Hirata K**, Dufour JF, Shibao K, Knickelbein R, O'Neill AF, Bode HP, Cassio D, St-Pierre MV, Larusso NF, Leite MF, Nathanson MH. Regulation of Ca(2+) signaling in rat bile duct epithelia by inositol 1,4,5-trisphosphate receptor isoforms. *Hepatology* 2002; **36**: 284-296 [PMID: [12143036](#) DOI: [10.1053/jhep.2002.34432](#)]
 - 8 **Pantazaka E**, Taylor CW. Differential distribution, clustering, and lateral diffusion of subtypes of the inositol 1,4,5-trisphosphate receptor. *J Biol Chem* 2011; **286**: 23378-23387 [PMID: [21550988](#) DOI: [10.1074/jbc.M111.236372](#)]
 - 9 **Tu H**, Wang Z, Nosyreva E, De Smedt H, Bezprozvany I. Functional characterization of mammalian inositol 1,4,5-trisphosphate receptor isoforms. *Biophys J* 2005; **88**: 1046-1055 [PMID: [15533917](#) DOI: [10.1529/biophysj.104.049593](#)]
 - 10 **Echevarría W**, Leite MF, Guerra MT, Zipfel WR, Nathanson MH. Regulation of calcium signals in the nucleus by a nucleoplasmic reticulum. *Nat Cell Biol* 2003; **5**: 440-446 [PMID: [12717445](#) DOI: [10.1038/ncb980](#)]
 - 11 **Streb H**, Irvine RF, Berridge MJ, Schulz I. Release of Ca²⁺ from a nonmitochondrial intracellular store in pancreatic acinar cells by inositol-1,4,5-trisphosphate. *Nature* 1983; **306**: 67-69 [PMID: [6605482](#) DOI: [10.1038/306067a0](#)]
 - 12 **Shibao K**, Hirata K, Robert ME, Nathanson MH. Loss of inositol 1,4,5-trisphosphate receptors from bile duct epithelia is a common event in cholestasis. *Gastroenterology* 2003; **125**: 1175-1187 [PMID: [14517800](#) DOI: [10.1016/S0016-5085\(03\)01201-0](#)]
 - 13 **Khamphaya T**, Chukijrunroat N, Saengsirisuwan V, Mitchell-Richards KA, Robert ME, Mennone A, Ananthanarayanan M, Nathanson MH, Weerachayaphorn J. Nonalcoholic fatty liver disease impairs expression of the type II inositol 1,4,5-trisphosphate receptor. *Hepatology* 2018; **67**: 560-574 [PMID: [29023819](#) DOI: [10.1002/hep.29588](#)]
 - 14 **Desmet VJ**. Ductal plates in hepatic ductular reactions. Hypothesis and implications. II. Ontogenic liver growth in childhood. *Virchows Arch* 2011; **458**: 261-270 [PMID: [21298286](#) DOI: [10.1007/s00428-011-1049-2](#)]
 - 15 **Huppert SS**, Iwafuchi-Doi M. Molecular regulation of mammalian hepatic architecture. *Curr Top Dev Biol* 2019; **132**: 91-136 [PMID: [30797519](#) DOI: [10.1016/bs.ctdb.2018.12.003](#)]
 - 16 **Dodds WJ**, Erickson SJ, Taylor AJ, Lawson TL, Stewart ET. Caudate lobe of the liver: anatomy, embryology, and pathology. *AJR Am J Roentgenol* 1990; **154**: 87-93 [PMID: [2104732](#) DOI: [10.2214/ajr.154.1.2104732](#)]
 - 17 **Sagoo MG**, Aland RC, Gosden E. Morphology and morphometry of the caudate lobe of the liver in two populations. *Anat Sci Int* 2018; **93**: 48-57 [PMID: [27586453](#) DOI: [10.1007/s12565-016-0365-7](#)]
 - 18 **Saxena R**, Theise ND, Crawford JM. Microanatomy of the human liver-exploring the hidden interfaces. *Hepatology* 1999; **30**: 1339-1346 [PMID: [10573509](#) DOI: [10.1002/hep.510300607](#)]
 - 19 **Wisse E**, Braet F, Luo D, De Zanger R, Jans D, Crabbé E, Vermoesen A. Structure and function of sinusoidal lining cells in the liver. *Toxicol Pathol* 1996; **24**: 100-111 [PMID: [8839287](#) DOI: [10.1177/019262339602400114](#)]
 - 20 **Maher JJ**. Cell-specific expression of hepatocyte growth factor in liver. Upregulation in sinusoidal endothelial cells after carbon tetrachloride. *J Clin Invest* 1993; **91**: 2244-2252 [PMID: [7683700](#) DOI: [10.1172/JCI116451](#)]
 - 21 **Crawford JM**. Development of the intrahepatic biliary tree. *Semin Liver Dis* 2002; **22**: 213-226 [PMID: [12360416](#) DOI: [10.1055/s-2002-34508](#)]
 - 22 **Strazzabosco M**, Fabris L. Functional anatomy of normal bile ducts. *Anat Rec (Hoboken)* 2008; **291**: 653-660 [PMID: [18484611](#) DOI: [10.1002/ar.20664](#)]
 - 23 **Krishna M**. Microscopic anatomy of the liver. *Clin Liver Dis (Hoboken)* 2013; **2**: S4-S7 [PMID: [30992875](#) DOI: [10.1002/cld.147](#)]
 - 24 **Torre C**, Perret C, Colnot S. Transcription dynamics in a physiological process: β -catenin signaling directs liver metabolic zonation. *Int J Biochem Cell Biol* 2011; **43**: 271-278 [PMID: [19914393](#) DOI: [10.1016/j.biocel.2009.11.004](#)]
 - 25 **Kietzmann T**. Metabolic zonation of the liver: The oxygen gradient revisited. *Redox Biol* 2017; **11**: 622-630 [PMID: [28126520](#) DOI: [10.1016/j.redox.2017.01.012](#)]
 - 26 **Halpern KB**, Shenhav R, Matcovitch-Natan O, Toth B, Lemze D, Golan M, Massasa EE, Baydatch S, Landen S, Moor AE, Brandis A, Giladi A, Avihail AS, David E, Amit I, Itzkovitz S. Single-cell spatial reconstruction reveals global division of labour in the mammalian liver. *Nature* 2017; **542**: 352-356 [PMID: [28166538](#) DOI: [10.1038/nature21065](#)]
 - 27 **Hata S**, Namae M, Nishina H. Liver development and regeneration: from laboratory study to clinical therapy. *Dev Growth Differ* 2007; **49**: 163-170 [PMID: [17335437](#) DOI: [10.1111/j.1440-169X.2007.00910.x](#)]
 - 28 **Gilgenkrantz H**, Collin de l'Hortet A. Understanding Liver Regeneration: From Mechanisms to Regenerative Medicine. *Am J Pathol* 2018; **188**: 1316-1327 [PMID: [29673755](#) DOI: [10.1016/j.ajpath.2018.03.008](#)]
 - 29 **Rodrigues MA**, Gomes DA, Leite MF, Grant W, Zhang L, Lam W, Cheng YC, Bennett AM, Nathanson MH. Nucleoplasmic calcium is required for cell proliferation. *J Biol Chem* 2007; **282**: 17061-17068 [PMID: [17420246](#) DOI: [10.1074/jbc.M700490200](#)]
 - 30 **Andrade V**, Guerra M, Jardim C, Melo F, Silva W, Ortega JM, Robert M, Nathanson MH, Leite F. Nucleoplasmic calcium regulates cell proliferation through legumain. *J Hepatol* 2011; **55**: 626-635 [PMID: [21237226](#) DOI: [10.1016/j.jhep.2010.12.022](#)]
 - 31 **Guimarães E**, Machado R, Fonseca MC, França A, Carvalho C, Araújo E Silva AC, Almeida B, Cassini P, Hissa B, Drumond L, Gonçalves C, Fernandes G, De Brot M, Moraes M, Barcelos L, Ortega JM, Oliveira A, Leite MF. Inositol 1, 4, 5-trisphosphate-dependent nuclear calcium signals regulate angiogenesis and cell motility in triple negative breast cancer. *PLoS One* 2017; **12**: e0175041 [PMID: [28126520](#) DOI: [10.1371/journal.pone.0175041](#)]

- 28376104 DOI: [10.1371/journal.pone.0175041](https://doi.org/10.1371/journal.pone.0175041)]
- 32 **Resende RR**, Andrade LM, Oliveira AG, Guimarães ES, Guatimosim S, Leite MF. Nucleoplasmic calcium signaling and cell proliferation: calcium signaling in the nucleus. *Cell Commun Signal* 2013; **11**: 14 [PMID: [23433362](https://pubmed.ncbi.nlm.nih.gov/23433362/) DOI: [10.1186/1478-811X-11-14](https://doi.org/10.1186/1478-811X-11-14)]
- 33 **Berridge MJ**, Bootman MD, Roderick HL. Calcium signalling: dynamics, homeostasis and remodelling. *Nat Rev Mol Cell Biol* 2003; **4**: 517-529 [PMID: [12838335](https://pubmed.ncbi.nlm.nih.gov/12838335/) DOI: [10.1038/nrm1155](https://doi.org/10.1038/nrm1155)]
- 34 **Oliveira AG**, Guimarães ES, Andrade LM, Menezes GB, Fatima Leite M. Decoding calcium signaling across the nucleus. *Physiology (Bethesda)* 2014; **29**: 361-368 [PMID: [25180265](https://pubmed.ncbi.nlm.nih.gov/25180265/) DOI: [10.1152/physiol.00056.2013](https://doi.org/10.1152/physiol.00056.2013)]
- 35 **Irvine RF**, Lloyd-Burton SM, Yu JC, Letcher AJ, Schell MJ. The regulation and function of inositol 1,4,5-trisphosphate 3-kinases. *Adv Enzyme Regul* 2006; **46**: 314-323 [PMID: [16857241](https://pubmed.ncbi.nlm.nih.gov/16857241/) DOI: [10.1016/j.advenzreg.2006.01.009](https://doi.org/10.1016/j.advenzreg.2006.01.009)]
- 36 **Connolly TM**, Bansal VS, Bross TE, Irvine RF, Majerus PW. The metabolism of tris- and tetraphosphates of inositol by 5-phosphomonoesterase and 3-kinase enzymes. *J Biol Chem* 1987; **262**: 2146-2149 [PMID: [3029066](https://pubmed.ncbi.nlm.nih.gov/3029066/)]
- 37 **Blaustein MP**, Lederer WJ. Sodium/calcium exchange: its physiological implications. *Physiol Rev* 1999; **79**: 763-854 [PMID: [10390518](https://pubmed.ncbi.nlm.nih.gov/10390518/) DOI: [10.1152/physrev.1999.79.3.763](https://doi.org/10.1152/physrev.1999.79.3.763)]
- 38 **Perocchi F**, Gohil VM, Girgis HS, Bao XR, McCombs JE, Palmer AE, Mootha VK. MICU1 encodes a mitochondrial EF hand protein required for Ca²⁺. *Nature* 2010; **467**: 291-296 [PMID: [20693986](https://pubmed.ncbi.nlm.nih.gov/20693986/) DOI: [10.1038/nature09358](https://doi.org/10.1038/nature09358)]
- 39 **Jiang QX**, Thrower EC, Chester DW, Ehrlich BE, Sigworth FJ. Three-dimensional structure of the type I inositol 1,4,5-trisphosphate receptor at 2.4 Å resolution. *EMBO J* 2002; **21**: 3575-3581 [PMID: [12110570](https://pubmed.ncbi.nlm.nih.gov/12110570/) DOI: [10.1093/emboj/cdf380](https://doi.org/10.1093/emboj/cdf380)]
- 40 **Shah SZA**, Zhao D, Khan SH, Yang L. Regulatory Mechanisms of Endoplasmic Reticulum Resident IP3 Receptors. *J Mol Neurosci* 2015; **56**: 938-948 [PMID: [25859934](https://pubmed.ncbi.nlm.nih.gov/25859934/) DOI: [10.1007/s12031-015-0551-4](https://doi.org/10.1007/s12031-015-0551-4)]
- 41 **Foskett JK**, White C, Cheung KH, Mak DO. Inositol trisphosphate receptor Ca²⁺ release channels. *Physiol Rev* 2007; **87**: 593-658 [PMID: [17429043](https://pubmed.ncbi.nlm.nih.gov/17429043/) DOI: [10.1152/physrev.00035.2006](https://doi.org/10.1152/physrev.00035.2006)]
- 42 **Baker MR**, Fan G, Serysheva II. Structure of IP₃R channel: high-resolution insights from cryo-EM. *Curr Opin Struct Biol* 2017; **46**: 38-47 [PMID: [28618351](https://pubmed.ncbi.nlm.nih.gov/28618351/) DOI: [10.1016/j.sbi.2017.05.014](https://doi.org/10.1016/j.sbi.2017.05.014)]
- 43 **Yang J**, Vais H, Gu W, Foskett JK. Biphasic regulation of InsP₃ receptor gating by dual Ca²⁺ release channel BH3-like domains mediates Bcl-xL control of cell viability. *Proc Natl Acad Sci USA* 2016; **113**: E1953-E1962 [PMID: [26976600](https://pubmed.ncbi.nlm.nih.gov/26976600/) DOI: [10.1073/pnas.1517935113](https://doi.org/10.1073/pnas.1517935113)]
- 44 **Choe CU**, Ehrlich BE. The inositol 1,4,5-trisphosphate receptor (IP3R) and its regulators: sometimes good and sometimes bad teamwork. *Sci STKE* 2006; **2006**: re15 [PMID: [17132820](https://pubmed.ncbi.nlm.nih.gov/17132820/) DOI: [10.1126/stke.3632006re15](https://doi.org/10.1126/stke.3632006re15)]
- 45 **Wang L**, Wagner LE 2nd, Alzayady KJ, Yule DI. Region-specific proteolysis differentially regulates type I inositol 1,4,5-trisphosphate receptor activity. *J Biol Chem* 2017; **292**: 11714-11726 [PMID: [28526746](https://pubmed.ncbi.nlm.nih.gov/28526746/) DOI: [10.1074/jbc.M117.789917](https://doi.org/10.1074/jbc.M117.789917)]
- 46 **Khan MT**, Wagner L 2nd, Yule DI, Bhanumathy C, Joseph SK. Akt kinase phosphorylation of inositol 1,4,5-trisphosphate receptors. *J Biol Chem* 2006; **281**: 3731-3737 [PMID: [16332683](https://pubmed.ncbi.nlm.nih.gov/16332683/) DOI: [10.1074/jbc.M509262200](https://doi.org/10.1074/jbc.M509262200)]
- 47 **Mikoshiha K**. IP₃ receptor/Ca²⁺ channel: from discovery to new signaling concepts. *J Neurochem* 2007; **102**: 1426-1446 [PMID: [17697045](https://pubmed.ncbi.nlm.nih.gov/17697045/) DOI: [10.1111/j.1471-4159.2007.04825.x](https://doi.org/10.1111/j.1471-4159.2007.04825.x)]
- 48 **Iwai M**, Michikawa T, Bosanac I, Ikura M, Mikoshiha K. Molecular basis of the isoform-specific ligand-binding affinity of inositol 1,4,5-trisphosphate receptors. *J Biol Chem* 2007; **282**: 12755-12764 [PMID: [17327232](https://pubmed.ncbi.nlm.nih.gov/17327232/) DOI: [10.1074/jbc.M609833200](https://doi.org/10.1074/jbc.M609833200)]
- 49 **Newton CL**, Mignery GA, Südhof TC. Co-expression in vertebrate tissues and cell lines of multiple inositol 1,4,5-trisphosphate (InsP₃) receptors with distinct affinities for InsP₃. *J Biol Chem* 1994; **269**: 28613-28619 [PMID: [7961809](https://pubmed.ncbi.nlm.nih.gov/7961809/)]
- 50 **Alzayady KJ**, Wang L, Chandrasekhar R, Wagner LE 2nd, Van Petegem F, Yule DI. Defining the stoichiometry of inositol 1,4,5-trisphosphate binding required to initiate Ca²⁺ release. *Sci Signal* 2016; **9**: ra35 [PMID: [27048566](https://pubmed.ncbi.nlm.nih.gov/27048566/) DOI: [10.1126/scisignal.aad6281](https://doi.org/10.1126/scisignal.aad6281)]
- 51 **Ramos-Franco J**, Fill M, Mignery GA. Isoform-specific function of single inositol 1,4,5-trisphosphate receptor channels. *Biophys J* 1998; **75**: 834-839 [PMID: [9675184](https://pubmed.ncbi.nlm.nih.gov/9675184/) DOI: [10.1016/S0006-3495\(98\)77572-1](https://doi.org/10.1016/S0006-3495(98)77572-1)]
- 52 **Hagar RE**, Burgstahler AD, Nathanson MH, Ehrlich BE. Type III InsP₃ receptor channel stays open in the presence of increased calcium. *Nature* 1998; **396**: 81-84 [PMID: [9817204](https://pubmed.ncbi.nlm.nih.gov/9817204/) DOI: [10.1038/23954](https://doi.org/10.1038/23954)]
- 53 **Finch EA**, Turner TJ, Goldin SM. Calcium as a coagonist of inositol 1,4,5-trisphosphate-induced calcium release. *Science* 1991; **252**: 443-446 [PMID: [2017683](https://pubmed.ncbi.nlm.nih.gov/2017683/) DOI: [10.1126/science.2017683](https://doi.org/10.1126/science.2017683)]
- 54 **De Young GW**, Keizer J. A single-pool inositol 1,4,5-trisphosphate-receptor-based model for agonist-stimulated oscillations in Ca²⁺ concentration. *Proc Natl Acad Sci USA* 1992; **89**: 9895-9899 [PMID: [1329108](https://pubmed.ncbi.nlm.nih.gov/1329108/) DOI: [10.1073/pnas.89.20.9895](https://doi.org/10.1073/pnas.89.20.9895)]
- 55 **Hagar RE**, Ehrlich BE. Regulation of the type III InsP(3) receptor by InsP(3) and ATP. *Biophys J* 2000; **79**: 271-278 [PMID: [10866953](https://pubmed.ncbi.nlm.nih.gov/10866953/) DOI: [10.1016/S0006-3495\(00\)76289-8](https://doi.org/10.1016/S0006-3495(00)76289-8)]
- 56 **Michikawa T**, Hirota J, Kawano S, Hiraoka M, Yamada M, Furuichi T, Mikoshiha K. Calmodulin mediates calcium-dependent inactivation of the cerebellar type I inositol 1,4,5-trisphosphate receptor. *Neuron* 1999; **23**: 799-808 [PMID: [10482245](https://pubmed.ncbi.nlm.nih.gov/10482245/) DOI: [10.1016/S0896-6273\(01\)80037-4](https://doi.org/10.1016/S0896-6273(01)80037-4)]
- 57 **Miyakawa T**, Maeda A, Yamazawa T, Hirose K, Kurosaki T, Iino M. Encoding of Ca²⁺ signals by differential expression of IP₃ receptor subtypes. *EMBO J* 1999; **18**: 1303-1308 [PMID: [10064596](https://pubmed.ncbi.nlm.nih.gov/10064596/) DOI: [10.1093/emboj/18.5.1303](https://doi.org/10.1093/emboj/18.5.1303)]
- 58 **Fiedler MJ**, Nathanson MH. The type I inositol 1,4,5-trisphosphate receptor interacts with protein 4.1N to mediate neurite formation through intracellular Ca waves. *Neurosignals* 2011; **19**: 75-85 [PMID: [21389686](https://pubmed.ncbi.nlm.nih.gov/21389686/) DOI: [10.1159/000324507](https://doi.org/10.1159/000324507)]
- 59 **Guatimosim S**, Amaya MJ, Guerra MT, Aguiar CJ, Goes AM, Gómez-Viquez NL, Rodrigues MA, Gomes DA, Martins-Cruz J, Lederer WJ, Leite MF. Nuclear Ca²⁺ regulates cardiomyocyte function. *Cell Calcium* 2008; **44**: 230-242 [PMID: [18201761](https://pubmed.ncbi.nlm.nih.gov/18201761/) DOI: [10.1016/j.ceca.2007.11.016](https://doi.org/10.1016/j.ceca.2007.11.016)]
- 60 **Futatsugi A**, Nakamura T, Yamada MK, Ebisui E, Nakamura K, Uchida K, Kitaguchi T, Takahashi-Iwanaga H, Noda T, Aruga J, Mikoshiha K. IP₃ receptor types 2 and 3 mediate exocrine secretion underlying energy metabolism. *Science* 2005; **309**: 2232-2234 [PMID: [16195467](https://pubmed.ncbi.nlm.nih.gov/16195467/) DOI: [10.1126/science.1114110](https://doi.org/10.1126/science.1114110)]
- 61 **Minagawa N**, Nagata J, Shibao K, Masyuk AI, Gomes DA, Rodrigues MA, Lesage G, Akiba Y, Kaunitz JD, Ehrlich BE, Larusso NF, Nathanson MH. Cyclic AMP regulates bicarbonate secretion in

- cholangiocytes through release of ATP into bile. *Gastroenterology* 2007; **133**: 1592-1602 [PMID: 17916355 DOI: 10.1053/j.gastro.2007.08.020]
- 62 **Kruglov EA**, Gautam S, Guerra MT, Nathanson MH. Type 2 inositol 1,4,5-trisphosphate receptor modulates bile salt export pump activity in rat hepatocytes. *Hepatology* 2011; **54**: 1790-1799 [PMID: 21748767 DOI: 10.1002/hep.24548]
- 63 **Feriod CN**, Oliveira AG, Guerra MT, Nguyen L, Richards KM, Jurczak MJ, Ruan HB, Camporez JP, Yang X, Shulman GI, Bennett AM, Nathanson MH, Ehrlich BE. Hepatic Inositol 1,4,5 Trisphosphate Receptor Type 1 Mediates Fatty Liver. *Hepatol Commun* 2017; **1**: 23-35 [PMID: 28966992 DOI: 10.1002/hep4.1012]
- 64 **Wang Y**, Li G, Goode J, Paz JC, Ouyang K, Screation R, Fischer WH, Chen J, Tabas I, Montminy M. Inositol-1,4,5-trisphosphate receptor regulates hepatic gluconeogenesis in fasting and diabetes. *Nature* 2012; **485**: 128-132 [PMID: 22495310 DOI: 10.1038/nature10988]
- 65 **Arruda AP**, Pers BM, Parlakgöl G, Güney E, Inouye K, Hotamisligil GS. Chronic enrichment of hepatic endoplasmic reticulum-mitochondria contact leads to mitochondrial dysfunction in obesity. *Nat Med* 2014; **20**: 1427-1435 [PMID: 25419710 DOI: 10.1038/nm.3735]
- 66 **Oliveira AG**, Andrade VA, Guimarães ES, Florentino RM, Sousa PA, Marques PE, Melo FM, Ortega MJ, Menezes GB, Leite MF. Calcium signalling from the type I inositol 1,4,5-trisphosphate receptor is required at early phase of liver regeneration. *Liver Int* 2015; **35**: 1162-1171 [PMID: 24814243 DOI: 10.1111/liv.12587]
- 67 **Nicou A**, Serrière V, Hilly M, Prigent S, Combettes L, Guillon G, Tordjmann T. Remodelling of calcium signalling during liver regeneration in the rat. *J Hepatol* 2007; **46**: 247-256 [PMID: 17125880 DOI: 10.1016/j.jhep.2006.08.014]
- 68 **Nagata J**, Guerra MT, Shugrue CA, Gomes DA, Nagata N, Nathanson MH. Lipid rafts establish calcium waves in hepatocytes. *Gastroenterology* 2007; **133**: 256-267 [PMID: 17631147 DOI: 10.1053/j.gastro.2007.03.115]
- 69 **Cruz LN**, Guerra MT, Kruglov E, Mennone A, Garcia CR, Chen J, Nathanson MH. Regulation of multidrug resistance-associated protein 2 by calcium signaling in mouse liver. *Hepatology* 2010; **52**: 327-337 [PMID: 20578149 DOI: 10.1002/hep.23625]
- 70 **Kruglov E**, Ananthanarayanan M, Sousa P, Weerachayaphorn J, Guerra MT, Nathanson MH. Type 2 inositol trisphosphate receptor gene expression in hepatocytes is regulated by cyclic AMP. *Biochem Biophys Res Commun* 2017; **486**: 659-664 [PMID: 28327356 DOI: 10.1016/j.bbrc.2017.03.086]
- 71 **Feriod CN**, Nguyen L, Jurczak MJ, Kruglov EA, Nathanson MH, Shulman GI, Bennett AM, Ehrlich BE. Inositol 1,4,5-trisphosphate receptor type II (InsP3R-II) is reduced in obese mice, but metabolic homeostasis is preserved in mice lacking InsP3R-II. *Am J Physiol Endocrinol Metab* 2014; **307**: E1057-E1064 [PMID: 25315698 DOI: 10.1152/ajpendo.00236.2014]
- 72 **Kele PG**, van der Jagt EJ, Gouw AS, Lisman T, Porte RJ, de Boer MT. The impact of hepatic steatosis on liver regeneration after partial hepatectomy. *Liver Int* 2013; **33**: 469-475 [PMID: 23311417 DOI: 10.1111/liv.12089]
- 73 **Leite MF**, Thrower EC, Echevarria W, Koulen P, Hirata K, Bennett AM, Ehrlich BE, Nathanson MH. Nuclear and cytosolic calcium are regulated independently. *Proc Natl Acad Sci U S A* 2003; **100**: 2975-2980 [PMID: 12606721 DOI: 10.1073/pnas.0536590100]
- 74 **Guerra MT**, Florentino RM, Franca A, Lima Filho AC, Dos Santos ML, Fonseca RC, Lemos FO, Fonseca MC, Kruglov E, Mennone A, Njei B, Gibson J, Guan F, Cheng YC, Ananthanarayanan M, Gu J, Jiang J, Zhao H, Lima CX, Vidigal PT, Oliveira AG, Nathanson MH, Leite MF. Expression of the type 3 InsP₃ receptor is a final common event in the development of hepatocellular carcinoma. *Gut* 2019; **68**: 1676-1687 [PMID: 31315892 DOI: 10.1136/gutjnl-2018-317811]
- 75 **Liang JQ**, Teoh N, Xu L, Pok S, Li X, Chu ESH, Chiu J, Dong L, Arfianti E, Haigh WG, Yeh MM, Ioannou GN, Sung JY, Farrell G, Yu J. Dietary cholesterol promotes steatohepatitis related hepatocellular carcinoma through dysregulated metabolism and calcium signaling. *Nat Commun* 2018; **9**: 4490 [PMID: 30367044 DOI: 10.1038/s41467-018-06931-6]
- 76 **Portela A**, Esteller M. Epigenetic modifications and human disease. *Nat Biotechnol* 2010; **28**: 1057-1068 [PMID: 20944598 DOI: 10.1038/nbt.1685]
- 77 **Jones PA**, Takai D. The role of DNA methylation in mammalian epigenetics. *Science* 2001; **293**: 1068-1070 [PMID: 11498573 DOI: 10.1126/science.1063852]
- 78 **Rodrigues MA**, Gomes DA, Nathanson MH. Calcium Signaling in Cholangiocytes: Methods, Mechanisms, and Effects. *Int J Mol Sci* 2018; **19** [PMID: 30563259 DOI: 10.3390/ijms19123913]
- 79 **Franca A**, Carlos Melo Lima Filho A, Guerra MT, Weerachayaphorn J, Loliola Dos Santos M, Njei B, Robert M, Xavier Lima C, Vieira Teixeira Vidigal P, Banales JM, Ananthanarayanan M, Leite MF, Nathanson MH. Effects of Endotoxin on Type 3 Inositol 1,4,5-Trisphosphate Receptor in Human Cholangiocytes. *Hepatology* 2019; **69**: 817-830 [PMID: 30141207 DOI: 10.1002/hep.30228]
- 80 **Weerachayaphorn J**, Amaya MJ, Spirli C, Chansela P, Mitchell-Richards KA, Ananthanarayanan M, Nathanson MH. Nuclear Factor, Erythroid 2-Like 2 Regulates Expression of Type 3 Inositol 1,4,5-Trisphosphate Receptor and Calcium Signaling in Cholangiocytes. *Gastroenterology* 2015; **149**: 211-222.e10 [PMID: 25796361 DOI: 10.1053/j.gastro.2015.03.014]
- 81 **Ananthanarayanan M**, Banales JM, Guerra MT, Spirli C, Munoz-Garrido P, Mitchell-Richards K, Tafur D, Saez E, Nathanson MH. Post-translational regulation of the type III inositol 1,4,5-trisphosphate receptor by miRNA-506. *J Biol Chem* 2015; **290**: 184-196 [PMID: 25378392 DOI: 10.1074/jbc.M114.587030]
- 82 **Uesilamongkol P**, Khamphaya T, Guerra MT, Rodrigues MA, Gomes DA, Kong Y, Wei W, Jain D, Trampert DC, Ananthanarayanan M, Banales JM, Roberts LR, Farshidfar F, Nathanson MH, Weerachayaphorn J. Type 3 Inositol 1,4,5-Trisphosphate Receptor Is Increased and Enhances Malignant Properties in Cholangiocarcinoma. *Hepatology* 2019 [PMID: 31251815 DOI: 10.1002/hep.30839]

Molecular Mechanism for Protection Against Liver Failure in Human Yellow Fever Infection

Fernanda de Oliveira Lemos,^{1*} Andressa França,^{1*} Antônio Carlos Melo Lima Filho,^{1*} Rodrigo M. Florentino,^{1*} Marcone Loiola Santos,¹ Dabny G. Missiaggia,¹ Gisele Olinto Libanio Rodrigues,² Felipe Ferraz Dias ,³ Ingredy Beatriz Souza Passos,⁴ Mauro M. Teixeira,² Antônio Márcio de Faria Andrade,⁵ Cristiano Xavier Lima,^{5,6} Paula Vieira Teixeira Vidigal,⁷ Vivian Vasconcelos Costa,⁴ Matheus Castro Fonseca,⁸ Michael H. Nathanson,⁹ and M. Fatima Leite¹

Yellow fever (YF) is a viral hemorrhagic fever that typically involves the liver. Brazil recently experienced its largest recorded YF outbreak, and the disease was fatal in more than a third of affected individuals, mostly because of acute liver failure. Affected individuals are generally treated only supportively, but during the recent Brazilian outbreak, selected patients were treated with liver transplant. We took advantage of this clinical experience to better characterize the clinical and pathological features of YF-induced liver failure and to examine the mechanism of hepatocellular injury in YF, to identify targets that would be amenable to therapeutic intervention in preventing progression to liver failure and death. Patients with YF liver failure rapidly developed massive transaminase elevations, with jaundice, coagulopathy, thrombocytopenia, and usually hepatic encephalopathy, along with pathological findings that included microvesicular steatosis and lytic necrosis. Hepatocytes began to express the type 3 isoform of the inositol trisphosphate receptor (ITPR3), an intracellular calcium (Ca^{2+}) channel that is not normally expressed in hepatocytes. Experiments in an animal model, isolated hepatocytes, and liver-derived cell lines showed that this new expression of ITPR3 was associated with increased nuclear Ca^{2+} signaling and hepatocyte proliferation, and reduced steatosis and cell death induced by the YF virus. **Conclusion:** Yellow fever often induces liver failure characterized by massive hepatocellular damage plus steatosis. New expression of ITPR3 also occurs in YF-infected hepatocytes, which may represent an endogenous protective mechanism that could suggest approaches to treat affected individuals before they progress to liver failure, thereby decreasing the mortality of this disease in a way that does not rely on the costly and limited resource of liver transplantation. (*Hepatology Communications* 2020;4:657-669).

The yellow fever virus (YFV) is the prototypical member of the Flaviviridae family, which also includes viruses such as hepatitis C virus, dengue, West Nile, Zika, and Japanese encephalitis.^(1,2) Yellow fever (YF) is endemic in 47 countries across Africa and Central and South America,⁽³⁾ and over

2,000 cases were reported in the Brazilian outbreak between July 2016 and June 2018.⁽⁴⁾ The infection was fatal in more than one-third of these patients, and the lethal cases were mostly attributed to acute liver failure.⁽⁵⁾ Therefore, YF remains a major health problem despite intense study about transmission

Abbreviations: 5mC, 5-methyl cytosine; ANOVA, analysis of variance; ATP, adenosine triphosphate; dpi, days post-infection; EGF, epidermal growth factor; ER, endoplasmic reticulum; FBS, fetal bovine serum; HCC, hepatocellular carcinoma; H&E, hematoxylin & eosin; ICG, indocyanine green; IFN, interferon; IHC, immunohistochemistry; ITPR, inositol trisphosphate receptor; KO, knockout; MAM, mitochondria-associated membranes; MOI, multiplicity of infection; mRNA, messenger RNA; PCNA, proliferating cell nuclear antigen; PCR, polymerase chain reaction; PFU, plaque-forming unit; R3KO, knockout for ITPR3; RPMI, Roswell Park Memorial Institute; UFMG, Universidade Federal de Minas Gerais; YF, yellow fever; YFV, yellow fever virus; YFV_{17DD}, YFV 17DD vaccine substrain; YFV_{WT}, YFV wild-type strain; WT, wild type.

Received December 3, 2019; accepted February 20, 2020.

Additional Supporting Information may be found at onlinelibrary.wiley.com/doi/10.1002/hep4.1504/supinfo.

*These authors contributed equally to this work.

Financial support: National Institute of Science and Technology in Dengue (573876/2008); Foundation for the National Institutes of Health (DK112797, DK114041, DK34989, and DK57751); Fundação de Amparo à Pesquisa de Minas Gerais; Coordenação de Aperfeiçoamento de Pessoal de Nível Superior; Fundação de Amparo à Pesquisa do Estado de São Paulo (2018/20014-0); Conselho Nacional de Desenvolvimento Científico e Tecnológico (159892/2018-0); and Liver Center at Universidade Federal de Minas Gerais.

and prophylaxis of the virus and the availability of an effective vaccine. The pathogenesis of the liver disease caused by YFV is poorly understood; indeed, treatment of infected individuals has typically been limited to supportive measures. During the recent Brazilian outbreak, however, selected patients with liver failure were considered for urgent liver transplant.^(6,7) This provided the opportunity to more carefully characterize the clinical and pathological features of YF-induced acute liver failure and to investigate the cell biology of its pathogenesis. Calcium signals in hepatocytes regulate pathological processes that are known to occur in YF, including changes in cell proliferation, lipid droplet formation,⁽⁷⁾ and cell death.^(2,8) Therefore, we examined cellular and molecular alterations in the calcium signaling machinery in livers of patients infected with YFV and in isolated liver cells and an animal model.

Materials and Methods

HUMAN LIVER SPECIMENS

Human liver samples and clinical data from patients with YF were obtained under the auspices of protocols approved by the Ethics Committee of Hospital Felício

Rocho (Belo Horizonte, Brazil) number CAAE: 90780318.9.0000.5125. YF specimens were from explanted livers, posttransplant liver biopsy of a patient who presented retroperitoneal bleeding 48 hours after the liver transplant, and autopsies of patients hospitalized at Hospital Felício Rocho in the 2018 YF outbreak. Healthy liver samples were obtained from biopsies of pretransplant liver grafts. YF diagnosis was confirmed by real-time polymerase chain reaction (PCR) in all cases. Patient selection for orthotopic liver transplantation was based on Clichy criteria.⁽⁹⁾

CELLS

HepG2 wild-type (WT) and inositol trisphosphate receptor (ITPR) 3 knockout (KO) cells were obtained from the laboratory of Dr. M. Nathanson (Yale University), maintained in Dulbecco's modified Eagle's medium supplemented with 10% fetal bovine serum, and kept at 37°C in 5% CO₂.

PRODUCTION OF VIRUSES AND PLAQUE ASSAY

For *in vitro* and *in vivo* experiments we used two YFV strains: (1) the 17DD vaccine substrain (YFV_{17DD}),

© 2020 The Authors. *Hepatology Communications* published by Wiley Periodicals, Inc., on behalf of the American Association for the Study of Liver Diseases. This is an open access article under the terms of the Creative Commons Attribution-NonCommercial-NoDerivs License, which permits use and distribution in any medium, provided the original work is properly cited, the use is non-commercial and no modifications or adaptations are made.

View this article online at wileyonlinelibrary.com.

DOI 10.1002/hep4.1504

Potential conflict of interest: Nothing to report.

ARTICLE INFORMATION:

From the ¹Department of Physiology and Biophysics, Universidade Federal de Minas Gerais, Belo Horizonte, Brazil; ²Department of Biochemistry and Immunology, Universidade Federal de Minas Gerais, Belo Horizonte, Brazil; ³Center of Microscopy, Universidade Federal de Minas Gerais, Belo Horizonte, Brazil; ⁴Department of Morphology, Universidade Federal de Minas Gerais, Belo Horizonte, Brazil; ⁵Hepatic Transplant Service, Hospital Felício Rocho, Belo Horizonte, Brazil; ⁶Surgery, Universidade Federal de Minas Gerais, Belo Horizonte, Brazil; ⁷Pathological Anatomy and Forensic Medicine, Universidade Federal de Minas Gerais, Belo Horizonte, Brazil; ⁸Brazilian Biosciences National Laboratory (LNBio), Brazilian Center for Research in Energy and Materials, Rua Giuseppe Máximo Solfaro, Campinas, Brazil; ⁹Section of Digestive Diseases, Department of Internal Medicine, Yale University School of Medicine, New Haven, CT.

ADDRESS CORRESPONDENCE AND REPRINT REQUESTS TO:

Michael H. Nathanson, M.D., Ph.D.
Section of Digestive Diseases, Department of Internal Medicine
Yale University School of Medicine
300 Cedar Street, TAC S241D

New Haven, CT 06520-8019
E-mail: michael.nathanson@yale.edu
Tel.: (+1) 203-785-5610

kindly donated by the Reference Laboratory for Flavivirus, Fiocruz, Brazilian Ministry of Health, and (2) The WT strain (YFV_{WT}), which was isolated in our Laboratory from a clinical specimen of serum from a symptomatic patient from the 2018 outbreak in Minas Gerais. 17DD virus stocks were passaged at a multiplicity of infection (MOI) of 0.01 in Vero cells (ATCC CCL81, existing collection in our laboratory from Banco de Células do Rio de Janeiro [BCRJ, access code 0245]) in Roswell Park Memorial Institute (RPMI) medium (Cultilab, Campinas, Brazil) supplemented with 10% segmented filamentous bacteria for 5 days at 37°C. The YFV_{WT} virus strain was propagated in mosquito cells (*Aedes albopictus* clone C6/36 [ATCC CRL-1660, existing collection in our laboratory from BCRJ, code 0343]) in L15 medium supplemented with 10% fetal bovine serum (FBS) (Cultilab) and maintained at 28°C. YFV_{WT} isolation was confirmed by real-time PCR as described subsequently. To concentrate the virus, 50 mL of the cell culture supernatant was loaded onto a VivaCell 100 centrifugal concentrator (Sartorius, Göttingen, Germany) and centrifuged at 2,000g for 10 minutes, and the supernatant remaining in the concentrator was aliquoted and stored at -80°C. For quantification of virus, Vero cells were grown to a confluent monolayer in RPMI 1640 medium with 10% FBS (Cultilab) and 1% penicillin-streptomycin-glutamine (Gibco) in 24-well plates at 37°C. The virus was serially diluted in serum-free medium and then inoculated into the cells at 37°C with gentle shaking every 15 minutes for 1 hour. Next, the medium was replaced with RPMI 1640 medium containing 2% carboxymethylcellulose and 2% FBS (Cultilab) (overlay medium) and the culture kept at 37°C. After 5 days, the cells were fixed in 3% formalin in phosphate-buffered saline for 1 hour, washed, and stained with 1% crystal violet in 10% formalin solution for 1 hour. Plates were washed with water, and plaques were counted manually.

ANIMALS AND YF MOUSE INFECTION

In vivo experiments were conducted using type I INF receptor deficient mice (A129^{-/-}) on a SV129 background. The A129^{-/-} mice were originally from the Jackson Laboratories (reference 010830) and were obtained from Bioterio de Matrizes da Universidade de Sao Paulo and kept under specific pathogen-free

conditions at the Immunopharmacology Lab at the Universidade Federal de Minas Gerais (UFMG). This mouse model was used because its use has already been described for studying the pathogenesis of YF.⁽¹⁰⁾ In particular, this model recapitulates key features of fatal human YF infection, including death, YFV replication and dissemination, proinflammatory cytokine release, and severe pathology in visceral organs, including the liver.⁽¹⁰⁾ The rationale for using the A129^{-/-} strain is that the resistance of mice to fatal viscerotropic YFV infection is mediated by interferons (IFNs), as it appears to be for dengue virus.⁽¹¹⁾ Mice were housed in filtered cages with autoclaved food and water available *ad libitum* on ventilated shelves (Alesco, Monte Mor, Brazil). Mice were housed under standard conditions with controlled temperature (18°C-23°C), humidity (40%-60%), and 12/12-hour dark-light cycle. Sample sizes for *in vivo* studies were determined using the G*Power 3.1 software package. The experimental protocol was approved by the Committee on Animal Ethics of the UFMG (permit protocol no. 84/2018). All surgeries were performed under ketamine/xylazine anesthesia. Studies with YFV were conducted under biosafety level 2 containment at Immunopharmacology Lab from the Instituto de Ciências Biológicas at the UFMG.

For the experiments, adult male and female A129^{-/-} mice (7-9 weeks old, 20-22 g) were inoculated with different inoculums of either YFV_{17DD} or YFV_{WT} viruses' strains through intravenous route/200 µL (tail vein). Control (noninfected) mice received 200 µL of C6/36 cell culture supernatant also through intravenous route (tail vein). Morbidity parameters such as lethality rates and bodyweight loss were evaluated daily. For clinical analysis, a kinetic of infection was performed and analysis was conducted on days 1, 3, and 6 following YFV infection.

STATISTICAL ANALYSIS

Data are presented as arithmetic mean ± SEM unless otherwise indicated. For statistical analysis, means between two groups were compared by Student *t* test, and comparisons among groups were analyzed by one-way analysis of variance (ANOVA) followed by Bonferroni's posttest. A *P* value of 0.05 or less was considered statistically significance.

FURTHER METHODOLOGICAL DETAILS

Detailed additional materials and methods are available in the Supporting Information.

Results

CLINICAL, PATHOLOGICAL, AND CELL BIOLOGICAL CHARACTERISTICS OF YFV-INDUCED LIVER FAILURE

We examined clinical presentations (Table 1) and liver biopsies (Fig. 1 and Supporting Fig. S1) of YFV-infected patients who were considered for liver transplant at Hospital Felício Rocho, Belo Horizonte, Brazil, during the 2018 outbreak. Fourteen patients were admitted, most of whom transferred from other hospitals specifically for transplant evaluation. Thirteen patients were male (92.8%) with an average age 47 (22-67 years), and all patients were exposed to forested areas. All but 1 of the patients were not vaccinated. Eight of the patients were deemed appropriate for listing for liver transplantation. These patients had high serum levels of transaminases at admission (9,000-27,000 U/mL), with aspartate aminotransferase > alanine aminotransferase; 6 developed acute kidney injury and required hemodialysis. All patients had severe coagulopathy, with thrombocytopenia (18,000-55,000), elevated international normalized ratio (1.5-10.0), and low factor V activity (11%-30%). Serum bilirubin also was elevated in nearly all of the patients, although serum alkaline phosphatase was in the normal range (not shown), suggesting that liver failure was due entirely to hepatocellular injury. Patients developed hepatic encephalopathy between 6 and 11 days after onset of symptoms, and progression from grade I to grade IV (24 hours) and then to death (36 hours) was very fast. After listing, 4 patients (50%) underwent orthotopic liver transplantation, whereas the other 4 died on the waiting list after a median of 24 hours. Two of the 4 transplanted patients died: one 3 hours after liver transplantation due to primary graft nonfunction, and the other 3 days after liver transplantation due to septic shock. The 2 patients who survived received sofosbuvir from 2 days before the surgery until 8 days following transplant. Both of these patients were in good health 18 months later.

TABLE 1. CLINICAL DATA OF PATIENTS HOSPITALIZED AT HOSPITAL FELÍCIO ROCHO IN 2018 YFV OUTBREAK

Patient	Age (years)	Gender	Platelets (per mL)	AST (IU/L)	ALT (IU/L)	Bilirubin (mg/dL)	INR	Creatinine (mg/dL)	Lactate (IU/L)	Encephalopathy	Transplantation (days)	Outcome
1	53	M	29,000	9,693	2,282	17.2	2.9	12.4	133	4	N	Dead
2	64	M	26,000	7,900	4,648	3.54	2.3	6.48	61	2	Y	Alive
3	37	M	58,000	8,151	7,206	8.16	>10	7.1	164	3	Y	Dead
4	49	M	89,000	5,160	2,463	5.12	1.81	8.74	40	n	N	Alive
5	39	M	58,000	8,707	4,509	6.81	2.9	8.81	125	4	N	Dead
6	58	M	12,000	12,590	7,446	21.9	1.65	1.17	42	n	N	Alive
7	69	M	35,000	8,572	3,987	5.9	>10	8.11	135	3	Y	Dead
8	57	M	29,000	8,451	3,854	10.1	4.4	7.49	184	4	N	Dead
9	57	F	46,000	28,266	9,680	4.47	>10	5.06	115	4	N	Dead
10	63	M	56,000	3,650	2,215	5.41	1.12	0.77	20	n	N	Alive
11	23	M	18,000	9,471	3,926	13.47	1.7	0.92	20	n	N	Alive
12	45	M	79,000	2,790	2,126	1.02	1.1	1.2	8	n	N	Alive
13	47	M	38,000	13,207	2,992	8.15	2.9	1.46	41	3	Y	Alive
14	40	M	49,000	157	288	0.49	1.1	0.82	15	n	N	Alive

Abbreviations: ALT, alanine aminotransferase; AST, aspartate aminotransferase; INR, international normalized ratio; N, no; Y, yes.

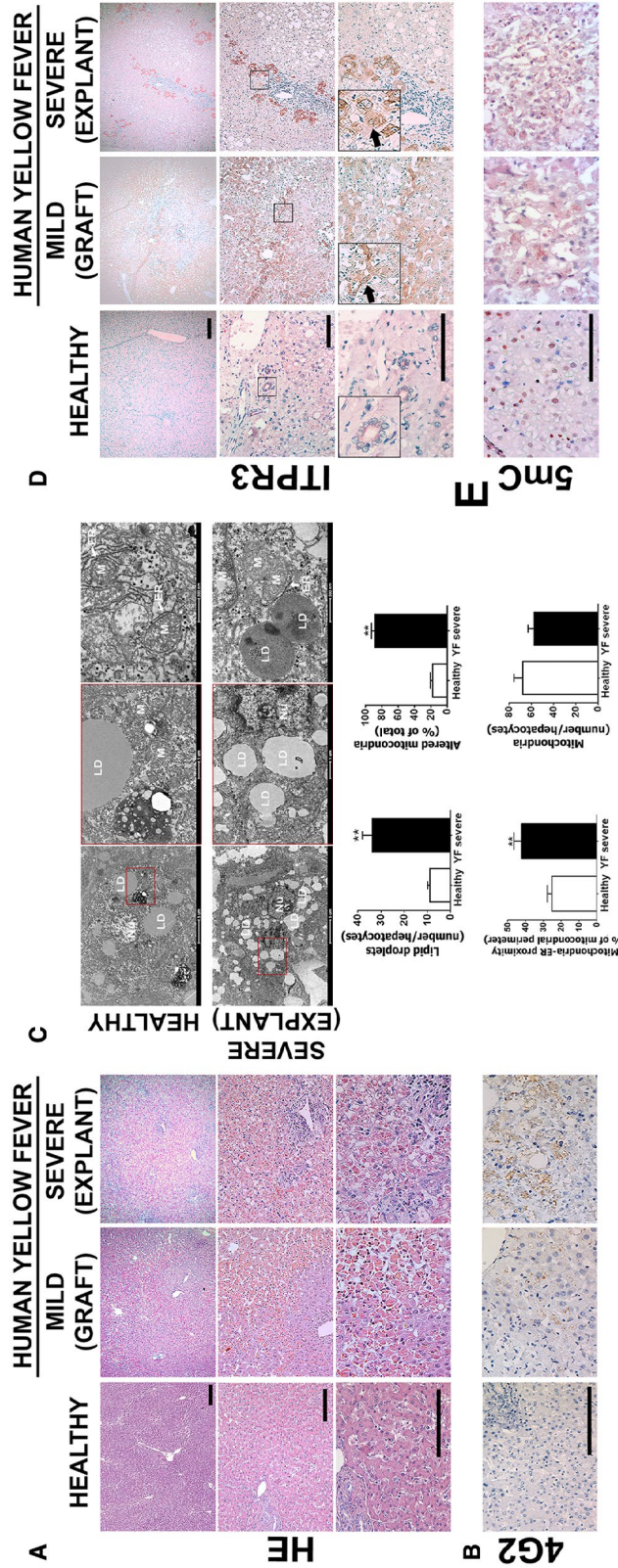


FIG. 1. Patients with acute liver failure from YF have steatosis, pan-lobular cell death, and new expression of ITPR3. (A) H&E-stained liver sections from healthy patient (left panel), YFV-infected patient showing mild liver disease (middle panel, biopsy from a liver graft), and a liver explant specimen from a patient with severe hepatic disease due to YFV infection (right panel). Patients were infected in 2018 during the YFV outbreak in Minas Gerais, Brazil. (B) Immunohistochemistry (IHC) staining for flavivirus envelope protein 4G2. (C) TEM images of liver samples from healthy patients (top panels) or YFV-infected patient displaying severe hepatic disease (bottom panels), showing mitochondria with disorganized or absent cristae, phagosomes, and lipid droplets. Graphs show quantification of number of lipid droplets, percentage of altered mitochondria, mitochondria-endoplasmic reticulum proximity, and mitochondrial number. Bars indicate the average values of samples from at least eight hepatocytes/group. (D) IHC liver slices stained for ITPR3. Arrows indicate ITPR3 localization in the cytoplasm and nucleus in hepatocytes of mild and severe cases of YF. (E) IHC stained for 5mC (scale bar: 50 μ m, 100 μ m, and 200 μ m for H&E and IHC, and 1 μ m and 5 μ m for TEM). Significance was analyzed using Student *t* test (***P* < 0.01). Abbreviations: LD, lipid droplet; Nu, nucleus; M, mitochondrion; Ph, phagosome.

Histological analysis of liver biopsy specimens showed severe hepatocellular damage throughout the hepatic lobule in the explants, while grafts developed mild injury in the midzone region (Fig. 1A and Supporting Fig. S1A). Pathological changes in explants included steatosis, lytic necrosis, hemorrhage, and inflammatory infiltrates, similar to what was described in a recent case report,⁽⁷⁾ and consistent with the clinical presentations of these patients. Pathological changes in midzonal hepatocytes of grafts included swelling, steatosis, apoptosis, and lytic necrosis (Fig. 1A, middle panel). All biopsy specimens also showed positive staining for the flavivirus envelope protein 4G2 (Fig. 1B and Supporting Fig. S1B), confirming the association between liver injury and YFV infection in these patients. Transmission electron microscopy (TEM) analysis demonstrated microvesicular steatosis in the YFV-infected hepatocytes (Fig. 1C), with a 3-fold increase in the number of lipid droplets relative to what was observed in normal control hepatocytes. Both steatosis and certain types of cell death have been linked to alterations in mitochondrial calcium signals in hepatocytes,⁽¹²⁻¹⁴⁾ which in turn may result from aberrant expression of the ITPRs that conduct calcium from the endoplasmic reticulum (ER) into mitochondria at mitochondria-associated membranes (MAMs).⁽¹⁴⁾ TEM analysis also showed that YFV-infected hepatocytes displayed mitochondrial alterations, including dissolved mitochondrial crests and presence of membrane pores, and an increased amount of MAMs, but no change in the total number of mitochondria (Fig. 1C). Transmission of calcium into mitochondria depends on which ITPR isoforms are expressed at the MAM,^(15,16) which varies among cell types and can change in disease states.^(13,14,17,18) Therefore, we examined whether expression of each of the three ITPR isoforms was altered in YF.

ITPR1 and ITPR2 are the isoforms principally expressed in normal hepatocytes,^(19,20) although hepatocytes begin to express ITPR3 as well in chronic liver diseases and in liver cancer, where it is responsible for certain pathological effects.^(21,22) Unexpectedly, ITPR3 expression markedly increased in hepatocytes during YF infection (Fig. 1D and Supporting Fig. S1C). Cytoplasmic, perinuclear, and nuclear ITPR3 staining was observed in hepatocytes in both explants and grafts (Fig. 1D). In contrast, there was no change in expression of ITPR1 (Supporting Fig. S1C), which is the isoform that normally localizes to

the MAM in hepatocytes,⁽¹⁴⁾ whereas ITPR2 expression was increased but to a much lesser extent than ITPR3 (Supporting Fig. S1C-E). Demethylation of its promoter can increase ITPR3 expression in hepatocytes,⁽²²⁾ and viral infection can promote DNA demethylation,^(23,24) so we analyzed the general methylation state in human YFV-infected tissue by examining tissue staining for 5-methyl cytosine (5mC), the methylated form of the DNA base cytosine targeted to DNA demethylases (Fig. 1E). Hepatocytes from normal liver were mostly positively stained (Fig. 1E, left panel), while hepatocytes were not labeled in either mild or severe liver injury from YFV (Fig. 1E, middle and right panels, respectively). Together, these findings demonstrate that YF infection induces hepatocytes to express ITPR3 and suggest that this occurs through DNA demethylation.

MOUSE MODEL OF YFV INFECTION REPLICATES HISTOLOGICAL AND FUNCTIONAL CHARACTERISTICS OF LIVER INVOLVEMENT IN HUMAN DISEASE

An animal model was used to investigate the mechanism of YF-induced liver injury and the role of ITPR3 in this. IFN α/β receptor KO SV129 mice were infected with YFV, and the time-course of ITPR3 expression was monitored. Mice were infected with either the attenuated YFV strain (YFV_{17DD}) used in the YF vaccine (Fig. 2) or with a sylvatic YFV strain (YFV_{WT}) that was isolated from a patient with YFV-liver failure in February 2018 (Supporting Fig. S2). Both strains caused loss of body weight and death (Fig. 2A and Supporting Fig. S2A). YFV_{17DD} reduced survival by 20% at 4×10^4 plaque-forming units (PFU) 7 days post-infection (dpi) (Fig. 2A), while all mice died by 7 dpi with 4×10^4 PFU of YFV_{WT} (Supporting Fig. S2A). Therefore, 4×10^4 PFU injections were used for further studies. Quantitative RT-PCR showed YFV_{17DD} messenger RNA (mRNA) in the mouse liver at 3 dpi, although the virus was not detected at 1 dpi and was completely eliminated by 6 dpi (Fig. 2B). Kinetics of indocyanine green (ICG) clearance from the blood was used to assess liver function in the YFV_{17DD}-infected mice (Fig. 2C). There was a significant

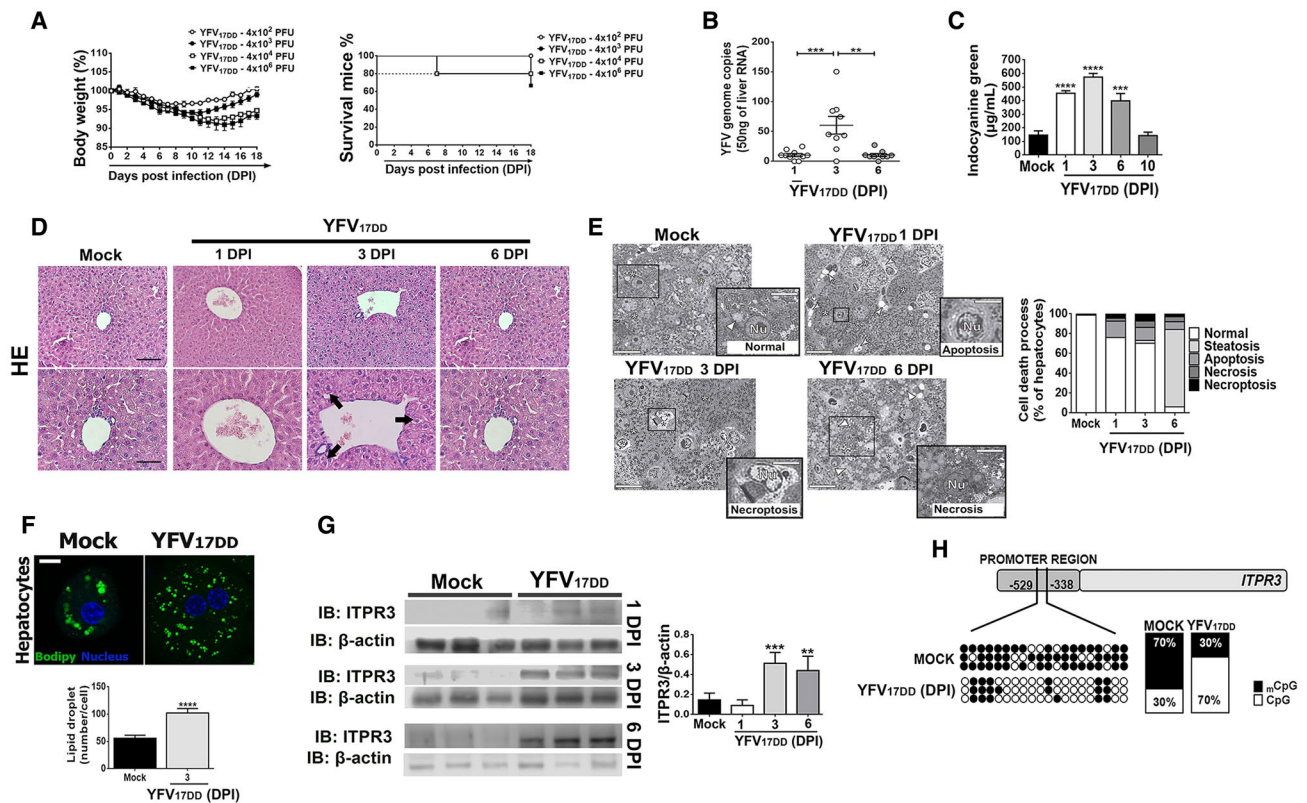


FIG. 2. Mouse model replicates histological findings in patients with liver failure from YF infection. IFN- α/β R^{-/-} SV129 mice (7–9 weeks old) were inoculated intravenously with YFV strain (YFV_{V17DD}) vaccine. (A) Changes in body weight (left panel) and Kaplan-Meier survival curve (right panel) after inoculums of 4×10^2 to 4×10^6 PFU. (B) Quantitative RT-PCR analysis of YFV viral load in the mice livers on 1 dpi, 3 dpi, and 6 dpi after inoculation of 4×10^4 PFU. Results are expressed as mean \pm SEM (** $P < 0.01$ and *** $P < 0.001$ using ANOVA, Bonferroni's posttest). (C) Liver function measured by the ICG clearance after inoculation of 4×10^4 PFU. Bars indicate mean \pm SEM of samples from 3–6 animals/group (*** $P < 0.001$ and **** $P < 0.0001$ using ANOVA, Bonferroni's posttest compared with mock samples). (D) Representative H&E-stained liver slices of mock and YFV_{17DD} inoculated animals on 1 dpi, 3 dpi, and 6 dpi. Scale bar: 50 μ m and 100 μ m. Arrows indicate hydropic degeneration characterized by the presence of swollen hepatocytes with clear and vacuolated cytoplasm and central nucleus. (E) Images of high-resolution light microscopy of 300- μ m-thick liver sections stained with toluidine blue, and representative images of mock and YFV_{17DD} inoculated mice on 1 dpi (B), 3 dpi (C), and 6 dpi (D) showing hepatocytes with normal aspect (white *) and ongoing different cell death processes (black *). Normal hepatocytes from mock animal with central nucleus, rough cytoplasm with many organelles, and few lipid droplets (arrowheads). Early apoptosis with initial cell and organelle condensation in hepatocyte from 1 dpi of YFV_{17DD}. Necroptosis characterized by pale and swollen nucleus and cytoplasm with plasma membrane integrity in hepatocyte from 3 dpi of YFV_{17DD}. Necrosis, illustrated by empty spaces of cytoplasm in hepatocyte from 6 dpi of YFV_{17DD} (left panel). Arrows indicate sinusoid capillaries; arrowheads indicate lipid droplets (scale bar: 25 μ m and 50 μ m). Frequency of cell death processes and steatosis analyzed in high-resolution images of 300-nm-thick sections (right panel). (F) Representative immunofluorescence images of isolated hepatocytes stained with Bodipy (green) and 4',6-diamidino-2-phenylindol (blue) from mock and YFV_{17DD} 3-dpi inoculated animals (upper panel) (scale bar: 20 μ m). Bottom panel shows the quantification of lipid droplets (number/cell). Bars indicate mean \pm SEM of samples from three animals/group (**** $P < 0.0001$ using Student t test). (G) ITPR3 expression is increased in liver 3 and 6 days after infection of mice with YFV_{17DD}. Left panel shows representative blots for ITPR3 expression in liver lysates from mock, and YFV_{17DD} 1-dpi, 3-dpi, and 6-dpi inoculated animals. Each lane reflects the blot for the lysate from a separate animal. Right panel shows quantification of ITPR3 expression, normalized by β -actin. Bars indicate mean \pm SEM of samples from 3–6 animals/group (** $P < 0.01$ and *** $P < 0.001$ using ANOVA, Bonferroni's posttest compared with mock samples). (H) Demethylation sites on cytosine-guanine dinucleotide (CpG) islands in mouse ITPR3 promoter region after 3 dpi with YFV_{17DD} virus. Black dots represent methylated sites, and white dots represent demethylated sites. Quantification of methylated/demethylated CpG island ratio in mock and YFV-infected liver samples. Abbreviations: IB, immunoblot; Nu, nucleus.

increase in ICG concentration in the blood after 1, 3, and 6 dpi, reflecting hepatic impairment, although the ICG concentration returned to normal at 10 dpi. Hematoxylin and eosin (H&E) stained liver specimens were microscopically examined. Hepatocytes displayed discrete hydropic degeneration (swollen cells with clear and vacuolated cytoplasm and central nucleus) in response to inoculation with 1 or 3 dpi of YFV_{17DD} (Fig. 2D) or YFV_{WT} (Supporting Fig. S2B); however, at 6 dpi, liver tissues were similar to controls. The frequency of apoptosis, steatosis, necroptosis, and necrosis were analyzed in 300-nm-thick sections stained with toluidine blue, and showed a progressive increase following infection, regardless of whether animals were infected with YFV_{17DD} (Fig. 2E) or YFV_{WT} (Supporting Fig. S2C). Hepatocytes isolated from YFV_{17DD}-infected mice at 3 dpi displayed an increased number of Bodipy-labeled lipid droplets compared with control hepatocytes (Fig. 2F). As in patients, livers of YFV-infected mice began to express ITPR3 (Fig. 2G and Supporting Fig. S2D). Western blot analysis demonstrated that expression of ITPR3 was significantly increased 3 dpi and 6 dpi in mice infected with either YFV_{17DD} (Fig. 2G) or YFV_{WT} (Supporting Fig. S2D). Similarly, 5mC staining showed that DNA methylation was decreased at 3 dpi with YFV_{WT} (Supporting Fig. S2E) compared with the noninfected group. Sequencing the ITPR3 promoter region of liver samples from mice at 3 dpi after YFV_{17DD} (Fig. 2H) or YFV_{WT} infection (Supporting Fig. S2F) confirmed demethylation, consistent with this being responsible for the new expression of ITPR3 in infected hepatocytes. Together, these results show that α/β KO SV129 mice infected with YFV display cellular and molecular alterations in the liver that are similar to what is observed in humans, including *de novo* expression of ITPR3.

ITPR3 EXPRESSION IN HEPATOCYTES PROTECTS YFV-INFECTED LIVER

To investigate the effects of YFV-induced *de novo* expression of ITPR3 in hepatocytes, experiments were performed in the liver-derived HepG2 cell line, which constitutively expresses ITPR3.^(22,25) These cells were compared with knockout for ITPR3 (R3KO) HepG2 cells, in which CRISPR was used to delete ITPR3 (Fig. 3A).⁽²²⁾

Calcium signal indicates the increase of free Ca²⁺ in a cell compartment relative to the basal level elicited by an agonist that directly or indirectly activates a calcium-dependent cascade. Cytosolic calcium signals were increased in YFV_{17DD}-infected cells relative to uninfected controls. The amplitude of the calcium signals was more than 3-fold greater in infected WT cells, but less than 2-fold greater in infected R3KO HepG2 cells, each relative to their uninfected controls (Fig. 3B,C). Calcium signaling can be regulated independently in the nucleus,⁽²⁵⁾ and nuclear calcium signals modulate progression through the cell cycle, hepatocyte proliferation, and liver regeneration,⁽²⁶⁻³⁰⁾ so we investigated Ca²⁺ signaling in the nucleus as well (Fig. 3D). YFV_{17DD} infection enhanced nuclear Ca²⁺ signals in both WT and R3KO cells, relative to uninfected cells. However, the amplitude of the nuclear Ca²⁺ signal was about 2.2-fold more pronounced in WT than in R3KO HepG2 cells (Fig. 3D). Consistent with this, a higher proliferation rate was observed in YFV_{17DD}-infected HepG2 cells compared with mock cells, whereas YFV_{17DD} did not induce proliferation in R3KO HepG2 cells (Fig. 3E). Moreover, cells lacking ITPR3 were more susceptible to the cytotoxic effect of YFV_{17DD} (Fig. 3F). This increased cytotoxic activity may have been due in part to the induction of apoptosis; Annexin V-positive cells were more prevalent in YFV_{17DD}-infected R3KO HepG2 cells than in uninfected cells, but not in YFV_{17DD}-infected WT HepG2 cells relative to their uninfected controls (Fig. 3F). Additionally, lipid droplet formation was higher in R3KO HepG2 cells than in WT cells, and this was even more pronounced after YFV_{17DD} infection (Fig. 4A). This preferential increase in steatosis in R3KO HepG2 was not related to mitochondrial Ca²⁺ signaling, because the amplitude of mitochondrial Ca²⁺ signals was increased to a similar extent in R3KO and WT HepG2 cells infected with YFV_{17DD} (Fig. 4B). However, the expression of *cpt1b* and *VLCAD*, which are genes related to β -oxidation, was down-regulated in YFV_{17DD}-infected R3KO HepG2 cells, whereas *VLCAD* was up-regulated in WT HepG2 cells (Fig. 4C,D). Therefore, the steatosis observed in R3KO HepG2 cells may have been due at least in part to inhibition of β -oxidation, which is responsible for breakdown of fatty acids derived from lipolysis of lipid droplets.⁽³¹⁾ YFV_{17DD} caused down-regulation of mRNA levels of the lipogenesis genes *SREBP1* and *FAS* in both HepG2 cell lines,

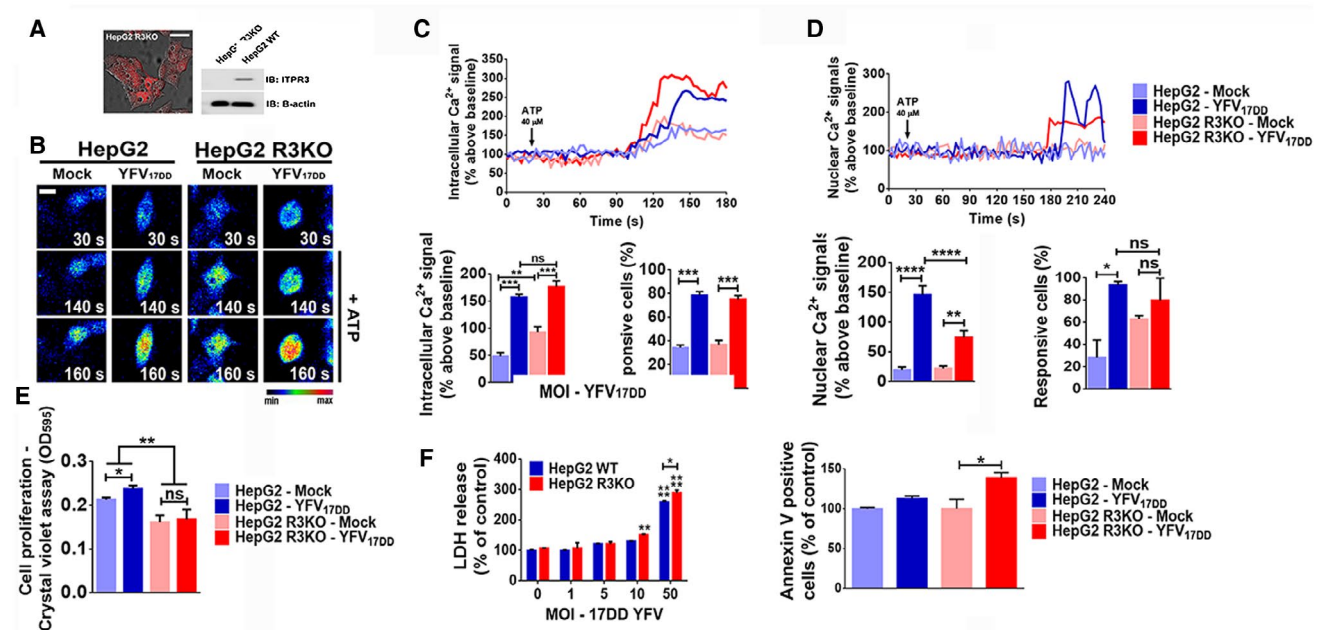


FIG. 3. ITPR3 expression is protective in a YFV-infected, liver-derived cell line. (A) Representative confocal images of HepG2 ITPR3 KO (HepG2 R3KO) cells and western blot for ITPR3 expression in HepG2 and HepG2 R3KO cells. (B) Confocal images of HepG2 and HepG2 R3KO cells loaded with Fluo-4/AM (6 μ M) and stimulated with 40 μ M ATP. The cells were infected with 50 MOI of YFV_{17DD} strain 24 hours before the Ca²⁺ analysis (scale bar: 20 μ m). (C) Representative time-course of total Ca²⁺ signal (upper panel), quantification of the peak fluorescence following stimulation with ATP (bottom-left panel), and percentage of responsive cells to increase of cytoplasmic Ca²⁺ signal (bottom-right panel). (D) Representative time-course of nuclear Ca²⁺ signal in the cells loaded with Fluo-4/AM (6 μ M) (upper graph). Bottom-left panel graph shows quantification of the peak fluorescence, and bottom-right graph shows percentage of responsive cells to increase of nuclear Ca²⁺ signal following stimulation with ATP. (E) Crystal violet proliferation assay 1 dpi with 50 MOI of YFV_{17DD}. (F) YFV_{17DD} cytotoxicity. Cell viability was measured by lactate-dehydrogenase release by the cells 1 dpi with different YFV_{17DD} inoculums (left panel). Proportion of apoptotic cells at day 1 of YFV_{17DD} 50 MOI infection, measured by flow cytometer analysis for annexin V-positive cells (right panel). Bars indicate the average values of samples from 3-6 biological replicates (>20 cells/replicate for Ca²⁺ signaling analysis). Significance was analyzed by the ANOVA, Bonferroni's posttest (* P < 0.05, ** P < 0.01, *** P < 0.001, and **** P < 0.0001) compared with mock samples. Abbreviations: IB, immunoblot; LDH, lactate dehydrogenase; ns, no statistical difference.

but more pronounced in R3KO HepG2 cells than in WT (Fig. 4E,F). These findings are consistent with the idea that ITPR3 stimulates nuclear Ca²⁺ signaling, cell proliferation, and lipolysis in YFV-infected hepatocytes, which collectively mitigates the deleterious effects of the infection.

To further investigate the effects of YFV infection on ITPR3 expression and calcium signaling, these were examined in freshly isolated primary mouse hepatocytes. Cells were stimulated with either epidermal growth factor (EGF) (Fig. 5A) or adenosine triphosphate (ATP) (Supporting Fig. S3), because both of these stimuli are important for calcium-mediated hepatocyte proliferation and liver regeneration.⁽³²⁻³⁵⁾ The amplitude of both cytosolic and nuclear Ca²⁺ signals induced by EGF was higher in hepatocytes

from YFV_{17DD}-infected mice than in mock hepatocytes (Fig. 5B,C, respectively). Cytosolic and nuclear Ca²⁺ signals in YFV_{17DD}-infected hepatocytes were also more pronounced in cells stimulated with ATP (Supporting Fig. S3A-C, respectively). ITPR3 expression was increased in the nucleus of YFV_{17DD}-infected hepatocytes, with its expression peak at 3 dpi (Fig. 5D), and this was associated with a higher number of proliferating cell nuclear antigen (PCNA)-positive hepatocytes in the YFV_{17DD}-infected mice as well (Fig. 5E). Specifically, nuclear staining for PCNA, a marker for proliferation, was significantly increased in YFV_{17DD}-infected mice at 1 dpi, 3 dpi, and 6 dpi (Fig. 5E). Consistent with these findings, a marked increase in PCNA staining was observed in the livers of YFV-infected patients with either mild

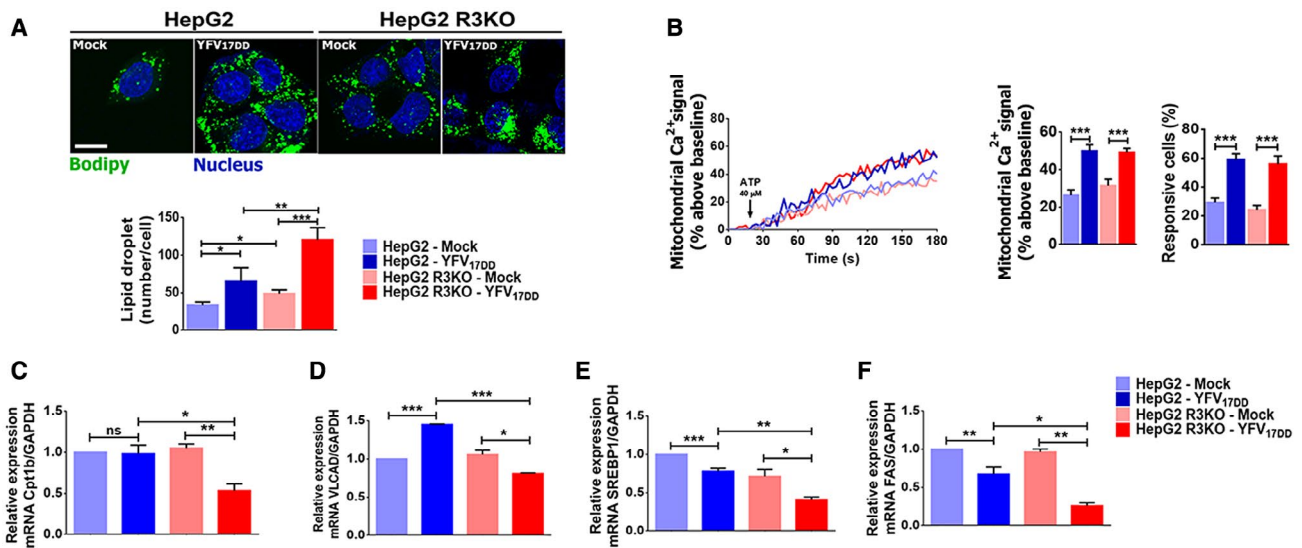


FIG. 4. ITPR3 expression decreases steatosis in a YFV-infected, liver-derived cell line. (A) Immunofluorescence images of HepG2 and HepG2 R3KO cells stained with Bodipy (green) and 4',6-diamidino-2-phenylindole (blue), both in mock and 1-dpi YFV_{17DD} cells (upper panel), and quantification of lipid droplets (number/cell) (scale bar: 20 μm) (bottom panel). (B) Representative time-course of mitochondrial Ca²⁺ signal (left graph). Cells were transfected with the mitochondrial matrix-targeted Ca²⁺ indicator inverse-pericam and stimulated with 40 μM ATP. Graphs show quantification of the peak of fluorescence following stimulation with ATP (middle graph) and percentage of responsive cells to increase of mitochondrial Ca²⁺ signals (right graph). Quantitative RT-PCR analysis for mRNA expression of β-oxidation, Cpt1b (C), VLCAD (D), lipogenesis, and SREBP1 (E) and FAS (F) genes. Bars indicate the average values of samples from three to six biological replicates (>20 cells/replicate for Ca²⁺ signaling analysis). Significance was analyzed by the ANOVA, Bonferroni's posttest (**P* < 0.05, ***P* < 0.01, ****P* < 0.001, and *****P* < 0.0001) compared with mock samples. Abbreviations: GAPDH, glyceraldehyde 3-phosphate dehydrogenase; ns, no statistical difference.

(Fig. 5F, middle panel) or severe (Fig. 5F, right panel) liver disease. Together, these results suggest that ITPR3 expression induced by YFV infection triggers a regenerative mechanism through a nuclear Ca²⁺ increase, in an attempt to protect the liver by stimulating hepatocyte proliferation.

Discussion

Despite extensive knowledge about YFV transmission and prophylaxis,⁽³⁶⁾ this infection remains a major threat to human health, and understanding of its pathogenesis remains limited. Here, we characterized the clinical and pathological findings in patients evaluated for liver transplant because they developed acute liver failure from their infection. The current findings complement and extend other recent clinical observations of YF liver failure, including the presence of massive hepatocellular necrosis and microvesicular steatosis, plus the rapid progression of coagulopathy, encephalopathy, and acute kidney injury.^(5-7,37)

Hepatocytes of infected patients also began to heavily express ITPR3, a calcium channel that is normally absent or minimally expressed in hepatocytes.^(19,20,38) This change was observed in a mouse model of YFV infection as well.

New expression of ITPR3 occurs in a variety of chronic liver diseases, and becomes more pronounced in hepatocellular carcinoma (HCC).⁽²²⁾ In that setting, pathological effects such as enhanced proliferation and resistance to apoptosis have been attributed to the ITPR3.⁽²²⁾ We report that ITPR3 can also become expressed in acute liver injury. Some of the ITPR3 in YFV infection localizes to the nucleus, where it is positioned to contribute to the enhanced nuclear calcium signaling observed here. This may have important therapeutic implications, as hepatocyte proliferation is dependent on calcium signals in the nucleus,⁽²⁶⁾ and the growth factors that are principally responsible for liver regeneration exert their effects by selectively activating nuclear calcium signaling pathways.^(27-30,39) It is less clear whether ITPRs that are localized to MAMs play a role in the

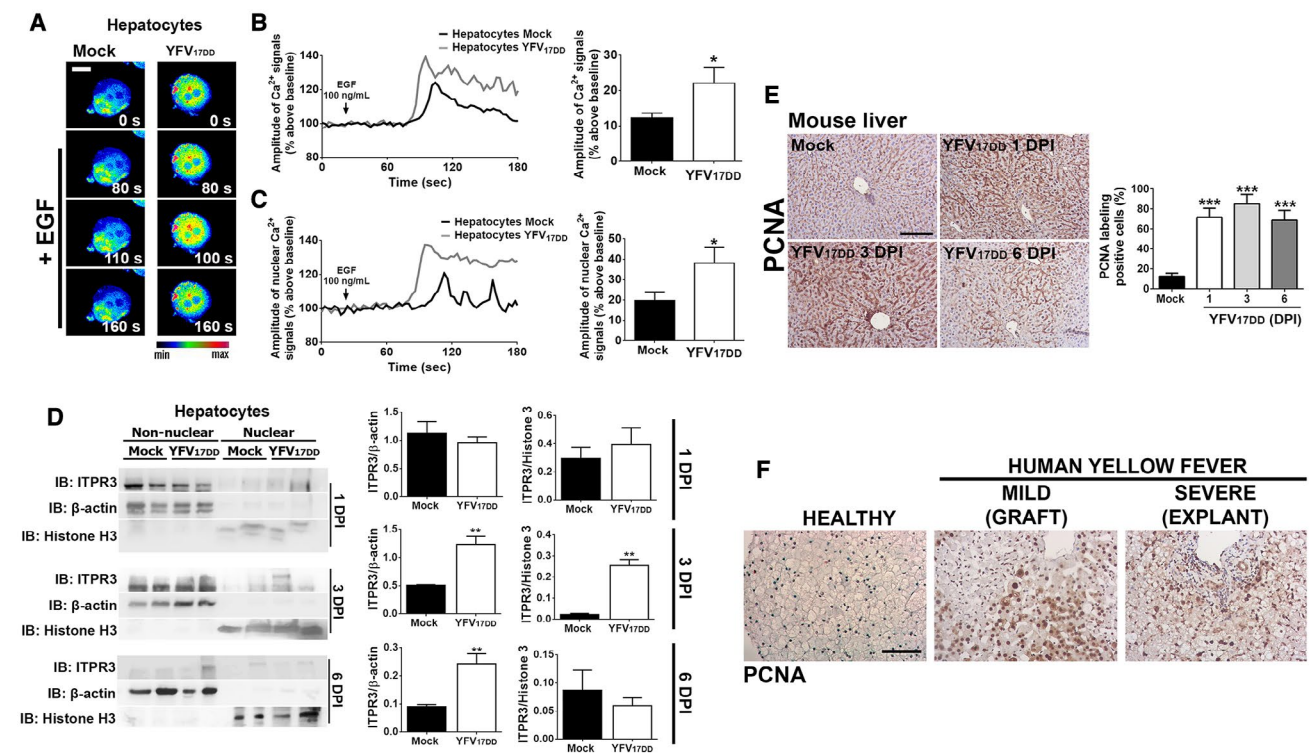


FIG. 5. YF infection increases Ca²⁺ signals in the nucleus and enhances proliferation of hepatocytes. (A) Confocal images of hepatocytes isolated from liver tissue of 3-dpi YFV_{17DD}-infected mice. Cells were loaded with Fluo-4/AM (6 μM) and stimulated with 100 ng/mL EGF (scale bar: 20 μm). (B) Representative time-course of total Ca²⁺ signal (left panel) and quantification of the peak fluorescence following stimulation with EGF (right panel). (C) Representative time-course of nuclear Ca²⁺ signal (left panel) and quantification of the peak fluorescence of nuclear Ca²⁺ signal following stimulation with EGF (right panel). (D) Nonnuclear and nuclear protein fractions of liver lysates from mock, 1-dpi, 3-dpi, and 6-dpi YFV_{17DD}-infected animals were tested for ITPR3 expression by western blot. Left panel shows representative blots; middle and right graphs show quantification of ITPR3 in nonnuclear and nuclear protein fractions. (E) IHC images of liver slices stained for PCNA in mock and YFV_{17DD}-infected animals on 1 dpi, 3 dpi, and 6 dpi (left panel). Scale bar: 100 μm. Quantification of PCNA-positive cells is shown in the right graph. (F) PCNA staining of liver slices from a healthy patient (left panel), YFV-infected hepatic human tissue from a graft biopsy with mild liver disease (middle panel), and an explant sample from a patient with severe hepatic disease (right panel). Scale bar: 50 μm. Bars indicate the average values of samples from three to six biological replicates (>20 cells/replicate for Ca²⁺ signaling analysis). Significance was analyzed by Student *t* test or the ANOVA, Bonferroni's posttest (**P* < 0.05, ***P* < 0.01, and ****P* < 0.001) compared with mock samples. Abbreviation: IB, immunoblot.

pathogenesis of YFV liver disease. These ITPRs are responsible for mitochondrial calcium signals, which in turn regulate lipid droplet formation and certain forms of cell death.^(12-14,16) Normally this is regulated by ITPR1 in hepatocytes,⁽¹⁴⁾ and expression of this isoform was not altered by YFV. ITPR2 can preferentially transmit calcium into mitochondria in some cell types,^(15,40) and ITPR2 expression was increased in YFV-infected hepatocytes, but there is disagreement about whether this isoform localizes to the MAM and does not regulate steatosis in hepatocytes.^(14,41) ITPR3 can preferentially transmit calcium into mitochondria in other cell types^(15-17,42). Indeed, we found that loss of ITPR3 sensitized YFV-infected cells to

apoptosis; however, effects of ITPR3 on steatosis may instead reflect concomitant changes in expression of enzymes involved in fatty acid oxidation and lipogenesis. The role of ITPR3 in controlling the expression of lipogenic genes is an open question that is just now being investigated. Several calcium signaling genes were recently shown to be important in human and mouse samples of HCC caused by nonalcoholic steatohepatitis. Among them, ITPR3 was aberrantly up-regulated in this disease,⁽²¹⁾ suggesting that this calcium channel could play a role in lipid metabolism. Chronic ITPR3 expression also modulates gene expression, triggering an anti-apoptotic response in HCC.⁽²²⁾ Together, these observations suggest the

possibility of a modulatory effect of ITPR3 on different molecular pathways in YFV-infected hepatocytes through regulation of gene expression, including genes related to lipid metabolism. Consistent with this, patients who develop symptoms from the YFV vaccine have enhanced ER stress,⁽⁴³⁾ which typically increases rather than decreases steatosis.⁽⁴⁴⁾ Lipid droplets are used by viruses from the Flaviviridae family, including YFV and hepatitis C virus (HCV), as an energy reservoir for replication, a platform for viral assembly⁽⁴⁵⁾ and a source of very low density lipoprotein, which is complexed to the HCV virus as a mechanism to evade the immune system.⁽⁴⁶⁾ Therefore, the current observation that ITPR3 inhibits steatosis may represent an additional protective role that it serves in YFV-infected hepatocytes.

A correlation between viral load and worse outcome has been reported in nonhuman primates infected with YFV⁽⁴⁷⁾ as well as in patients with YFV,⁽⁵⁾ and this relationship was recapitulated in our mouse model. Therefore, even though our findings suggest that *de novo* expression of ITPR3 in hepatocytes may be an endogenous protective mechanism in YFV infection, there also may be limits to the extent of this beneficial effect. It remains to be determined whether and to what extent the regulation of ITPR3 expression and targeting of this calcium channel to the nucleus can mitigate the liver damage that commonly contributes to the morbidity and mortality of this disease.

Author Contributions: F.O.L. designed and performed experiments, analyzed the data, and wrote the manuscript. A.F., A.C.M.L.F., R.M.F., M.L.S., D.G.M., and G.O.L.R. performed *in vitro* and *in vivo* experiments and analyzed the data. G.O.L.R., I.B.S.P., and V.V.C. performed the wild-type YF virus isolation, YFV propagation, and *in vivo* experiments, and analyzed the data related to the YF mouse model. F.F.D. processed tissue samples and performed TEM and morphometric analysis in the YF specimens. A.M.F.A., C.X.L., and P.T.V. identified and diagnosed human YF-infected specimens. M.M.T., V.V.C., M.C.F., M.H.N., and M.F.L. supervised the project, formulated the hypothesis, designed the experiments, and edited the manuscript.

Acknowledgments: The authors thank the Center of Microscopy at the Universidade Federal de Minas Gerais (<http://www.microscopia.ufmg.br>) for providing the equipment and technical support for experiments involving electron microscopy.

REFERENCES

- 1) Barrett AD, Monath TP. Epidemiology and ecology of yellow fever virus. *Adv Virus Res* 2003;61:291-315.
- 2) Monath TP. Yellow fever: an update. *Lancet Infect Dis* 2001;1:11-20.
- 3) Klitting R, Gould EA, Paupy C, de Lamballerie X. What does the future hold for yellow fever virus? *Genes (Basel)* 2018;9. pii: E291.
- 4) **Faria NR, Kraemer MUG, Hill SC, Goes de Jesus J, Aguiar RS, Iani FCM**, et al. Genomic and epidemiological monitoring of yellow fever virus transmission potential. *Science* 2018;361:894-899.
- 5) Kallas EG, D'Elia Zanella L, Moreira CHV, Buccheri R, Diniz GBF, Castineiras ACP, et al. Predictors of mortality in patients with yellow fever: an observational cohort study. *Lancet Infect Dis* 2019;19:750-758.
- 6) Duarte-Neto AN, Cunha MDP, Marcilio I, Song ATW, de Martino RB, Ho YL, et al. Yellow fever and orthotopic liver transplantation: new insights from the autopsy room for an old but re-emerging disease. *Histopathology* 2019;75:638-648.
- 7) Song ATW, Abdala E, de Martino RB, Malbouisson LMS, Tanigawa RY, Andrade GM, et al. Liver transplantation for fulminant hepatitis attributed to yellow fever. *Hepatology* 2019;69:1349-1352.
- 8) Quaresma JA, Barros VL, Fernandes ER, Pagliari C, Takakura C, da Costa Vasconcelos PF Jr., et al. Reconsideration of histopathology and ultrastructural aspects of the human liver in yellow fever. *Acta Trop* 2005;94:116-127.
- 9) Bernuau J, Goudeau A, Poynard T, Dubois F, Lesage G, Yvonnet B, et al. Multivariate analysis of prognostic factors in fulminant hepatitis B. *Hepatology* 1986;6:648-651.
- 10) Meier KC, Gardner CL, Khoretonenko MV, Klimstra WB, Ryman KD. A mouse model for studying viscerotropic disease caused by yellow fever virus infection. *PLoS Pathog* 2009;5:e1000614.
- 11) Shresta S, Sharar KL, Prigozhin DM, Beatty PR, Harris E. Murine model for dengue virus-induced lethal disease with increased vascular permeability. *J Virol* 2006;80:10208-10217.
- 12) **Mansouri A, Gattolliat CH**, Asselah T. Mitochondrial dysfunction and signaling in chronic liver diseases. *Gastroenterology* 2018;155:629-647.
- 13) Ferioud CN, Gustavo Oliveira A, Guerra MT, Nguyen L, Mitchell Richards K, Jurczak MJ, et al. Hepatic inositol 1,4,5 trisphosphate receptor type 1 mediates fatty liver. *Hepatology Commun* 2017;1:23-35.
- 14) **Arruda AP, Pers BM**, Parlakgul G, Guncy E, Inouye K, Hotamisligil GS. Chronic enrichment of hepatic endoplasmic reticulum-mitochondria contact leads to mitochondrial dysfunction in obesity. *Nat Med* 2014;20:1427-1435.
- 15) Bartok A, Weaver D, Golenar T, Nichtova Z, Katona M, Bansaghi S, et al. IP3 receptor isoforms differently regulate ER-mitochondrial contacts and local calcium transfer. *Nat Commun* 2019;10:3726.
- 16) **Mendes CC, Gomes DA**, Thompson M, Souto NC, Goes TS, Goes AM, et al. The type III inositol 1,4,5-trisphosphate receptor preferentially transmits apoptotic Ca²⁺ signals into mitochondria. *J Biol Chem* 2005;280:40892-40900.
- 17) **Kuo IY, Brill AL**, Lemos FO, Jiang JY, Falcone JL, Kimmerling EP, et al. Polycystin 2 regulates mitochondrial Ca²⁺ signaling, bioenergetics, and dynamics through mitofusin 2. *Sci Signal* 2019;12. pii: eaat7397.
- 18) **Ueasilomngkol P, Khamphaya T**, Guerra MT, Rodrigues MA, Gomes DA, Kong Y, et al. Type 3 inositol 1,4,5-trisphosphate receptor is increased and enhances malignant properties in cholangiocarcinoma. *Hepatology* 2020;71:583-599.

- 19) Hirata K, Pusch T, O'Neill AF, Dranoff JA, Nathanson MH. The type II inositol 1,4,5-trisphosphate receptor can trigger Ca²⁺ waves in rat hepatocytes. *Gastroenterology* 2002;122:1088-1100.
- 20) Kruglov EA, Gautam S, Guerra MT, Nathanson MH. Type 2 inositol 1,4,5-trisphosphate receptor modulates bile salt export pump activity in rat hepatocytes. *Hepatology* 2011;54:1790-1799.
- 21) **Liang JQ, Teoh N**, Xu L, Pok S, Li X, Chu ESH, et al. Dietary cholesterol promotes steatohepatitis related hepatocellular carcinoma through dysregulated metabolism and calcium signaling. *Nat Commun* 2018;9:4490.
- 22) **Guerra MT, Florentino RM**, Franca A, Lima Filho AC, dos Santos ML, Fonseca RC, et al. Expression of the type 3 InsP3 receptor is a final common event in the development of hepatocellular carcinoma. *Gut* 2019;68:1676-1687.
- 23) Gomes AV, de Souza Morais SM, Menezes-Filho SL, de Almeida LG, Rocha RP, Ferreira JM, et al. Demethylation profile of the TNF- α promoter gene is associated with high expression of this cytokine in Dengue virus patients. *J Med Virol* 2016;88:1297-1302.
- 24) Fan H, Cui Z, Zhang H, Mani SK, Diab A, Lefrancois L, et al. DNA demethylation induces SALL4 gene re-expression in subgroups of hepatocellular carcinoma associated with Hepatitis B or C virus infection. *Oncogene* 2017;36:2435-2445.
- 25) Leite MF, Thrower EC, Echevarria W, Koulen P, Hirata K, Bennett AM, et al. Nuclear and cytosolic calcium are regulated independently. *Proc Natl Acad Sci U S A* 2003;100:2975-2980.
- 26) Rodrigues MA, Gomes DA, Leite MF, Grant W, Zhang L, Lam W, et al. Nucleoplasmic calcium is required for cell proliferation. *J Biol Chem* 2007;282:17061-17068.
- 27) Gomes DA, Rodrigues MA, Leite MF, Gomez MV, Varnai P, Balla T, et al. c-Met must translocate to the nucleus to initiate calcium signals. *J Biol Chem* 2008;283:4344-4351.
- 28) **De Angelis Campos AC, Rodrigues MA**, de Andrade C, de Goes AM, Nathanson MH, Gomes DA. Epidermal growth factor receptors destined for the nucleus are internalized via a clathrin-dependent pathway. *Biochem Biophys Res Commun* 2011;412:341-346.
- 29) Rodrigues MA, Gomes DA, Andrade VA, Leite MF, Nathanson MH. Insulin induces calcium signals in the nucleus of rat hepatocytes. *Hepatology* 2008;48:1621-1631.
- 30) Amaya MJ, Oliveira AG, Guimaraes ES, Casteluber MC, Carvalho SM, Andrade LM, et al. The insulin receptor translocates to the nucleus to regulate cell proliferation in liver. *Hepatology* 2014;59:274-283.
- 31) Houten SM, Wanders RJ. A general introduction to the biochemistry of mitochondrial fatty acid β -oxidation. *J Inher Metab Dis* 2010;33:469-477.
- 32) Runge DM, Runge D, Dorko K, Pizarov LA, Leckel K, Kostrubsky VE, et al. Epidermal growth factor- and hepatocyte growth factor-receptor activity in serum-free cultures of human hepatocytes. *J Hepatol* 1999;30:265-274.
- 33) Tackett BC, Sun H, Mei Y, Maynard JP, Cheruvu S, Mani A, et al. P2Y2 purinergic receptor activation is essential for efficient hepatocyte proliferation in response to partial hepatectomy. *Am J Physiol Gastrointest Liver Physiol* 2014;307:G1073-G1087.
- 34) Michalopoulos GK, Khan Z. Liver regeneration, growth factors, and amphiregulin. *Gastroenterology* 2005;128:503-506.
- 35) Besnard A, Gautherot J, Julien B, Tebbi A, Garcin I, Doignon I, et al. The P2X4 purinergic receptor impacts liver regeneration after partial hepatectomy in mice through the regulation of biliary homeostasis. *Hepatology* 2016;64:941-953.
- 36) Klitting R, Fischer C, Drexler JF, Gould EA, Roiz D, Paupy C, de Lamballerie X. What does the future hold for yellow fever virus? *Genes (Basel)* 2018;9:425-462.
- 37) Ribeiro AF, Cavalin RF, Abdul Hamid Suleiman JM, Alves da Costa J, Januaria de Vasconcelos M, Sant'Ana Malaque CM, Sztajnbock J. Yellow fever: factors associated with death in a hospital of reference in infectious diseases, Sao Paulo, Brazil, 2018. *Am J Trop Med Hyg* 2019;10:180-188.
- 38) Dufour JF, Luthi M, Forestier M, Magnino F. Expression of inositol 1,4,5-trisphosphate receptor isoforms in rat cirrhosis. *Hepatology* 1999;30:1018-1026.
- 39) Garcin I, Tordjmann T. Calcium signalling and liver regeneration. *Int J Hepatol* 2012;2012:630670.
- 40) **Wu S, Lu Q**, Wang Q, Ding Y, Ma Z, Mao X, et al. Binding of FUN14 domain containing 1 with inositol 1,4,5-trisphosphate receptor in mitochondria-associated endoplasmic reticulum membranes maintains mitochondrial dynamics and function in hearts *in vivo*. *Circulation* 2017;136:2248-2266.
- 41) Feriod CN, Nguyen L, Jurczak MJ, Kruglov EA, Nathanson MH, Shulman GI, et al. Inositol 1,4,5-trisphosphate receptor type II (InsP3R-II) is reduced in obese mice, but metabolic homeostasis is preserved in mice lacking InsP3R-II. *Am J Physiol Endocrinol Metab* 2014;307:E1057-E1064.
- 42) De Stefani D, Bononi A, Romagnoli A, Messina A, De Pinto V, Pinton P, et al. VDAC1 selectively transfers apoptotic Ca²⁺ signals to mitochondria. *Cell Death Differ* 2012;19:267-273.
- 43) Chan KR, Gan ES, Chan CYY, Liang C, Low JZH, Zhang SL, et al. Metabolic perturbations and cellular stress underpin susceptibility to symptomatic live-attenuated yellow fever infection. *Nat Med* 2019;25:1218-1224.
- 44) Lebeauin C, Vallee D, Hazari Y, Hetz C, Chevet E, Bailly-Maitre B. Endoplasmic reticulum stress signalling and the pathogenesis of non-alcoholic fatty liver disease. *J Hepatol* 2018;69:927-947.
- 45) Martins AS, Martins IC, Santos NC. Methods for lipid droplet biophysical characterization in flaviviridae infections. *Front Microbiol* 2018;9:1951.
- 46) Filipe A, McLauchlan J. Hepatitis C virus and lipid droplets: finding a niche. *Trends Mol Med* 2015;21:34-42.
- 47) Engelmann F, Josset L, Girke T, Park B, Barron A, Dewane J, et al. Pathophysiologic and transcriptomic analyses of viscerotropic yellow fever in a rhesus macaque model. *PLoS Negl Trop Dis* 2014;8:e3295.

Author names in bold designate shared co-first authorship.

Supporting Information

Additional Supporting Information may be found at onlinelibrary.wiley.com/doi/10.1002/hep4.1504/supinfo.